

REPRESENTATION OF UNCERTAINTY AND CORRIDOR DP FOR HYDROPOWER  
OPTIMIZATION

A Dissertation

Presented to the Faculty of the Graduate School

of Cornell University

In Partial Fulfillment of the Requirements for the Degree of

Doctor of Philosophy

by

Jonathan Richard Lamontagne

January 2015

© 2015 Jonathan Richard Lamontagne

# REPRESENTATION OF UNCERTAINTY AND CORRIDOR DP FOR HYDROPOWER OPTIMIZATION

Jonathan Richard Lamontagne, Ph.D.

Cornell University 2015

This thesis focuses on optimization techniques for multi-reservoir hydropower systems operation, with a particular concern with the representation and impact of uncertainty. The thesis reports on three research investigations: 1) examination of the impact of uncertainty representations, 2) efficient solution methods for multi-reservoir stochastic dynamic programming (SDP) models, and 3) diagnostic analyses for hydropower system operation.

The first investigation explores the value of sophistication in the representation of forecast and inflow uncertainty in stochastic hydropower optimization models using a sampling SDP (SSDP) model framework. SSDP models with different uncertainty representation ranging in sophistication from simple deterministic to complex dynamic stochastic models are employed when optimize a single reservoir systems [similar to Faber and Stedinger, 2001]. The effect of uncertainty representation on simulated system performance is examined with varying storage and powerhouse capacity, and with random or mean energy prices. In many cases very simple uncertainty models perform as well as more complex ones, but not always.

The second investigation develops a new and efficient algorithm for solving multi-reservoir SDP models: Corridor SDP. Rather than employing a uniform grid across the entire state space, Corridor SDP efficiently concentrates points in where the

system is likely to visit, as determined by historical operations or simulation. Radial basis functions (RBFs) are used for interpolation. A greedy algorithm places points where they are needed to achieve a good approximation. In a four-reservoir test case, Corridor DP achieves the same accuracy as spline-DP and linear-DP with approximately 1/10 and 1/1100 the number of discrete points, respectively. When local curvature is more pronounced (due to minimum-flow constraints), Corridor DP achieves the same accuracy as spline-DP and linear-DP with approximately 1/30 and 1/215 the number of points, respectively.

The third investigation explores three diagnostic approaches for analyzing hydropower system operation. First, several simple diagnostic statistics describe reservoir volume and powerhouse capacity in units of time, allowing scale-invariant comparisons and classification of different reservoir systems and their operation. Second, a regression analysis using optimal storage/release sequences identifies the most useful hydrologic state variables. Finally spectral density estimation identifies critical time scales for operation for several single-reservoir systems considering mean and random energy prices.

Deregulation of energy markets has made optimization of hydropower operations an active concern. Another development is publication of Extended Streamflow Forecasts (ESP) by the National Weather Service (NWS) and others to describe flow forecasts and their precision; the multivariate Sampling SDP models employed here are appropriately structured to incorporate such information in operational hydropower decisions. This research contributes to our ability to structure and build effective hydropower optimization models.

## BIOGRAPHICAL SKETCH

Jonathan Richard Lamontagne was born in Nashua, New Hampshire on November 11, 1986. After obtaining his high school diploma at Pembroke Academy in Pembroke, New Hampshire he attended the University of New Hampshire where he received a B.S. in Civil Engineering in 2009. During summer and winter breaks he worked as a construction laborer, an engineering intern for Appledore Engineering, and as a hazardous waste enforcement intern for the New Hampshire Department of Environmental Services. He entered graduate studies at Cornell in 2009 to pursue a lifelong interest in water resources engineering, and received his M.S. in Civil and Environmental Engineering in 2014. Upon graduation he accepted a post-doctoral research position at Cornell. He currently lives in Ithaca with his wife Katie.

This thesis is dedicated to the generations of my family who made my success possible,  
and especially to my Katie.

## ACKNOWLEDGMENTS

Very few people are truly self-made and I am certainly not one. My success in obtaining a doctorate is the culmination of generations of my family's dedication to hard work and education. I would be remiss not to acknowledge the profound influence those who have gone before have had in showing me the way and providing inspiration.

I would also like to acknowledge the untiring support and encouragement of my advisor and special committee chair Professor Jerry R. Stedinger. My graduate education has been the most intense and rewarding learning experience I have ever had. Professor Stedinger's constant patience and creativity have been indispensable to the completion of this thesis.

I especially acknowledge the hard work, support, understanding, and love of my wife Katie which has gotten me through the rough patches and long hours of the past 5 years. This thesis is yours as much as mine.

Finally, I would like to gratefully acknowledge the Hydro Research Foundation and the Bonneville Power Administration whose financial support made my graduate studies possible.

## TABLE OF CONTENTS

BIOGRAPHICAL SKETCH.....	5
ACKNOWLEDGMENTS.....	7
TABLE OF CONTENTS.....	8
LIST OF FIGURES.....	11
LIST OF TABLES.....	21
CHAPTER 1.....	23
REFERENCES.....	29
CHAPTER 2.....	31
Section 2.1 Dynamic Programming and Stochastic Dynamic Programming.....	32
Section 2.2 Sampling Stochastic Dynamic Programming.....	36
Section 2.3 The Evolution of SDP Algorithms for Reservoir Optimization.....	38
Section 2.4 Special Concerns addressed in this Thesis.....	44
Section 2.4.1 Representations of Uncertainty.....	44
Section 2.4.2 Addressing the Curse of Dimensionality.....	49
Aggregation Approaches.....	50
Stochastic Dual Dynamic Programming.....	51
Surrogate Approximation of Future Value Function.....	51
Sparse Sampling of the State Space.....	52
The Fitted-Q-Iteration Method.....	53
Section 2.5 Conclusion.....	54
REFERENCES.....	56
CHAPTER 3.....	65
Section 3.1 The Kennebec River.....	65
Section 3.2 The Kennebec Hydropower System.....	67
Section 3.3 Hypothetical Systems and Synthetic Hydrology.....	69
Section 3.3.1 Generation of Synthetic Inflows.....	73
Selecting Reference Streams.....	75
“Single-Reservoir” System.....	78
Brassua and Moosehead Lakes.....	79
Flagstaff Lake.....	81
Wyman Lake.....	83
Section 3.4 Conclusion.....	83
REFERENCES.....	85
CHAPTER 4.....	87
Section 4.1 Introduction and Motivation.....	87
Section 4.2 SDP Algorithms for Reservoir Operation.....	90
Implementation of SDP and SSDP Policies.....	95
Section 4.3 Transition Probabilities and Representations of Uncertainty.....	96
Transition Probabilities based on Forecasts.....	98
Transition Probabilities based on Multiple Forecasts.....	101
Section 4.4 Proposed Algorithm Structure.....	104
Section 4.4.1 Comparison of Proposed Algorithm and Past Work.....	109
Section 4.4.2 Representations of Uncertainty for the Proposed Algorithm.....	111
Section 4.5 Metrics for Measuring Algorithm Performance in Hydro Studies ...	112

Section 4.6	Test Problem .....	114
Section 4.6.1	Study Basins .....	115
Section 4.6.2	Economic Objective .....	117
Section 4.6.3	Rule Curve Operation .....	119
Section 4.7	Results and Discussion .....	120
	Mean Price Scheme.....	121
	Variable Price Scheme .....	129
Section 4.8	Summary and Conclusions .....	134
	REFERENCES .....	137
	Appendix 1: Synthetic Forecast Generation .....	141
	Appendix 2: “Mean Price” Model Runs .....	143
	Appendix 3: “Variable Price” Model Runs .....	149
CHAPTER 5	.....	154
Section 5.1	Introduction and motivation for Corridor Concept.....	155
Section 5.1.1	Corridor SDP and the use of corridors in deterministic DP.....	157
Section 5.2	Dynamic Programming (DP) for Reservoir Operation.....	157
Section 5.3	Addressing the Curse .....	159
	Aggregation Approaches .....	159
	Stochastic Dual Dynamic Programming.....	160
	Surrogate Approximation of Future Value Function .....	161
	Sparse Sampling of the State Space.....	161
Section 5.4	Corridor DP.....	163
Section 5.5	RBF Interpolation and Least-Squares Approximation .....	166
Section 5.6	Basis Functional Forms and Parameterization.....	171
Section 5.6.1	RBF Function Shape and Parameterization for two-dimensional test cases	172
Section 5.7	Selection of Corridor Points .....	178
Section 5.7.1	Step One: Filling .....	179
Section 5.7.2	Step Two: Inserting a Backbone .....	181
Section 5.7.3	Step Three: Corridor Thinning.....	182
Section 5.8	Results.....	186
Section 5.8.1	Test Basin.....	186
Section 5.8.2	Comparison of Traditional and Corridor SDP: Easy Case.....	189
	Convergence Analysis .....	193
Section 5.8.3	Comparison of Traditional and Corridor DP: Hard Case.....	195
Section 5.8.4	Speed-up from smooth surfaces .....	199
Section 5.8.5	On the Selection of Basis Functional Form .....	202
Section 5.9	Discussion.....	207
Section 5.10	Conclusions .....	208
	REFERENCES .....	209
	Appendix: SDP Diagnostics .....	212
CHAPTER 6	.....	217
Section 6.1	Introduction.....	217
Section 6.2	Literature Search.....	218
Section 6.3	Diagnostic Metrics .....	220

Section 6.3.1	Simple Diagnostic Metrics .....	221
Section 6.3.2	The Regression Approach .....	227
Section 6.3.3	The Spectral Density Function Approach .....	228
Section 6.4	Results .....	230
Section 6.4.1	Study Systems .....	230
Section 6.4.2	Application of Diagnostic Metrics .....	233
	'Mean Price' Scheme Results .....	234
	'Real Price' Scheme Results .....	241
Section 6.5	The value of the Spectral Density Analysis .....	245
Section 6.6	Conclusion .....	247
	REFERENCES .....	249
	Appendix: 'Mean Price' Economic Scheme PSDF < <b>SRR</b> > .....	251
	Appendix: 'Mean Price' Economic Scheme CPSDF < <b>SIR</b> > .....	255
	Appendix: 'Mean Price' Economic Scheme CPSDF < <b>SSR</b> > .....	259
	Appendix: 'Real Price' Economic Scheme PSDF < <b>SRR</b> > .....	263
	Appendix: 'Real Price' Economic Scheme CPSDF < <b>SIR</b> > .....	267
	Appendix: 'Real Price' Economic Scheme CPSDF < <b>SSR</b> > .....	271
CHAPTER 7	.....	276
	Chapter 4 Conclusions .....	276
	Chapter 5 Conclusions .....	278
	Chapter 6 Conclusions .....	278
	Future Work .....	280
	REFERENCES .....	282

## LIST OF FIGURES

Figure 3-1: Schematic of the Kennebec Hydropower System .....	70
Figure 3-2: Schematic of “single-reservoir” system where $X$ is the reservoir storage and $Y$ is the powerhouse turbine capacity. ....	72
Figure 3-3: Schematic of “four-reservoir” system .....	72
Figure 3-4: Map showing the location of the target basins (in blue) and the reference record basins (in green). ....	77
Figure 3-5: Scaled (by DA) Brassua mean annual inflow hydrograph and Scaled (by DA) mean annual inflow hydrographs for reference records. ....	79
Figure 3-6: Brassua mean annual inflow hydrograph and Scaled (by DA) mean annual inflow hydrographs for reference records. ....	80
Figure 3-7: Flagstaff mean annual inflow hydrograph and Scaled (by annual inflow) mean annual inflow hydrographs for reference records. ....	83
Figure 4-1: Probability of transitioning from scenario $i$ to scenario $j$ for the F and M cases vs. the streamflow volume in scenario $j$ .....	100
Figure 4-2: Structure of the Proposed Adaptive Time Step SSDP Model .....	106
Figure 4-3: Alternative approaches to time decomposition for reservoir operations models.....	110
Figure 4-4: Uncertainty structures from various configurations of the time decomposition algorithm. ....	112
Figure 4-5: Schematic of a Hypothetical Single Reservoir System .....	116
Figure 4-6: Range of the $STdays$ vs. $PHdays$ of the test systems considered. ....	117
Figure 4-7: Price profile versus generation .....	118
Figure 4-8: Structure of the RCO algorithm.....	120
Figure 4-9: PR for (Big, 8300) system for various algorithms, mean price scheme. ....	122
Figure 4-10: $Eff$ for (Big, 8300) system for various algorithms, mean price scheme. ....	122
Figure 4-11: $Eff$ for Big reservoirs with varying turbine capacity for various algorithms, mean price scheme. ....	123
Figure 4-12: $Eff$ for (Big, 8300) system for select algorithms, mean price scheme .....	124
Figure 4-13: $Eff$ for Small reservoirs with varying turbine capacity for various re-optimization forecast precision, mean price scheme. ....	125
Figure 4-14: $Eff$ for Mid reservoirs with varying turbine capacity for various re-optimization forecast precision, mean price scheme. ....	125
Figure 4-15: $Eff$ for Turbine Capacity (8300 cfs) with varying storage for various algorithms, mean price scheme. ....	126

Figure 4-16: <i>Eff</i> of uncertainty models with increasing sophistication, for system (Big, 8300) and forecast precision $R2 = 0.95$ , ‘mean price’ scheme.....	127
Figure 4-17: <i>Eff</i> of uncertainty models with increasing sophistication, for system (Big,3500) and forecast precision $R2 = 0.95$ , ‘mean price’ scheme.....	128
Figure 4-18: Least sophisticated uncertainty model which matches the <i>Eff</i> of sophisticated F/F/F uncertainty model, ‘mean price’ scheme, forecast precision $R2 = 0.95$ .....	129
Figure 4-19: <i>Eff</i> for Mid reservoirs with varying turbine capacity for various re-optimization forecast precision, variable price scheme.....	130
Figure 4-20: <i>Eff</i> for Turbine Capacity (8300 cfs) with varying storage for various algorithms, variable price scheme.....	132
Figure 4-21: <i>Eff</i> for (Big, 8300) system for several algorithms, variable price scheme.....	132
Figure 4-22: <i>Eff</i> for (Small, 2000) system for several algorithms, variable price scheme.....	133
Figure 4-23: Least sophisticated uncertainty model which matches the <i>Eff</i> of sophisticated F/F/F uncertainty model, ‘variable price’ scheme, forecast precision $R2 = 0.95$ .....	134
Figure 4-24: The effect of forecast precision and reservoir size on <i>Eff</i> for stochastic programming models, with fixed turbine capacity (2000 cfs), ‘mean price’ scheme.	144
Figure 4-25: The effect of forecast precision and reservoir size on <i>Eff</i> for stochastic programming models, with fixed turbine capacity (3500 cfs), ‘mean price’ scheme.	144
Figure 4-26: The effect of forecast precision and reservoir size on <i>Eff</i> for stochastic programming models, with fixed turbine capacity (5000 cfs), ‘mean price’ scheme.	144
Figure 4-27: The effect of forecast precision and reservoir size on <i>Eff</i> for stochastic programming models, with fixed turbine capacity (8300 cfs), ‘mean price’ scheme.	145
Figure 4-28: The effect of forecast precision and turbine capacity on <i>Eff</i> for stochastic programming models, with fixed storage capacity (Small), ‘mean price’ scheme.....	145
Figure 4-29: The effect of forecast precision and turbine capacity on <i>Eff</i> for stochastic programming models, with fixed storage capacity (Mid), ‘mean price’ scheme.....	146
Figure 4-30: The effect of forecast precision and turbine capacity on <i>Eff</i> for stochastic programming models, with fixed storage capacity (Big), ‘mean price’ scheme.....	146
Figure 4-31: The effect of forecast precision and reservoir size on <i>Eff</i> for stochastic programming models, with fixed turbine capacity (2000 cfs), ‘variable price’ scheme.....	149

Figure 4-32: The effect of forecast precision and reservoir size on <i>Eff</i> for stochastic programming models, with fixed turbine capacity (3500 cfs), ‘variable price’ scheme. ....	149
Figure 4-33: The effect of forecast precision and reservoir size on <i>Eff</i> for stochastic programming models, with fixed turbine capacity (5000 cfs), ‘variable price’ scheme. ....	150
Figure 4-34: The effect of forecast precision and reservoir size on <i>Eff</i> for stochastic programming models, with fixed turbine capacity (8300 cfs), ‘variable price’ scheme. ....	150
Figure 4-35: The effect of forecast precision and turbine capacity on <i>Eff</i> for stochastic programming models, with fixed storage capacity (Small), ‘mean price’ scheme. ....	150
Figure 4-36: The effect of forecast precision and turbine capacity on <i>Eff</i> for stochastic programming models, with fixed storage capacity (Mid), ‘mean price’ scheme. ....	151
Figure 4-37: The effect of forecast precision and turbine capacity on <i>Eff</i> for stochastic programming models, with fixed storage capacity (Big), ‘mean price’ scheme. ....	151
Figure 5-1: 3-dimensional projection of a 4-dimensional lattice with 10 discrete points evaluated in each dimension. ....	164
Figure 5-2: Quadratic Test Function .....	173
Figure 5-3: Interpolating Gaussian RBF surface ( $\gamma = 0.1$ ) with 9 grid points .....	174
Figure 5-4: Interpolating Gaussian RBF surface ( $\gamma = 0.6$ ) with 9 grid points .....	175
Figure 5-5: Interpolating Gaussian RBF surface ( $\gamma = 2.1$ ) with 9 grid points .....	175
Figure 5-6: Interpolating Gaussian RBF surface ( $\gamma = 4.6$ ) with 9 grid points .....	175
Figure 5-7: Interpolating RBF cubic Spline RBF surface with 9 grid points.....	176
Figure 5-8: Matlab ‘Peaks’ Function.....	176
Figure 5-9: Interpolating Gaussian RBF ( $\gamma = 0.65$ ) surface for Matlab ‘Peaks’ with 9 grid points.....	176
Figure 5-10: Interpolating Cubic Spline RBF surface for Matlab ‘Peaks’ with 9 grid points .....	177
Figure 5-11: Corridor Basis Points before and after Filling.....	181
Figure 5-12: Corridor Basis Points with Backbone points.....	182
Figure 5-13: Maximum Residual Error ( $\max e_i$ ) versus Iteration of the Greedy Basis Selection Algorithm.....	184
Figure 5-14: Corridor Basis Points with Backbone after thinning using the Greedy Algorithm, for the <i>easy case</i> .....	185

Figure 5-15: Corridor Basis Points with Backbone after thinning using the Greedy Algorithm, for the <i>hard case</i> .....	185
Figure 5-16: Schematic of the Kennebec Hydropower System .....	188
Figure 5-17: Schematic of four-reservoir test system used in Section 5.8.2. ....	189
Figure 5-18: SSE in the Corridor Region vs. Number of Basis Points, <i>easy case</i> .....	192
Figure 5-19: Relative RMSE in the Corridor Region vs. Number of Basis Points, <i>easy case</i> .....	192
Figure 5-20: MSE in the Corridor Region vs. Number of Basis Points, <i>hard case</i> ...	198
Figure 5-21: Relative RMSE in the Corridor Region vs. Number of Basis Points, <i>hard case</i> .....	198
Figure 5-22: SSE in Corridor for various RBF functional forms, for two discretization levels, <i>easy case</i> .....	204
Figure 5-23: SSE in Corridor for various RBF functional forms, for two discretization levels with gamma ( $N = 40/N = 175$ ), <i>hard case</i> .....	205
Figure 5-24: Future Value Function of Corridor DP after one time step (green) and fitted polynomial (red).....	214
Figure 5-25: Future Value Function of Corridor DP after three time step (green) and fitted polynomial (red) if the sub-optimal termination in Figure 5-23 is ignored. ....	215
Figure 5-26: Future Value Function of Corridor DP after three time step (green) and fitted polynomial (red) if the sub-optimal termination in Figure 5-23 is addressed. .	215
Figure 6-1: Storage Capacity Factor, $CS$ , versus coefficient of variation for various active storage volumes, $Va$ .....	224
Figure 6-2: Powerhouse Flexibility Factor, $CPH$ , versus coefficient of variation for various powerhouse hydraulic capacities, $PHmax$ .....	226
Figure 6-3: $R2$ vs. Duration ( $\tau$ ) for various reservoir storages (in $106ft^3$ ) for $PHmax = 1000$ (in $ft^3/s$ ). .....	235
Figure 6-4: $R2$ vs. Duration ( $\tau$ ) for various reservoir storages (in $106ft^3$ ) for $PHmax = 2000$ (in $ft^3/s$ ). .....	235
Figure 6-5: $R2$ vs. Duration ( $\tau$ ) for various reservoir storages (in $106ft^3$ ) for $PHmax = 3500$ (in $ft^3/s$ ). .....	236
Figure 6-6: $R2$ vs. Duration ( $\tau$ ) for various reservoir storages (in $106ft^3$ ) for $PHmax = 8300$ (in $ft^3/s$ ). .....	236
Figure 6-7: Autocorrelation vs. Lag for daily inflow volume into hypothetical Kennebec reservoir. ....	237
Figure 6-8: Ensemble PSDF of optimal release $R$ for System (Big, 2000), $STdays = 162.1$ , $PHdays = 114$ , with the ‘mean-price’ economic scheme. ....	238

Figure 6-9: Ensemble CPSDF of optimal release $R$ and inflow $I$ for System (Big, 2000), $STdays = 162.1$ , $PHdays = 114$ , with the ‘mean-price’ economic scheme .....	239
Figure 6-10: Ensemble PSDF of optimal release $R$ for System (Small, 2000), $STdays = 16.9$ , $PHdays = 11.4$ , with the ‘mean-price’ economic scheme. ....	240
Figure 6-11: Ensemble CPSDF of optimal release $R$ and reservoir storage $S$ for System (Small, 2000), $STdays = 16.9$ , $PHdays = 11.4$ , with the ‘mean-price’ economic scheme.....	240
Figure 6-12: Ensemble PSDF of optimal release $R$ for System (Big, 2000), $STdays = 162.14$ , $PHdays = 114$ , with the ‘real-price’ economic scheme. ....	242
Figure 6-13: Ensemble CPSDF of optimal release $R$ and inflow $I$ for System (Big, 2000), $STdays = 162.14$ , $PHdays = 114$ , with the ‘real-price’ economic scheme. ....	243
Figure 6-14: Ensemble PSDF of optimal release $R$ for System (Big, 8300), $STdays = 162.14$ , and $PHdays = 27.47$ , with the ‘real-price’ economic scheme. ....	244
Figure 6-15: Ensemble CPSDF of optimal release $R$ for System (Big, 8300), $STdays = 162.14$ , and $PHdays = 27.47$ , with the ‘real-price’ economic scheme. ....	244
Figure 6-16: Ensemble PSDF of optimal release $R$ for System (Small, 8300), $STdays = 16.19$ , and $PHdays = 2.75$ , with the ‘real-price’ economic scheme. ....	245
Figure 6-17: Ensemble PSDF of optimal release $R$ for System (Small, 8300), ‘mean price’ scheme, 1-week short-term SSDP horizon.....	246
Figure 6-18: Ensemble PSDF of optimal release $R$ for System (Small, 8300), ‘mean price’ scheme, 2-week short-term SSDP horizon.....	247
Figure 6-19: Ensemble PSDF of optimal release $R$ for System (Small, 2000), $STdays = 16.19$ , $PHdays = 11.4$ , with the ‘mean-price’ economic scheme. ....	251
Figure 6-20: Ensemble PSDF of optimal release $R$ for System (Mid, 2000), $STdays = 82.19$ , $PHdays = 57.00$ ,with the ‘mean-price’ economic scheme. ....	251
Figure 6-21: Ensemble PSDF of optimal release $R$ for System (Big, 2000), $STdays = 162.14$ , $PHdays = 114$ , with the ‘mean-price’ economic scheme. ....	251
Figure 6-22: Ensemble PSDF of optimal release $R$ for System (Small, 3500), $STdays = 16.18$ , $PHdays = 6.51$ , with the ‘mean-price’ economic scheme. ....	252
Figure 6-23: Ensemble PSDF of optimal release $R$ for System (Mid, 3500), $STdays = 82.19$ , $PHdays = 32.57$ , with the ‘mean-price’ economic scheme. ....	252
Figure 6-24: Ensemble PSDF of optimal release $R$ for System (Big, 3500), $STdays = 162.14$ , $PHdays = 65.15$ , with the ‘mean-price’ economic scheme. ....	252
Figure 6-25: Ensemble PSDF of optimal release $R$ for System (Small, 5000), $STdays = 16.19$ , $PHdays = 4.56$ , with the ‘mean-price’ economic scheme. ....	253

Figure 6-26: Ensemble PSDF of optimal release $R$ for System (Mid, 5000), $STdays = 82.19$ , $PHdays = 22.8$ , with the ‘mean-price’ economic scheme. ....	253
Figure 6-27: Ensemble PSDF of optimal release $R$ for System (Big, 5000), $STdays = 162.14$ , $PHdays = 45.60$ , with the ‘mean-price’ economic scheme. ....	253
Figure 6-28: Ensemble PSDF of optimal release $R$ for System (Small, 8300), $STdays = 16.19$ , $PHdays = 2.75$ , with the ‘mean-price’ economic scheme. ....	254
Figure 6-29: Ensemble PSDF of optimal release $R$ for System (Mid, 8300), $STdays = 82.19$ , $PHdays = 13.74$ , with the ‘mean-price’ economic scheme. ....	254
Figure 6-30: Ensemble PSDF of optimal release $R$ for System (Big, 8300), $STdays = 162.14$ , $PHdays = 27.47$ , with the ‘mean-price’ economic scheme. ....	254
Figure 6-31: Ensemble CPSDF of optimal release $R$ and inflow $I$ for System (Small, 2000), $STdays = 16.19$ , $PHdays = 11.40$ , with the ‘mean-price’ economic scheme. ....	255
Figure 6-32: Ensemble CPSDF of optimal release $R$ and inflow $I$ for System (Mid, 2000), $STdays = 82.19$ , $PHdays = 57.00$ , with the ‘mean-price’ economic scheme. ....	255
Figure 6-33: Ensemble CPSDF of optimal release $R$ and inflow $I$ for System (Big, 2000), $STdays = 162.14$ , $PHdays = 114.00$ , with the ‘mean-price’ economic scheme. ....	255
Figure 6-34: Ensemble CPSDF of optimal release $R$ and inflow $I$ for System (Small, 3500), $STdays = 16.19$ , $PHdays = 6.51$ , with the ‘mean-price’ economic scheme. ....	256
Figure 6-35: Ensemble CPSDF of optimal release $R$ and inflow $I$ for System (Mid, 3500), $STdays = 82.19$ , $PHdays = 32.57$ , with the ‘mean-price’ economic scheme. ....	256
Figure 6-36: Ensemble CPSDF of optimal release $R$ and inflow $I$ for System (Big, 3500), $STdays = 162.14$ , $PHdays = 65.15$ , with the ‘mean-price’ economic scheme. ....	256
Figure 6-37: Ensemble CPSDF of optimal release $R$ and inflow $I$ for System (Small, 5000), $STdays = 16.19$ , $PHdays = 4.56$ , with the ‘mean-price’ economic scheme. ....	257
Figure 6-38: Ensemble CPSDF of optimal release $R$ and inflow $I$ for System (Mid, 5000), $STdays = 82.19$ , $PHdays = 22.8$ , with the ‘mean-price’ economic scheme. ....	257
Figure 6-39: Ensemble CPSDF of optimal release $R$ and inflow $I$ for System (Big, 5000), $STdays = 162.14$ , $PHdays = 45.6$ , with the ‘mean-price’ economic scheme. ....	257

Figure 6-40: Ensemble CPSDF of optimal release $R$ and inflow $I$ for System (Small, 8300), $STdays = 16.19$ , $PHdays = 2.75$ , with the ‘mean-price’ economic scheme. .....	258
Figure 6-41: Ensemble CPSDF of optimal release $R$ and inflow $I$ for System (Mid, 8300), $STdays = 82.19$ , $PHdays = 13.74$ , with the ‘mean-price’ economic scheme. .....	258
Figure 6-42: Ensemble CPSDF of optimal release $R$ and inflow $I$ for System (Big, 8300), $STdays = 162.14$ , $PHdays = 27.47$ , with the ‘mean-price’ economic scheme. .....	258
Figure 6-43: Ensemble CPSDF of optimal release $R$ and reservoir storage $S$ for System (Small, 2000), $STdays = 16.19$ , $PHdays = 11,40$ , with the ‘mean-price’ economic scheme.....	259
Figure 6-44: Ensemble CPSDF of optimal release $R$ and reservoir storage $S$ for System (Mid, 2000), $STdays = 82.19$ , $PHdays = 32.57$ , with the ‘mean-price’ economic scheme.....	259
Figure 6-45: Ensemble CPSDF of optimal release $R$ and reservoir storage $S$ for System (Big, 2000), $STdays = 162.14$ , $PHdays = 114.00$ , with the ‘mean-price’ economic scheme.....	259
Figure 6-46: Ensemble CPSDF of optimal release $R$ and reservoir storage $S$ for System (Small, 3500), $STdays = 16.19$ , $PHdays = 6.51$ , with the ‘mean-price’ economic scheme.....	260
Figure 6-47: Ensemble CPSDF of optimal release $R$ and reservoir storage $S$ for System (Mid, 3500), $STdays = 82.19$ , $PHdays = 32.57$ , with the ‘mean-price’ economic scheme.....	260
Figure 6-48: Ensemble CPSDF of optimal release $R$ and reservoir storage $S$ for System (Big, 3500), $STdays = 162.14$ , $PHdays = 65.15$ , with the ‘mean-price’ economic scheme.....	260
Figure 6-49: Ensemble CPSDF of optimal release $R$ and reservoir storage $S$ for System (Small, 5000), $STdays = 16.19$ , $PHdays = 4.56$ , with the ‘mean-price’ economic scheme.....	261
Figure 6-50: Ensemble CPSDF of optimal release $R$ and reservoir storage $S$ for System (Mid, 5000), $STdays = 82.19$ , $PHdays = 22.80$ , with the ‘mean-price’ economic scheme.....	261
Figure 6-51: Ensemble CPSDF of optimal release $R$ and reservoir storage $S$ for System (Big, 5000), $STdays = 162.14$ , $PHdays = 45.60$ , with the ‘mean-price’ economic scheme.....	261
Figure 6-52: Ensemble CPSDF of optimal release $R$ and reservoir storage $S$ for System (Small, 8300), $STdays = 16.19$ , $PHdays = 2.75$ , with the ‘mean-price’ economic scheme.....	262

Figure 6-53: Ensemble CPSDF of optimal release $R$ and reservoir storage $S$ for System (Mid, 8300), $STdays = 82.19$ , $PHdays = 13.74$ , with the ‘mean-price’ economic scheme.....	262
Figure 6-54: Ensemble CPSDF of optimal release $R$ and reservoir storage $S$ for System (Big, 8300), $STdays = 162.14$ , $PHdays = 27.47$ , with the ‘mean-price’ economic scheme.....	262
Figure 6-55: Ensemble PSDF of optimal release $R$ for System (Small, 2000), $STdays = 16.19.14$ , $PHdays = 11.40$ , with the ‘real-price’ economic scheme. ....	263
Figure 6-56: Ensemble PSDF of optimal release $R$ for System (Mid, 2000), $STdays = 82.19$ , $PHdays = 57.00$ , with the ‘real-price’ economic scheme. ....	263
Figure 6-57: Ensemble PSDF of optimal release $R$ for System (Big, 2000), $STdays = 162.14$ , $PHdays = 114.00$ , with the ‘real-price’ economic scheme.....	263
Figure 6-58: Ensemble PSDF of optimal release $R$ for System (Small, 3500), $STdays = 16.19$ , $PHdays = 6.51$ , with the ‘real-price’ economic scheme.....	264
Figure 6-59: Ensemble PSDF of optimal release $R$ for System (Mid, 3500), $STdays = 82.19$ , $PHdays = 32.57$ , with the ‘real-price’ economic scheme. ....	264
Figure 6-60: Ensemble PSDF of optimal release $R$ for System (Big, 3500), $STdays = 162.14$ , $PHdays = 65.15$ , with the ‘real-price’ economic scheme.....	264
Figure 6-61: Ensemble PSDF of optimal release $R$ for System (Small, 5000), $STdays = 16.19$ , $PHdays = 4.56$ , with the ‘real-price’ economic scheme.....	265
Figure 6-62: Ensemble PSDF of optimal release $R$ for System (Mid, 5000), $STdays = 82.19$ , $PHdays = 22.8$ , with the ‘real-price’ economic scheme. ....	265
Figure 6-63: Ensemble PSDF of optimal release $R$ for System (Big, 5000), $STdays = 162.14$ , $PHdays = 45.60$ , with the ‘real-price’ economic scheme.....	265
Figure 6-64: Ensemble PSDF of optimal release $R$ for System (Small, 8300), $STdays = 16.19$ , $PHdays = 2.75$ , with the ‘real-price’ economic scheme.....	266
Figure 6-65: Ensemble PSDF of optimal release $R$ for System (Mid, 8300), $STdays = 82.19$ , $PHdays = 13.74$ , with the ‘real-price’ economic scheme. ....	266
Figure 6-66: Ensemble PSDF of optimal release $R$ for System (Big, 8300), $STdays = 162.14$ , $PHdays = 27.47$ , with the ‘real-price’ economic scheme.....	266
Figure 6-67: Ensemble CPSDF of optimal release $R$ and inflow $I$ for System (Small, 2000), $STdays = 16.19$ , $PHdays = 11.40$ , with the ‘real-price’ economic scheme. ....	267
Figure 6-68: Ensemble CPSDF of optimal release $R$ and inflow $I$ for System (Mid, 2000), $STdays = 82.19$ , $PHdays = 57.00$ , with the ‘real-price’ economic scheme. ....	267

Figure 6-69: Ensemble CPSDF of optimal release $R$ and inflow $I$ for System (Big, 2000), $STdays = 162.14$ , $PHdays = 114$ , with the ‘real-price’ economic scheme. .....	267
Figure 6-70: Ensemble CPSDF of optimal release $R$ and inflow $I$ for System (Small, 3500), $STdays = 16.19$ , $PHdays = 6.51$ , with the ‘real-price’ economic scheme.	268
Figure 6-71: Ensemble CPSDF of optimal release $R$ and inflow $I$ for System (Mid, 3500), $STdays = 82.19$ , $PHdays = 32.57$ , with the ‘real-price’ economic scheme. .....	268
Figure 6-72: Ensemble CPSDF of optimal release $R$ and inflow $I$ for System (Big, 3500), $STdays = 162.14$ , $PHdays = 65.15$ , with the ‘real-price’ economic scheme. .....	268
Figure 6-73: Ensemble CPSDF of optimal release $R$ and inflow $I$ for System (Small, 5000), $STdays = 16.19$ , $PHdays = 4.56$ , with the ‘real-price’ economic scheme.	269
Figure 6-74: Ensemble CPSDF of optimal release $R$ and inflow $I$ for System (Mid, 5000), $STdays = 82.19$ , $PHdays = 22.8$ , with the ‘real-price’ economic scheme.	269
Figure 6-75: Ensemble CPSDF of optimal release $R$ and inflow $I$ for System (Big, 5000), $STdays = 162.14$ , $PHdays = 45.6$ , with the ‘real-price’ economic scheme. .....	269
Figure 6-76: Ensemble CPSDF of optimal release $R$ and inflow $I$ for System (Small, 8300), $STdays = 16.19$ , $PHdays = 2.75$ , with the ‘real-price’ economic scheme.	270
Figure 6-77: Ensemble CPSDF of optimal release $R$ and inflow $I$ for System (Mid, 8300), $STdays = 82.19$ , $PHdays = 13.74$ , with the ‘real-price’ economic scheme. .....	270
Figure 6-78: Ensemble CPSDF of optimal release $R$ and inflow $I$ for System (Big, 8300), $STdays = 162.14$ , $PHdays = 27.47$ , with the ‘real-price’ economic scheme. .....	270
Figure 6-79: Ensemble CPSDF of optimal release $R$ and reservoir storage $S$ for System (Small, 2000), $STdays = 16.19$ , $PHdays = 11.4$ , with the ‘real-price’ economic scheme.....	271
Figure 6-80: Ensemble CPSDF of optimal release $R$ and reservoir storage $S$ for System (Mid, 2000), $STdays = 82.19$ , $PHdays = 57.00$ , with the ‘real-price’ economic scheme.....	271
Figure 6-81: Ensemble CPSDF of optimal release $R$ and reservoir storage $S$ for System (Big, 2000), $STdays = 162.14$ , $PHdays = 114.00$ , with the ‘real-price’ economic scheme.....	271
Figure 6-82: Ensemble CPSDF of optimal release $R$ and reservoir storage $S$ for System (Small, 3500), $STdays = 16.19$ , $PHdays = 6.51$ , with the ‘real-price’ economic scheme.....	272

Figure 6-83: Ensemble CPSDF of optimal release $R$ and reservoir storage $S$ for System (Mid, 3500), $STdays = 82.19$ , $PHdays = 32.57$ , with the ‘real-price’ economic scheme.....	272
Figure 6-84: Ensemble CPSDF of optimal release $R$ and reservoir storage $S$ for System (Big, 3500), $STdays = 162.14$ , $PHdays = 65.15$ , with the ‘real-price’ economic scheme.....	272
Figure 6-85: Ensemble CPSDF of optimal release $R$ and reservoir storage $S$ for System (Small, 5000), $STdays = 16.19$ , $PHdays = 4.56$ , with the ‘real-price’ economic scheme.....	273
Figure 6-86: Ensemble CPSDF of optimal release $R$ and reservoir storage $S$ for System (Mid, 5000), $STdays = 82.19$ , $PHdays = 22.80$ , with the ‘real-price’ economic scheme.....	273
Figure 6-87: Ensemble CPSDF of optimal release $R$ and reservoir storage $S$ for System (Big, 5000), $STdays = 162.14$ , $PHdays = 45.60$ , with the ‘real-price’ economic scheme.....	273
Figure 6-88: Ensemble CPSDF of optimal release $R$ and reservoir storage $S$ for System (Small, 8300), $STdays = 16.19$ , $PHdays = 2.75$ , with the ‘real-price’ economic scheme.....	274
Figure 6-89: Ensemble CPSDF of optimal release $R$ and reservoir storage $S$ for System (Mid, 8300), $STdays = 82.19$ , $PHdays = 13.74$ , with the ‘real-price’ economic scheme.....	274
Figure 6-90: Ensemble CPSDF of optimal release $R$ and reservoir storage $S$ for System (Big, 8300), $STdays = 162.14$ , $PHdays = 27.47$ , with the ‘real-price’ economic scheme.....	274

## LIST OF TABLES

Table 3-1: Configurations of “single-reservoir” considered in Chapters 4 and 6 .....	73
Table 3-2: Candidate Reference Records and Target Basin Drainage Area, Mean Annual Inflow Rate, Mean Summer Inflow Rate.....	78
Table 3-3: Summary of proration method used to generate synthetic inflows for Kennebec River .....	82
Table 4-1: Single Reservoir System Configurations .....	116
Table 4-2: Proposed runs for Time Decomposition Model.....	121
Table 4-3: P-values of a two-sided paired t-test of the difference between the simulated benefits of several algorithms on the (Big, 8300) system.....	124
Table 4-4: Benefits ( <i>Ben</i> ), Performance Ratio ( <i>PR</i> ), and Efficiency ( <i>Eff</i> ) for systems with turbine capacity 2000 and “mean price” scheme. ....	147
Table 4-5: Benefits ( <i>Ben</i> ), Performance Ratio ( <i>PR</i> ), and Efficiency ( <i>Eff</i> ) for systems with turbine capacity 3500 and “mean price” scheme. ....	147
Table 4-6: Benefits ( <i>Ben</i> ), Performance Ratio ( <i>PR</i> ), and Efficiency ( <i>Eff</i> ) for systems with turbine capacity 5000 and “mean price” scheme. ....	148
Table 4-7: Benefits ( <i>Ben</i> ), Performance Ratio ( <i>PR</i> ), and Efficiency ( <i>Eff</i> ) for systems with turbine capacity 8300 and “mean price” scheme. ....	148
Table 4-8: Benefits ( <i>Ben</i> ), Performance Ratio ( <i>PR</i> ), and Efficiency ( <i>Eff</i> ) for systems with turbine capacity 2000 and “variable price” scheme. ....	152
Table 4-9: Benefits ( <i>Ben</i> ), Performance Ratio ( <i>PR</i> ), and Efficiency ( <i>Eff</i> ) for systems with turbine capacity 3500 and “variable price” scheme. ....	152
Table 4-10: Benefits ( <i>Ben</i> ), Performance Ratio ( <i>PR</i> ), and Efficiency ( <i>Eff</i> ) for systems with turbine capacity 5000 and “variable price” scheme. ....	153
Table 4-11: Benefits ( <i>Ben</i> ), Performance Ratio ( <i>PR</i> ), and Efficiency ( <i>Eff</i> ) for systems with turbine capacity 8300 and “variable price” scheme. ....	153
Table 5-1: Basis Functional Forms and Conditions (Regis and Shoemaker, 2007)...	172
Table 5-2: Greedy Algorithm for basis selection for Interpolating RBF Surface .....	183
Table 5-3: Summary of DP Schemes tested, <i>easy case</i> .....	190
Table 5-4: Summary of DP Schemes tested with flow penalty, <i>hard case</i> .....	197
Table 5-5: Run time and relative RMSE in the Corridor for the 4-reservoir system for various discretization levels for DP with spline and linear interpolation for the <i>easy case</i> .....	200
Table 5-6: Run time and relative RMSE in the Corridor for various discretization levels for DP with spline and linear interpolation for the <i>hard case</i> .....	201

Table 6-1: $Va$ , $VPH$ , and $PHdays$ for projects on the Kennebec, Merrimack and Columbia Rivers.....	225
Table 6-2: Turbine Capacity and Storage Capacity for each of the 12 system configurations.....	232
Table 6-3: Storage Capacity Factor $CS\tau = 1 Day$ , Storage-days $STdays$ , Powerhouse-days $PHdays$ , and the Powerhouse Flexibility Factor $CPH$ for twelve system configurations.....	233

## CHAPTER 1

### INTRODUCTION

The objective in reservoir operations optimization is to select an operating policy which maximizes some objective over a planning horizon. This is a sequential decision problem: the operator must make a decision every month, week, day, or even hour. It is also a stochastic problem: at the time the operator must make a decision there are uncertainties that could affect the consequences of that decision. It can be a consequential problem: environmental and public safety, not to mention profit and recreational benefits could be affected. In some cases it might even be a what Rittel and Webber [1973] call a ‘wicked’ problem, one which the operator has no right to get wrong: in flooding situations people might die.

In light of these realizations the prospect of designing any optimization tool for planning or managing real-world reservoir systems can seem a daunting task.

However, water resources systems engineers have a long and successful history of applying optimization techniques to real-world decision making [Yeh, 1985; Labadie, 2004,2005]. The research presented in this thesis builds on the body of past work reservoir operations optimization modeling. My thesis has two primary focuses: the representation of streamflow uncertainty in reservoir optimization models, and the reduction of the computational burden of multi-reservoir dynamic programming models.

A fundamental challenge in reservoir operations optimization is that reservoir system is often incentivized to operate in a risky way. The more water that is in

storage the higher the head, and the more energy which is produced per unit volume of water released. Running the reservoir at or near full can be very risky as a sudden inflow could cause a spill, wherein water is not passed through the turbines and generates no energy. Thus the dilemma of the reservoir operator is when and how far to drawdown. To avoid any spill the reservoir might be kept low, but this is inefficient with respect to energy generation. In arid regions like California a large multi-use reservoir might draw down in anticipation of a large storm, but then be unable to refill and meet its irrigation demands later in the summer growing season. Failing to drawdown enough and being forced to spill can be dangerous (particularly at Folsom Dam which is just 15 miles upstream of Sacramento, CA).

One approach to aiding reservoir operators is through the use of dynamic programming (DP) models. Discrete DP (just denoted DP) is an optimization technique which, at each decision point weighs the immediate benefit of a decision immediately taken with the future benefits of a decision made in the future. In reservoir operation DP weighs the benefit of an immediate release with the benefit of a future release. If the benefits of the immediate release are greater than the benefits of waiting the release is made now, and vice versa. Such models have long been successfully applied to the reservoir optimization problem [Young, 1967; Hall et al., 1968; Roeffs and Bodin, 1970; Yakowitz, 1982]. Such models can inform operating rules for reservoirs, which give an operator an optimal release based on current reservoir storage. However such models do not take into account the stochasticity of inflows and will not hedge against uncertainty because they implicitly assume that inflows are known with certainty.

Stochastic DP (SDP) is an extension of DP to consider uncertainty in forcings, typically uncertainty in inflow. Remarkably the application of SDP to the reservoir optimization problem pre-dates the simpler deterministic DP, seeing its first use in 1946 by Masse, followed in 1955 by Little. SDP models select optimal releases considering a range of future (and in some cases current) reservoir inflows. Because the future is now uncertain, at each decision point SDP weighs the benefits of an immediate release with the expected benefits of a future release. Typically the distribution of future inflows is modeled as a Markov process where, for example the distribution of flows tomorrow is conditional on the flow today, or the distribution flows today might be modeled as conditional on the flow yesterday [see Yakowitz, 1982 and Loucks et al., 1981]. How the uncertainty in inflows is modeled is a widely studied topic, and is a primary focus of Chapter 4 of this thesis.

How the uncertainty is modeled is important for at least two reasons. First, if the SDP model is to adequately weigh the benefits of future releases, then the representation of uncertainty must reflect the ability of the decision maker to resolve uncertainty when making future releases. Second, the way in which uncertainty is modeled affects the representation of streamflow, and realistic representation of streamflow persistence is critical if SDP is to properly assess the expected benefits of future releases.

Addressing the first point, Stedinger et al. [1984] shows that improved SDP performance can be achieved by conditioning the distribution of future inflows on a flow forecast. Using this method in an SDP model better reflects the skill of the reservoir operator when making a decision. Using forecasts also potentially improves

the representation of the persistence of flow, which can also improve the performance of SDP models.

Sampling SDP (SSDP) is a variation on SDP that rose largely to address the concern about the representation of inflows in SDP models. In SDP inflows are represented by intact streamflow scenarios which might be historical flows [Kelman et al., 1990; Cote et al, 2011], ensemble forecasts [Faber and Stedinger, 2001; Kim et al., 2007], or they might be climate projections [Vicuna et al., 2010]. In any case the persistence of flow is doubtlessly better represented by time series than Markov Processes, allowing SSDP to better assess the value of future releases, as demonstrated by Cote et al. [2011].

Like SDP, SSDP considers a range of potential scenarios when selecting a current decision, but unlike SDP, SSDP evaluates the benefits of that decision on an intact scenario. How the uncertainty is represented when SSDP selects an optimal release can have a large impact on the value of the resulting optimal operating policy, as demonstrated by Faber and Stedinger [2001] for a reservoir in Colorado, and later by Kim et al. [2007] for a reservoir in Korea.

Chapter 4 of this thesis extends that work in four ways.

- 1) It considers much shorter time steps: most previous SSDP studies use weekly time steps, whereas Chapter 4 considers time steps as short as 6-hours. This tests the SSDP methodology for sub-daily operation, a relevant research topic as short-term ensemble forecasts become available.
- 2) It considers a wide range of systems by fixing the hydrology and drastically changing the storage and turbine capacity. Unlike previous studies which focus on a single system, the analysis in Chapter 4 is able to draw more general conclusions across different categories of reservoirs.

- 3) It compares operation of the different reservoir systems with different economic models, allowing us to isolate the effects of hydrologic uncertainty and price variability on operations.
- 4) Finally it utilizes synthetically generated inflow forecasts which have a desired precision which allows the examination of the value of forecast precision on SSDP model performance.

In support of the study in Chapter 4, Chapter 5 of this thesis introduces a number of non-parametric statistics which allow for the classification of reservoir types (i.e. run-of-river, storage only, generating reservoir) regardless of the scale of the reservoir in question. Chapter 4 reports results comparing some of the largest hydropower reservoirs in North America with small reservoirs in Northern Maine, demonstrating that the magnitude of the project alone is not a good indicator of how the project operates or should be modeled. A regression procedure and a spectral analysis procedure which help a modeler determine the critical time scales of operation for a reservoir which can answer the question: do we operate at an hourly, daily, weekly, monthly cycle (or perhaps decadal cycle for Hoover Dam on the Colorado River). The Spectral analysis approach is novel for water resources systems analysis, and shows great potential as a diagnostic technique.

Dynamic programming models become very computationally difficult to solve in high dimensions, or for the reservoir operations case, for multiple reservoirs. This is a well-documented problem, dating back to Richard Bellman who coined the term the ‘curse of dimensionality’ in 1961 [Bellman, 1961]. Chapter 2 of this thesis explains in detail why high dimensional problems are difficult in dynamic programming, and some of the techniques which are commonly used to diminish the ‘curse.’ Chapter 5 presents a new approach called Corridor DP, which achieves

computational savings by focusing on storage combinations which a multi-reservoir system is most likely to visit. It is shown that the Corridor DP algorithm is more computationally efficient than other traditional DP methods.

Finally Chapter 7 provides some concluding remarks and discussion of planned extensions for the methods presented in this thesis.

## REFERENCES

- Cote, P., Haguma, D., Leconte, R. & Krauc, S. 2011, "Stochastic Optimization of Hydro-Quebec hydropower installations: a statistical comparison between SDP and SSDP methods", *Canadian Journal of Civil Engineering*, vol. 38, no. 12, pp. 1427-1434.
- Hall, W.A., Butcher, W.S. & Esogbue, A. 1968, "Optimization of the operation of a multiple-purpose reservoir by dynamic programming", *Water Resources Research*, vol. 4, no. 3, pp. 471.
- Kelman, J., Stedinger, J.R., Cooper, L.A., Hsu, E. & Yuan, S. 1990, "Sampling stochastic dynamic programming applied to reservoir operation", *Water Resources Research*, vol. 26, no. 3, pp. 447-454.
- Kim, Y., Eum, H., Lee, E. & Ko, I. 2007, "Optimizing Operational Policies for a Korean Multireservoir System using Sampling Stochastic Dynamic Programming with Ensemble Streamflow Prediction", *Journal of Water Resources Planning and Management*, vol. 133, no. 1, pp. 4-14.
- Labadie, J.W. 2005, "Closure to "Optimal Operation of Multi-Reservoir Systems: State-of-the-Art Review"", *Journal of Water Resources Planning and Management*, vol. 131, no. 5, pp. 407.
- Labadie, J.W. 2004, "Optimal Operation of Multireservoir Systems: State-of-the-Art Review", *Journal of Water Resources Planning and Management*, vol. 130, no. 2, pp. 93-111.
- Little, J.D.C. 1955, "Use of Storage Water in a hydroelectric System", *Journal of Operations Research*, vol. 3, pp. 187-197.
- Loucks, D.P., Stedinger, J.R. & Haith, D.A. 1981, *Water Resources Systems PLanning and Analysis*, 1st edn, Prentice-Hall, Englewood Cliffs, N.J.
- Masse, P.B.D. 1946, *Les Reserves et al Regulation de l'Avenir dans la Vie Economique*, Hermann and Cie, Paris.
- Rittel, H.W.J. & Webber, M.M. 1973, "Dilemmas in a General Theory of Planning", *Policy Science*, vol. 4, pp. 155.

- Roefs, T.G. & Bodin, L.D. 1970, "Multireservoir operation studies", *Water Resources Research*, vol. 6, no. 2, pp. 410.
- Stedinger, J.R., Sule, B.F. & Loucks, D.P. 1984, "Stochastic dynamic programming models for reservoir operation optimization.", *Water Resources Research*, vol. 20, no. 11, pp. 1499-1505.
- Vicuna, S., Dracup, J.A., Lund, J.R., Dale, L.L. & Maurer, E.P. 2010, "Basin-scale water system operations with uncertain future climate conditions: Methodology and case studies", *Water Resources Research*, vol. 46, no. W04505, pp. 1-19.
- Yakowitz, S. 1982, "Dynamic programming applications in water resources", *Water Resources Research*, vol. 18, no. 4, pp. 673-679.
- Yeh, W.W. 1985, "Reservoir Management and Operations Models: A State-of-the-Art Review", *Water Resources Research*, vol. 21, no. 12, pp. 1797-1818.
- Young, G.K. 1967, "Finding reservoir operating rules", *Journal of Hydraulics Division American Society of Civil Engineers*, vol. 93, no. HY6, pp. 297.

## CHAPTER 2

### A REVIEW OF DYNAMIC PROGRAMMING MODELS FOR HYDROPOWER OPTIMIZATION

This chapter provides a brief introduction to dynamic programming techniques commonly applied to reservoir operations optimization problems, along with a short history and literature review on the topic. Dynamic programming algorithms have found widespread application across a variety of fields including natural resource economics [Insley and Rollins, 2005; Dixit, 1990; Conrad and Clark, 1987], product distribution networks [Topaloglu and Kunnumkal, 2006], power system control [Yu et al., 2014], and of course water resources systems analysis to name a few. This chapter will focus on application to reservoir operations problems and will primarily focus on the issues of uncertainty representation and efficient high-dimensional dynamic programming for reservoir problems. For a broader discussion of reservoir optimization and dynamic programming applied to water resources see Labadie [2004, 2005], Yeh [1985], and Yakowitz [1982]. For a more in-depth discussion of the dynamic programming more broadly Powell [2007] and Bertsekas [2011] are excellent reference sources. Section 2.1 introduces dynamic programming and stochastic dynamic programming for reservoir operations problems. Section 2.2 introduces and describes the use of sampling stochastic dynamic programming algorithms. Section 2.3 is a brief narrative describing the evolution of DP and SDP methods in water resources systems analysis since the mid-1950s. Section 2.4 provides particular discussion on the areas of DP and SDP which addressed in Chapters 4 and 5, and finally Section 2.5 includes some concluding remarks.

### ***Section 2.1 Dynamic Programming and Stochastic Dynamic Programming***

Operation of a reservoir system requires the operator to select a series of releases which satisfy a host of constraints and hopefully maximize the value of some objective or set of objectives. This is a challenging problem because system forcing, both hydrologic and economic, are uncertain at the time a decision must be made. As the system responds to forcings and to actions taken by the operator, its state will evolve and present new optimization problem each time an action must be taken. Further complicating the problem, objectives and constraints are often non-linear in reservoir systems, rendering many mathematical solution techniques inadequate.

Dynamic Programming (DP) and Stochastic DP (SDP) are well suited to this type of problem. They impose virtually no restriction on the functional form of the objective and constraints of a problem, and they provide a dynamic operating rule that accounts for the evolution of the system in response to an operator's control and in the case of SDP to realizations of random forcing variables.

The DP framework assumes a simple additive model of reservoir system benefits over a planning horizon (equation (2-1)). In each discrete time a decision (a release for reservoirs),  $R_t$ , must be made. The incremental benefit of  $R_t$ ,  $B_t$ , also depends on the current reservoir storage,  $S_t$ , and the current inflow  $Q_t$ . It is assumed that at the end of the planning period (index  $T$ ) storage remaining in the reservoir has some terminal value,  $v(S_{T+1})$ .

$$Z = \sum_{t=1}^T B_t(S_t, R_t, Q_t) + v(S_{T+1}) \quad (2-1)$$

The evolution of the reservoir system in response to the operator's decision  $R_t$  is given by

$$S_{t+1} = S_t + Q_t - R_t - e_t(S_t, S_{t+1}) \quad (2-2)$$

where  $e_t$  is an evaporation/seepage loss term. The challenge of the operator is to pick the best series of releases or equivalently the best sequence of reservoir storages over the planning period  $t = 1, \dots, T$ .

Because of the assumption of sequential evolution of the system state and the additive benefit function DP can be used to solve this planning problem. The DP solution to the planning problem posed by equations (2-1) and (2-2) is given by:

$$f_t(S_t) = \max_{R_t} \{B_t(S_t, Q_t, R_t) + \alpha f_{t+1}(S_{t+1}) \quad \forall S_t \text{ and } t \in \{1, \dots, T\}$$

$$S_{t+1} = S_t + Q_t - R_t - e_t(S_t, S_{t+1}) \quad (2-3)$$

where  $\alpha$  and  $f_{T+1} = v(S_{T+1})$ . The traditional solution technique for the DP model is start with  $f_T(S_T)$ , and to solve equation (2-3) recursively backwards in time until one arrives at present time and has  $f_1(S_1)$  [Bellman, 1957]. The result of the DP solution process is a decision rule which specifies an optimal  $R_t$  for any  $S_t$  and future value function of water in storage  $f_t(S_t)$  for each time step in the  $t$  in the planning period. In the DP formulation in equation (2-3) the current storage  $S_t$  is the state-variable, meaning that the state of the reservoir system is fully described by  $S_t$ . In multiple reservoir DP models it is common to assign a storage state to each reservoir, so  $S_t$  would become a  $k$ -dimensional vector.

SDP is a natural extension of the DP framework to consider the stochastic nature of the forcings such as the inflows  $Q_t$ . Given a description of the stochastic forcings, one must compute the expected benefits associated with each decision  $R_t$ . To describe the hydrologic state of the basin, it is common to add a hydrologic state variable. A simple hydrologic state variable might be the previous or current period's

inflow,  $Q_t$ . If one then assumes that the  $Q_t$  is known in time  $t$  [as in Loucks et al., 1981 and Tejada et al., 1995] one obtains the model.

$$f_t(S_t, Q_t) = \max_{R_t} \left\{ B_t(S_t, Q_t, R_t) + \alpha \mathop{\text{E}}_{Q_{t+1}|Q_t} [f_{t+1}(S_{t+1}, Q_{t+1})] \right\} \quad (2-4)$$

$$\forall S_t, Q_t, t \in \{1, \dots, T\}$$

Here the expected future benefits are computed with the probability  $P_t[Q_{t+1}|Q_t]$ , which is the probability of the next period's flow given the flow in the current period. Many papers have explored alternative hydrologic states including snow-water equivalent or antecedent soil moisture [Cote et al., 2011] or an inflow forecast [Stedinger et al., 1984, Kelman et al., 1990; Maceira and Kelman, 1991; Karamouz and Vasiliadis, 1992; Tejada et al., 1995; Kim and Palmer, 1997; and Kim et al., 2007]. Computing correct transition probabilities based on flow forecasts is described at length in Chapter 4 of this thesis. An SDP model which uses a generic  $H_t$  is given by equations (2-5) and (2-6):

$$f_t(S_t, H_t) = \max_{R_t^*} \mathop{\text{E}}_{Q_t|H_t} [B_t(S_t, R_t, Q_t) + \alpha f_{t+1}(S_{t+1}, H_{t+1})] \quad (2-5)$$

$$\forall S_t, H_t \text{ and } t \in \{1, \dots, T\}$$

$$R_t = \max\{\min\{R_t^*, S_t + Q_t\}, (S_t + Q_t - S_{max} - e(S_t, S_{t+1}))\} \quad (2-6)$$

where  $S_{max}$  is the maximum reservoir storage level and  $R_t^*$  is the optimal target release in time  $t$ . The distinction between  $R_t^*$  and  $R_t$  is necessary because  $R_t^*$  may not be feasible because  $Q_t$  is no longer known. Equation (2-6) ensures that the final selected  $R_t$  is feasible. It should be noted that multiple hydrologic states might be employed. For example Karamouz and Vasiliadis [1992] assign a state variable to the current inflows and a state variable to the next period's inflows. Tejada [1993] experiment with three hydrologic state variables, and Turgeon [2005] shows how

information from several previous days' flows can be leveraged into a single hydrologic state variable. Chapter 4 describes in great detail how one might generate the needed probabilities to compute  $E_{Q_t|H_t}$  if  $H_t$  is a vector of hydrologic (or economic) states.

The backwards recursive DP and SDP procedure described above provides an optimal policy for each system state at discrete time steps over the planning period. To develop these policies numerically the storage state space is often discretized, and the "optimal" policy is computed for each discrete state at each time.

When implementing the numerically derived policy, the reservoir is unlikely to reside only in the discrete points which happened to have been sampled, and will more likely fall between the discrete points. One solution to this problem is to interpolate within the policy table, or to fit some simple function to that table. Another approach is *re-optimization* which selects an optimal release given the current state by performing a one-step SDP optimization with the current reservoir conditions (Tejada et al., 1993). Equation (2-7) describes the *re-optimization* step.

$$\max_{R_t} \left\{ B_t(S_t, Q_t, R_t) + \alpha E_{i|Q_t, H_t} [f_{t+1}(S_{t+1}, i)] \right\} \quad (2-7)$$

where  $H_t$  is the current hydrologic information. Tejada et al. [1993] compared the performance of models which interpolate in the policy table to select an optimal release and models which use *re-optimization*. They found that *re-optimization* generally results in better operation, particularly when coarse grids were used in the initial backwards moving that derived the future value function. Furthermore they found that use of *re-optimization* improved the reliability of meeting both energy and

water targets. *Re-optimization* is used when implementing optimal policies derived from sampling SDP models in Chapter 4.

### ***Section 2.2 Sampling Stochastic Dynamic Programming***

SDP models often overestimate the benefits actually attainable with particular release decisions because decisions are evaluated with the same simplified streamflow description used in developing the SDP policy [Tejada et al., 1993]. This has led to the develop of sampling SDP models. SSDP represents future streamflow with an ensemble of scenarios, which are time series of reservoir inflow and other variables (like energy price). This provides a discrete description of streamflow that implicitly captures the joint distribution of streamflow, forecasts, and other variables across time and space, without requiring an explicit probability distribution [Kelman et al., 1990; Faber and Stedinger, 2001; Kim et al., 2007; Vicuna et al., 2011; Eum et al., 2011; Cote et al., 2011].

Kelman et al. [1990] present a SSDP model for optimizing hydropower operation for a system in California. Their model (equations (2-8) and (2-9)) takes reservoir storage,  $S_t$ , inflow forecast,  $F_t$ , and the current scenario trace as state variables (i.e. the hydrologic state,  $H_t$ , is described by both a forecast and a scenario). Their SSDP formulation is given by:

$$\max_{R_t} \left\{ B_t(S_t, Q_t(i), R_t) + \alpha E_{i|F_t} \left[ E_{F_{t+1}|F_t, j} [f_{t+1}(S_{t+1}, F_{t+1}, j)] \right] \right\} \quad (2-8)$$

$$\forall S_t \text{ and } t \in \{1, \dots, T\}$$

$$f_t(S_t, F_t, i) = B_t(S_t, Q_t(i), R_t) + \alpha E_{F_{t+1}|F_t, i} [f_{t+1}(S_{t+1}, F_{t+1}, i)] \quad (2-9)$$

$$\forall S_t \text{ and } t \in \{1, \dots, T\}$$

where  $Q_t(i)$  is the reservoir inflow in time  $t$  and scenario  $i$ , and  $F_t$  is a flow forecast in time  $t$ .

Equation (2-8) is the Decision Model which is used to select an optimal  $R_t$  and equation (2-9) is the Simulation Model which is used to assess the benefits of the optimal release. This is the key difference between SSDP and SDP: SDP uses the same model to select an optimal release and assess its benefit (for example equation (2-5)). The Decision Model considers possible transitions between scenario traces, whereas the Simulation Model simulates the operational benefits on a single intact scenario, thus preserving the persistence of hydrologic inflows. To numerically solve this SSDP model, equations (2-8) and (2-9) must be solved for each discrete pair of  $(S_t, F_t)$ , for each trace  $i$ , for every time step in the planning period.

The double expectation in equation (2-8) captures both the probability of a future forecast given the current forecast and an inflow, and the transition probability of a future scenario given the current forecast. Faber and Stedinger [2001] avoid the need for a double expectation and a forecast state variable by utilizing the historical forecast series associated with each trace. Thus the forecast state variable is embedded in the scenario state variable, and the scenario state variable becomes the sole hydrologic state variable. This allows a very large reduction in the computational demands of the solution algorithm by reducing the dimension of the implicit hydrologic state variable (going from  $i$  and  $H_t$  to just use of  $i$  which has an  $H_t$  with it). A reasonable concern is if all combinations of  $i$  and  $H_t$  were reasonable, or likely. In many cases the answer is that some were not likely, and thus the modeling process

was not efficient. For single reservoir systems such as that considered by Kelman et al. [1990], this is not particularly important. However, as we strive to model multiple reservoir systems, economy in the computational algorithm becomes much more important. The corridor model explored in Chapter 5 addresses this issue. The Faber and Stedinger [2001] SSDP formulation is:

$$\max_{R_t} \left\{ B_t(S_t, Q_t(i), R_t + \alpha E_{j|i} [f_{t+1}(S_{t+1}, j)]) \right\} \quad (2-10)$$

$$\forall S_t, i, \text{ and } t \in \{1, \dots, T\}$$

$$f_t(S_t, i) = B_t(S_t, Q_t(i), R_t) + \alpha f_{t+1}(S_{t+1}, i) \quad (2-11)$$

$$\forall S_t, i, \text{ and } t \in \{1, \dots, T\}$$

where equation (2-10) is the SSDP Decision Model and equation (2-11) is the SSDP Simulation Model. This is the SSDP formulation which is adopted in this study. To compute  $E_{j|i}$ , the probability  $P_t[j|i]$  is needed. The computation of these probabilities is discussed in great detail in Chapter 4. Faber and Stedinger [2001] and Kim et al. [2007] used ESP forecasts and historical inflows as SSDP traces, whereas Kelman et al. [1990] and Cote et al. [2011] use only historical flows. Vicuna et al. [2011] used climate scenarios from different GCM results with different greenhouse gas scenarios as SSDP traces.

### ***Section 2.3 The Evolution of SDP Algorithms for Reservoir Optimization***

The name ‘Dynamic Programming’ is somewhat of a misnomer in that it is not programming in the same way that linear programming is a solution method for a subset of optimization models. Rather, DP is a theory of multi-stage decision processes: it is a way of modeling a decision process, which might be solved by any number of programming methods, including linear programming models (see Loucks,

1968 for just one example). Richard Bellman, the father of DP, later regretted the name “Dynamic Programming,” but explained the choice was influenced by a desire to make the new theory sound interesting to funding agencies in a time when great advances in linear programming were taking place [Bellman, 1989].

Yakowitz [1982] and Esogbue [1989] see the solution of water resources problems as a major impetus for the early development of DP methods. In fact, Bellman’s foundational book on DP [Bellman, 1957] prominently features a water resources problem. Yakowitz [1982] sees water resources as an ideal laboratory for the development of DP methods. Yakowitz [1982] and Esogbue [1989] are concerned with DP applied to water resources problems in general, whereas this section will focus on DP for reservoir problems.

The first application of an SDP model to reservoir operations was demonstrated by Masse [1946]. The earliest example in the English literature is Little [1955]. That work considers the optimal operation of a single reservoir for hydropower, and provided the prototypical SDP formulation for much of the later work in SDP for reservoirs [Yakowitz, 1982]. Little’s model used a Markov description of reservoir inflow wherein the distribution of the current inflow is conditioned on the value of the previous period’s inflow. Thus, the state of the single reservoir system is described by a storage state and a hydrologic state (previous period’s inflow). Little applied his SDP model to the operation of Grand Coulee Dam on the Columbia River. Interestingly, he found that simulated operation using a policy derived by the SDP model resulted in only a 1% performance over existing rule curve

policies. The study described in Chapter 4 of this thesis experienced similar gains, and develops appropriate metrics for comparison of algorithms.

Gessford and Karlin [1958] considered an SDP model for a single reservoir wherein the inflows are independent, so a hydrologic state variable is not required. This analysis allowed them to derive more general optimal operating strategies using inventory theory. Russell [1972] extended this work to include penalties on releases. The value of this work is that it allows one to draw general conclusions about optimal reservoir operating behavior. Whether the assumption of independently distributed inflows is valid depends on the time step of the model and the hydrology of the system. Buras et al. [1963] adopt such an approach in a study of the joint operation of a reservoir and aquifer with a monthly time step. Other early examples include Askew [1974a,b, 1975] and Rossman [1977].

Loucks [1968] presents steady-state SDP models, along with equivalent linear programming (LP) formulations. Those models used either the current inflow or the previous period's inflow as hydrologic states. Similarly, Loucks and Faulkson [1970] and Butcher [1971] present SDP models which derive a steady state optimal policy, with a hydrologic state variable. Loucks and Gablinger [1970] provide an SDP and equivalent LP formulation to solve for the optimal policy in the transient case with discounting.

Su and Deininger [1974] apply an SDP model the operation of Lake Superior, using a hydrologic state variable of the previous period's inflow, which is represented as a Markov process. To reflect seasonal variations in hydrologic conditions the

transition probabilities of the Markov process in that formulation are transient, whereas most previous applications considered stationary Markov models of inflow.

Subsequent improvements in SDP models resulted from the use of better hydrologic information as a state variable. Bras et al. [1983] showed that incorporation of current hydrologic forecast information in an SDP model can lead to more efficient operations in a study of the High Aswan Dam. Revisiting the High Aswan Dam problem, Stedinger et al. [1984] incorporated available hydrologic information into the SDP decision model by using the inflow forecast as the hydrologic state variable. The resultant steady-state operating policy allowed decisions to depend on current forecasts without the need to re-formulate and re-solve a new SDP at each time step. Tejada et al. [1995] illustrated the use of forecasts in an SDP model of reservoirs in the Central Valley of California. Turgeon [2005] illustrates the advantages of a comparable algorithm. Similarly Krzystofowicz and Watada [1986], Krzystofowicz and Reese [1991], and Krzystofowicz [1999] develop a description of forecast-streamflow uncertainty that employs Bayesian decision theory. Karamouz and Vasiliadis [1992] and Kim and Palmer [1997] explored the use of such Bayesian SDP models. Kelman et al. [1989, 1990], Faber [2000], Faber and Stedinger [2001], Kim et al. [2007], Cote et al. [2011], and Eum et al. [2011] focus on better descriptions of the joint distribution of flows and forecasts using sampling SDP (SSDP).

Kelman et al. [1989;1990] introduced sampling SDP to optimize water systems operations on the Feather River in California, using multiple historical time-series as scenarios to capture by example the variability of streamflow processes. A scenario is

defined here as a streamflow hydrograph and the associated volume forecast time-series and energy market parameters and loads. In this case the hydrologic state variable is the set of streamflow scenarios.

If the probabilities assigned to historical streamflow series are appropriately conditioned on historical volume forecasts as described by Kelman et al. [1990] and Faber and Stedinger [2001], many historical streamflow series may be extremely unlikely, in effect reducing the number of relevant streamflow scenarios available to compute the expected future value of water in storage. This is identified by Labadie [2004] as a primary drawback of SSDP.

It would seem then to be better to use sets of streamflow series that are consistent with anticipated basin flows. The National Weather Service's Ensemble Streamflow Prediction (NWS ESP) procedure produces streamflow forecasts in the form of multiple hydrographs, each a possible realization of seasonal streamflow [Day, 1985; Schaake and Larson, 1998]. Because such hydrographs are often derived from historical weather sequences, historical (or modified historical) energy market signals could very easily be embedded in the ESP forecasts. Such sets of hydrographs (and other embedded signals) capture by example the temporal and spatial correlation structure of the streamflow series. One advantage of using SSDP algorithms with ESP for multiple reservoir optimization is that the ESP captures the interrelationships among streamflows in those basins by utilizing historical weather patterns for different years [Faber, 2000; Faber and Stedinger, 2001]. Faber and Stedinger [2001] demonstrate the use of NWS ESPs for operation of a reservoir in Colorado, and more

recently Kim et al. [2007] and Eum et al. [2011] demonstrate the use of ESP forecasts for basins in Korea.

Askew [1974a, b, 1975] introduced chance-constrained SDP in which probability of failure to meet some constraint must be less than a prescribed level,  $y_t$ . Yakowitz [1982] points out that Askew's approach satisfies the chance constraint, but is not guaranteed to be the optimal policy satisfying that constraint. Sneidovich and Davis [1975] propose adding  $y_t$  as a state variable for the chance constrained SDP model, with added conditions for the chance constraint. Askew [1974b] proposes a variation on chance constraints in which the expected number of constraint violations is bounded. Rossman [1977] presents an approach for solving such a model based in Lagrangian duality theory. If a state variable is added for the number of failures, then Rossman's expectation constraints are equivalent to probabilistic constraints [Sneidovich,1979].

The previous discussion in this section has focused nearly exclusively on single-reservoir applications of SDP. Solution of multi-reservoir SDP and DP models is more difficult, and was somewhat more limited in early applications of SDP for reservoir optimization. Section 2.4.2 discusses solution techniques for reducing the burden of multi-reservoir optimization and Chapter 5 of this thesis presents new developments in this area. The first SDP model for multiple reservoirs was presented by Schweig and Cole [1968], who consider a two reservoir system. Yakowitz [1982] points out that their model is essentially the same as the joint reservoir-aquifer model developed by Buras [1963]. Roefs and Bodin [1970] and Heidari et al. [1971] provide early examples of multi-reservoir deterministic DP models. Because deterministic DP

models do not include a hydrologic state variable, the number of reservoirs included in early studies was generally greater for deterministic DP models compared to stochastic DP models. In fact a four reservoir deterministic DP model is presented as early as Larson [1968], and a 10-reservoir deterministic DP model is solved using ‘constrained differential dynamic programming’ by Murray and Yakowitz [1979]. Pereira and Pinto [1985] solve a 39 reservoir problem using stochastic dual dynamic programming. This and other methods for solving DP and SDP models for large systems are described in more detail in Section 2.4.2.

#### ***Section 2.4 Special Concerns addressed in this Thesis***

Chapter 4 of this thesis is concerned with the representation of uncertainty in reservoir optimization models and the value of forecasts to hydropower operation. Section 2.4.1 provides an overview of previous work in this area. Chapter 5 of this thesis develops a new method to cope with the curse of dimensionality. Section 2.4.2 provides a brief overview of previous efforts to address the curse of dimensionality for multi-reservoir dynamic programming models.

##### ***Section 2.4.1 Representations of Uncertainty***

How uncertainty is represented in a reservoir optimization model can have a major impact on the quality of the resulting ‘optimal decision’ [Tejada-Guibert et al., 1995]. One might intuitively guess that the more complex the model, the more hydrologic information included, the better the resulting decisions, but Klemes [1977] reminds us that this often is not so. Precisely how uncertainty should be modeled in SDP models for reservoirs has remained an active area of research since SDP models were first applied to the reservoir optimization problem.

Many studies have focused on the application of a single model, with a single uncertainty representation, to a specific reservoir system. These studies are important in that they add valuable experience to the literature, but they necessarily draw narrower insight into how uncertainty ought to be represented than the analysis presented in Chapter 4 of this thesis. This section focuses on past works which seek to draw broader conclusions by comparing the application of different uncertainty models to the same system, or different systems.

An early example of such a study is Klemes [1977], who builds a very simple model of a single reservoir and concludes that simple deterministic DP models perform no better than more complex SDP models. This study is particularly interesting because it considers 1) the value of considering uncertainty in optimization models for reservoirs with a wide range of storage sizes, 2) the effect of reduced hydrologic and economic uncertainty on the value of the derived ‘optimal’ policy, and 3) a framework for quantitatively comparing the effects of hydrologic and economic uncertainties on the ‘optimal’ policy. Stedinger [1978] objects to the generality of the results claimed by Klemes [1977] contending that the example simplified to the point of being unrealistic. Stedinger [1978] claims that the loss of realistic representation of hydrology and reservoir operations leave Klemes [1977]’s results interesting, but ultimately of limited practical value, an opinion supported by this author.

This early exchange highlights a central difficulty in studies which seek generality: the more realistic the system model, often the more specific the findings. This line is tread carefully by all studies which seek general findings, and great care

was taken in Chapter 4 of this thesis to make the various hypothetical hydropower systems credible.

Like Klemes [1977], Karamouz and Houck [1987] examine the relative value of deterministic DP and SDP models, but unlike Klemes [1977], Karamouz and Houck use real hydrologic series as the basis of their analysis. They select three study basins with different hydrology (located in Maryland, Missouri, and Utah), and imagine four reservoirs in each study basin, for a total of 12 hypothetical systems. To aid in comparison between basins, the reservoir storages are set to specific fractions of the mean annual inflow. They found that for medium and large reservoirs deterministic DP performed as well as SDP, but for small reservoirs SDP outperformed deterministic DP.

Tejada-Guibert et al. [1995] take a somewhat different tack. Rather than applying an SDP model to different systems, Tejada-Guibert et al. applies various formulations of an SDP model for a reservoir system in the Central Valley of California. Rather than changing system physical characteristics, Tejada-Guibert et al. examines the relative performance of various SDP models with different objectives, and provide a discussion of the choice of hydrologic state depending on the objective of the system operator. Kelman et al. [1990] and Faber and Stedinger [2001] extend a similar analysis to the SSDP framework.

Other studies which have examined the choice of hydrologic state variable and the impact of different probability models for those state variables for SDP models for a specific system include Esmail-Beik and Yu [1984], Picardi and Soncini-Sessa [1991], Estralich and Buras [1991], Huang et al. [1991], Turgeon [2005], Turgeon

[2007], and Desreumaux et al. [2014]. Picardi and Soncini-Sessa [1991] is also notable for providing an early demonstration of the power of parallelization in SDP models for reservoir optimization.

Cote et al [2011] studies the relative of value of SSDP and SDP models with different hydrologic state variables, including a composite variable of snow-water-equivalent and antecedent soil moisture (depending on season). Faber and Stedinger [2001] examine the efficacy of SSDP models utilizing either ESP forecast or historical flows series as scenarios. They go a step further by examining the value of different scenario tree structures, some of which can be solved with simple stochastic programming techniques rather than dynamic optimization techniques like SSDP and SDP. A similar analysis is provided by Eum et al. [2011]. Faber [2000] and Kim et al. [2007] extend this type of analysis to multi-reservoir systems.

Kim and Plamer [1997] provide a somewhat broader study. Like Klemes [1977] and Karamouz and Houck [1987], Kim and Palmer vary the size of the single study reservoir. Like Tejada-Guibert [1995] and Faber and Stedinger [2001], Kim and Palmer vary the objective function by varying the energy demand and price. For a variety of reservoir size, demand, and price cases they examine the effectiveness of different uncertainty representations and the value of seasonal forecasts for stochastic programming models. By providing realistic cases for a wide range of storages and economic conditions, Kim and Palmer present somewhat general findings about the value of uncertainty representations, as is provided by the analysis in Chapter 4 of this thesis.

More recently Georgakakos and Graham [2008] provide an analytical examination of the sensitivity of optimal reservoir operation to inflow uncertainty for different sized reservoirs. That work also examined when inflow forecasts are of most value. That study utilized a relatively simple objective: meeting an end-of-period storage target. Graham and Georgakakos [2010] expand that work to a multi-objective analysis and provide a numerical example. Importantly, the later work reports its findings for non-dimensional time and storage units so the work is more easily transferred to other systems. Both works find that forecasts are generally more important for smaller reservoir systems, and the latter work shows that operation of small systems are most sensitive to forecast uncertainty. A problem with the analysis in Graham and Georgakakos [2010] is that the results are not easily comparable across hypothetical systems with different storages. For instance, they report the size of the squared deviations from the storage targets across a wide range of reservoir storages. As reservoir storage increases, one would expect squared deviations to also increase: a more meaningful metric might be percent deviations from storage target. Comparison of model performance is a major consideration in Chapter 4 of this thesis.

Zhao et al. [2011] provides a similar analysis to Kim and Palmer [1997], but examine the value of incorporating various forecast products (with varying levels of precision) into a decision support model. They generalize their findings by varying 1) reservoir size and 2) inflow variability. They find that forecast precision is most important for highly variable hydrology and for small reservoirs. An important contribution of Zhao et al. [2011] is a model for the evolution of forecast precision over the forecast horizon. This is important because the error in the inflow forecast

increases with time (is greater farther from the forecast point). This point is also explored by Xu et al. [2014].

All of the studies described in this section have involved conclusions arrived at from building competing optimization models. Hejazi et al. [2008] makes the point that much can be learned by observing historical operations using data mining techniques to identify relationships between hydrologic variables and system operation. This represents an a-priori analysis which can inform the choice of hydrologic state variable. Zhao et al. [2012] and Chapter 6 of this thesis examine similar issues by identifying what forecast length is most critical to system operation, but Hejazi et al. [2008] is unique in that it identifies critical hydrologic variables for 79 reservoirs in California and across the Great Plains. This allows Hejazi et al. [2008] to draw general conclusions about the sizes of reservoirs and seasons for which forecasts and SDP are most valuable. A short coming of that analysis is that it does not explicitly consider operational objectives for specific reservoirs: for instance there is no distinction between hydropower reservoirs and irrigation reservoirs. A further shortcoming is that the analysis does not explicitly consider forecast uncertainty. Still by considering operation across a huge range of reservoirs Hejazi et al. provide an interesting discussion of how one might construct a representation of uncertainty for a given system.

### ***Section 2.4.2 Addressing the Curse of Dimensionality***

To numerically solve equation (2-5), the state space is often discretized and solved at  $N$  specified points, generally a grid. If  $f_t$  is non-linear, then as  $N$  increases

the precision of an approximation of  $f_t$  based on  $N$  points using linear interpolation should also increase.

In the case that a  $k$ -reservoir system is considered,  $S_t$ ,  $R_t$ , and  $Q_t$  become  $k$ -dimensional vectors of reservoir storage  $\mathbf{S}_t$ , releases,  $\mathbf{R}_t$ , and inflows  $\mathbf{Q}_t$  at each of the  $k$  reservoirs in time  $t$ . The state space becomes a  $k$ -dimensional cube, and if each dimension is divided into  $N$  discrete points in each dimension, then equation (2-5) must be solved at  $N^k$  points, resulting in an exponential growth of computational effort and memory required to resolve equation (2-5) with an increase in  $k$ . An additional problem is that solving equation (2-5) at each point becomes more difficult as  $k$  increases, further adding to the computational burden of traditional DP in high dimension. The following discussion describes several approaches to reducing the cost of high-dimensional DP models.

### ***Aggregation Approaches***

Perhaps the most obvious approach to reduce the computational burden of high-dimensional DP models is aggregation, wherein several reservoirs are represented by a combined state variable such as total storage or total energy [Arvanitidis and Rosing, 1970; Quintana and Chikhani, 1981; Gilbert and Shane, 1982; Duran et al., 1985; Saad and Turgeon, 1988; Turgeon and Charbonneau, 1998]. This approach can be very effective, particularly in systems where the critical operation is well represented by a subset of the original state variables (eigenvectors for the full state space). Saad et al. [1992] demonstrate such an example using principle component analysis to determine which state variables account for the majority of the variability in system performance. For their 4-reservoir example, upwards of 90% of

the variability was described by a single state variable, and upwards of 97% of the variability was described by two state variables. This suggested that modeling the system with two state variables is sufficient to capture the critical aspects of system operation. A potential downside of such a representation is that aggregation can often result in a loss of modeling resolution of constraints and system dynamics which may not be acceptable.

### ***Stochastic Dual Dynamic Programming***

A second approach to addressing the “curse” is through use of Bender’s Decomposition in Sampling Dual Dynamic Programming (SDDP) [Pereira and Pinto, 1985]. That algorithm uses simulation of the system to obtain points where the future value function is evaluated. The future value function is approximated by piecewise linear Benders cuts. This involves iterative optimization and simulation till the desired precision is achieved. The linear approximation allows evaluation of the future value function over the entire volume of the state space. Remarkably, the Pereira and Pinto [1985] solve a 39 reservoir problem using this method. The SDDP approach has also been successfully applied more recently [see Tilmant and Kelman, 2007; Goor et al., 2011]. However, if  $f_t$  is non-linear, the SDDP piecewise linear approximation might not be sufficiently precise.

### ***Surrogate Approximation of Future Value Function***

A third approach is to use a surrogate surface to represent  $f_t$  between discrete  $\mathcal{S}_t$  at which equation (2-5) has been solved. This allows for a coarser grid of discrete points to achieve the desired precision in  $f_t$  (i.e. allows for smaller  $N$  to achieve the same accuracy). A simple method is to use linear, or multi-linear interpolation

between discrete  $\mathcal{S}_t$ . This can work well when  $f_t$  is nearly linear, but will require an increasingly fine mesh (i.e. larger  $N$ ) as  $f_t$  becomes more non-linear. Another concern is that a piecewise linear representations will have discontinuous first derivatives at the knots,  $\mathcal{S}_t$ , which make solution of equation (2-5) more difficult.

Johnson et al. [1993] compare cubic splines, Hermite polynomials, and multi-linear interpolation for a multi-reservoir problem. They demonstrate that for a 4-reservoir system, using cubic splines resulted in a 330 times speed-up compared to multi-linear interpolation in order to achieve a 0.5% mean relative error. The speed up is both because a coarser lattice of points is sufficient, and because a faster, derivative based, optimizer could be used to solve equation (2-5) because cubic splines have continuous first derivatives.

### *Sparse Sampling of the State Space*

The previous discussion has assumed that the selected discrete state-space points,  $\mathcal{S}_t$ , are arrayed on a regular grid, or lattice of points. This is called a full-factorial lattice because the same discretization level is used in all dimensions, and a basis point is placed at every combination of discretization levels across the dimensions [Chen et al., 1999]. Full factorial lattices are preferable for fitting multi-linear and cubic-spline interpolation surfaces. However, other work has explored the use of irregularly placed points and partial grid designs as a means of reducing the required size of  $\mathcal{S}_t$ .

One example of partial grid design is the use of sparse grids [see Bungartz and Griebel, 2004]. Sparse grids are built using a hierarchical discretization scheme. In this approach, rather than having discrete levels in each dimension, the discretization

is divided into degrees characterized by the distance between adjacent points in a degree. As the degree of discretization increases the distance between adjacent points in that degree is smaller. Under certain conditions, sparse grids can be shown to achieve the same accuracy as full grids, with a fraction of the points. Adaptive sparse grids change the degree of the discretization adaptively across the state-space in response to the complexity of the function being approximated [Brumm and Scheidegger, 2014].

Another example of partial grid design is provided Chen et al. [1999] who use orthogonal arrays to select discrete points in the state-space. To represent  $f_t$  they use multivariate adaptive regression splines, which do not require a regular lattice of points. The work presented in Chapter 5 uses irregularly placed points, with radial basis functions (RBFs) to approximate  $f_t$ . Rather than using orthogonal arrays to select the points to sample in the state space, this work uses *a priori* knowledge of system behavior to select relevant points.

### ***The Fitted-Q-Iteration Method***

More recently, Q-learning algorithms have been applied to solve SDP models for water resources problems [Castelletti et al., 2010; Castelletti et al., 2013; Pianosi et al., 2013]. Q-learning is a reinforced learning technique which can be applied to solve traditional Dynamic Programming models [Bertsekas, 2011; Ernst, 1999; Ernst et al., 2005]. The Fitted-Q-Iteration approach proposed by Castelletti et al. [2010] solves the DP model by sampling and simulating state-action pairs. The state-action pairs might be selected through historical operation (as suggested in Chapter 5 of this thesis), through standard discretization and sampling of the state-action space, or through

efficient sampling using Latin Hypercubes or Orthogonal arrays, as suggested by Chen et al. [1999]. To determine the optimal policy between sampled points in the state-space, Castelletti et al. [2010, 2013] use randomized regression trees [Geurts et al.; 2006]. Numerical experiments by Castelletti et al. [2010] suggests their fitted Q-iteration method can have enormous computational speed up over traditional iterative DP solution techniques.

### ***Section 2.5 Conclusion***

DP, SDP, and SSDP are powerful tools which allow an analyst to model complex systems and derive an optimal control rule. Since the mid-1950s water resources systems engineers have employed SDP models to manage reservoir systems. The SDP methodology particularly lends itself to the reservoir operations problem because it can accommodate non-linear constraints and objectives and selects an optimal policy considering hydrologic uncertainty. More recently SSDP has been developed and shows great promise as it provides a natural framework to accommodate ensemble forecasts in a management model, and ensemble forecasts are becoming more common in meteorology and hydrology.

This chapter begins with a very brief introduction to DP, SDP, and SSDP as they have been applied to reservoir optimization problems. This chapter primarily supports Chapters 4 and 5 which employ a single-reservoir SSDP model and multi-reservoir DP model respectively. In particular Section 2.4 highlights the relevant literature in the areas of research which Chapters 4 and 5 seek to advance. The reader who is interested in reservoir operation more generally is referred to Labadie

[2004,2005], and the reader who is interested in DP and SDP more generally is referred to Powell [2007].

## REFERENCES

- Arvanitidis, N.V. & Rosing, J. 1970, "Optimal operation of multireservoir systems using composite representation", *IEEE Trans Power Appl Syst*, vol. 89, no. 2, pp. 327.
- Askew, A.J. 1975, "Use of risk premium in chance-constrained dynamic programming", *Water Resources Research*, vol. 11, no. 6, pp. 862-866.
- Askew, A.J. 1974, "Chance-constrained dynamic programming and the optimization of water resources system", *Water Resources Research*, vol. 10, no. 6, pp. 1099-1106.
- Askew, A.J. 1974, "Optimum reservoir operating policies and the imposition of a reliability constraint", *Water Resources Research*, vol. 10, no. 1, pp. 51-56.
- Bellman, N. 1989, "On the Origin of the Name Dynamic Programming" in *Dynamic Programming for Optimal Water Resources Systems Analysis*, ed. A. Esogbue, 1st edn, Prentice Hall, Englewood Cliffs, NJ, pp. 3.
- Bellman, R. 1957, *Dynamic Programming*, Princeton University Press, Princeton, NJ.
- Bellman, R. 1957, *Dynamic Programming*, 1st edn, Princeton University Press, Princeton, NJ.
- Bertsekas, D.P. 2011, *Dynamic Programming and Optimal Control*, 3rd edn, Athena Scientific, Belmont, MA.
- Bras, R.L., Buchanan, R. & Curry, K.C. 1983, "Real Time Adaptive Closed Loop Control of Reservoirs with the High Aswan Dam as a Case Study", *Water Resources Research*, vol. 19, no. 1, pp. 33-52.
- Brumm, J. & Scheidegger, S. 2014, "using Adaptive Sparse Grids to Solve High-Dimensional Dynamic Models", *Social Science Research Network*, .
- Bungartz, H. & Griebel, M. 2004, "Sparse Grids", *Acta Numerica*, , pp. 1-123.

- Buras, N. 1963, "Conjunctive Operation of Dams and Aquifers", *Proceedings of the American Society of Civil Engineers*, vol. 89, no. HY6, pp. 111-131.
- Butcher, W.S. 1971, "Stochastic dynamic programming for optimum reservoir operation", *Water Resources Bulletin*, vol. 7, no. 1.
- Castelletti, A., Galelli, S., Restelli, M. & Soncini-Sessa, R. 2010, "Tree-based reinforcement learning for optimal water reservoir operation", *Water Resources Research*, vol. 46, no. W09507.
- Castelletti, A., Pianosi, F. & Restelli, M. 2013, "A multiobjective reinforcement learning approach to water resources systems operation: Pareto frontier approximation in a single run", *Water Resources Research*, vol. 49.
- Chen, V.C.P., Ruppert, D. & Shoemaker, C.A. 1999, "Applying experimental design and regression splines to high-dimensional continuous-state stochastic dynamic programming", *Operations Research*, vol. 47, no. 1, pp. 38-53.
- Cote, P., Haguma, D., Leconte, R. & Krauc, S. 2011, "Stochastic Optimization of Hydro-Quebec hydropower installations: a statistical comparison between SDP and SSDP methods", *Canadian Journal of Civil Engineering*, vol. 38, no. 12, pp. 1427-1434.
- Day, G.N. 1985, "Extended Streamflow Forecasting Using NWSRFS", *Journal of Water Resources Planning and Management*, vol. 111, no. 2, pp. 157-170.
- Desreumaux, Q., Cote, P. & Leconte, R. 2014, "Role of hydrologic information in stochastic dynamic programming: a case study of the Kemano hydropower system in British Columbia", *Canadian Journal of Civil Engineering*, vol. 41, pp. 839.
- Dixit, A.k. 1990, *Optimization in Economic Theory*, 2nd edn, Oxford University Press, Oxford, UK.
- Draper, N.R. & Smith, H. 1966, *Applied Regression Analysis*, 1st edn, John Wiley & Sons, Inc., New York.

- Ernst, D. 1999, *Newar optimal closed-loop control. Application to electric power systems.*, University of Liege.
- Ernst, D., Geurts, P. & Wehenkel, L. 2005, "Tree-based batch mode reinforcement learning", *Journal of Machine Learning Research*, vol. 6, pp. 503-556.
- Esmail-Beik, S. & Yu, Y.-. 1984, "Optimal Operation of Multipurpose pool of Elk City Lake", *Water Resources Planning and Management*, vol. 110, no. 1, pp. 1.
- Esogbue, A. 1989, "A Taxonomic Treatment of Dynamic Programming Models of Water Resources Systems" in *Dynamic Programming for Optimal Water Resources Systems Analysis*, ed. A. Esogbue, 1st edn, Prentice Hall, Englewood Cliffs, NJ, pp. 27.
- Estralrich, B. & Buras, N. 1991, "Alternative Specifications of State Variables in Stochastic-Dynamic-Programming Models of Reservoir Operation", *Applied Mathematics and Computation*, vol. 44, pp. 143.
- Eum, H., Kim, Y. & Palmer, R.N. 2011, "Optimal Drought Management Using Sampling Stochastic Dynamic Programming with a Hedging Rule", *Journal of Water Resources Planning and Management*, vol. 137, no. 1.
- Faber, B.A. 2001, *Real-time Reservoir Optimization Using Ensemble Streamflow Forecasts*, Cornell.
- Faber, B.A. 2001, *Real-Time Reservoir Optimization Using Ensemble Streamflow Forecasts*, PhD edn, Cornell University, Ithaca, NY.
- Gablinger, M. & Loucks, D.P. 1970, "Markov models for flow regulation", *Journal of Hydraulics Division American Society of Civil Engineers*, vol. 96, no. HY1, pp. 165-181.
- Georgakakos, K.P. & Graham, N.E. 2008, "Potential Benefits of Seasonal Inflow Prediction Uncertainty for Reservoir Release Decisions", *Journal of Applied Meteorology and Climatology*, vol. 47, pp. 1297.
- Gessford, J. & Karlin, S. 1958, "Optimal policy for hydroelectric operations" in *Studies in the Mathematical Theory of Inventory and Production*, eds. K.J.

- Arrow, S. Karlin & H. Scarf, 1st edn, Stanford university Press, Stanford, CA, pp. 179-200.
- Geurts, P., Ernst, D. & Wehenkel, L. 2006, "Extremely randomized trees", *Machine Learning*, vol. 63, no. 1, pp. 3-42.
- Gilbert, K.C. & Shane, R.M. 1982, "TVA hydro scheduling model: Theoretical aspects", *Journal of Water Resources Planning and Management*, vol. 108, pp. 21-36.
- Goor, Q., Kelman, R. & Tilmant, A. 2011, "Optimal Multipurpose-Multireservoir Operation Model with Variable Productivity of Hydropower Plants", *Journal of Water Resources Planning and Management*, vol. 137, no. 3, pp. 258-267.
- Graham, N.E. & Georgakakos, K.P. 2010, "Toward Understanding the Value of Climate Information for Multiobjective Reservoir Management under Present and Future Climate and Demand Scenarios", *Journal of Applied Meteorology and Climatology*, vol. 49, pp. 557.
- Heidari, M., Chow, V.T., Kokotovic, P.V. & Meredith, D.D. 1971, "Discrete differential dynamic programming approach to water resources systems optimization", *Water Resources Research*, vol. 7, no. 2, pp. 273.
- Hejazi, M.I., Cai, X.M. & Ruddell, B.J. 2008, "The role of hydrologic information in reservoir operation – Learning from historical releases", *Advances in Water Resources*, vol. 31, pp. 1636-1650.
- Hsu, W., Holmes, T.J. & Morgan, F. 2014, "Optimal city hierarchy: A dynamic programming approach to central place theory", *Journal of Economic Theory*, vol. 154, pp. 245.
- Huang, W.-., Harboe, R. & Bogardi, J.J. 1991, "Testing Stochastic Dynamic Programming Models Conditioned on Observed or Forecasted Inflows", *Journal of Water Resources Planning and Management*, vol. 117, pp. 28.
- Insley, M. & Rollins, K. 2005, "On solving the multirotational timber harvesting problem with stochastic prices: a linear complementarity formulation", *American Journal of Agriculture Economics*, vol. 83, no. 5, pp. 735-755.

- Johnson, S.A., Stedinger, J.R., Shoemaker, C.A., Li, Y. & Tejada-Guibert, J.A. 1993, "Numerical Solution of Continuous-State Dynamic Programs Using Linear and Spline Interpolation", *Operations Research*, vol. 41, no. 3.
- Karamouz, M. & Houck, M.H. 1987, "Comparison of Stochastic and Deterministic Dynamic Programming for Reservoir Operating Rule Generation", *Water Resources Bulletin*, vol. 23, no. 1, pp. 1.
- Karamouz, M. & Vasiliadis, H.V. 1992, "Bayesian Stochastic Optimization of Reservoir Operation Using Uncertain Forecasts", *Water Resources Research*, vol. 28, no. 5, pp. 1221-1232.
- Kelman, J., Stedinger, J.R., Cooper, L.A., Hsu, E. & Yuan, S. 1990, "Sampling stochastic dynamic programming applied to reservoir operation", *Water Resources Research*, vol. 26, no. 3, pp. 447-454.
- Kelman, J., Stedinger, J.R., Cooper, L.A., Hsu, E. & Yuan, S. 1989, "Use of Probabilistic Constraints in Reservoir Operating Policies with Sampling Stochastic Dynamic Programming", *Proceedings of 3rd Water Resources Operations Management Workshop: Computerized Decision Report Systems for Water Managers*, pp. 266.
- Kim, Y., Eum, H., Lee, E. & Ko, I. 2007, "Optimizing Operational Policies for a Korean Multireservoir System using Sampling Stochastic Dynamic Programming with Ensemble Streamflow Prediction", *Journal of Water Resources Planning and Management*, vol. 133, no. 1, pp. 4-14.
- Kim, Y. & Palmer, R.N. 1997, "Value of Seasonal Flow Forecasts in Bayesian Stochastic Programming", *Journal of Water Resources Planning and Management*, vol. 123, no. 6, pp. 327-335.
- Klemes, V. 1977, "Value of Information in Reservoir Optimization", *Water Resources Research*, vol. 13, no. 5, pp. 837.
- Krzysztofowicz, R. 1999, "Bayesian theory of probabilistic forecasting via deterministic hydrologic model", *Water Resources Research*, vol. 35, no. 9, pp. 2739.

- Krzysztofowicz, R. & Reese, S. 1991, "Bayesian Analyses of Seasonal Runoff Forecasts", *Stochastic Hydrology and Hydraulics*, vol. 5, no. 4, pp. 295.
- Krzysztofowicz, R. & Watada, L.M. 1986, "Stochastic Model of Seasonal Runoff Forecasts", *Water Resources Research*, vol. 22, no. 3, pp. 296.
- Labadie, J.W. 2004, "Optimal Operation of Multireservoir Systems: State-of-the-Art Review", *Journal of Water Resources Planning and Management*, vol. 130, no. 2, pp. 93-111.
- Larson, R. 1968, *State Ubcrenebt Dynamic Programming*, Elsevier, New York.
- Little, J.D.C. 1955, "Use of Storage Water in a hydroelectric System", *Journal of Operations Research*, vol. 3, pp. 187-197.
- Loucks, D.P. 1968, "Computer Models for Reservoir Regulation", *Journal of the Sanitary Engineering Division, ASCE*, vol. 94, no. SA4.
- Loucks, D.P. & Falkson, L.M. 1970, "A Comparison of Some Dynamic, Linear and Policy Iteration Methods for Reservoir Operation", *Water Resources Bulletin*, vol. 6, no. 3.
- Loucks, D.P., Stedinger, J.R. & Haith, D.A. 1981, *Water Resources Systems PLanning and Analysis*, 1st edn, Prentice-Hall, Englewood Cliffs, N.J.
- Maceira, M.E. & Kelman, J. 1991, *Long Term Hydro-Thermal Coordination based on Sampling Stochastic Dynamic Programming*, CEPTEL-Centro de Pesquisas de Energia Electrica, Brazil, Brazil.
- Masse, P.B.D. 1946, *Les Reserves et al Regulation de l'Avenir dans la Vie Economique*, Hermann and Cie, Paris.
- Murray, D. & Yakowitz, S. 1979, "Constrained differential dynamic programming and its application to multireservoir control", *Water Resources Research*, vol. 15, no. 4, pp. 1017.

- Pereira, M.V.F. & Pinto, L.M.V.G. 1985, "Stochastic optimization of a multireservoir hydroelectric system-a decomposition approach", *Water Resources Research*, vol. 21, no. 6.
- Pianosi, F., Castelletti, A. & Restelli, M. 2013, "Tree-based fitted Q-iteration for multi-objective Markov decision processes in water resource management", *Journal of Hydroinformatics*, vol. 15, no. 2, pp. 258-270.
- Piccardi, C. & Soncini-Sessa, R. 1991, "Stochastic Dynamic Programming for Reservoir Optimal Control: Dense Discretization and Inflow Correlation Assumption Made Possible by Parallel Computing", *Water Resources Research*, vol. 27, no. 5, pp. 729.
- Powell, W.B. 2007, *Approximate Dynamic Programming*, 2nd edn, Wiley, New York.
- Quintana, V.H. & Chikhani, A.Y. 1981, "A Stochastic Model for Mid-Term Operation Planning of Hydro-Thermal Systems with Random Reservoir Inflows", *IEEE Trans Power Appl Syst*, vol. 100, no. 3, pp. 1119.
- Roefs, T.G. & Bodin, L.D. 1970, "Multireservoir operation studies", *Water Resources Research*, vol. 6, no. 2, pp. 410.
- Rossmann, L. 1977, "Reliability-constrained dynamic programming and randomized release rules in reservoir management", *Water Resources Research*, vol. 13, no. 2, pp. 247-255.
- Russell, C.B. 1972, "An optimal policy for operating a multipurpose reservoir", *Operations Research*, vol. 20, no. 6, pp. 1181-1189.
- Saad, M. & Turgeon, A. 1988, "Application of principal component analysis to long-term reservoir management", *Water Resources Research*, vol. 24, pp. 907-912.
- Saad, M., Turgeon, A. & Stedinger, J.R. 1992, "Censored-data Correlation and Principle Component Dynamic Programming", *Water Resources Research*, vol. 28, no. 8, pp. 2135-2140.
- Schaake, J. & Larson, L. 1998, "Ensemble streamflow prediction (ESP): progress and research needs", *Special Symposium on Hydrology*.

- Schweig, Z. & Cole, A. 1968, "Optimal control of linked reservoirs", *Water Resources Research*, vol. 4, no. 3, pp. 479-498.
- Sneidovich, M. 1979, "Reliability-constrained reservoir control problems, 1, Methodological issues", *Water Resources Research*, vol. 15, no. 6, pp. 1574.
- Stedinger, J.R. 1978, "Comment on 'Value of Information in Reservoir Optimization' by V. Klemes", *Water Resources Research*, vol. 14, no. 5, pp. 984.
- Stedinger, J.R., Sule, B.F. & Loucks, D.P. 1984, "Stochastic dynamic programming models for reservoir operation optimization.", *Water Resources Research*, vol. 20, no. 11, pp. 1499-1505.
- Su, S.U. & Deininger, R.A. 1974, "Modeling the regulation of Lake Superior under uncertainty of future water supplies", *Water Resources Research*, vol. 10, no. 1, pp. 11-25.
- Tejada-Guibert, J.A., Johnson, S.A. & Stedinger, J.R. 1995, "The value of hydrologic information in stochastic dynamic programming models of a multireservoir system", *Water Resources Research*, vol. 31, no. 10, pp. 2571-2579.
- Tilmant, A. & Kelman, R. 2007, "A stochastic approach to analyze trade-offs and risks associated with large-scale water resources systems", *Water Resources Research*, vol. 43, no. W06425, pp. 1-11.
- Topaloglu, H. & Kunnumkal, S. 2006, "Approximate dynamic programming methods for an inventory allocation problem under uncertainty", *Naval Research Logistics*, vol. 53, pp. 782-805.
- Turgeon, A. 2007, "Stochastic optimization of multireservoir operation: the optimal reservoir trajectory approach", *Water Resources Bulletin*, vol. 43, no. W05420.
- Turgeon, A. 2005, "Solving a stochastic reservoir management problem with multilag autocorrelated inflows", *Water Resources Research*, vol. 41, no. W12414.
- Turgeon, A. & Charbonneau, R. 1998, "An aggregation-disaggregation approach to long-term reservoir management", *Water Resources Research*, vol. 34, no. 12, pp. 3585-3594.

- Vicuna, S., Dracup, J.A., Lund, J.R., Dale, L.L. & Maurer, E.P. 2010, "Basin-scale water system operations with uncertain future climate conditions: Methodology and case studies", *Water Resources Research*, vol. 46, no. W04505, pp. 1-19.
- Xu, W., Zhang, C., Peng, Y., Fu, G. & Zhou, H. 2014, "A two stage Bayesian stochastic optimization model for cascaded hydropower systems considering varying uncertainty of flow forecasts", *Water Resources Research*, vol. 50.
- Yakowitz, S. 1982, "Dynamic programming applications in water resources", *Water Resources Research*, vol. 18, no. 4, pp. 673-679.
- Yeh, W.W. 1985, "Reservoir Management and Operations Models: A State-of-the-Art Review", *Water Resources Research*, vol. 21, no. 12, pp. 1797-1818.
- Yu, M., Lu, C. & Liu, Y. 2014, "Direct Heuristic Dynamic Programming Method for Power System Stability Enhancement", *2014 American Control Conference (ACC)*, pp. 747.
- Zhao, T., Cai, X. & Yang, D. 2011, "Effect of streamflow forecast uncertainty on real-time reservoir operation", *Advances in Water Resources*, vol. 34, no. 4, pp. 495.
- Zhao, T., Yang, D., Cai, X., Zhao, J. & Wang, H. 2012, "Identifying effective forecast horizon for real-time reservoir operation under a limited inflow forecast", *Water Resources Research*, vol. 48, no. W01540.

## CHAPTER 3

### THE KENNEBEC RIVER AND GENERATION OF SYNTHETIC HYDROLOGY FOR HYDROPOWER STUDIES

This section describes two hypothetical hydropower systems which are based on the facilities on the Kennebec River in Maine. The original plan for this thesis was to obtain flow and reservoir characteristic data from the system operator, NextEra Energy. Unfortunately, given legal considerations NextEra was unwilling to provide system information. However, there are a number of USGS gauges in the basin and adjacent basins with public information, and most important plant characteristics can be obtained from Federal Energy Regulatory Commission (FERC) re-licensing documentation or other public sources. Section 3.1 of this chapter describes the Kennebec River hydrology while Section 3.2 describes its installed hydroelectric system. Section 3.3 describes the hypothetical systems which are used in later chapters of this thesis, and the procedures used to generate synthetic inflows for those systems. Finally, Section 3.4 provides concluding remarks.

#### ***Section 3.1 The Kennebec River***

The Kennebec River basin is located in north-central Maine in the eastern United States. The Kennebec originates near the US/Canada border and flows 150 miles to the Atlantic Ocean at Merrymeeting Bay. The river has a drainage area of 5,870 square miles and includes a wide range of topography from mountains in the headwaters to flat coastal plains. The major tributaries are the Moose, Dead, Carrabassett, Sandy, and Sebasticook Rivers. The average gradient of the main channel is 8.5 feet per mile, The Dead and Sandy Rivers have channel gradients of 25

and 22 feet per mile respectively. The average annual discharge of the Kennebec River is 287.5 billion cubic feet (bcf) [Kennebec Water Power Co. (KWPC), 1997].

The average annual temperature in the basin is 42° F, with average monthly temperatures ranging from nearly 70° F in July to 10° F in January. Temperature extremes in the basin have ranged from 90° F to -30° F, with rapid changes in daily weather a common occurrence. The land cover is 8% agriculture, 75% wooded, 5% lakes and ponds, with the remaining 12% consisting of other land use, such as residential, urban, and industrial [KWPC, 1997]. The majority of the 'other' land use is in the lower reaches of the basin. The headwaters are largely undeveloped.

The Kennebec River basin generally receives a large winter snowpack [Hodgkins et al., 2005], and the spring snowmelt represents the most significant feature of the annual hydrograph. For example, nearly 60% of the annual inflow to Flagstaff Lake on the Dead River occurs between March and May. To accommodate the spring freshet and any large winter storms, the large storage reservoirs in the headwaters of the Kennebec are typically drawn down to 30% of full rated capacity [KWPC] at the end of October. The time of arrival of the spring thaw varies from year to year, and is often marked by the 'ice out' date. This is the earliest date in the year when it is possible to traverse the main body of the lake in a boat unobstructed by ice. Historically, the 'ice out' date is early May for the storage reservoirs in the headwaters, although a recent study suggests global warming is causing earlier 'ice out' [Hodgkins et al., 2002].

A major hydrologic consideration during the summer months is strong and localized thunderstorms. It is not uncommon for spatial variability to cause one basin

to receive twice as much rainfall from a storm as an adjacent basin [KWPC, 1997]. This can cause difficulty when managing a network of storage reservoirs: where the rain falls might be more important than how much falls. On average, the basin receives between 40-50 inches of rain a year, with higher elevations often receiving more [US Geological Survey, 2005] This is typical for highland in interior New England. Average annual hydrographs of Brassua and Flagstaff Lake are provided in Section 3.3.

With modest temperatures over most of the year, the role of evaporation and transpiration on the annual water balance are relatively minor. During an average summer, evaporation losses for the largest reservoirs are generally on the order of 1-1.5 feet of lake level. Combined with transpiration, summer time losses are as high as 81% of precipitation, however losses during the fall and winter months (when most of the precipitation falls), are much lower, so on an annual water balance they account for very small losses. In fact, evapo-transpiration losses are often neglected in optimization models in this region of North America [Cote, 2011].

### ***Section 3.2 The Kennebec Hydropower System***

There are ten hydro-electric generation facilities as well as two storage-only reservoirs (Moosehead and Flagstaff Lakes) located in the basin. The elevation change from the first facility to the last is 1073 vertical feet. The total installed hydro-electric generation capacity is 256 MW. The available storage in the Kennebec's three primary reservoirs, Moosehead Lake, Flagstaff Lake, and Brassua Lake is 44.7 billion cubic feet, or about 15% of the average annual runoff. Figure 3-1 shows a schematic of the Kennebec Hydropower system.

Essentially the system contains three storage reservoirs (Brassua, Flagstaff, and Moosehead Lakes) and two generating reservoirs (Harris and Wyman Station), followed by seven run-of-river plants. Run-of-river plants have virtually no storage so the only water available is the river flow. Brassua Lake is primarily a storage reservoir, though a small single-turbine 5 MW powerhouse is in operation. The outlet of Brassua Lake is the Moose River which flows 3 miles to Moosehead Lake. Moosehead Lake is the largest lake in Maine and one of the largest lakes in New England. The natural lake level has been raised approximately 7.5 feet to provide storage for hydropower operations. Artificial outlet structures on Moosehead lake pre-date hydropower generation on the Kennebec, and were initially installed for moving cut timber dating back to the mid-19<sup>th</sup> century [KWPC, 1997]. The active storage for hydropower operation only includes the artificial storage, and other operational constraints apply throughout the year. Moosehead Lake has two outlet structures into the Kennebec River.

Approximately 12 miles down-stream of Moosehead Lake is Harris Station. Harris Station's reservoir is known as Indian Pond. Harris Station is the largest hydropower plant, by generation capacity, in Maine [Maine Department of Environmental Protection (DEP), 2010] with a capacity of 89.5 MW. There is very little unregulated inflow to the Kennebec River between Moosehead Lake and Harris Station. Below Harris Station the Kennebec is joined by the Dead River at The Forks. The Dead River flows from Flagstaff Lake, which is a storage-only reservoir and entirely manmade.

Below The Forks the Kennebec River enters Wyman Lake, which is the Storage Reservoir for Wyman Station. Wyman Station is the second largest hydropower plant in Maine with a total generation capacity of 83.0 MW [Maine DEP, 2010]. After Wyman Station the Kennebec River flows through seven run-of-river plants, the last of which is located near Waterville.

Harris Station and Wyman Station have large turbine capacity and appreciable storage and are largely used for peaking during weekdays [FERC, 1999]. The three storage reservoirs in the Upper Kennebec are used to supplement incremental inflow into the Kennebec River through the generally dry summer months [FERC, 1997].

### ***Section 3.3 Hypothetical Systems and Synthetic Hydrology***

The majority of the Kennebec system is owned and/or operated by NextEra Energy. At the outset of this research it seemed that hydrologic and powerplant data would be available for the major projects on the Kennebec. Unfortunately, much of this data is proprietary, and it proved impossible to arrive at an arrangement to obtain the necessary data. Because this research is largely an exploratory and illustrative exercise, we deemed it appropriate to study hypothetical basins resembling subsets of the real Kennebec System. As long as the characteristics and hydrology of the hypothetical systems represent realistic systems which might exist, this was deemed to be a reasonable approach to describe operation of possible systems in this region of the United States.

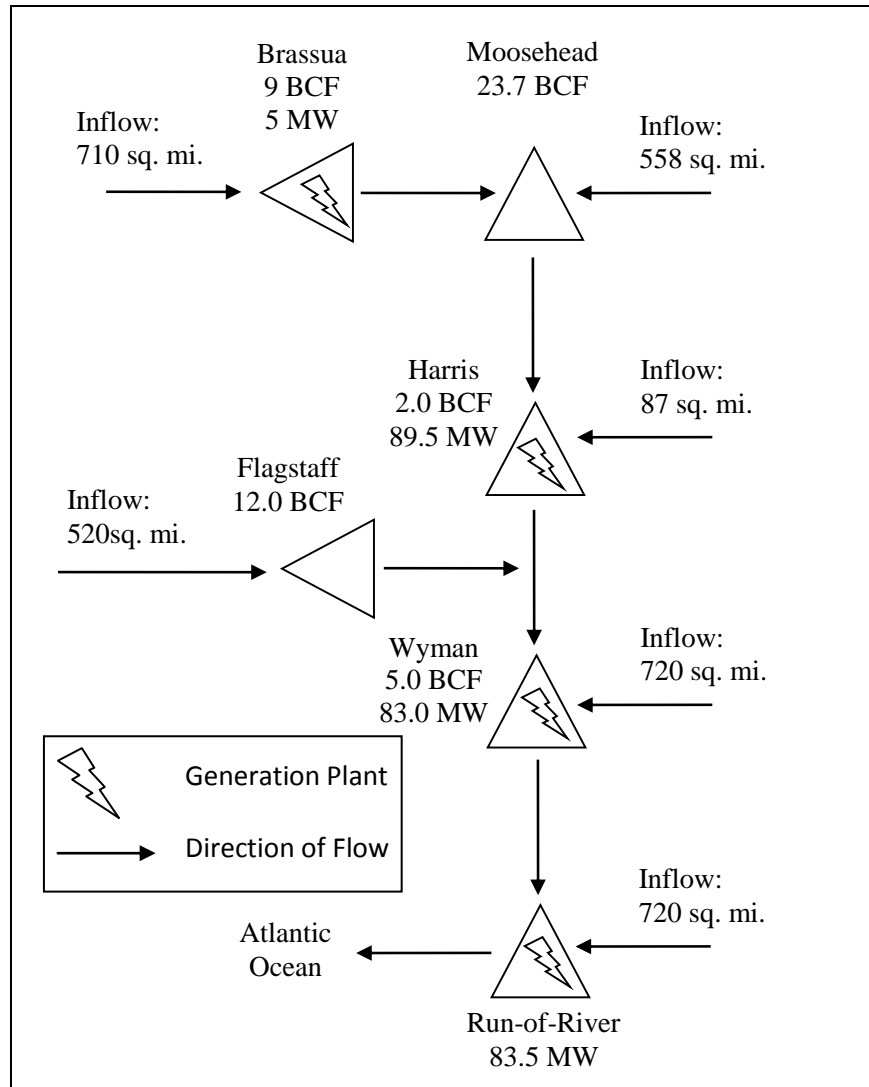


Figure 3-1: Schematic of the Kennebec Hydropower System

Two hypothetical system configurations were created: a “single-reservoir” system and a “four-reservoir” system. The “single-reservoir” system is created by

imagining Harris Station with no upstream regulation (see

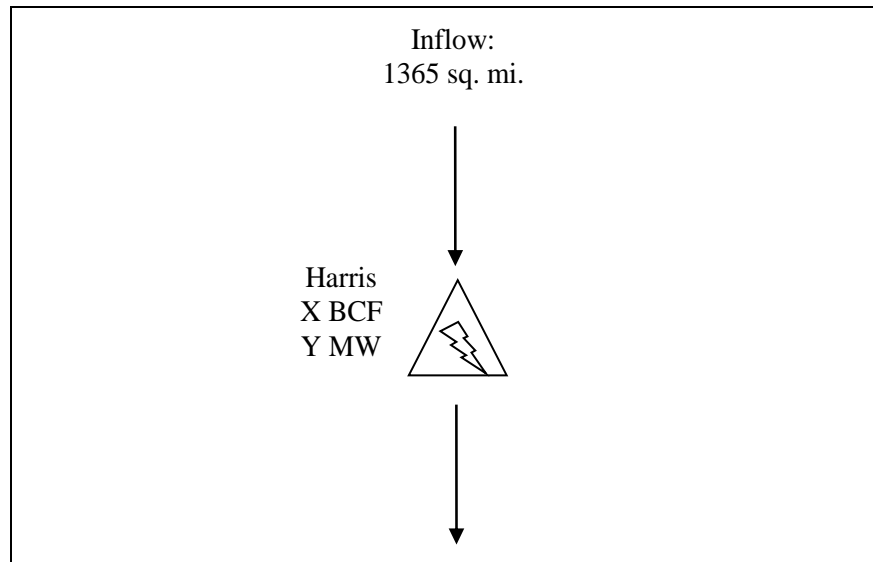


Figure 3-2). This is used in the SSDP study described in Chapter 4 and the diagnostic study in Chapter 6 of this thesis. The “four reservoir” system consists of Brassua, Flagstaff, an aggregation of Moosehead and Harris, and Wyman Station (see Figure 3-3). This system is used in the Corridor DP work described in Chapter 5 of this thesis.

As described in Chapters 4 and 6, a wide range of variations on System A are also considered. These are obtained by retaining the same inflow time series, but assuming that the system has more or less storage and more or less powerhouse turbine capacity. The System A variations considered in Chapters 5 and 6 are summarized in Table 3-1. These represent a wide range of storage-powerhouse capacity ratios.

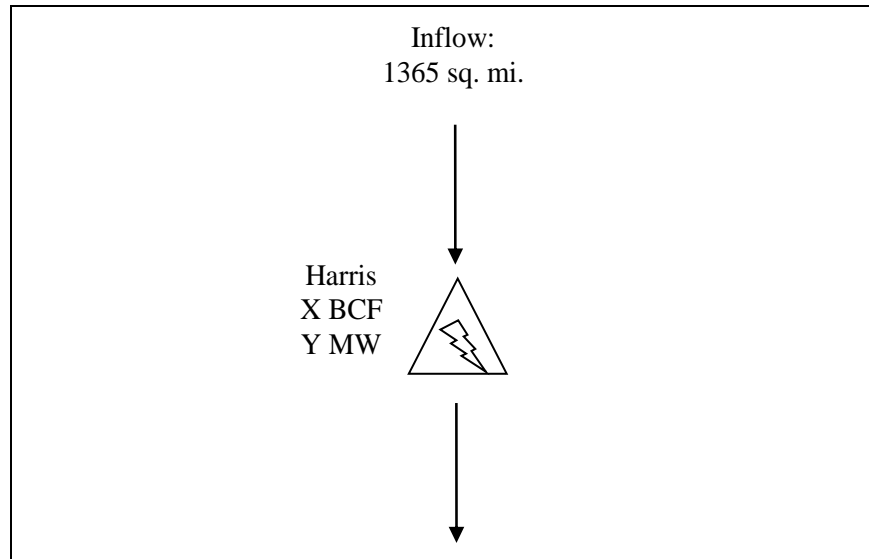


Figure 3-2: Schematic of “single-reservoir” system where  $X$  is the reservoir storage and  $Y$  is the powerhouse turbine capacity.

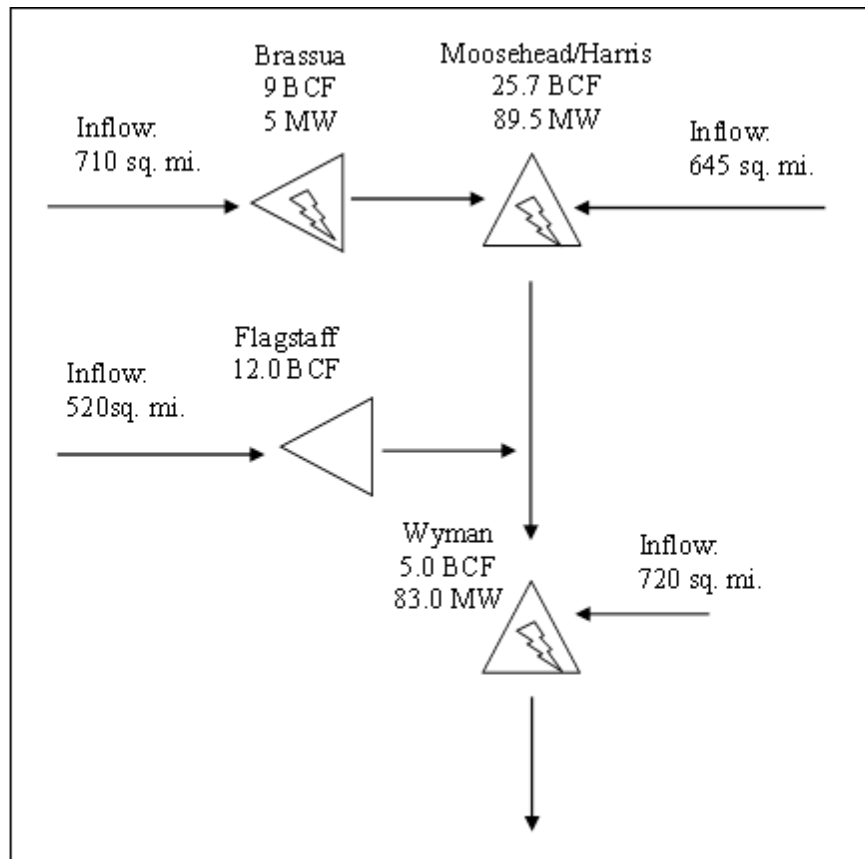


Figure 3-3: Schematic of “four-reservoir” system

Table 3-1: Configurations of “single-reservoir” considered in Chapters 4 and 6

System Name	Storage Capacity (BCF)	Powerhouse Capacity (MW; CFS)
(Small, 2000)	2.0	21.6; 2000
(Small, 3500)	2.0	37.7; 3500
(Small, 5000)	2.0	53.9; 5000
(Small, 8300)*	2.0	89.5; 8300
(Mid, 2000)	10.0	21.6; 2000
(Mid, 3500)	10.0	37.7; 3500
(Mid, 5000)	10.0	53.9; 5000
(Mid, 8300)	10.0	89.5; 8300
(Big, 2000)	20.0	21.6; 2000
(Big, 3500)	20.0	37.7; 3500
(Big, 5000)	20.0	53.9; 5000
(Big, 8300)**	20.0	89.5; 8300

\*Actual storage and powerhouse capacity.

\*\*Nearly the aggregate storage of Moosehead and Harris, with Harris powerhouse capacity

Plant and reservoir storage relationships for most of the system’s facilities are available in the FERC relicensing materials [FERC, 1999; FERC, 1997; FERC, 2010]. Additionally, information on the installed units were available through Oak Ridge National Lab [Kao, 2011]. These data were sufficient to build fairly accurate representations of plant characteristics.

### ***Section 3.3.1 Generation of Synthetic Inflows***

When this research was started, it was hoped that natural inflow data for each of the storage projects on the Kennebec River would become available. Unfortunately, much of this data is out of the public domain and was not available. Thus, it was necessary to generate realistic synthetic inflow records for the each of the reservoirs to be studied. This was deemed acceptable, as the objective of this research was to study optimization algorithms for hydropower systems like those in the Northeast United States, rather than a particular system. The methodology adopted for

generation of synthetic inflows was the proration of flows from nearby unregulated streams based on drainage area or mean annual flow. The objective in this exercise is to select a reference river which experiences similar hydrology and exhibits similar responses to a target river.

Archfield and Vogel [2010] identify the selection of an appropriate reference stream as the primary challenge in synthesizing daily flow data for an ungauged site using proration. In a case study in southern New England, they demonstrate that selection of the closest unregulated gauge does not always yield the best results, but that it is preferable to select the gauge for which flows are most correlated with the ungauged site. To determine this, they utilize a variogram based procedure and demonstrate that in most cases, their procedure does select the most correlated gauge record. While their procedure is interesting, the motivation of their study was to support water resources assessments in southern New England, where replicating actual historic flows are important. In this study, we are merely attempting to synthesize a realistic approximation of northern New England Hydrology, so the added sophistication in Achfield and Vogel [2010] was not deemed necessary.

Daily hydrologic data for the hydropower projects of the Kennebec River are proprietary and were unavailable for this study. However, average annual inflow hydrographs are available for most storage projects, in Exhibit B of the Federal Energy Regulatory Commission (FERC) license application. Given this, it is possible to ensure that a flow record being used to synthesize daily inflows is realistically capturing the annual hydrologic characteristics of each reservoir.

As is the case in much of North America, the river basins of Maine, New Hampshire, and the adjacent region of Quebec are highly impacted by dams and diversions. The selection of unregulated records required careful consideration, as many available records contain both pre- and post-regulation flows since dams have been constructed or removed during the period of record. A review of the unregulated gauging sites in southeastern Quebec revealed no record of sufficient length which could be used for this study. Slack and Landwehr [1992] and Slack et al. [1993] conducted an assessment of the nation's streamflow monitoring network to identify records, or periods of records through water year 1988 which have not been effected by regulation. Their report also gives such important statistics as mean basin elevation, percent lakes and pond coverage, average slope, and main channel length. These data were used when considering the suitability of unregulated gauged watersheds for proration to the storage basins of interest. The required synthetic inflow data for the analyses in Chapters 4, 5, and 6 include:

1. Summer inflows for "single-reservoir" system
2. Summer inflows for Brassua and Moosehead Lakes
3. Summer inflows for Flagstaff Lake
4. Summer inflows for Wyman Lake.

### ***Selecting Reference Streams***

Several USGS stream gauging stations are located on the main stem of the Kennebec River. Streamflow at many of these stations is partially or fully regulated by the operation of upstream dams. Regulation on the main stem of the Kennebec River began as early as the 1830s, with construction of wooden dams on Moosehead Lake to support the timber industry [KWPC, 1997]. Thus, regulation on the Kennebec River pre-dates any gauging activity, so natural flows are not available from those

gauges. However, some gauges on the tributaries to the Kennebec, such as the Carrabassett, Dead, and Sandy rivers experience little or no regulation, or have an extended period of pre-regulation record. For example, USGS Gauge #0104500 provides a daily record for the periods 1902-1906 and 1910-1979 for the Dead River at its junction with the Kennebec River (The Forks), while regulation of flows on the Dead River did not begin until 1948 with the construction of the Long Falls Dam and the formation of Flagstaff Lake.

Gages lying in the adjacent Penobscot and Androscoggin River Basins as well as the nearby St Johns River Basin were considered for reference records. Using the data base assembled by Slack et al. [1993], five potential reference gages were selected, as summarized in Table 3-2. These five sites were selected as they were deemed geographically close enough to the Kennebec basins, hydrologically similar, and of comparable size. Figure 3-4 shows the locations of the reference record basins and the target basins on a map of northern Maine and southern Quebec.

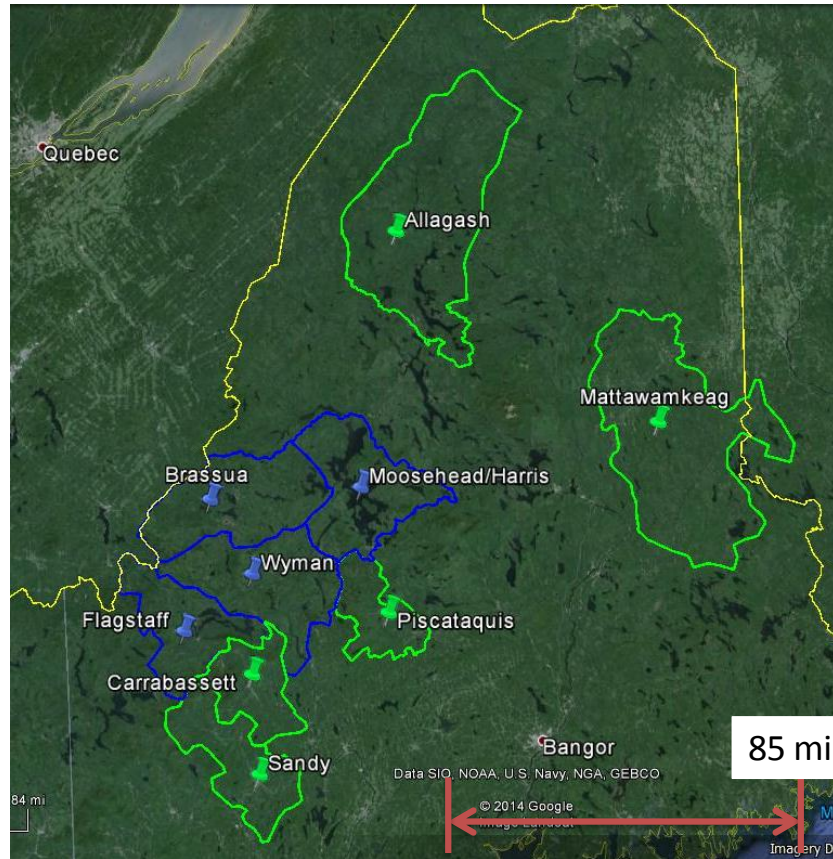


Figure 3-4: Map showing the location of the target basins (in blue) and the reference record basins (in green).

Proration involves scaling a flow record by some ratio. Three different ratios were considered: drainage area ratio, average annual flow rate ratio, and average summer flow rate ratio. The quality of a match between a reference record and a target basin involved the comparison of the mean annual hydrograph (or some substitute) of the target basin to the scaled average annual hydrograph of the reference stream. The following section explains what scaling method and reference stream was used for each target basin. That information is also summarized in Table 3-3.

Table 3-2: Candidate Reference Records and Target Basin Drainage Area, Mean Annual Inflow Rate, Mean Summer Inflow Rate

Name	Drainage Area (sq. miles)	Mean Annual Inflow (cfs)	Mean Summer Inflow (cfs)
Reference Records			
Carrabassett River (01047000)	353	728	381
Mattawamkeag River (01030500)	1418	2511	1187
Piscataquis River (01031500)	298	603	293
Sandy River (01048000)	516	977	453
Allagash River (01011000)	1229	1956	1418
Target Basins			
System A	1365	*	*
Brassua Lake	710	1322	860
Moosehead Lake	867	*	*
Flagstaff Lake	516	1393	847
Wyman Lake	720	*	*

\*Not Available

***“Single-Reservoir” System***

Because the hypothetical system does not exist, it was impossible to obtain an average annual inflow hydrograph from FERC license material. On the other hand, Brassua Lake is nested within the system watershed (in fact composing more than ½ its total watershed area), so it seemed reasonable to use the shape of the Brassua Lake annual hydrograph as a model for the “single-reservoir” inflow. The scaled annual hydrographs of each of the five reference records were compared to the scaled annual hydrograph of Brassua Lake. It was found that the Mattawamkeag River generally matched the hydrograph best (Figure 3-5). Furthermore, the watershed size of the Mattawmkeag River and the “single-reservoir” watershed are similar, and both basins

are nearly entirely wooded and undeveloped. Thus the Mattawamkeag record was used as the reference record for the “single-reservoir” system.

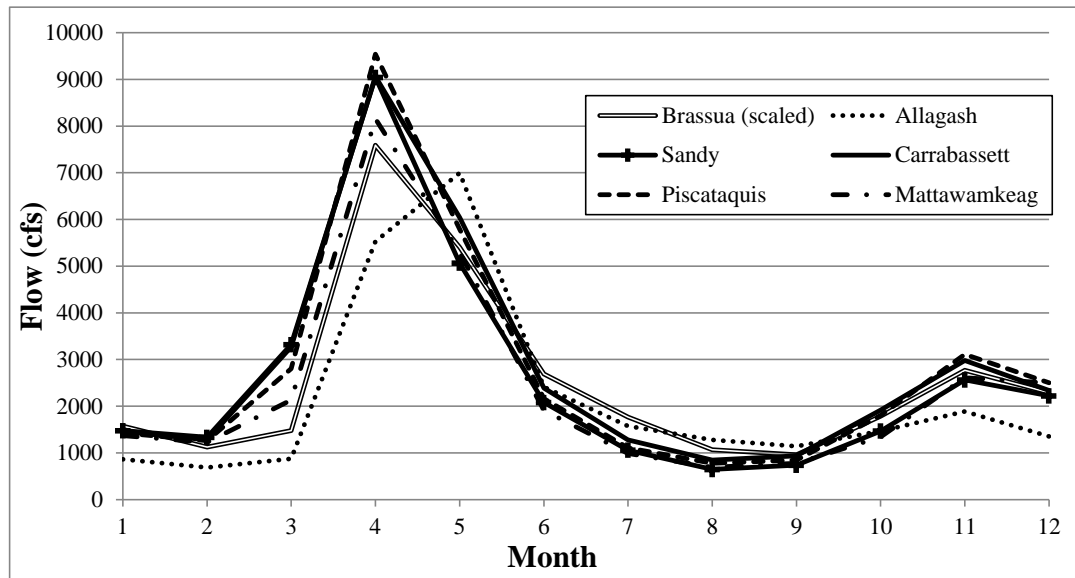


Figure 3-5: Scaled (by DA) Brassua mean annual inflow hydrograph and Scaled (by DA) mean annual inflow hydrographs for reference records.

### ***Brassua and Moosehead Lakes***

Exhibit E of the FERC license application contains the mean monthly inflow based on the years 1989-2007 [FERC, 2010]. This mean annual hydrograph was compared to the scaled mean annual hydrographs for the five reference rivers (Figure 3-6). In general, the average peak inflow, occurring in April, is less pronounced for Brassua Lake than most of the reference records, and the average summer flows are higher than the reference records. The Moose River passes through a number of ponds and minor lakes before flowing into Brassua Lake. As a result, there is more natural storage of snowmelt waters in the basin relative to other nearby basins, which likely causes a higher streamflow persistence through the dry summer months relative to other nearby streams (Clark, 2011).

The FERC license application for Moosehead Lake is only available to be viewed on Microfilm at the FERC headquarters in Washington DC. As a result, I was unable to obtain an inflow hydrograph for Mooshead Lake, but it seems unlikely that inflow characteristics for the two reservoirs, separated by a mere 2 mile stretch of the Moose River, would experience dissimilar inflow characteristics. Thus, a single candidate proration river was selected for the natural inflow into each reservoir, based on the Brassua inflow hydrograph.

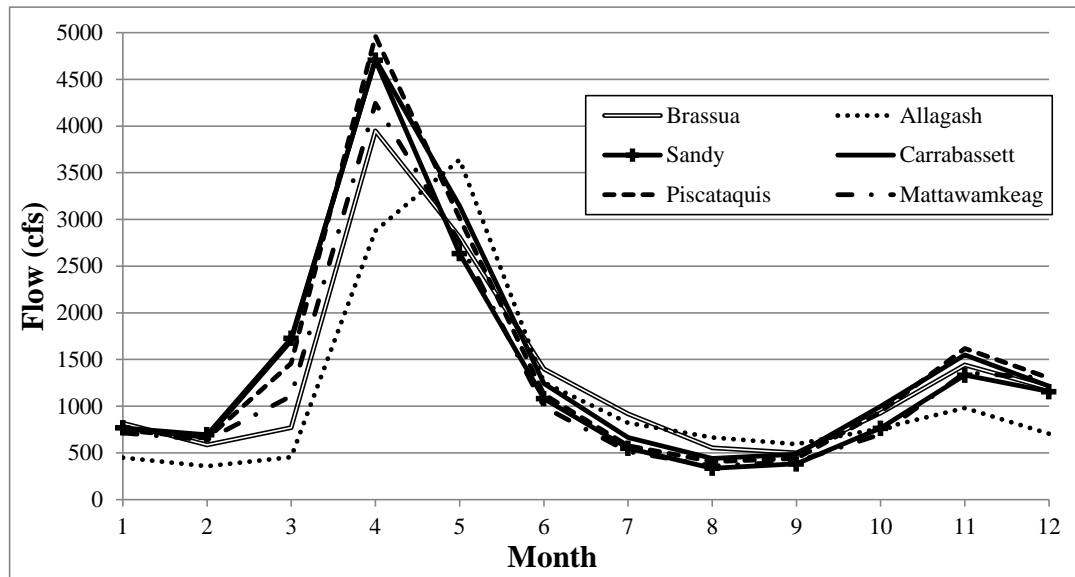


Figure 3-6: Brassua mean annual inflow hydrograph and Scaled (by DA) mean annual inflow hydrographs for reference records.

The Mattawamkeag River was selected as the reference record for Moosehead and Brassua Lakes. The scaling was based on relative drainage area as this resulted in smallest sum of squared errors in average monthly flow. For much of the year the scaled hydrograph of the Mattawamkeag is virtually indistinguishable from the majority of the other reference records, but it matches the spring run-off characteristics of Brassua Lake much better than the other records considered.

### *Flagstaff Lake*

Flagstaff Lake is impounded by the Long Falls Dam on the Dead River, which is located 16 miles upstream of its junction with the Kennebec River and was constructed between 1948 and 1950. No impoundment had previously existed at that site [KWPC, 1997]. The drainage area of the Dead River at the Long Falls Dam is 516 sq mi. The USGS operated a streamflow gauge near the site of the Long Falls Dam (USGS 01043500) from 1939-1982 and also operated a gage at the confluence of the Dead River and the Kennebec River (USGS 0104500) from 1902-1906 and 1910-1979. More recently, the USGS has operated a stream gauging station on a tributary to the Dead River, Spencer Stream (USGS 01044550), which has been in operation from 1999-2011. The average annual hydrograph based on years 1985-1993 is also available through FERC licensing application materials [FERC, 1993; FERC 1995].

Comparison of the pre-regulation records from the two USGS gauging stations on the Dead River showed strong agreement with the annual inflow hydrograph published in the FERC licensing application [FERC, 1993; FERC, 1995]. Furthermore, comparison of the concurrent record of the two Dead River records showed strong agreement with each other, indicating that the gage located at The Forks (USGS 0104500) is a reasonable candidate as a reference record. By prorating the Dead River (pre-regulation) and Spencer Stream records, it is possible to generate unregulated daily inflows into Flagstaff Lake for the years 1902-1906, 1910-1948, and 1999-2011. Unfortunately, much of the USGS gauging network in Northern Maine was not installed until the late 1920s or early 1930s, so finding concurrent reference

records for the other reservoirs in the system proved difficult. Thus, reference records outside of the Dead River watershed were necessary.

Table 3-3: Summary of proration method used to generate synthetic inflows for Kennebec River

<b>Target Watershed</b>	<b>Reference Record</b>	<b>Proration Ratio</b>
<b>“Single-Reservoir” System</b>	Mattawamkeag River (01030500)	Watershed Area
<b>Brassua/Moosehead Lakes</b>	Mattawmkeag River (0103500)	Watershed Area
<b>Flagstaff Lake</b>	Allagash River—April-June (01011000) Carrabassett River—July-March (01047000)	Mean Annual Inflow
<b>Wyman Lake</b>	Piscataquis River (01030500)	Watershed Area

Figure 3-7 plots the mean inflow hydrograph for Flagstaff Lake obtained from FERC documentation and the average inflow hydrographs for the five reference records, scaled by mean annual inflow. Unlike most of the Maine records considered in this study, the inflows to Flagstaff Lake peak in May rather than April. This is likely because the Dead River drains somewhat more northern areas than most of the reference record rivers and drains a mountainous region which retains its snowpack later into the spring. However, the Allagash River, which is the northernmost reference river considered in this study matches the spring snowmelt hydrograph of Flagstaff Lake better than other reference streams, when scaled by its mean annual inflow. However, during the summer months the Flagstaff Lake hydrograph is more closely matched by the other reference streams. Thus a hybrid proration approach is taken wherein the Allagash River is the reference record for April, May, and June, and the Carrabassett River is the reference record for the rest of the year. In both cases the scaling is by the ratio of mean annual flow.

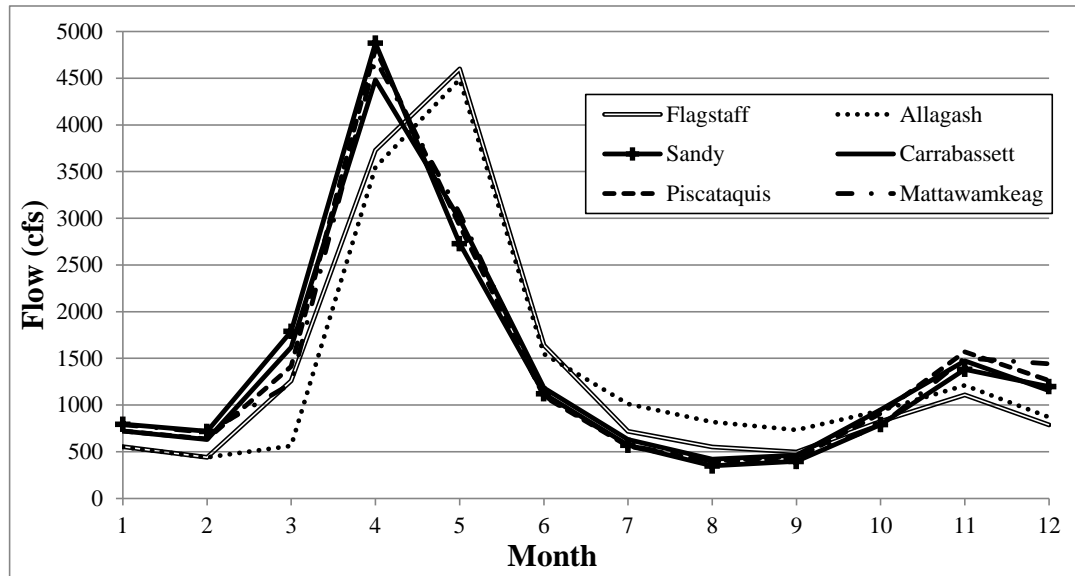


Figure 3-7: Flagstaff mean annual inflow hydrograph and Scaled (by annual inflow) mean annual inflow hydrographs for reference records.

The Carrabasset River was chosen because it is directly adjacent to the Dead River watershed and drains similar mountainous terrain.

### ***Wyman Lake***

Because Wyman Lake is not a storage reservoir and last re-licensed before FERC E-library records were made available, a natural inflow hydrograph is not available through licensing documentation. However, the Piscataquis River is located directly adjacent to the Wyman Lake watershed. Because of its proximity to the Wyman Lake drainage area the Piscataquis river was chosen as a reference basin for Wyman Lake. As a default, the ratio of drainage areas was used for the proration.

### ***Section 3.4 Conclusion***

This Chapter describes the Kennebec River, the Kennebec River hydropower system, the hypothetical systems modeled in Chapter 4, 5, and 6, and the process used to obtain power plant characteristic data, and the process used to generate realistic synthetic inflows for each of the reservoir systems. It was difficult to obtain

powerplant characteristics and necessary to generate synthetic inflow data because the powerplants are privately owned and that data is considered proprietary. Much of the necessary plant characteristic data was available through FERC re-licensing material and other publically available sources. Synthetic inflows were generated by prorating inflows from nearby unregulated rivers whose annual hydrographs approximately matched those of reservoirs in the system. While this does not preserve the correlation structure of inflows between reservoirs, this was deemed an acceptable procedure for generating a reasonable representation of a hydropower system like the Kennebec River. For the exploratory research presented in this study this was deemed sufficient.

## REFERENCES

- KWPC. 1997, *Maine's Multiple-Use River: Kennebec River--Past and Present*, Kennebec Water Power Company.
- Archfield, S.A. & Vogel, R.M. 2010, "Map correlation method: Selection of a reference streamgage to estimate daily streamflow at ungaged catchments", *Water Resources Research*, vol. 46, no. W10513.
- FERC: Central Maine Power Company 1995, *Application for New License for Major Project Existing Dam, Flagstaff Project FERC No. 2612*, Vol. 1 edn.
- FERC: Central Maine Power Company 1993, *Initial Consultation Document Flagstaff Storage Project, FERC No. 2612-ME*.
- Clark, C. 2011, *Personal Communication, phone conversation*.
- Cote, P., Haguma, D., Leconte, R. & Krauc, S. 2011, "Stochastic Optimization of Hydro-Quebec hydropower installations: a statistical comparison between SDP and SSDP methods", *Canadian Journal of Civil Engineering*, vol. 38, no. 12, pp. 1427-1434.
- Federal Energy Regulatory Commission 1997, *Order Issuing New License, Project No. 2671-002*, Federal Energy Regulatory Commission.
- FERC: FPL Energy Maine Hydro LLC 1999, *Application for License for the Indian Pond Project, FERC No. 2142*, FERC, FERC-E.
- FERC: FPL Energy Maine Hydro LLC 1999, *Application for License for the Indian Pond Project, FERC No. 2142.*, FERC.
- FERC: FPL Energy Maine Hydro LLC, Madison Paper Industries & Merimil Limited Partnership 2010, *Brassua Hydroelectric Project FERC No. 2615: Application For New License For Major Water power Project Under 5MW*, FERC.
- Hodgkins, G.A., Dudley, R.W. & Loiselle, M.C. 2005, *Historical Late-Winter and Spring Snowpack Depth and Equivalent Water-Content Data for Maine*, U.S. Geological Survey.
- Hodgkins, G.A., James II, I.C. & Huntington, T.G. 2002, "Historical Changes in Lake Ice-Out Dates as Indicators of Climate Change in New England, 1850-2000.", *International Journal of Climatology*, vol. 22, pp. 1819-1827.
- Kao, S. 2011, *Generator Data for the Kennebec*.

Maine Department of Environmental Protection 2010, *Hydropower Projects in Maine*,  
Maine Department of Environmental Protection.

Slack, J.R. & Landwehr, J.M. 1992, *Hydro-Climatic Data Network (HCDN): A U.S.  
Geological Survey Streamflow Data Set for the United States for the Study of  
Climate Variations, 1874-1988*, U.S. Geological Survey, Reston, VA.

Slack, J.R., Lumb, A.M. & Landwehr, J.M. 1993, *Hydro-climatic data network:  
streamflow data set*, U.S. Geological Survey, Reston, VA.

## CHAPTER 4

### SAMPLING STOCHASTIC DYNAMIC PROGRAMMING ALGORITHMS FOR RESERVOIR OPTIMIZATION

The development of the Sampling Stochastic Dynamic Programming (SSDP) algorithm in this chapter builds on prior work by Faber and Stedinger [2001] who applied SSDP to a seasonal planning problem, with weekly time steps. That study focused on snow melt hydrology for a high-elevation basin in Colorado, and considered a wide range of SSDP models, including some which used seasonal snowmelt run-off forecasts to inform operation.

This study focuses on a seasonal planning problem for a small reservoir in Maine, with time steps as short as 6 hours. The end of the spring snowmelt, summer operations and Fall drawdown are modeled. Synthetically generated flows for this basin are generally very small (with occasional storms), while energy prices fluctuate and can have very high peaks. The operator must weigh the immediate benefits of releasing water against the cost of operating at a lower head and opportunity cost of being unable to sell in the future when prices might peak.

#### ***Section 4.1 Introduction and Motivation***

Reservoir operation requires the decision maker to select a series of releases which maximize the benefits (or expected benefits) over a planning horizon. In the case of a hydropower electric reservoir, this requires the decision maker to balance the present benefit of an immediate release with potential future benefits of later releases. This is a stochastic sequential decision problem because future hydrologic and energy market conditions are generally uncertain at the time a decision must be made.

Stochastic Dynamic Programming (SDP) and Sampling SDP (SSDP) are well suited for such problems because they provide optimal sequential decisions under uncertainty and can accommodate non-linear objectives and constraints, which are common in hydropower.

An important consideration when constructing a stochastic optimization model is how uncertainty is represented. It is a key issue considered here. A good uncertainty representation can be critical to assuring the quality of the resulting optimal decision, and the computational efficiency of the model. Many authors have considered the value of forecasts in reservoir operation, as described in the literature search in Chapter 2. As just one example, Tejada et al. [1995] used SDP models to illustrate the consequences and improved efficiencies of reservoir operation over policies which ignored uncertainty for snow-melt hydrology for the Central Valley Project in California.

The work presented here builds on previous work by Faber and Stedinger [2001] and Kim et al. [2007] by exploring the utility of a wide range of representations of uncertainty in an SSDP model framework. Faber and Stedinger [2001] found that relatively simple uncertainty models with a single branching point performed as well as much more complex models which considered hydrologic uncertainty throughout the planning horizon for a high altitude system in Colorado. This chapter extends that work to the summer operation of a hydropower reservoir in Maine. To more readily compare the operational efficiency of different models, new metrics for measuring operating policy performance are presented.

When building an uncertainty model for a stochastic system it is critical to identify which uncertainties are most critical to system operation on the time scale of interest. Most hydropower operations research has focused on incorporating hydrologic uncertainty (see Hejazi et al. [2008] and the sources cited therein), but it might be the case that economic uncertainty is more critical to efficient system operation. This is particularly important in de-regulated, competitive energy markets like those found in New England. In Maine where the study basin presented here is located, summer flows generally do not vary much day-to-day (see flow auto-correlation plot in Chapter 6) but the price of energy might fluctuate by 3-4 times over a two days.

Another important consideration is what forecast time scale is of most utility to efficient operation of the system. Many previous dynamic programming studies have focused on longer-term operation with time steps of several days, a week, or even a month. For example: Pereira and Pinto [1985], Faber et al. [2001], and Cote et al. [2011] consider weekly time steps and Kim et al. [2007] consider monthly time steps. With the increase in computational power, SSDP is a feasible tool for short-term hydropower operation, with sub-daily time steps. The shorter time step presents new challenges to the formulation of the stochastic model. Neither the frequency nor the duration of forecasts will necessarily align with the time step of the model. Furthermore the hydrologic time scales of interest might exceed the time step length of the model, but the economic time scale of operation necessitates short time steps.

The models presented here suggest an SSDP model framework for such short-term reservoir planning applications. Chapter 6 explores the question of hydrologic time scales of interest in more detail.

Finally, an important consideration is the value of accurate forecasts. Rather than using an existing forecast product, this study uses synthetically generated forecasts with specified duration and precision. This allows for the study of the value of forecasts with different accuracies.

#### ***Section 4.2 SDP Algorithms for Reservoir Operation***

In reservoir operations optimization, the objective is to maximize the expected benefit of operating a reservoir over a planning period,  $Z$ . In practice, time is broken into discrete time steps in which a release decision,  $R_t$ , must be made. The incremental benefit of  $R_t$ ,  $B_t$ , also depends on the current reservoir storage,  $S_t$ , the current inflow  $Q_t$ , and the energy price  $P_t$ . SDP models select a sequence of  $R_t$  which maximize the expected sum of  $B_t$  from the present time  $t = 1$  to the end of the planning horizon,  $t = T$  plus a terminal value of storage,  $v(S_{T+1})$ . The expected benefit from the reservoir operation is

$$Z = E \left[ \sum_{t=1}^T B_t(S_t, R_t, Q_t, P_t) + v(S_{T+1}) \right] \quad (4-1)$$

The expectation is necessary because both  $Q_t$  and  $P_t$  are stochastic. The stochastic nature of  $P_t$  is often overlooked, which may or may not be appropriate depending on the economic context of the system. Variability in prices has become more important as the energy industry has been deregulated [Aggarwal et al., 2009]. Thus large power utilities need to buy energy and reserve power in volatile energy

markets, rather than implicitly buying it from themselves. The introduction of large amounts of wind energy into the energy production mix makes energy markets even more variable [Fernandez, et al., 2012]. Thus there are great opportunities for money to be made if hydropower facilities can gauge when to generate power given their limited reserves of stored energy, and likely future streamflow levels.

In any time it is assumed that the state of the system is described by a state variable. In reservoir optimization reservoir storage,  $S_t$ , is usually a state variable. In SDP it is also common to add a hydrologic state variable,  $H_t$ , which might be the current period's inflow, snow-water equivalent or antecedent soil moisture [Cote et al., 2011], or an inflow forecast [Stedinger et al., 1984, Kelman et al., 1990; Maceira and Kelman, 1991; Karamouz and Vasiliadis, 1992; Tejada et al., 1995; Kim and Palmer, 1997; and Kim et al., 2007]. Introduction of  $H_t$  allows development of policies that use the best available information on the distribution of future streamflows. An SDP formulation of the reservoir operations optimization problem is then given by [Stedinger et al., 1984]:

$$f_t(S_t, H_t) = \max_{R_t^*} \mathbb{E}_{Q_t|H_t} [B_t(S_t, R_t, Q_t) + \alpha f_{t+1}(S_{t+1}, H_{t+1})] \quad (4-2)$$

$$\forall S_t \text{ and } t \in \{1, \dots, T\}$$

$$S_{t+1} = S_t + Q_t - R_t - e_t(S_t, S_{t+1}) \quad (4-3)$$

$$R_t = \max\{\min\{R_t^*, S_t + Q_t\}, (S_t + Q_t - S_{max} - e(S_t, S_{t+1}))\} \quad (4-4)$$

where,

- $f_t$  is the value function in time  $t$ ,
- $S_t$  is the reservoir storage in time  $t$ ,
- $H_t$  is the hydrologic state variable in time  $t$ ,
- $R_t$  is the release in time  $t$ ,
- $R_t^*$  is the optimal target release in time  $t$ ,

$Q_t$  is the reservoir inflow in time  $t$ ,  
 $S_{max}$  is the maximum reservoir storage,  
 $\alpha$  is a discount factor,  
 and  $e_t$  is an evaporation/seepage loss term for time  $t$ .

Here the Functional Model (equation (4-2)) provides the value for any state  $(S_t, H_t)$  in time  $t$ ,  $f_t(S_t, H_t)$ . The Storage Transition Equation (equation (4-3)) describes the change in storage state resulting from the release decision  $R_t$ , inflows  $Q_t$ , and evaporation/seepage losses  $e_t$ . Evaporation losses are assumed to be negligible in this study. Equation (4-4) is necessary because in this formulation the immediate inflow,  $Q_t$ , is not known when the target release,  $R_t^*$ , is selected and that target  $R_t^*$  may not be feasible.

Numerical solution of the SDP model generally requires the discretization of the state space  $(S_t, H_t)$ , and the solution of equation (4-2) for every combination of discrete  $(S_t, H_t)$  pairs in every period over the entire planning horizon [Powell, 2007]. This is done through a recursive process, where equation (4-2) is solved backwards in time starting in time step  $T$  and ending in time step 1.

Alternatively, if one assumes current inflow,  $Q_t$ , is known, it allows the computation of  $B_t$  to remain outside the expectation, and eliminates the need for equation (4-4) [Loucks and Falkson, 1970]. Stedinger et al. [1984] makes the argument that reservoir operators can adapt their release over the time step to account from deviations in inflow, so the assumption that  $Q_t$  is known is a reasonable modeling approach that is both computationally simpler and more realistic.

$$\begin{aligned}
 f_t(S_t, H_t) = \max_{R_t} & \left( B_t(S_t, R_t, Q_t) + \alpha \mathbb{E}_{H_{t+1}|H_t} [f_{t+1}(S_{t+1}, H_{t+1})] \right) \\
 & \forall S_t \text{ and } t \in \{1, \dots, T\}
 \end{aligned} \tag{4-5}$$

$$S_{t+1} = S_t + Q_t - R_t - e_t(S_t, S_{t+1}) \quad (4-6)$$

The expectation in equation (4-5) is computed using the conditional probability  $P_t[H_{t+1}|H_t]$ , which is the probability of transitioning into hydrologic state  $H_{t+1}$  given the current hydrologic state  $H_t$ . When  $H_t$  is the current reservoir inflow,  $Q_t$ , a first-order Markov process can be used to model future streamflow [Tejada-Guibert et al., 1995], as discussed in Chapter 2. In contrast SSDP represents future streamflow with an ensemble of scenarios, which are time series of reservoir inflow and other variables (like energy price). This provides a discrete description of streamflow that implicitly captures the joint distribution of streamflow, forecasts, and other variables across time and space, without requiring an explicit probability distribution [Faber and Stedinger, 2001].

Kelman et al. [1990] present a SSDP model for optimizing hydropower operation for a system in California. Their model (equations (4-7) and (4-8)) takes reservoir storage,  $S_t$ , inflow forecast,  $F_t$ , and the current scenario trace as state variables (i.e. the hydrologic state,  $H_t$ , is described by both a forecast and a scenario). Their SSDP formulation is given by:

$$\max_{R_t} \left\{ B_t(S_t, Q_t(i), R_t) + \alpha E_{i|F_t} \left[ E_{F_{t+1}|F_t, j} [f_{t+1}(S_{t+1}, F_{t+1}, j)] \right] \right\} \quad (4-7)$$

$$\forall S_t \text{ and } t \in \{1, \dots, T\}$$

$$f_t(S_t, F_t, i) = B_t(S_t, Q_t(i), R_t) + \alpha E_{F_{t+1}|F_t, i} [f_{t+1}(S_{t+1}, F_{t+1}, i)] \quad (4-8)$$

$$\forall S_t \text{ and } t \in \{1, \dots, T\}$$

where  $Q_t(i)$  is the reservoir inflow in time  $t$  and scenario  $i$ .

Equation (4-7) is the Decision Model which is used to select an optimal  $R_t$  and equation (4-8) is the Simulation Model which is used to assess the benefits of the optimal release. This is a key difference between SSDP and SDP is that SDP uses the same model to select an optimal release and assess its benefit (for example equation (4-5)). The Decision Model considers possible transitions between scenario traces, whereas the Simulation Model simulates the operational benefits on a single intact scenario, thus preserving the persistence of hydrologic inflows. To numerically solve this SSDP model, equations (4-7) and (4-8) must be solved for each discrete pair of  $(S_t, F_t)$ , for each trace  $i$ , for every time step in the planning period.

The double expectation in equation (4-7) captures both the probability of a future forecast given the current forecast and an inflow, and the transition probability of a future scenario given the current forecast. Faber and Stedinger [2001] avoid the need for a double expectation and a forecast state variable by utilizing the historical forecast series associated with each trace. Thus the forecast state variable is embedded in the scenario state variable, and the scenario state variable becomes the sole hydrologic state variable. This allows a very large reduction in the computational demands of the solution algorithm by reducing the dimension of the implicit hydrologic state variable (going from  $i$  and  $H_t$  to just use of  $i$  which has an  $H_t$  with it).

A reasonable concern is if all combinations of  $i$  and  $H_t$  were reasonable, or likely. In many cases the answer is that some were not likely, and thus the modeling process was not efficient. For single reservoir systems such as that considered by Kelman et al. [1990], this is not particularly important. However, as we strive to model multiple reservoir systems, economy in the computational algorithm becomes

much more important. The corridor model explored in Chapter 5 addresses this issue by seeking to focus modeling efforts on realistic regions of the state space. The Faber and Stedinger [2001] SSDP formulation is:

$$\max_{R_t} \left\{ B_t(S_t, Q_t(i), R_t) + \alpha E_{j|i} [f_{t+1}(S_{t+1}, j)] \right\} \quad (4-9)$$

$$\forall S_t, i, \text{ and } t \in \{1, \dots, T\}$$

$$f_t(S_t, i) = B_t(S_t, Q_t(i), R_t) + \alpha f_{t+1}(S_{t+1}, i) \quad (4-10)$$

$$\forall S_t, i, \text{ and } t \in \{1, \dots, T\}$$

where equation (4-9) is the SSDP Decision Model and equation (4-10) is the SSDP Simulation Model. This is the SSDP formulation which is adopted in this study. Here  $E_{j|i}$  is computed using  $P_t[j|i]$  which is the probability of transitioning into trace  $j$  in time  $t + 1$  given the system is in trace  $i$  in time  $t$ . The computation of this probability is described in Section 4.3. Faber and Stedinger used ESP forecasts and historical inflows as SSDP scenarios, whereas this study uses only historical inflow series as scenario traces.

### ***Implementation of SDP and SSDP Policies***

The backwards recursive SDP and SSDP procedures described above provide an “optimal” policy for each system state at discrete time steps over the planning period. To develop these policies numerically the storage state space is often discretized, and the “optimal” policy is computed for each discrete state at each time.

In actual practice, the reservoir is unlikely to reside only in the discrete points which happened to have been sampled, and will more likely fall between the discrete points. One solution to this problem is to interpolate within the policy table, or to fit some simple function to that table. Another approach is *re-optimization* which selects

an optimal release given the current state by performing a one-step SDP optimization with the current reservoir conditions (Tejada-Guibert et al., 1993). Equation (4-11) describes the *re-optimization* step.

$$\max_{R_t} \left\{ B_t(S_t, Q_t, R_t) + \alpha \mathop{\text{E}}_{i|Q_t, H_t} [f_{t+1}(S_{t+1}, i)] \right\} \quad (4-11)$$

where  $H_t$  is the current hydrologic information. Tejada-Guibert et al. [1993] compared the performance of models which interpolate in the policy table to select an optimal release and models which use *re-optimization*. They found that *re-optimization* generally results in better operation, particularly when coarse grids were used in the initial backwards moving that derived the future value function. Furthermore they found that use of *re-optimization* improved the reliability of meeting both energy and water targets. It also allows for the revision of the benefit function for the current period to reflect special circumstances such as temporary fish flow or water quality requirements, or machinery that is down or inoperative due to maintenance or failures.

The SSDP model described in equations (4-9) and (4-10) is used in this study to compute the future value function, and the *re-optimization* model described in equation (4-11) is used to select a release when simulating system operation. The procedure used is described in detail in Section 4.4

### **Section 4.3 Transition Probabilities and Representations of Uncertainty**

An important consideration for the SDP, SSDP, and *re-optimization* models described in the previous section is how the expectation of future benefits should be computed. The SSDP model used in this study (equation (4-9) and (4-10)) describes

possible future events with a series of potential realizations or scenarios which might occur with corresponding probabilities. The resulting representation of uncertainty can vary greatly depending on the structure and source of the scenarios (how many are chosen, and when transitions between scenarios are considered), and the method used to assign a probability of each scenario or scenario transition. This section discusses the different transition probability cases for the SSDP and *re-optimization* models described in the previous section.

The expectation in equation (4-9) employs the probability of transitioning from scenario trace  $i$  in time  $t$  to scenario trace  $j$  in time  $t + 1$ , denoted  $P_t[j|i]$ . If one considers  $m$  potential scenarios, then the  $P_t[j|i]$  form an  $m \times m$  transition matrix whose  $(i, j)$  element is  $P_t[j|i]$ . The choice of transition matrix dictates the representation of uncertainty in the transitions in the optimization in equation (4-9).

The simplest choice of transition matrix is the identity matrix, whose elements are 1 on the diagonal and 0 otherwise. This means that transitions between scenarios are not considered, and it is equivalent to performing an independent deterministic optimization on each of the traces, which in our case are the historical series. This will be referred to as the “I” case following Faber and Stedinger, [2001].

Alternatively, if every element of the transition matrix is  $1/m$ , then every transition is modeled as being equally likely in the next time step. This will be referred to as the “M” case. This case recognizes uncertainty, but neglects any hydrologic persistence, because each scenario transition is equally likely at each step, despite how dissimilar two scenarios might be [Faber and Stedinger, 2001].

However, in some instances the “M” case is correct. For example, were one to use ESP traces as scenarios, then each scenario is initially equally likely by construction. If the “M” case is used at the time a forecast is made, it will properly represent the persistence in flow because each ESP scenario is an intact hydrograph. If the “M” case is used after the ESP forecast date then persistence will be misrepresented.

### ***Transition Probabilities based on Forecasts***

An attractive alternative to the “I” and “M” cases is to use the best available hydrologic or energy price forecast,  $F_t$ . This will be referred to as the “F” case.

Stedinger, et al. (1984) employ the “F” case by using an inflow forecast for the current time as a hydrologic state variable in their SDP model for the High Aswan Dam in Egypt (i.e.  $H_t = F_{t-1}$  in equation (4-5)). The expectation in (4-5) requires two sets of transition probabilities:

1.  $P_t(Q_t|F_{t-1})$  which is the probability of a future flow given a flow forecast.
2.  $P_t(F_t|Q_t, F_{t-1})$  which describes the evolution of forecasts given the current inflow and forecast.

Note that here  $F_t$  is the streamflow forecast of  $Q_{t+1}$ .

Kelman, et al. [1990] take a similar, Bayesian approach to the computation of the expectations in equation (4-7). The dual expectation in equation (4-7) requires two probabilities:

3.  $P_t(j, F_t)$  which is the probability of scenario trace  $j$  given a flow forecast
4.  $P_t(F_{t+1}|j, F_t)$  which describes the evolution of the forecast given the current scenario and the current forecast.

Faber and Stedinger [2001] avoid the need for a double expectation by embedding the historical forecast series in each trace as opposed to evaluating a forecast hydrologic variable at discrete points across each scenario trace (as in Kelman et al., [1990]). Kim et al. [2007], Eum et al. [2010], Vicuna et al. [2010], and Cote et al. [2011] also take the same approach as Faber and Stedinger [2001]. Because each trace has a unique inflow and forecast series, the probability of transitioning from trace  $i$  to trace  $j$  is modeled as the probability of experiencing the flow volume from trace  $j$  ( $V_{t+1}(j)$ ) given the forecast of  $V_{t+1}$  from trace  $i$ :

$$P_t[j|i] = P_t[V_{t+1}(j)|F_t(i)] \quad (4-12)$$

The probability of a flow volume  $V_{t+1}$  given forecast  $F_t$  can be computed using Bayes theorem (Faber and Stedinger,2001):

$$P_t[V_{t+1}(j)|F_t] = \frac{P[F_t|V_{t+1}(j)]P[j]}{\sum_{k=1}^m (P[F_t|V_{t+1}(k)]P[k])} \quad (4-13)$$

where  $P[F_t|V_{t+1}(j)]$  is the likelihood function (i.e. the probability of a forecast given the actual flow volume), and  $P[j]$  is the prior probability of scenario trace  $j$ , assumed to be  $1/m$  before the forecast is announced. A different prior might be used if scenarios have been combined. The likelihood function  $P[F_t|V_{t+1}(j)]$  can be obtained by regressing  $F_t(i)$  on  $V_{t+1}(i)$  [perhaps employing some transformation] for each scenario trace  $i$  and assuming normal residual error. Thus,

$$P[F_t|V_{t+1}(j)] \sim N(qf_t(V_{t+1}(j)), \sigma_\varepsilon^2) \quad (4-14)$$

where  $qf_t(V_{t+1})$  is the regression prediction  $F_t$  given  $V_{t+1}$  and  $\sigma_\varepsilon^2$  is the residual error variance. Use of a logarithmic transformation, would yield a multivariate lognormal distribution. Equations (4-12), (4-13), and (4-14) provide the needed transition

probabilities to solve the backwards recursive SSDP model in equation (4-9). For the forward-moving re-optimization step (equation (4-11)), the probability of transitioning into any trace based on the current hydrologic or market conditions is needed. In this study, this is described by a flow volume forecast  $F_1$ . The needed probability is given by

$$P_1[j|F_1] = P[V_2(j)|F_1] \quad (4-15)$$

Figure 4-3 plots  $P_t[j|i]$  for the F and M cases. The I case would be zero over all the scenario  $j$  inflows, except the inflow for scenario  $i$  where it would be 1.

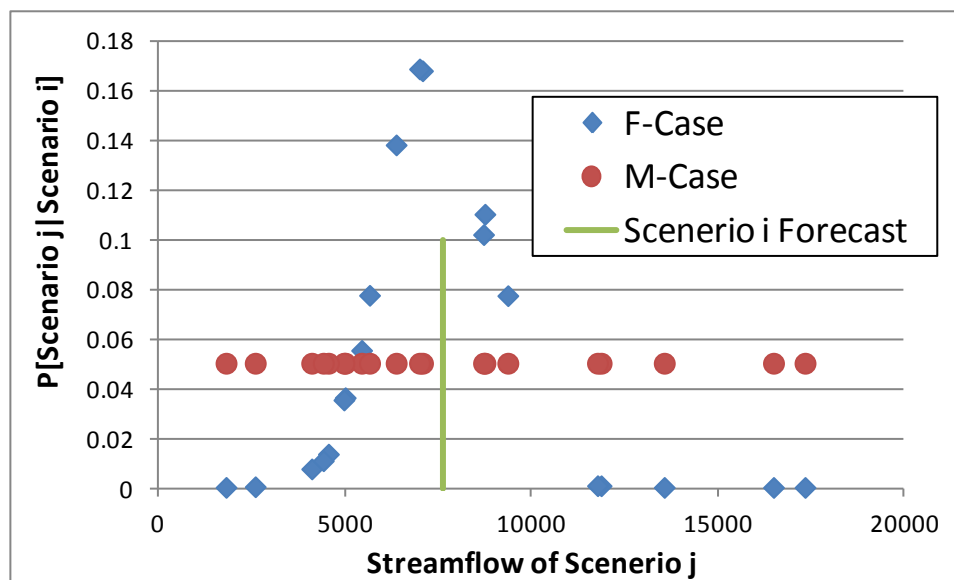


Figure 4-1: Probability of transitioning from scenario  $i$  to scenario  $j$  for the F and M cases vs. the streamflow volume in scenario  $j$

Stedinger and Kim [2010] develop a PDF ratio procedure which is designed to re-weight ESP traces given new forecast information. That procedure is both simple, is applicable to multi-variate forecasts (described in the next section), and makes fewer assumptions. The Appendix of that paper

compares the PDF ratio procedure to that proposed by Faber and Stedinger [2001] and adopted here, and finds the two approaches are identical for the normal distribution case with an informative forecast.

### ***Transition Probabilities based on Multiple Forecasts***

The previous discussion has considered use of a single forecast product, but it might be the case that multiple forecast products are available. For example, there might be an 18-hour forecast and a weekly forecast. The following discussion provides a Bayesian framework for incorporating multiple forecasts in the scenario transition probability following a procedure laid out by Faber (2001) for transition probabilities for multivariate ESP forecasts.

Each scenario now consists of a single streamflow trace that has multiple forecast for each time period considering possible streamflow volumes for different forecast durations).  $\vec{F}_t$  and  $\vec{V}_t$  are now  $l$  dimensional vectors, where  $l$  is the number of forecasts included in the analysis.  $\vec{V}_t$  represents the actual flows that occur over the specified time periods. Let  $(\vec{F}_t(i))_k$  denote the  $k^{th}$  forecast ( $k = 1, \dots, l$ ) of scenario  $i$  in time  $t$ . Likewise  $(\vec{V}_{t+1}(i))_k$  is the actual inflow volume for hydrologic scenario  $i$  over the duration of  $(\vec{F}_t(i))_k$  (e.g. 18-hours, 7-days, etc). For simplicity, the discussion will focus on the case that  $l = 2$ .

Equation (4-12) becomes

$$P_t[j|i] = P_t[\vec{V}_{t+1}(j)|\vec{F}_t(i)] \quad (4-16)$$

and the Bayesian likelihood in equation (4-14) becomes

$$P[\vec{F}_t|\vec{V}_{t+1}(j)] \sim MVN\left(\vec{q}_t(\vec{V}_{t+1}(j)), \Sigma\right) \quad (4-17)$$

where  $\vec{qf}_t(\vec{V}_{t+1}(j))$  is a 2 dimensional mean vector and  $\Sigma$  is a  $2 \times 2$  covariance matrix. Again, some transformation may be employed. As in the univariate case in equation (4-14), the parameters of the multivariate normal distribution in equation (4-17) can be estimated using regression. This is done by regressing each forecast  $(\vec{F}_t)_k$  on its corresponding  $(\vec{V}_{t+1})_k$ . It might be advantageous to include additional flow-durations as explanatory variables in the regression. For instance, one can regress  $(\vec{F}_t)_1$  or  $(\vec{F}_t)_2$  on  $(\vec{V}_{t+1})_1$  AND  $(\vec{V}_{t+1})_2$ . Whether or not this is advisable likely depends on the number of historical forecasts available, and the relative duration of the different forecasts.

Krzysztofowicz and Watada [1986], Krzysztofowicz and Reese [1991], and Krzysztofowicz [1999] provide an elegant Bayesian alternative to the regression approach taken here to describe forecast-streamflow uncertainty.

***A Special Case of Using known current inflows***

As discussed in Section 4.2, the SSDP formulation used in this study assume inflows in the present time are known (see equations (4-9) and (4-10)). Thus, one might choose to condition the transition probability on a forecast  $F_t$  AND the known current inflow  $Q_t$ . This can be computed as a special case of the multi-forecast computation discussed in this section. Equation (4-16) now becomes

$$P_t[j|i] = P_t[V_{t+1}(j)|F_t(i), Q_t(i)] \tag{4-18}$$

Note that there is only a single forecast, but the probability is now also conditioned on the current inflow. The Bayesian likelihood in equation (4-17) becomes

$$P[F_t, Q_t | V_{t+1}(j)] \sim MVN(\vec{qf}_t(V_{t+1}(j)), \Sigma) \quad (4-19)$$

To compute the elements of the two dimensional conditional mean vector

$\vec{qf}_t(V_{t+1}(j))$ , regression is used. In this case  $F_t$  is regressed on  $V_{t+1}(j)$ , and  $F_t$  is regressed on  $Q_t$ .  $\Sigma$  is estimated from the residual errors and their correlation, as demonstrated below.

### *Sample Computation for Multi-forecast Likelihood*

This section contains an example of the computation for the multi-forecast likelihood. Suppose that we wish to compute  $P_t[j|i]$  using both a forecast  $F_t$  and the current inflow  $Q_t$ . In order to compute the Bayesian likelihood in equation (4-19), we would at least regress  $F_t$  on  $V_{t+1}$  and  $Q_t$  on  $V_{t+1}$ . Let

$$X = \begin{bmatrix} \vec{1} & \vec{V}_{t+1} \end{bmatrix} \quad (4-20)$$

where  $\vec{1}$  is an  $m$  dimensional column vector of ones, and  $\vec{V}_{t+1}$  is an  $m$  dimensional column vectors containing the flow volume for the forecast duration. A linear model is assumed:

$$F = X\beta + \varepsilon \quad (4-21)$$

where  $\beta$  is a  $2 \times 1$  vector of model parameters and  $\varepsilon$  is an  $m$  dimensional vector of errors which are assumed to be normally distributed. The least-squares estimates of  $\beta$  is

$$b = (X^T X)^{-1} X^T F \quad (4-22)$$

and the associated residual error variance is

$$\sigma_e^2 = \frac{(F - Xb)^T (F - Xb)}{m - p} = \frac{e^T e}{m - p} \quad (4-23)$$

where  $e$  is an  $m$  dimensional vector of residuals, and  $p = 2$  in this case.

The model parameters  $b_1$  and  $b_2$  are then defined as

$$b_1 = (X_1^T X_1)^{-1} X_1^T \vec{F}_t$$

and (4-24)

$$b_2 = (X_2^T X_2)^{-1} X_2^T \vec{Q}_t$$

respectively. The associated residual vectors are  $e_1$  and  $e_2$  respectively, which have residual error variance  $\sigma_{e_1}^2$  and  $\sigma_{e_2}^2$  respectively (as computed using the formula in equation (4-23)). These residual error variances are combined to form  $\Sigma$  from the multivariate Bayesian likelihood in equation (4-19):

$$\Sigma = \begin{bmatrix} \sigma_{e_1}^2 & r(e_1, e_2) \sigma_{e_1} \sigma_{e_2} \\ r(e_1, e_2) \sigma_{e_1} \sigma_{e_2} & \sigma_{e_2}^2 \end{bmatrix} \quad (4-25)$$

where  $r(e_1, e_2)$  is the correlation of the residuals from model 1 and model 2. For a specific  $V_{t+1}(j)$ ,  $\vec{qf}_t(V_{t+1}(j))$  is computed as

$$\vec{qf}_t(V_{t+1}(j)) = \begin{bmatrix} b_1(1) + V_{t+1}(j) b_1(2) \\ b_2(1) + V_{t+1}(j) b_2(2) \end{bmatrix} \quad (4-26)$$

#### **Section 4.4 Proposed Algorithm Structure**

Past applications of SSDP to reservoir operation have considered seasonal or long-term planning problems with weekly time steps (Kelman et al., 1990; Faber and Stedinger, 2001; Cote et al., 2011). This work considers a seasonal planning problem (summer operations), but is concerned with short-term (sub-daily) planning. To accommodate the short-time step length, a new SSDP approach is used, as described in this section. A new approach is required because the short-time step, necessary to

capture the dynamics of the energy market, lengths no longer necessarily correspond to the time scale of the hydrologic uncertainty. This raises the question, how should uncertainty be modeled in a stochastic model to best capture hydrologic and market variability while remaining computationally efficient.

First, we make the distinction between the uncertainty time step and operational time step of the model. In SSDP, the uncertainty time step is the length of time between scenario transitions. The operational time step is the temporal resolution of the model of system operation. In most SSDP applications the operational and uncertainty time steps are the same so no distinction is needed.

In this work, the uncertainty time step changes over the course of the planning period. Specifically, a 6-hour uncertainty time step is used for the near term (the next week), and a weekly uncertainty time step is used for the long-term. Let  $u$  be the index for the near-term 6-hour uncertainty time step and  $t$  be the index for the weekly uncertainty time step.

In most SSDP applications the uncertainty and operational time steps remain constant over the planning horizon, whereas in this work the uncertainty time step changes over the planning horizon. Thus, we make the distinction between the planning horizon and the uncertainty horizon. The planning horizon is the point in time where the planning model terminates and assumes a terminal value function. The uncertainty horizon is the point in time where the uncertainty time step changes length. If the uncertainty time step is constant then no distinction is needed. Let  $T$  be the index of the planning horizon and  $U$  be the index of the uncertainty horizon.

Finally, it is necessary to define the SSDP model frequency, which is the frequency with which the SSDP model is re-run or updated. This should correspond to the frequency with which knowledge of the system becomes available. In the multi-tiered models, like the one described in this section, different parts of the same model might have different model frequencies. That is to say that one might re-run a short-term planning model every day, but only re-run a long-term planning model once per week.

The proposed SSDP algorithm has two parts: a long-term model and a short-term model. Figure 4-2 provides a diagram of the proposed SSDP model structure.

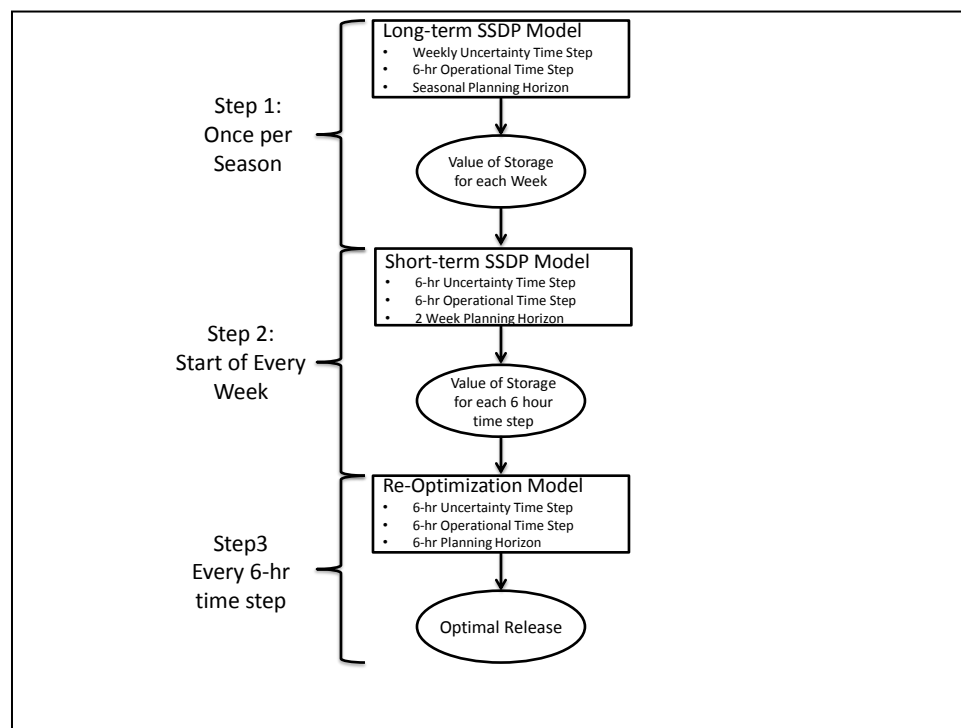


Figure 4-2: Structure of the Proposed Adaptive Time Step SSDP Model

The long-term model has a weekly uncertainty time step, a 6-hr operational time step and a 3-month planning horizon. The frequency of the long-term model is

once per 3-month planning period. Equations (4-27) and (4-28) describe the long-term model:

$$\max_{R_t} \left\{ B_t(S_t, Q_t(i), R_t + \alpha E_{j|i} [f_{t+1}(S_{t+1}, j)]) \right\} \quad (4-27)$$

$$\forall S_t, i, \text{ and } t \in \{1, \dots, T\}$$

$$f_t(S_t, i) = B_t(S_t, Q_t(i), R_t) + \alpha f_{t+1}(S_{t+1}, i) \quad (4-28)$$

$$\forall S_t, i, \text{ and } t \in \{1, \dots, T\}$$

The short-term model has a 6-hr uncertainty time step, a 6-hr operational time step, and a two week planning horizon. The frequency of the long-term model is once per week. Equations (4-29), (4-30), and (4-31) describe the short-term model:

$$\max_{R_u} \left\{ B_u(S_u, Q_u(i), R_u + \alpha E_{j|i} [g_{u+1}(S_{u+1}, j)]) \right\} \quad (4-29)$$

$$\forall S_u, i, \text{ and } u \in \{1, \dots, U\}$$

$$g_u(S_u, i) = B_u(S_u, Q_u(i), R_u) + \alpha g_{u+1}(S_{u+1}, i) \quad (4-30)$$

$$\forall S_u, i, \text{ and } u \in \{1, \dots, U\}$$

$$g_{U+1} = f_z \quad (4-31)$$

where  $z$  is the index of  $t$  corresponding to the time  $U + 1$ , i.e. two weeks from the time  $u = 1$ . Equation (4-31) is the link between the long-term and short-term models: it assures that terminal value from short-term model is provided by the future value function of the short-term model. Thus the entire algorithm can be viewed as a single SSDP model with a constant operational time step, and an adjustable uncertainty time step.

There was concern that some error might be introduced into the short-term model via the use  $f_z$  as a terminal value function because of small inconsistencies in how the short- and long-term models represent uncertainty. For example, if  $f_z$

undervalues water storage, then we would expect the short-term model to try to drain the reservoir over each planning period, resulting in a myopic ‘saw-tooth’ storage time-series. These errors were expected to be small, and to predominantly affect the end of the short-term planning horizon. As a simple solution, the short-term model is run for an extra week which is disregarded when assigning the  $g_u$  for the current week.

When simulating system performance the *re-optimization* approach described in Section 4.2 is taken:

$$\max_{R_u} \left\{ B_u(S_u, Q_u, R_u) + \alpha \mathop{\text{E}}_{i|Q_u, H_u} [g_{u+1}(S_{u+1}, i)] \right\} \quad (4-32)$$

A 6-hr time step is used in simulation, and the *re-optimization* model uses the value function from the short-term model as its terminal value.

Section 4.3 discusses transition probability cases and the computation of transition probabilities using forecasts. No real forecasts were available for this study, so a statistical procedure was developed for generating inflow volume forecasts with a specified precision and duration (discussed in Appendix). It is assumed that flow in the next 6-hours is known, so forecasts start on hour 7 and run to end of forecast duration (i.e. a 6-hour forecast duration would produce a forecast for hours 7-12). An important consideration is what forecast duration is used. Chapter 6 describes some metrics which can be used to help an analyst determine the forecast duration which is important for a given system. Through the analysis in Chapter 6 it was determined that a 24-hour forecast duration is appropriate for the hydrology of this study basin.

#### ***Section 4.4.1 Comparison of Proposed Algorithm and Past Work***

Pairing a long-term and short-term models in a single planning model

framework is not a new concept and is widely applied in practice [Yeh, 1986]. For example, Yeh [1992] used such an approach to optimize the hourly operation of a hydrothermal power system with a yearly planning horizon. That algorithm consists of a monthly model with a planning horizon of one year, a daily model with a planning horizon of one month, and an hourly model with a planning horizon of one week. The model frequencies correspond to their time step. The shorter-term models represent the system in more detail than the longer-term models (Yeh, 1992). There are many other examples [Bechard, 1981; Dudley, et al., 1973; Shelton, 1979; Vedula, et al., 1996; Vedula, et al., 1992; Wunderlich, 1979; Yeh, 1979]. The approach proposed in this section is unique for two reasons:

5. Because the same modeling approach is taken in the long- and short-term models the algorithm can be formulated as a single model.
6. The long-term model passes a value function rather than constraints to the short-term model.

The linking of models in a multi-tiered modeling approach is a non-trivial consideration. One approach is for the longer-term models to pass explicit release targets (constraints) to the shorter-term models (see Approach 1 in Figure 4-3). For example a monthly model might select an optimal release for each month, while a weekly model distributes that release within the month. Such an approach ensures that the resulting optimal policy is consistent across the models and stable through the planning horizon (i.e. not engaging in myopic behavior at model boundaries). Yeh 1992 took this approach, as have others [Bechard, 1981; Dudley, et al., 1973; Shelton, 1979; Vedula, et al., 1996; Vedula, et al., 1992; Wunderlich, 1979; Yeh, 1979]. A

potential problem with this approach is that the longer-term policy may not be optimal or even feasible in the short-term because it uses a coarser representation of the system and uncertainty.

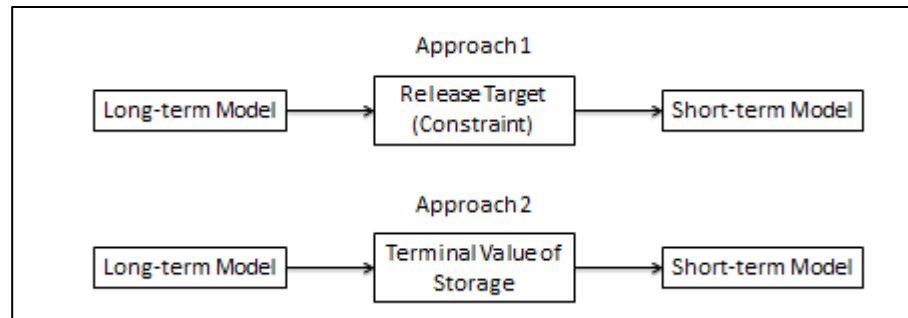


Figure 4-3: Alternative approaches to time decomposition for reservoir operations models.

A second approach is for the longer-term models to pass the terminal value of storage to the shorter-term models (see Approach 2 in Figure 4-3). This approach frees the short-term model from meeting release constraints imposed by a long-term model, potentially resulting in improved policies. This approach is closely related to stochastic dual dynamic programming (Goor, et al., 2011; Pereira, et al., 1985; Timant, et al., 2007), which relies on Bender's decomposition (discussed below).

A potential problem arises if the terminal value function provided to the short-term model is poor: the short-term model might engage in myopic behavior. For example, if a monthly model consistently underestimates the terminal value of storage at the end of each week, a nested weekly model will attempt to draw the reservoir down in each week. To avoid this it is critical that the value function of the long-term model is sufficiently accurate.

The two approaches can be understood by considering similar decompositions in linear programming. The Dantzig-Wolfe decomposition is a method for solving

large linear programming problems with a special structure. The method decomposes the original problem into a master program and independent subprograms. The master program sets parameters for the subprograms, which in turn pass their solution back to the master program (Ladson, 1970 p. 144). This is somewhat analogous to the first approach to multi-tiered modeling, in which the long-term models supply a total release volume to the short-term model. On the other hand, Benders' partitioning algorithm divides linear (or nonlinear) programming problems into two stages (Ladson, 1970 p. 370). The stage-two model can be thought of as providing a terminal value for the stage-one model. This is similar to the second approach to time decomposition, in which the long-term model passes the terminal value of storage to the short-term model.

#### ***Section 4.4.2 Representations of Uncertainty for the Proposed Algorithm***

Figure 4-1 shows an example of the transition probabilities assigned to 20 traces given the M and F transition matrix cases described above. A case must be chosen for each step of the proposed algorithm described in this section. A wide variety of representations of uncertainty can be generated by adopting different transition cases for each of the algorithm models (i.e. the long-term, short-term, and *re-optimization* models). For example, one might choose the "I" case for both the long- and short-term models, then the "M" case for the forwards *re-optimization* model. The resulting algorithm would be referred to as the I/I/M configuration. Figure 4-4 provides an example of a few uncertainty cases.

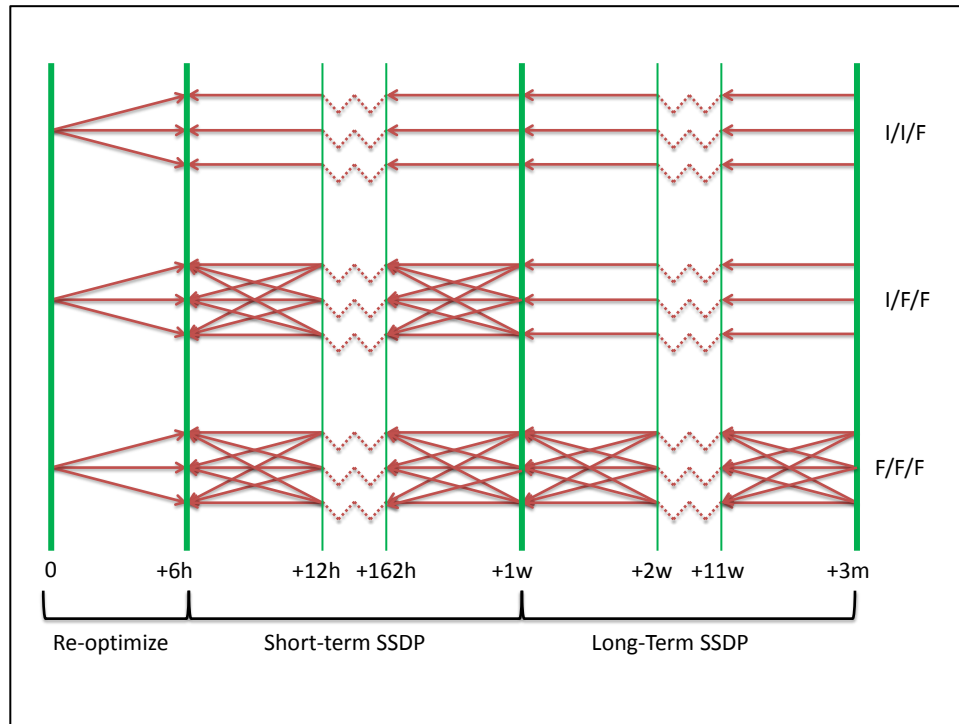


Figure 4-4: Uncertainty structures from various configurations of the time decomposition algorithm.

In the I/I/F case it is assumed that uncertainty is resolved after the immediate decision is made. This could be solved with a complex SSDP model, or with a simpler stochastic programming scheme. The I/F/F scheme considers uncertainty through the end of the current week, but then assumes that uncertainty has been resolved at the end of the current week. The F/F/F model considers uncertainty in the current week and also on a week-to-week basis.

By comparing various model configurations we can draw general conclusions on the utility of different representations of uncertainty for hydropower planning in the variable hydrology of Northern New England.

#### ***Section 4.5 Metrics for Measuring Algorithm Performance in Hydro Studies***

Many hydropower studies, including this chapter, compare the performance of different algorithms (or configurations of the same algorithm) in optimizing a study

system. The idea is to simulate system operation over a number of years or seasons using each of the candidate algorithms and to compare the results against some ideal. In the case of hydropower operation it is possible to identify a ‘*Perfect*’ operating rule by performing a deterministic DP on the simulation period. This is equivalent to the I/I case from Section 4.4. Thus, a natural metric of model performance is the *performance ratio*:

$$PR(X) = \frac{E[B(X)]}{E[B(Perfect)]} \quad (4-33)$$

where  $E[B(X)]$  is the average benefits achieved using algorithm  $X$  and  $E[B(Perfect)]$  is the average benefits from the *Perfect* decision rule.  $PR$  will range from 0 to 1; the better the algorithm performance the higher the  $PR$  will be. As is shown in 0 of this Chapter,  $PR$  is often quite high, even for unsophisticated algorithms: in some cases in 0 deterministic models achieve a  $PR > 0.9$ . The problem is that for many systems and in many seasons any reasonable policy will achieve a good performance: possible improvements will be relatively small, though not insignificant to the system owner. Thus a metric is needed which accounts for the baseline benefits which any unsophisticated policy will achieve.

To estimate this baseline performance we define run-of-river (ROR) operation. In this case it is assumed that the reservoir is held at its maximum allowable elevation and can only pass the inflow in any time period. For a reservoir with active storage this would be the most naïve but rational policy possible. For a true run-of-river (see discussion in Chapter 6) this operation will be the only possible operating policy. Having defined ROR operation, we define the algorithm *efficiency* as:

$$Eff(X) = \frac{E[B(X)] - E[B(ROR)]}{E[B(Perfect)] - E[B(ROR)]} \quad (4-34)$$

where  $E[B(ROR)]$  is the mean benefits of ROR operation over the simulation period. As shown in 0, by considering improvements over an appropriate baseline the difference between competing algorithms becomes more distinct and compelling.

Chapter 6 of this thesis describes new metrics for diagnosing reservoir behavior and classifying reservoir operating types. Two metrics which are applied here are storage days ( $ST_{days}$ ) and powerhouse days ( $PH_{days}$ ) defined as:

$$ST_{days} = \frac{V_a}{\mu_{day}} \quad (4-35)$$

and

$$PH_{days} = \frac{V_a}{V_{PH}} \quad (4-36)$$

respectively, where  $V_a$  is the reservoir active storage,  $\mu_{day}$  is the average daily inflow, and  $V_{PH}$  is the volume of water which can be passed through the powerhouse turbines in a day.  $ST_{days}$  is the number of days of average inflow the active storage can hold.  $PH_{days}$  is the number of days it would take to drain the active storage through the powerhouse turbines.

#### **Section 4.6 Test Problem**

To examine the value of various representations of uncertainty and the value of forecast precision a single reservoir test problem based is presented. This section describes the system characteristics, and the economic objective employed in the tests presented in Section 4.7.

### ***Section 4.6.1 Study Basins***

The proposed SSDP algorithm described in Section 4.4 is applied here to summer operation of a single hypothetical reservoir based on Harris Station on the Upper Kennebec River in Maine, USA. Chapter 3 describes the Kennebec River system and hydrology in more detail and Figure 4-5 provides a schematic of the hypothetical system lay-out. The total drainage area is 1365 square miles. The actual storage of Harris Station is 2.0 billion cubic feet (BCF), the actual generation capacity is 89 MW, but a wide range of system configurations are considered (see Table 4-1). This will allow the study of a wide range of ‘types’ of hydropower systems (for more discussion see Chapter 6). Figure 4-6 plots the range of  $ST_{days}$  and  $PH_{days}$  for the systems considered in this study.

In reality there are two large (mostly-storage) reservoirs upstream of Harris Station: Brassua Lake and Moosehead Lake. These are neglected from the reservoir model in order to make short-term operation of this reservoir a more interesting test case. It is assumed that the entire 1365 square miles basin produces unregulated inflow. Additionally, many operational constraints on storage usage are relaxed. It is assumed that by October 31 the system must be drawn down to meet flood storage. Operation is modeled from May 1 till the end of October. This corresponds roughly with the summer operational period in Maine.

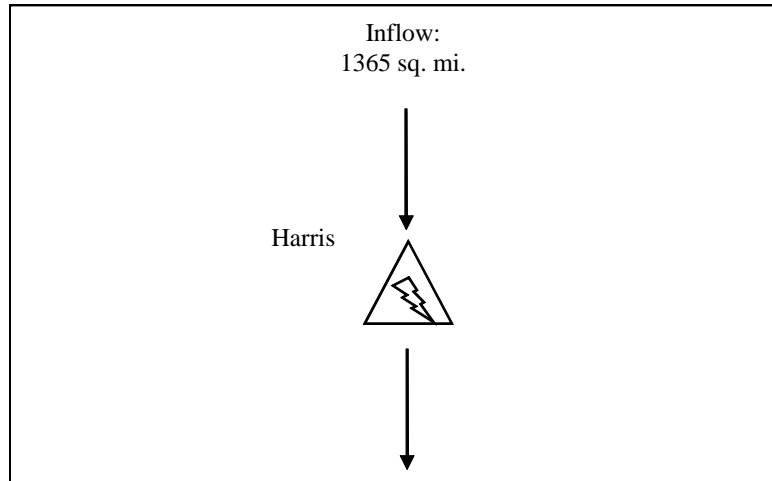


Figure 4-5: Schematic of a Hypothetical Single Reservoir System

Natural inflows were not available for any of the reservoirs on the Kennebec River, so flows were synthetically generated from a ‘reference’ record using a simple pro-ration method. This is discussed more in Chapter 3. To generate a sufficient number of scenario traces, the 20-year historical record was ‘shifted’ forward one week and back one week to generate a total of 60 ‘historical’ traces for the SSDP algorithm.

Table 4-1: Single Reservoir System Configurations

Name	Storage Capacity (BCF)	Turbine Capacity (cfs)
(Small, 2000)	1.97	2000
(Mid, 2000)	9.85	2000
(Big, 2000)	19.70	2000
(Small, 3500)	1.97	3500
(Mid, 3500)	9.85	3500
(Big, 3500)	19.70	3500
(Small, 5000)	1.97	5000
(Mid, 5000)	9.85	5000
(Big, 5000)	19.70	5000
(Small, 8300)	1.97	8300
(Mid, 8300)	9.85	8300
(Big,8300)	19.70	8300

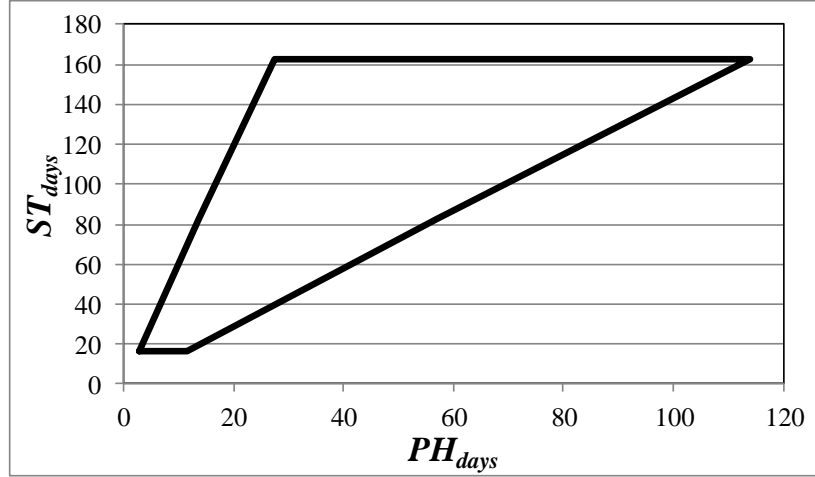


Figure 4-6: Range of the  $ST_{days}$  vs.  $PH_{days}$  of the test systems considered.

#### Section 4.6.2 Economic Objective

The system operational objective is to maximize revenue:

$$\max_{R_t} \left\{ \sum_{t=1}^T B_t \right\} \quad (4-37)$$

where the incremental benefit in each time,  $B_t$  is a function of  $R_t$ , the current and next time period's reservoir storage,  $S_t$  and  $S_{t+1}$  respectively, and the energy price profile in the present time. A time step of 6-hours is considered here. The incremental benefits are computed as:

$$B_t = \frac{\alpha R_t [0.5(\Delta H(S_t, R_t) + \Delta H(S_{t+1}, R_t))]}{\zeta} \times PP_t(R_t, S_t), \quad R_t \geq 140 \frac{ft^3}{s} \quad (4-38)$$

$$B_t = 0, \quad \text{otherwise}$$

where  $\alpha$  is an efficiency factor,  $\zeta$  is a unit conversion factor,  $\Delta H$  is the net head which is a function of storage and release, and  $PP_t$  is the integral of the energy price profile, which is computed as:

$$PP_t = \int_0^{P_t} Price_t(p) dp = cP_t + (a/b) \sin(bP_t) \quad (4-39)$$

where  $a$  and  $b$  and  $c$  are parameters of the price model,  $P_t$  is the generation in time  $t$ , and  $Price_t$  is the price profile:

$$Price_t(P_t) = c + a\cos(bP_t) \quad (4-40)$$

$Price_t$  varies continuously between  $(c + a)$  and  $(c - a)$  as a function of the power generated  $P_t$ . Figure 4-7 plots  $Price_t$  versus  $P_t$ . This model does not imply that the hypothetical one reservoir system can affect price, which would be unreasonable.

Rather, this model reflects the fact that system operators will spread generation across the highest price hours first and will only generate during the lowest price hour in any time step if it is necessary or economically beneficial to do so. Thus, rather than assuming a constant release over the period, we assume the operators will start by generating only in the highest price hours.

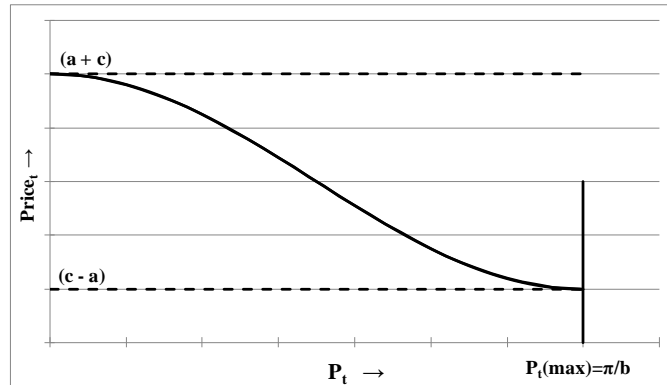


Figure 4-7: Price profile versus generation

The real Kennebec hydropower system is part of the ISO New England market. In that market prices vary throughout the day and across days. Two price schemes are considered in the following runs. To isolate the effect of hydrologic processes on the system a ‘mean price’ scheme is used. In this case each day is divided into three ‘on-peak’ periods and one ‘off-peak’ period. Every ‘on-peak’ period has the same price

parameters  $a$ ,  $b$ , and  $c$  and each ‘off-peak’ period has the same price parameters  $a$ ,  $b$ , and  $c$ . Price variability is important to the operation of the real system, so a ‘real price’ scheme is also used. In this case each time period has a unique  $a$ ,  $b$ , and  $c$  based on real day-ahead price data from New England ISO.

A price profile is developed for each 6-hour period over the planning period. Each day therefore consists of four 6-hour timesteps. As explored in Chapter 6, there is a distinct diurnal cycle in the energy price signal, corresponding to ‘on-peak’ and ‘off-peak’ prices. This cycle is reflected in both the ‘mean price’ and ‘real price’ schemes. For the ‘mean price’ scheme in each day there are three ‘on-peak’ periods with the same price profile and one ‘off-peak’ period with a price profile. These profiles are the same each day. In the ‘real-price’ scheme the price profiles are selected based on New England ISO price data associated with each simulation period.

### ***Section 4.6.3 Rule Curve Operation***

This research focuses on the benefit of forecast precision and representations of uncertainty. A valid question is whether uncertainty need be considered at all: would a deterministic optimization approach perform as well as the stochastic approach? To address this questions, we define rule curve operation (RCO). In RCO a deterministic DP is run on the mean of the historical traces, then an actual release is chosen for each stage of each trace using *re-optimization* (see Figure 4-8). This implicitly provides a rule curve in that for each time-step and for each reservoir storage state, there is a deterministic rule which provides an optimal decision. The RCO algorithm is a reasonable deterministic approach to compare against the stochastic algorithm described in Section 4.4.

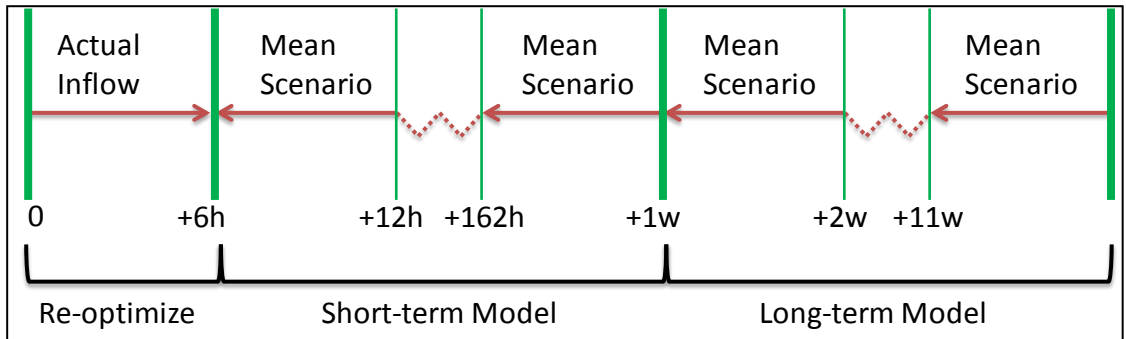


Figure 4-8: Structure of the RCO algorithm

#### **Section 4.7 Results and Discussion**

To study the utility of various representations of uncertainty to hydropower operations optimization, the operation of the systems described in Section 4.6.1 was simulated over 60 summer seasons of operation using various configurations of the algorithm described in Section 4.4.

A second research question is how the precision of forecasts affects the utility of different model configurations. To examine this, the system operation is simulated using forecasts with varying precision. These forecasts are generated using the procedure described in the Appendix of this chapter.

A third research question is how the relative size of the turbine and storage capacity affects the answers to the first two research questions. This might be viewed as comparing different systems, or representative of the same system but with different seasonal hydrology.

To address these three questions, for both the ‘mean price’ and the ‘variable price’ schemes the following runs were completed for each of the 12 hypothetical systems in Table 4-1.

The I/I/I runs represent operation with “perfect” foresight and will be a benchmark for measuring algorithm performance. By comparing I/I/F runs with I/F/F and

F/F/F runs with the same forecast precision and duration we can explore how the representation of uncertainty resolution affects simulated system performance. By comparing I/I/F models or F/F/F models with varying precision but fixed duration, we can explore the value of forecast precision to system operation. Comparing the performance of each algorithm configuration on different system configurations will allow more general conclusions to be drawn about the value of forecast precision for different types of hydropower systems.

Table 4-2: Proposed runs for Time Decomposition Model

	Forecast Precision	Price Scheme
I/I/I	-	Mean, Variable
I/I/M	-	Mean, Variable
I/I/F	75, 85, 95	Mean, Variable
I/M/M	-	Mean, Variable
I/F/F	75, 85, 95	Mean, Variable
M/M/M	-	Mean, Variable
M/F/F	75, 85, 95	Mean, Variable
F/F/F	75, 85, 95	Mean, Variable
RCO	-	Mean, Variable

### ***Mean Price Scheme***

Each algorithm described in Table 4-2 was run for each system model in Table 4-1 for the mean price scheme. A full table containing these results is provided in the Appendix of this chapter. Figure 4-9 plots the *PR* of each algorithm considered for the (Big, 8300) system configuration for the mean price scheme. Incredibly, ROR operation achieves a *PR* of about 0.84. This is because with large turbine capacity the reservoir rarely spills. This suggests that the room for improvement in for this system (Big, 8300) is relatively small, and will mostly come from shifting generation into the

‘on-peak’ periods. Improvements are not easily observed from *PR* in such cases.

Figure 4-10 plots the *Eff* for the same algorithms and system.

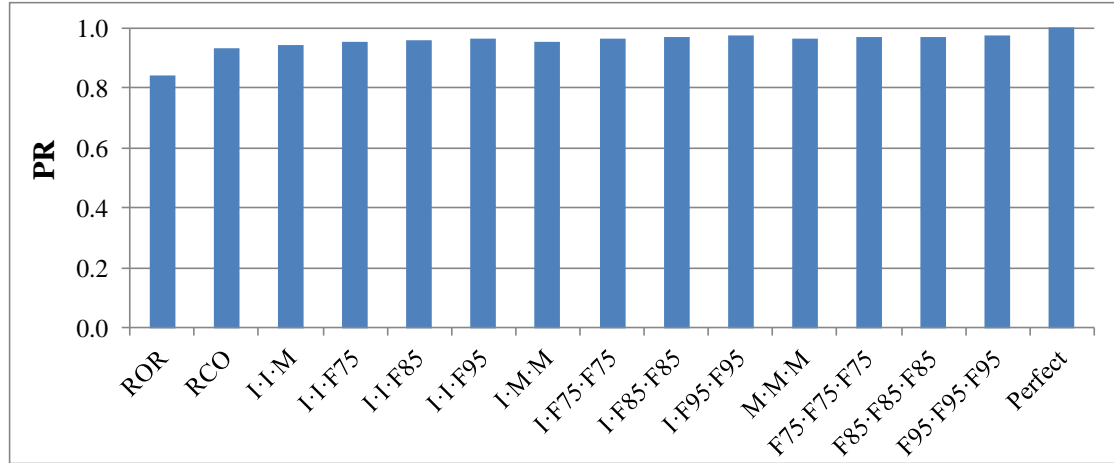


Figure 4-9: PR for (Big, 8300) system for various algorithms, mean price scheme.

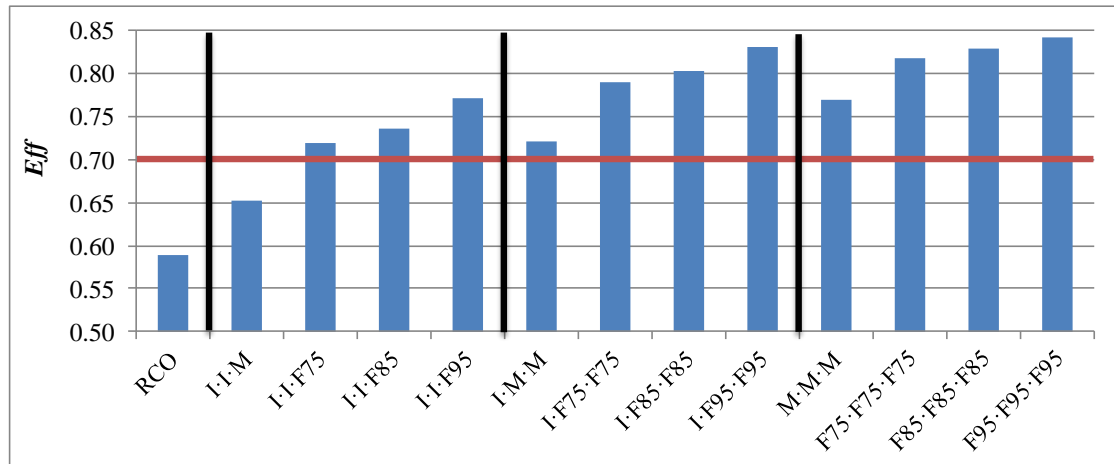


Figure 4-10: *Eff* for (Big, 8300) system for various algorithms, mean price scheme.

When the ROR baseline is removed, the differences in algorithm performance become more apparent. Figure 4-11 plots the *Eff* for a variety of runs, with a fixed storage (Big) and varying turbine capacity. Note that as turbine capacity increases, the efficiency decreases. This is because as the turbine capacity increases, the ROR operational run spills less and the room for improvement becomes smaller.

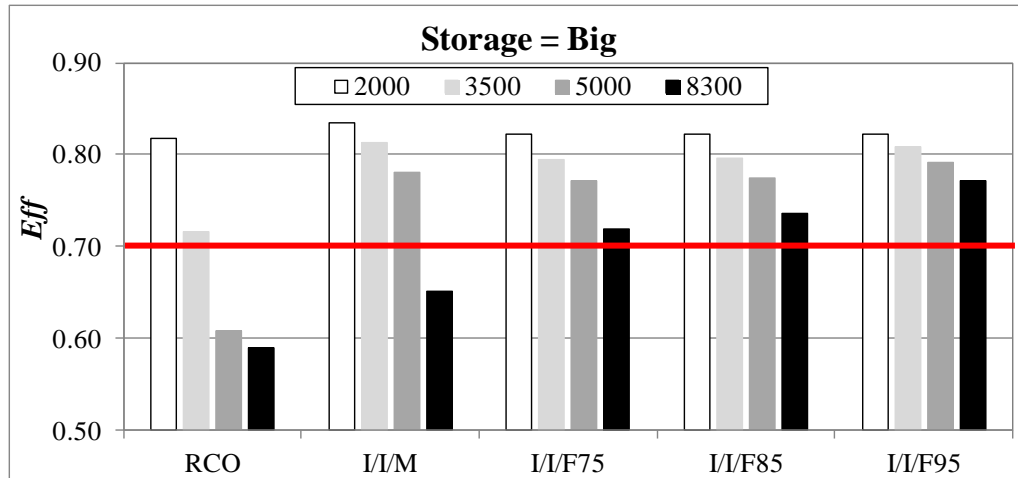


Figure 4-11:  $Eff$  for Big reservoirs with varying turbine capacity for various algorithms, mean price scheme.

The groupings (besides RCO) in Figure 4-11 correspond to the same algorithm, but with increasing information about the next day's flow (i.e. higher forecast precision). Interestingly, the efficiency of the systems with smaller turbine capacity (2000, 3500, 5000) are essentially unaffected by the precision of the forecast. In contrast the performance of system (Big, 8300) improves with increasing forecast precision. When the turbines are small, the reservoir is relatively constrained and is limited in how much it can shift across days.

Figure 4-12 plots the (Big, 8300) results from Figure 4-11. Compare the I/I/M case to the I/I/F75 case. By employing a poor forecast the efficiency is raised from 0.65 to 0.72. Furthermore as the precision of the forecast increases, so too does the algorithm efficiency, and a paired t-test (which is reported in Table 4-3) shows that the improvements are statistically significant. These results are typical of all the algorithms tested on system (Big, 8300); i.e. improvement in forecast precision at any stage of the algorithm described in Section 4.4 precipitates a statistically significant improvement in system operational efficiency.

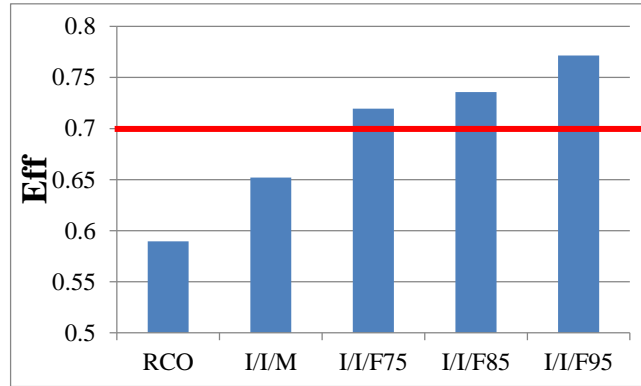


Figure 4-12: *Eff* for (Big, 8300) system for select algorithms, mean price scheme

Table 4-3: P-values of a two-sided paired t-test of the difference between the simulated benefits of several algorithms on the (Big, 8300) system.

	I/I/F75	I/I/F85	I/I/F95
I/I/M	0.004	0.002	0.000
I/I/F75		0.000	0.000
I/I/F85			0.000

The finding that efficiency decreases with increased turbine capacity was shown across the range of storages considered in this study, as shown in Figure 4-13 and Figure 4-14. As the storage capacity becomes smaller, the efficiency of systems with smaller turbine capacity becomes sensitive to *re-optimization* forecast precision. For example, the efficiency in system (Small, 3500) significantly (statistically) improves with increased forecast precision. However, the efficiency of system (Mid, 3500) does not improve (statistically) with increased *re-optimization* forecast precision.

To more clearly understand the role storage has on efficiency, Figure 4-15 plots efficiency for various optimization model configurations for systems with different storages, but with a fixed turbine capacity. Note that as storage increases, so

too does efficiency. This was true across a wide range of algorithm configurations tested.

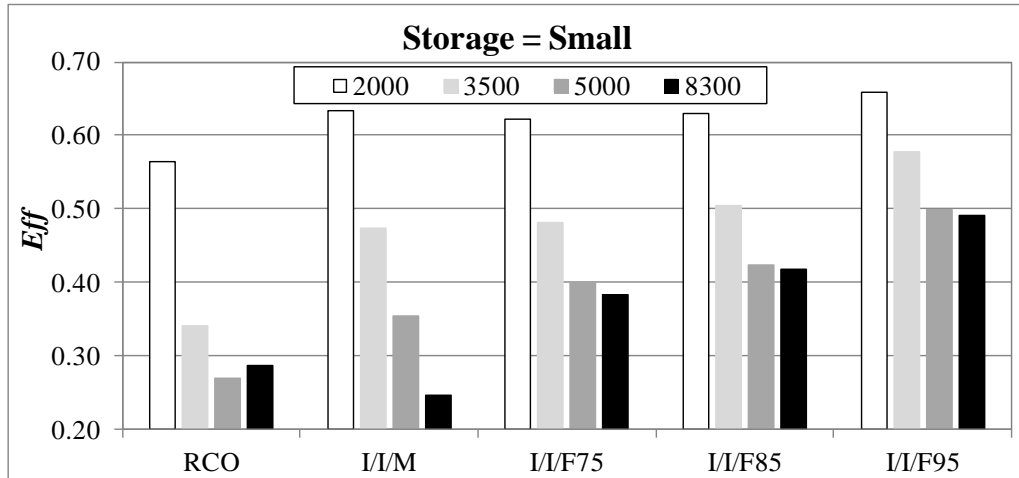


Figure 4-13: *Eff* for Small reservoirs with varying turbine capacity for various re-optimization forecast precision, mean price scheme.

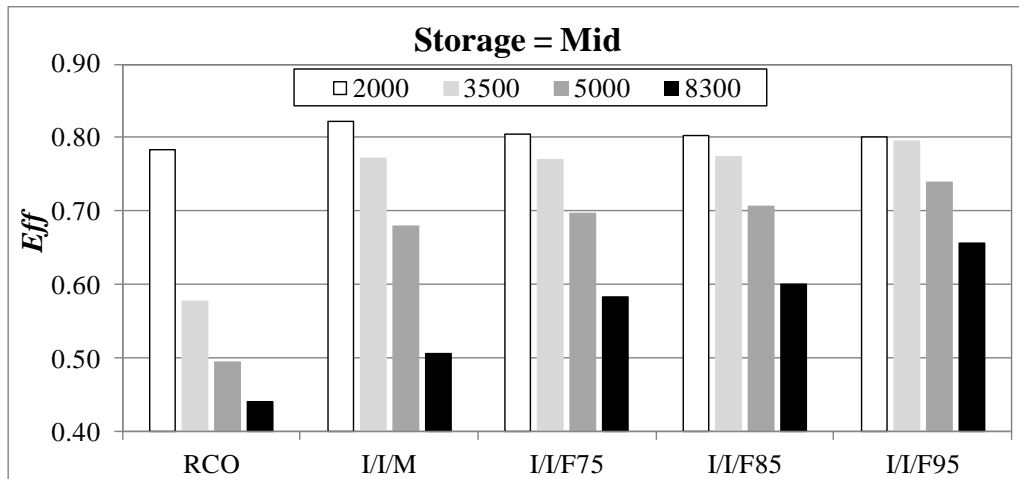


Figure 4-14: *Eff* for Mid reservoirs with varying turbine capacity for various re-optimization forecast precision, mean price scheme.

The efficiency increases with reservoir storage because larger reservoirs have greater operational flexibility to absorb high flows and shape releases to generate ‘on-peak.’ As storage becomes smaller, the system has less flexibility. If a reservoir had no storage then it would be ‘run-of-river’ and there would be no opportunity to

improve operations (i.e.  $Eff$  would be zero). Efficiency was found to increase with storage in every system tested. Plots like Figure 4-15 for other storages are available in the Appendix of this chapter.

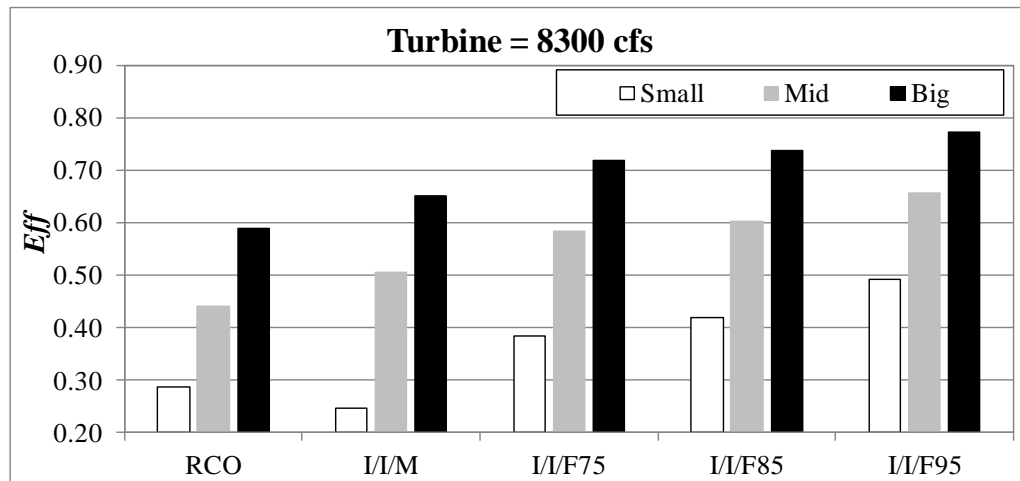


Figure 4-15:  $Eff$  for Turbine Capacity (8300 cfs) with varying storage for various algorithms, mean price scheme.

Having explored how the relative size of the turbine and storage capacity can affect the algorithm *efficiency* and the effect of *re-optimization* forecast precision, we look closer at how uncertainty should be modeled. One expects that increased uncertainty model sophistication should improve model efficiency. In their single-reservoir example in Colorado, Faber and Stedinger [2001] found that a simple two-stage model performed as well as more sophisticated multi-stage models. We expand that analysis here by considering a wide range of system configurations.

First, we must describe more thoroughly what we mean by uncertainty model sophistication. The least sophisticated model is I/I/M. This model has only a single branching point, and makes no use of forecast information. Slightly more sophisticated are the I/M/M and M/M/M models. While these models do not use forecast precision, they do recognize uncertainty (through scenario transitions) after

the end of the current time step. The I/I/F model is considered more sophisticated than the M models because it uses forecast information about future hydrologic conditions. The I/F/F model is more sophisticated because it also uses forecast information, but considers uncertainty (through scenario transitions) through the end of the current week. Finally, the F/F/F model is the most sophisticated model considered. One expects that the model efficiency should be non-decreasing with increased uncertainty model sophistication:

$$Eff(I/I/M) \leq Eff(I/I/F) \leq Eff(I/F/F) \leq Eff(F/F/F)$$

First, consider the effect of uncertainty model sophistication on the (Big, 8300) system which has both large storage and turbine capacity. Figure 4-16 plots the *efficiency* of select algorithms with increasing uncertainty model sophistication. Note that in this case increased uncertainty model sophistication always results in improved efficiency (F/F/F efficiency is greater than I/F/F efficiency using paired t-test with  $\alpha = 0.1$ ).

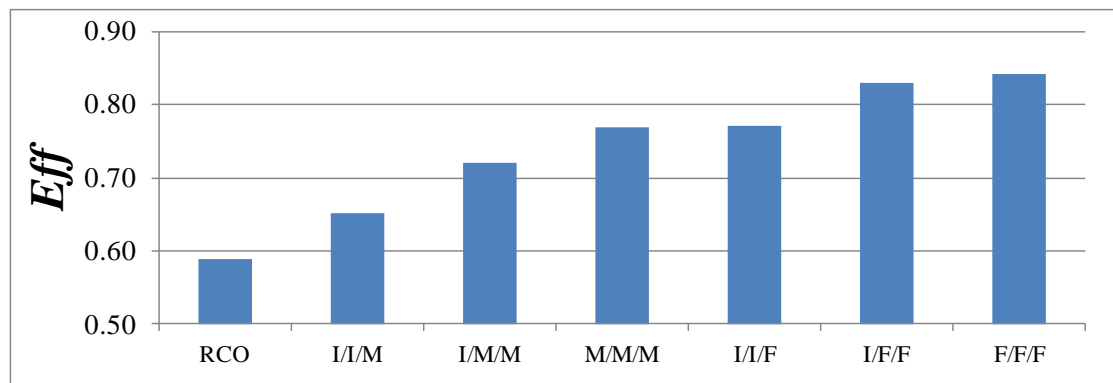


Figure 4-16: *Eff* of uncertainty models with increasing sophistication, for system (Big, 8300) and forecast precision  $R^2 = 0.95$ , ‘mean price’ scheme.

This result is by no means universal across the systems considered. As a counter example consider the system (Big, 3500), which has large storage capacity but

only moderately sized turbines. Figure 4-17 plots the efficiency of different algorithms utilizing increasing levels of uncertainty model sophistication. Note that in this case, increased sophistication does not always result in improved *efficiency*, in fact there is no statistical difference between the efficiency of I/I/M and F/F/F using a paired t-test with  $\alpha = 0.1$ .

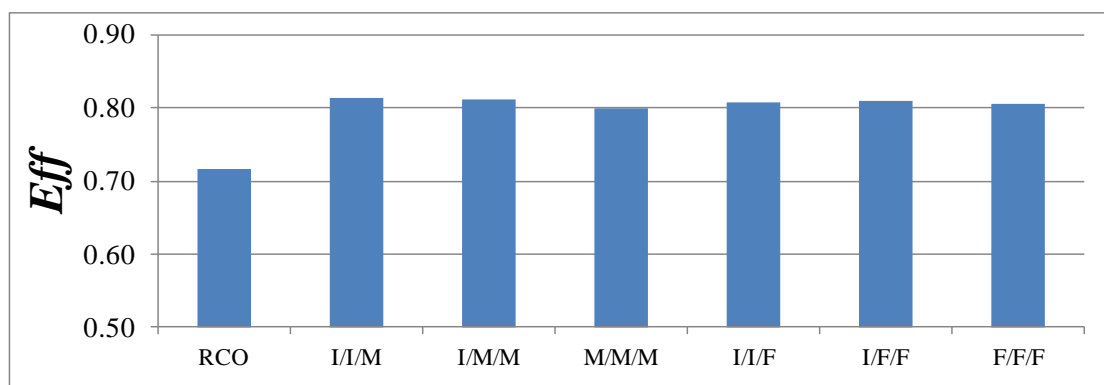


Figure 4-17: *Eff* of uncertainty models with increasing sophistication, for system (Big,3500) and forecast precision  $R^2 = 0.95$ , ‘mean price’ scheme.

These are just two examples, but 12 different systems were considered in this analysis. To understand trends across different systems Figure 4-18 reports the least sophisticated model which matched the performance of the most sophisticated F/F/F model. To generalize the results, they are plotted in terms of  $ST_{days}$  and  $PH_{days}$ .

Recall that points in the upper right corner (high  $ST_{days}$  and high  $PH_{days}$ ) correspond to systems with large reservoir storage and small turbines. We see that unsophisticated models which make no use of forecasts perform as well as sophisticated F/F/F models. This makes intuitive sense: with large storage the system is able to absorb most inflows so spilling is not a great concern except in very large storm events. Forecasts don’t help in those events because it takes so long to draft enough for large storms with small turbines that it is actually more optimal to

occasionally spill than to operate at reduced head. As the turbines get larger this is not true: the system is able to rapidly draft to make room, so it is no longer optimal to spill occasionally for large events.

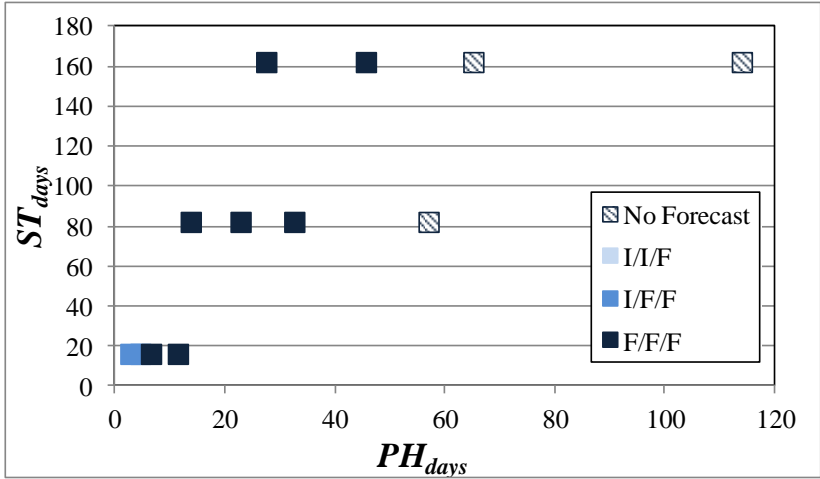


Figure 4-18: Least sophisticated uncertainty model which matches the *Eff* of sophisticated F/F/F uncertainty model, ‘mean price’ scheme, forecast precision  $R^2 = 0.95$ .

Over a wide range of  $ST_{days}$  and  $PH_{days}$  the most sophisticated uncertainty models results in the best *efficiency*, but this is not the case for a few systems in the lower left of Figure 4-18. Points in the lower left of the plot (low  $ST_{days}$  and low  $PH_{days}$ ) correspond to systems with small storage and large turbine capacity. In this case considering uncertainty on a week-to-week basis doesn’t help. The storage for these systems is not large enough for over-week planning, and the turbines are large enough so that spilling is almost never a concern.

**Variable Price Scheme**

The previous discussion focused on the ‘mean price’ scheme in which the price of energy varied within each day, but the price profile was identical for each day. This allowed the previous section to focus on the value of hydrologic forecasts and

representations of uncertainty in the presence of solely hydrologic uncertainty. In the ‘variable price’ scheme the price profile varies from day to day. This variability is not explicitly accounted for in the computation of transition probabilities, though Section 4.3 describes how one might do so. However, the price uncertainty is embedded in the computation of the future value function: each historical scenario includes both a price profile series and a reservoir inflow series.

The introduction of variable prices can potentially change how the system operates. Before there was no preference between on peak generation on one day or another, but now it is potential beneficial to store water for days to generate on a future high price day. The ability of a reservoir system to do this will depend on the size of storage relative to the turbine capacity. Figure 4-19 plots the *efficiency* for various algorithm configurations and turbine capacities with fixed storage capacity (Big).

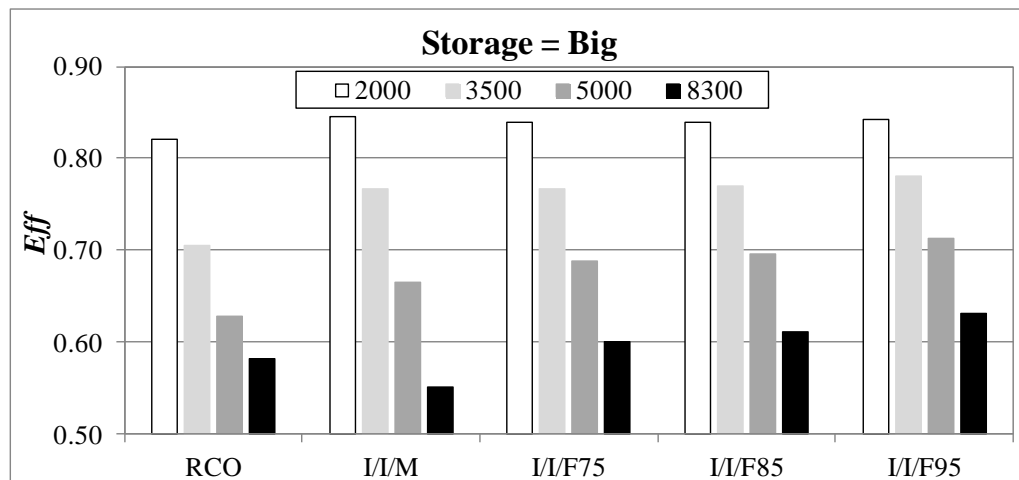


Figure 4-19: *Eff* for Mid reservoirs with varying turbine capacity for various re-optimization forecast precision, variable price scheme.

The *efficiency* falls much more dramatically with increased turbine capacity than in the ‘mean price’ case. In fact, the ‘variable price’ efficiency of nearly every

algorithm has decreased compared to ‘mean price’ efficiency. This is primarily because the ‘Perfect’ algorithm is able to exploit the variable prices to generate significantly more benefit. For every single system configuration the mean benefits over the simulation period increased in the ‘variable price’ scheme compared to the ‘mean price’ scheme. This causes the efficiency relative to ROR operation to decrease for nearly every stochastic algorithm tested. The notable exception is the system (Big, 2000), which has a large storage but a small turbine capacity. The turbines in that case are small enough compared to the storage that the system is unable to put much more on peak than it was in the ‘variable price’ scheme. As a result the mean benefits increased only slightly, and the efficiencies between the two price schemes are nearly the same.

Figure 4-20 plots the *efficiency* for various algorithms for a fixed turbine capacity but varying storage capacities. As storage increases, so does the efficiency. This is because the greater the storage, the longer the system is able to hold flows and release on-peak, and during high price days.

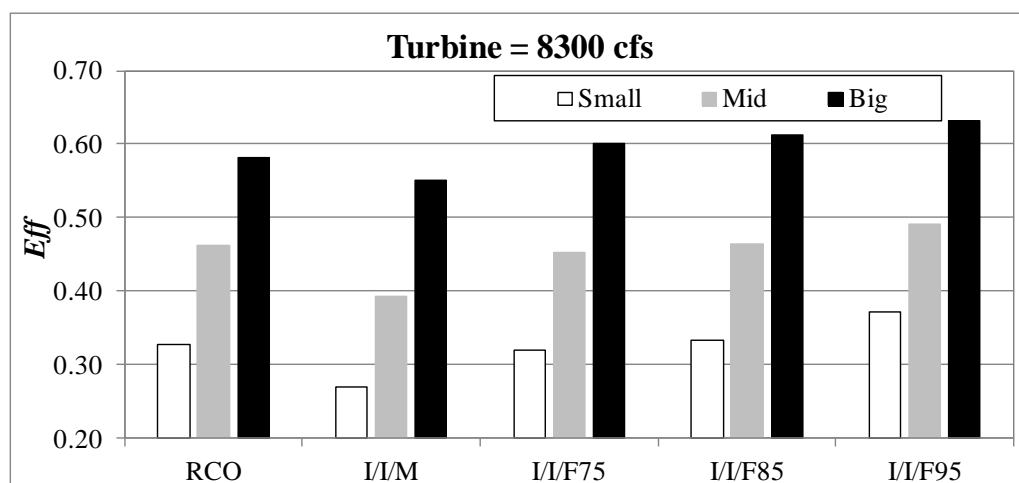


Figure 4-20: *Eff* for Turbine Capacity (8300 cfs) with varying storage for various algorithms, variable price scheme.

As one would expect from Figure 4-19 and Figure 4-20, the most efficient operating policy is achieved by the largest reservoir with the smallest turbine capacity (Big, 2000). The least efficient operating policy is achieved by the system with the smallest storage and the biggest turbines (Small, 8300).

Figure 4-21 plots several algorithm configurations for the system (Big, 8300). Unlike in the ‘mean price’ scheme plotted in Figure 4-12, we now find that the deterministic RCO algorithm outperforms the stochastic model without forecasts (I/I/M), so in this case a deterministic model performs better than a naïve stochastic model. This is because the RCO algorithm operates under the assumption that the next period will be average. At most times during summer operation this is a reasonable approach: if nothing else it will avoid getting into trouble. On the other hand, the I/I/M algorithm assumes that any scenario in the next time period is equally likely: be it normal hydrology, flood, or drought. As a result the I/I/M algorithm behaves too conservatively and is unable to exploit the occasional high price spikes.

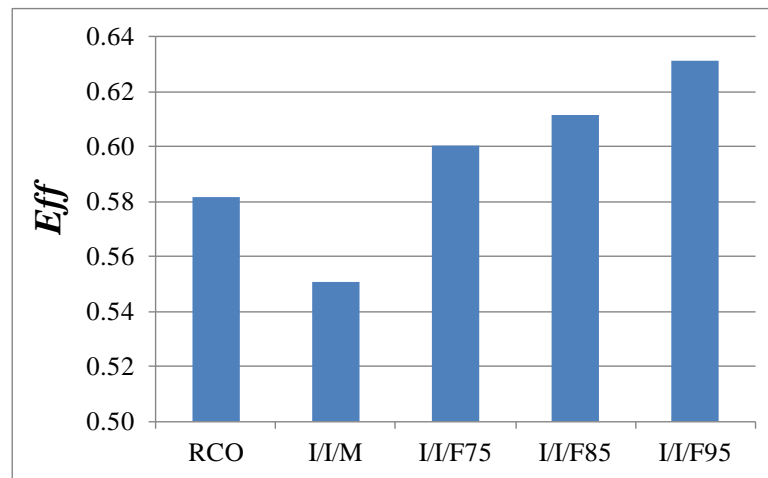


Figure 4-21: *Eff* for (Big, 8300) system for several algorithms, variable price scheme.

For every algorithm configuration applied to the (Big, 8300) system it was found that increasing forecast precision increased the operational efficiency. Furthermore, it was found that incorporating forecast information into each stage of the algorithm (i.e. F/F/F models) outperformed simpler models which did not consider uncertainty transitions past the current day or the current week. This result is consistent with the finding for the ‘mean price’ scheme.

However, unlike the mean price scheme it was found that the use of forecasts and stochastic models did not always improve operation. For example consider the system (Small, 2000), which has very small storage and turbine capacity. In this case, there is no statistical difference between the deterministic model and the two-stage branching model (I/I/F) (see Figure 4-22). Thus we are unable to determine if forecasts improve performance. Furthermore, the deterministic model achieves a higher operational efficiency than many models which use lower precision forecasts.

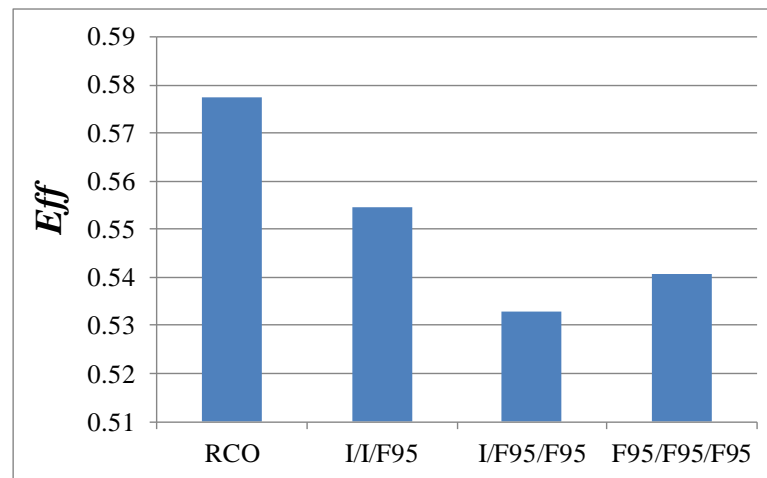


Figure 4-22: *Eff* for (Small, 2000) system for several algorithms, variable price scheme.

To obtain a broader understanding of how uncertainty model sophistication affects the *efficiency* of system performance Figure 4-23 reports the least sophisticated

model which matches the performance of the sophisticated F/F/F model. Again to be more general the results are reported in terms of  $ST_{days}$  and  $PH_{days}$ .

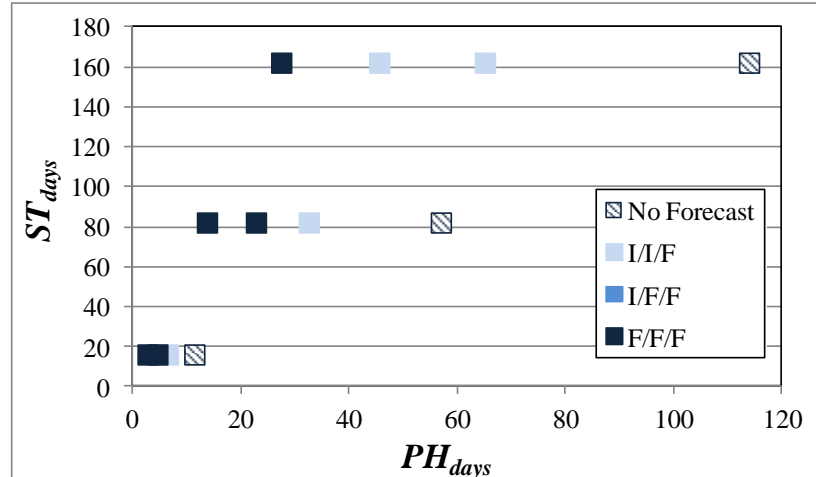


Figure 4-23: Least sophisticated uncertainty model which matches the  $Eff$  of sophisticated F/F/F uncertainty model, ‘variable price’ scheme, forecast precision  $R^2 = 0.95$ .

We now see that uncertainty model sophistication is most beneficial for systems with large turbines (points roughly to the left side of the plot in Figure 4-23). As the turbines become smaller relative to the storage (to the right and top of Figure 4-23) the less model sophistication is needed to match the performance of the most sophisticated F/F/F model. For a wide range of systems with mid-sized turbine capacities, I/I/F models match the performance of the more sophisticated F/F/F model, confirming the finding of Faber and Stedinger [2001].

#### Section 4.8 Summary and Conclusions

This chapter introduced an SSDP algorithm for optimizing short-term hydropower operation. This model is unique in that it makes the distinction between the operational time step and the uncertainty time step. This distinction is needed because unlike most SSDP models, the uncertainty time step in the proposed algorithm changes over the planning horizon. This allows the generalization of the SSDP model

to accommodate a wide array scenario trees which provide diverse representations of uncertainty.

This SSDP algorithm is leveraged to answer three research questions. First, what is the utility of various representations of uncertainty? Second, what is the value of forecast precision to hydropower operations? And third, how do the answers to the first two questions depend on the characteristics of the system under study.

To explore each of these questions the operation of a number of hypothetical reservoir systems is simulated over 60 summer operating periods. Two economic models were used: one with a constant energy price profile for each day and one with a variable energy price profile.

To answer the first question a number of SSDP models with varying levels of uncertainty sophistication were used to optimize each of the reservoir systems' operation over the simulation period. It was found that for the 'mean price' scheme very unsophisticated uncertainty models, which do not utilize forecasts match the *efficiency* of the most sophisticated models for systems with large storage, but small turbines. For most other systems in the 'mean price' scheme, increased uncertainty model sophistication always results in improved *efficiency*. For the 'variable price' scheme it was found that simple 'two-stage' stochastic models match the performance of more sophisticated dynamic uncertainty models for systems with mid-sized turbines over a range of system storage sizes. It was found that when turbines were large that increased uncertainty model sophistication always resulted in increased *efficiency*. As in the 'mean price' scheme, when storage is large and turbines are small, then very

unsophisticated models which use no forecasts match the performance of the more sophisticated uncertainty models.

It was found that improved forecast precision generally improved algorithm performance, though it was found that as turbine size becomes smaller the efficiency of the optimization algorithm is less sensitive to the precision of the forecast. This is particularly true for reservoirs with large storage, and in the ‘variable price’ case.

Finally it was found that algorithm efficiency is generally very low for the ‘variable price’ case compared to the ‘mean price’ case. This is partially because there is now an added layer of uncertainty and partially because the *Eff* is distorted by an improvement in the ‘perfect’ model performance. Future studies should consider incorporating price forecast information into the computation of scenario probabilities, as described in this chapter.

## REFERENCES

- Aggarwal, S.K., Saini, L.M. & Kumar, A. 2009, "Electricity price forecasting in deregulated markets: A review and evaluation", *Electrical Power and Energy Systems*, vol. 31, pp. 13.
- Bechar, D. 1981, "The Ottawa River regulation modeling system (ORRMS)", *Proceedings of the International Symposium on Real-Time Operation of Hydrosystems*.
- Cote, P., Haguma, D., Leconte, R. & Krauc, S. 2011, "Stochastic Optimization of Hydro-Quebec hydropower installations: a statistical comparison between SDP and SSDP methods", *Canadian Journal of Civil Engineering*, vol. 38, no. 12, pp. 1427-1434.
- Dudley, N.J. & Burt, O.R. 1973, "Stochastic Reservoir Management and System Design for Irrigation", *Water Resources Research*, vol. 9, no. 3, pp. 507-522.
- Eum, H., Kim, Y. & Palmer, R.N. 2011, "Optimal Drought Management Using Sampling Stochastic Dynamic Programming with a Hedging Rule", *Journal of Water Resources Planning and Management*, vol. 137, no. 1.
- Faber, B.A. 2001, *Real-Time Reservoir Optimization Using Ensemble Streamflow Forecasts*, PhD edn, Cornell University, Ithaca, NY.
- Faber, B.A. & Stedinger, J.R. 2001, "Reservoir optimization using sampling SDP with ensemble streamflow prediction (ESP) forecasts", *Journal of Hydrology*, vol. 249, pp. 113-133.
- Fernandez, A., Blumsack, S. & Reed, P.M. 2012, "Evaluating wind-following and ecosystem services for hydroelectric dams in PJM", *Journal of Regulatory Economics*, vol. 41, pp. 139.
- Goor, Q., Kelman, R. & Tilmant, A. 2011, "Optimal Multipurpose-Multireservoir Operation Model with Variable Productivity of Hydropower Plants", *Journal of Water Resources Planning and Management*, vol. 137, no. 3, pp. 258-267.

- Grygier, J.C., Stedinger, J.R. & Yin, H. 1989, "A Generalized Maintenance of Variance Extension Procedure for Extending Correlated Series", *Water Resources Research*, vol. 25, no. 3, pp. 345-349.
- Hejazi, M.I., Cai, X.M. & Ruddell, B.J. 2008, "The role of hydrologic information in reservoir operation – Learning from historical releases", *Advances in Water Resources*, vol. 31, pp. 1636-1650.
- Karamouz, M. & Vasiliadis, H.V. 1992, "Bayesian Stochastic Optimization of Reservoir Operation Using Uncertain Forecasts", *Water Resources Research*, vol. 28, no. 5, pp. 1221-1232.
- Kelman, J., Stedinger, J.R., Cooper, L.A., Hsu, E. & Yuan, S. 1990, "Sampling stochastic dynamic programming applied to reservoir operation", *Water Resources Research*, vol. 26, no. 3, pp. 447-454.
- Kim, Y., Eum, H., Lee, E. & Ko, I. 2007, "Optimizing Operational Policies for a Korean Multireservoir System using Sampling Stochastic Dynamic Programming with Ensemble Streamflow Prediction", *Journal of Water Resources Planning and Management*, vol. 133, no. 1, pp. 4-14.
- Kim, Y. & Palmer, R.N. 1997, "Value of Seasonal Flow Forecasts in Bayesian Stochastic Programming", *Journal of Water Resources Planning and Management*, vol. 123, no. 6, pp. 327-335.
- Krzysztofowicz, R. 1999, "Bayesian theory of probabilistic forecasting via deterministic hydrologic model", *Water Resources Research*, vol. 35, no. 9, pp. 2739.
- Krzysztofowicz, R. & Reese, S. 1991, "Bayesian Analyses of Seasonal Runoff Forecasts", *Stochastic Hydrology and Hydraulics*, vol. 5, no. 4, pp. 295.
- Krzysztofowicz, R. & Watada, L.M. 1986, "Stochastic Model of Seasonal Runoff Forecasts", *Water Resources Research*, vol. 22, no. 3, pp. 296.
- Ladson, L.S. 1970, *Optimization Theory for large Systems*, 1st edn, MacMillan, New York, NY.

- Loucks, D.P. & Falkson, L.M. 1970, "A Comparison of Some Dynamic, Linear and Policy Iteration Methods for Reservoir Operation", *Water Resources Bulletin*, vol. 6, no. 3.
- Loucks, D.P., Stedinger, J.R. & Haith, D.A. 1981, *Water Resources Systems PLanning and Analysis*, 1st edn, Prentice-Hall, Englewood Cliffs, N.J.
- Maceira, M.E. & Kelman, J. 1991, *Long Term Hydro-Thermal Coordination based on Sampling Stochastic Dynamic Programming*, CEPEL-Centro de Pesquisas de Energia Electrica, Brazil, Brazil.
- Pereira, M.V.F. & Pinto, L.M.V.G. 1985, "Stochastic optimization of a multireservoir hydroelectric system-a decomposition approach", *Water Resources Research*, vol. 21, no. 6.
- Powell, W.B. 2007, *Approximate Dynamic Programming*, 2nd edn, Wiley, New York.
- Shelton, R.A. 1979, "Management of TVA reservoir systems", *Proceedings of the National Workshop on Reservoir Systems Operation*.
- Stedinger, J.R. & Kim, Y. 2010, "Probabilities for ensemble forecasts reflecting climate information", *Journal of Hydrology*, vol. 391, no. 1-2, pp. 9-23.
- Stedinger, J.R., Sule, B.F. & Loucks, D.P. 1984, "Stochastic dynamic programming models for reservoir operation optimization.", *Water Resources Research*, vol. 20, no. 11, pp. 1499-1505.
- Tejada-Guibert, J.A., Johnson, S.A. & Stedinger, J.R. 1995, "The value of hdyrologic information in stochastic dynamic programming models of a multireservoir system", *Water Resources Research*, vol. 31, no. 10, pp. 2571-2579.
- Tejada-Guibert, J.A., Johnson, S.A. & Stedinger, J.R. 1993, "Comparison of two approaches for implementing multireservoir operating policies derived using stochastic dynamic programing", *Water Resources Research*, vol. 29, no. 12, pp. 3969-3980.

- Tilmant, A. & Kelman, R. 2007, "A stochastic approach to analyze trade-offs and risks associated with large-scale water resources systems", *Water Resources Research*, vol. 43, no. W06425, pp. 1-11.
- Vedula, S. & Kumar, D.N. 1996, "An integrated model for optimal reservoir operation for irrigation of multiple crops", *Water Resources Research*, vol. 32, no. 4, pp. 1101-1108.
- Vedula, S. & Mujumdar, P.P. 1992, "Optimal reservoir operation for irrigation of multiple crops", *Water Resources Research*, vol. 28, no. 1, pp. 1-9.
- Vicuna, S., Dracup, J.A., Lund, J.R., Dale, L.L. & Maurer, E.P. 2010, "Basin-scale water system operations with uncertain future climate conditions: Methodology and case studies", *Water Resources Research*, vol. 46, no. W04505, pp. 1-19.
- Yeh, W.W. 1992, "Optimization of real-time hydrothermal system operation", *Water Resources Planning and Management*, vol. 118, no. 6.
- Yeh, W.W. 1985, "Reservoir Management and Operations Models: A State-of-the-Art Review", *Water Resources Research*, vol. 21, no. 12, pp. 1797-1818.
- Yeh, W.W. 1979, "Real-time reservoir operation: The Central Valley Project case study", *Proceedings of the National Workshop on Reservoir System Operation*.
- Zhao, T., Cai, X. & Yang, D. 2011, "Effect of streamflow forecast uncertainty on real-time reservoir operation", *Advances in Water Resources*, vol. 34, no. 4, pp. 495.

### ***Appendix 1: Synthetic Forecast Generation***

This research does not use an existing forecast product, but instead uses synthetic forecasts created using the generalized maintenance of variance extension procedure (GMOVE) proposed by Grygier et al. [1989] and the model of forecast error proposed by Stedinger & Kim [2010].

Let  $\mathbf{Q}$  be a vector of inflows to a reservoir and  $\mathbf{F}$  be a vector of corresponding forecasts. The Stedinger & Kim [2010] additive forecast error model is

$$\mathbf{Q} = \mathbf{F} + \boldsymbol{\varepsilon} \quad (4-41)$$

where  $\boldsymbol{\varepsilon}$  is a vector of forecast errors. Assuming  $\mathbf{F}$  is uncorrelated with  $\boldsymbol{\varepsilon}$ , the variance of  $\mathbf{Q}$ ,  $\sigma_{\mathbf{Q}}^2$  is given by

$$\sigma_{\mathbf{Q}}^2 = \sigma_{\mathbf{F}}^2 + \sigma_{\boldsymbol{\varepsilon}}^2 \quad (4-42)$$

The covariance of  $\mathbf{Q}$  and  $\mathbf{F}$ ,  $\sigma_{\mathbf{QF}}$ , can be defined as

$$\sigma_{\mathbf{QF}} = \rho_{\mathbf{QF}}\sigma_{\mathbf{Q}}\sigma_{\mathbf{F}} \quad (4-43)$$

where  $\rho_{\mathbf{QF}}$  is the correlation between the forecasts and the actual flow.  $\sigma_{\mathbf{QF}}$  can also be defined as

$$\begin{aligned} \sigma_{\mathbf{QF}} &= E[\mathbf{QF}] + E[\mathbf{Q}]E[\mathbf{F}] = E[(\mathbf{F} + \boldsymbol{\varepsilon})\mathbf{F}] - E[\mathbf{F} + \boldsymbol{\varepsilon}]E[\mathbf{F}] \\ \sigma_{\mathbf{QF}} &= E[\mathbf{F}^2] + E[\boldsymbol{\varepsilon}\mathbf{F}] - E[\mathbf{F}]^2 + E[\boldsymbol{\varepsilon}]E[\mathbf{F}] \\ \sigma_{\mathbf{QF}} &= E[\mathbf{F}^2] - E[\mathbf{F}]^2 = \sigma_{\mathbf{F}}^2 \end{aligned} \quad (4-44)$$

The final step in equation (4-44) follows from the assumption that the forecasts are unbiased which means that  $E[\mathbf{Q}] = E[\mathbf{F}]$  and  $E[\boldsymbol{\varepsilon}] = 0$ , and that the forecasts are uncorrelated to forecast error, meaning that  $E[\boldsymbol{\varepsilon}\mathbf{F}] = 0$ . Combining equations (4-43) and (4-44) yields

$$\rho_{QF} = \frac{\sigma_F^2}{\sigma_Q \sigma_F} = \frac{\sigma_F}{\sigma_Q} \quad (4-45)$$

which yields

$$\sigma_F^2 = \rho_{QF}^2 \sigma_Q^2 \quad (4-46)$$

Substituting this expression into equation (4-42) yields

$$\sigma_\varepsilon^2 = (1 - \rho_{QF}^2) \sigma_Q^2 \quad (4-47)$$

Thus given the correlation between the true flows and the forecast, equations (4-46) and (4-47) give expressions for the variance of the forecasts and the variance of the forecast error respectively. But how should  $\rho_{QF}$  be understood in terms of forecast precision? If  $F$  is the result of a linear regression procedure, then the  $R^2$  of the regression is  $\rho_{QF}^2$ .  $R^2$  is a convenient way to communicate the precision of synthetic forecasts.

Given the moments of  $Q$ ,  $F$ , and  $\varepsilon$  the GMOVE procedure is used to generate  $F$  with the desired  $R^2$ . The GMOVE model for generating  $F$  is given by Grygier et al. [1989]:

$$F = \mu_F + b(X - \bar{X}) + c(Q - \bar{Q}) \quad (4-48)$$

where  $\mu_F$  is the mean of  $F$ ,  $X$  is the previous time step's inflow into the reservoir,  $b$  and  $c$  are GMOVE parameters, and  $\bar{X}$  and  $\bar{Q}$  are the sample means of  $X$  and  $Q$  respectively. Grygier et al. [1989] show that  $c$  is given by

$$c = \frac{\sigma_{QF} - b s_{XQ}}{s_Q^2} \quad (4-49)$$

where  $s_{XQ}$  is the sample covariance of  $X$  and  $Q$ , and  $s_Q^2$  is the sample variance of  $Q$ .  $b$  can be computed by taking the root of [Grygier, et al., 1989]

$$b^2 = \frac{\sigma_F^2 - \frac{\sigma_{QF}^2}{s_Q^2}}{s_X^2 - \frac{s_{XQ}^2}{s_Q^2}} \quad (4-50)$$

where  $s_X^2$  is the sample variance of  $X$ . If the sample moments of  $Q$  are used in equations (4-46) and (4-47), equation (4-48) can be used to generate synthetic  $F$  for any desired  $R^2$ . This allows for the examination of the benefit of forecast precision to hydropower operations optimization. For example, how much do reservoir operations improve if forecasts with  $R^2 = 0.95$  rather than  $R^2 = 0.65$  are used. We can examine this by comparing the I/I/F95 and I/I/F65 model configurations, where F65 is the “F” case with  $R^2 = 0.65$ .

#### ***Appendix 2: “Mean Price” Model Runs***

This appendix contains the results for the “mean price” scheme as figures and tables. We consider the effect of forecast uncertainty by fixing the representation of uncertainty (i.e. I/I/\* or a stochastic programming model) and changing the quality of the forecast. It is observed in the chapter that as the forecast improves, the *Eff* also generally improves. To examine how the storage capacity affects this assumption, consider the following figures, in which the turbine size is fixed but the size of the reservoir is varied.

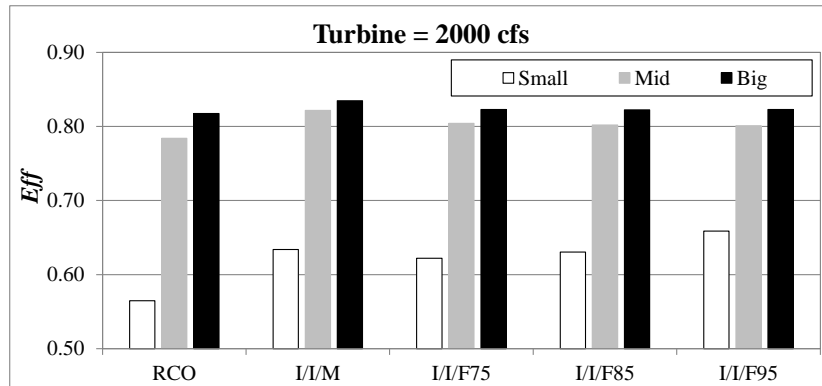


Figure 4-24: The effect of forecast precision and reservoir size on  $Eff$  for stochastic programming models, with fixed turbine capacity (2000 cfs), 'mean price' scheme.

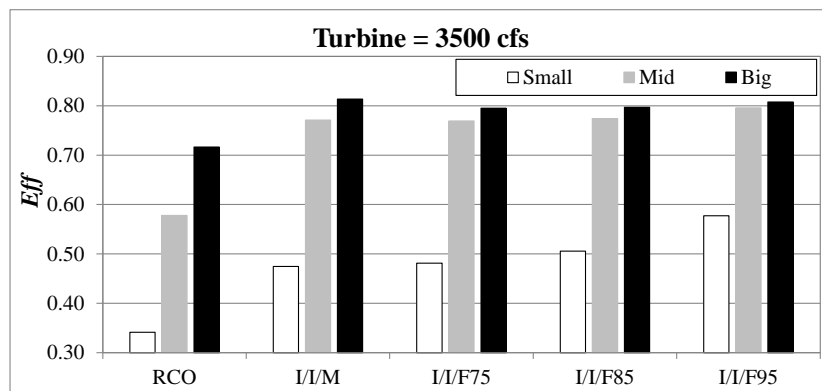


Figure 4-25: The effect of forecast precision and reservoir size on  $Eff$  for stochastic programming models, with fixed turbine capacity (3500 cfs), 'mean price' scheme.

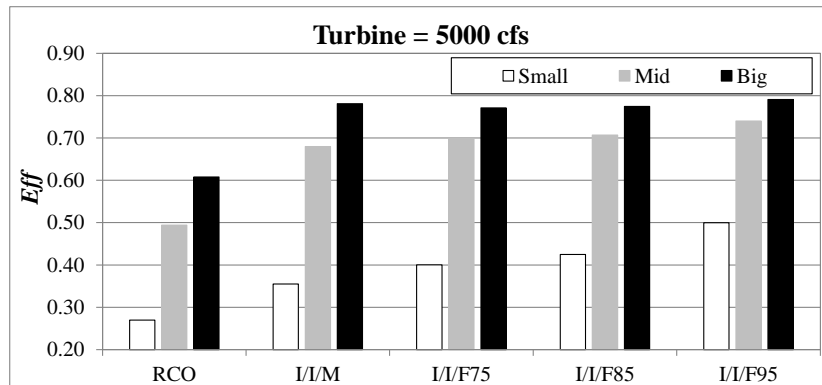


Figure 4-26: The effect of forecast precision and reservoir size on  $Eff$  for stochastic programming models, with fixed turbine capacity (5000 cfs), 'mean price' scheme.

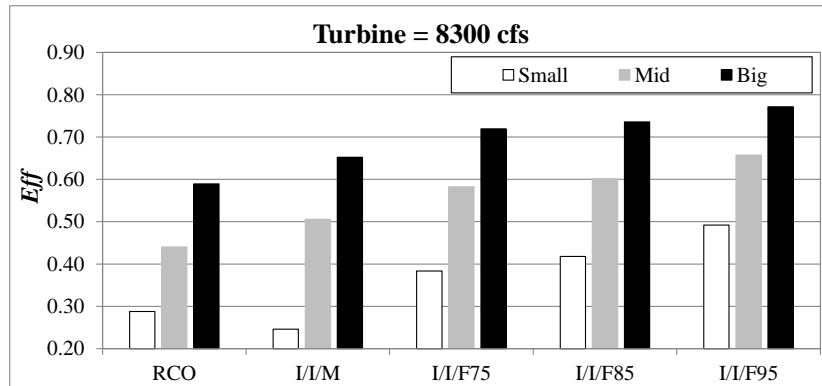


Figure 4-27: The effect of forecast precision and reservoir size on  $Eff$  for stochastic programming models, with fixed turbine capacity (8300 cfs), ‘mean price’ scheme.

The following figures consider the effect of forecast precision and turbine capacity by plotting efficiency for the same stochastic programming models, but with fixed storage capacity.

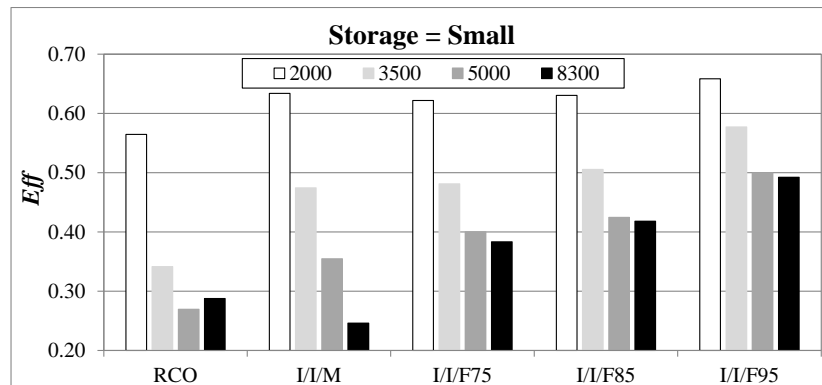


Figure 4-28: The effect of forecast precision and turbine capacity on  $Eff$  for stochastic programming models, with fixed storage capacity (Small), ‘mean price’ scheme.

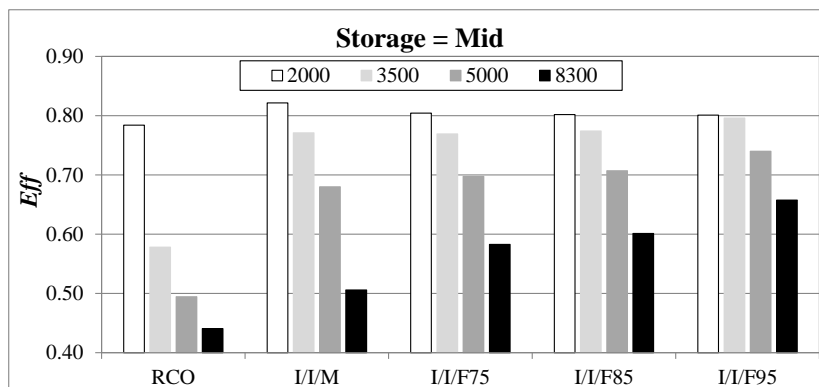


Figure 4-29: The effect of forecast precision and turbine capacity on  $Eff$  for stochastic programming models, with fixed storage capacity (Mid), ‘mean price’ scheme.

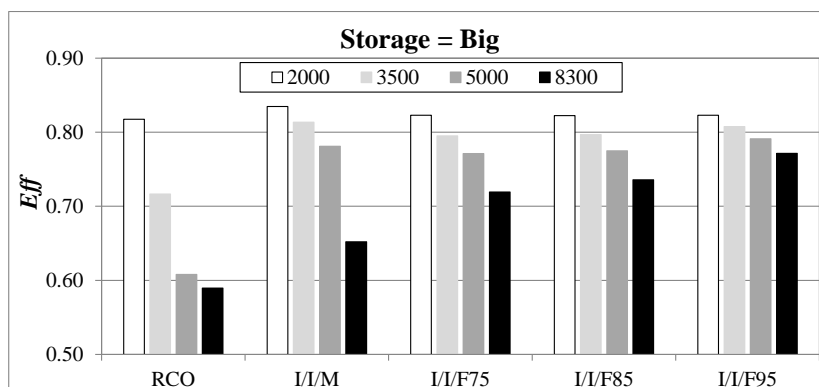


Figure 4-30: The effect of forecast precision and turbine capacity on  $Eff$  for stochastic programming models, with fixed storage capacity (Big), ‘mean price’ scheme.

The following tables report the results of all of the ‘mean price’ scheme model runs.

Table 4-4: Benefits (*Ben*), Performance Ratio (*PR*), and Efficiency (*Eff*) for systems with turbine capacity 2000 and “mean price” scheme.

Model	(Small, 2000)			(Mid, 2000)			(Big, 2000)		
	<i>Ben</i>	<i>PR</i>	<i>Eff</i>	<i>Ben</i>	<i>PR</i>	<i>Eff</i>	<i>Ben</i>	<i>PR</i>	<i>Eff</i>
ROR	1,802,155	0.836	0	2,307,456	0.806	0	2,840,278	0.867	0
RCO	2,001,321	0.929	0.565	2,743,162	0.958	0.784	3,197,043	0.976	0.818
I/I/M	2,025,683	0.940	0.634	2,764,021	0.965	0.822	3,204,625	0.978	0.835
I/I/F75	2,021,481	0.938	0.622	2,754,376	0.962	0.804	3,199,436	0.976	0.823
I/I/F85	2,024,498	0.940	0.630	2,753,104	0.962	0.802	3,199,216	0.976	0.822
I/I/F95	2,034,428	0.944	0.659	2,752,551	0.961	0.801	3,199,407	0.976	0.823
I/M/M	2,026,973	0.941	0.638	2,762,042	0.965	0.818	3,203,602	0.978	0.833
I/F75/F75	2,024,319	0.939	0.630	2,751,921	0.961	0.800	3,197,040	0.976	0.818
I/F85/F85	2,027,306	0.941	0.638	2,750,839	0.961	0.798	3,196,914	0.976	0.817
I/F95/F95	2,037,578	0.946	0.668	2,750,121	0.961	0.797	3,197,284	0.976	0.818
M/M/M	2,026,098	0.940	0.635	2,757,810	0.963	0.810	3,199,926	0.977	0.824
F75/F75/F75	2,025,188	0.940	0.632	2,744,738	0.959	0.787	3,194,010	0.975	0.811
F85/F85/F85	2,027,890	0.941	0.640	2,742,692	0.958	0.783	3,193,645	0.975	0.810
F95/F95/F95	2,038,759	0.946	0.671	2,741,651	0.958	0.781	3,193,641	0.975	0.810
I/I/I	2,154,801	1	1	2,863,124	1	1	3,276,681	1	1

Table 4-5: Benefits (*Ben*), Performance Ratio (*PR*), and Efficiency (*Eff*) for systems with turbine capacity 3500 and “mean price” scheme.

Model	(Small, 3500)			(Mid, 3500)			(Big, 3500)		
	<i>Ben</i>	<i>PR</i>	<i>Eff</i>	<i>Ben</i>	<i>PR</i>	<i>Eff</i>	<i>Ben</i>	<i>PR</i>	<i>Eff</i>
ROR	2,248,821	0.848	0	2,785,954	0.806	0	3,498,139	0.806	0
RCO	2,386,011	0.900	0.341	3,173,842	0.918	0.578	4,100,170	0.945	0.717
I/I/M	2,439,546	0.920	0.475	3,303,465	0.956	0.771	4,181,702	0.964	0.814
I/I/F75	2,442,231	0.921	0.481	3,302,135	0.955	0.769	4,166,172	0.960	0.795
I/I/F85	2,451,956	0.925	0.505	3,305,493	0.956	0.774	4,167,621	0.961	0.797
I/I/F95	2,480,813	0.936	0.577	3,320,111	0.960	0.796	4,176,700	0.963	0.808
I/M/M	2,446,317	0.923	0.491	3,307,745	0.957	0.778	4,179,159	0.963	0.811
I/F75/F75	2,458,148	0.927	0.521	3,314,279	0.959	0.787	4,166,549	0.960	0.796
I/F85/F85	2,468,335	0.931	0.546	3,318,010	0.960	0.793	4,167,698	0.961	0.797
I/F95/F95	2,493,874	0.941	0.610	3,331,415	0.964	0.813	4,177,760	0.963	0.809
M/M/M	2,446,738	0.923	0.492	3,301,443	0.955	0.768	4,170,010	0.961	0.800
F75/F75/F75	2,459,354	0.928	0.524	3,315,707	0.959	0.789	4,163,489	0.960	0.792
F85/F85/F85	2,470,019	0.932	0.550	3,319,574	0.960	0.795	4,166,682	0.960	0.796
F95/F95/F95	2,495,124	0.941	0.613	3,337,312	0.965	0.822	4,175,374	0.962	0.806
I/I/I	2,650,685	1	1	3,456,994	1	1	4,338,286	1	1

Table 4-6: Benefits (*Ben*), Performance Ratio (*PR*), and Efficiency (*Eff*) for systems with turbine capacity 5000 and “mean price” scheme.

Model	(Small, 5000)			(Mid, 5000)			(Big, 5000)		
	<i>Ben</i>	<i>PR</i>	<i>Eff</i>	<i>Ben</i>	<i>PR</i>	<i>Eff</i>	<i>Ben</i>	<i>PR</i>	<i>Eff</i>
ROR	2,485,396	0.858	0	3,035,478	0.822	0	3,781,931	0.814	0
RCO	2,596,528	0.896	0.270	3,361,104	0.910	0.494	4,307,033	0.927	0.608
I/I/M	2,631,674	0.908	0.355	3,483,539	0.943	0.680	4,456,428	0.959	0.781
I/I/F75	2,650,469	0.915	0.400	3,495,137	0.946	0.698	4,448,036	0.957	0.771
I/I/F85	2,660,434	0.918	0.425	3,501,317	0.948	0.707	4,451,127	0.958	0.775
I/I/F95	2,691,357	0.929	0.500	3,523,089	0.954	0.740	4,465,218	0.961	0.791
I/M/M	2,641,337	0.912	0.378	3,504,156	0.949	0.711	4,472,139	0.963	0.799
I/F75/F75	2,681,859	0.926	0.477	3,535,973	0.957	0.760	4,480,122	0.964	0.808
I/F85/F85	2,695,129	0.930	0.509	3,542,446	0.959	0.769	4,482,866	0.965	0.812
I/F95/F95	2,723,075	0.940	0.577	3,562,574	0.964	0.800	4,493,794	0.967	0.824
M/M/M	2,641,310	0.912	0.378	3,511,695	0.951	0.723	4,486,319	0.966	0.816
F75/F75/F75	2,685,683	0.927	0.486	3,549,470	0.961	0.780	4,503,772	0.969	0.836
F85/F85/F85	2,695,825	0.930	0.510	3,559,388	0.963	0.795	4,506,625	0.970	0.839
F95/F95/F95	2,723,942	0.940	0.579	3,578,677	0.969	0.824	4,518,724	0.973	0.853
I/I/I	2,897,647	1	1	3,694,315	1	1	4,645,533	1	1

Table 4-7: Benefits (*Ben*), Performance Ratio (*PR*), and Efficiency (*Eff*) for systems with turbine capacity 8300 and “mean price” scheme.

Model	(Small, 8300)			(Mid, 8300)			(Big, 8300)		
	<i>Ben</i>	<i>PR</i>	<i>Eff</i>	<i>Ben</i>	<i>PR</i>	<i>Eff</i>	<i>Ben</i>	<i>PR</i>	<i>Eff</i>
ROR	2,717,186	0.874	0	3,293,404	0.851	0	4,036,113	0.840	0
RCO	2,829,777	0.910	0.288	3,546,721	0.917	0.440	4,488,534	0.934	0.590
I/I/M	2,813,487	0.905	0.246	3,584,269	0.927	0.506	4,536,538	0.944	0.652
I/I/F75	2,867,287	0.922	0.384	3,628,485	0.938	0.583	4,588,156	0.955	0.719
I/I/F85	2,880,790	0.927	0.418	3,639,263	0.941	0.601	4,600,698	0.958	0.736
I/I/F95	2,909,816	0.936	0.492	3,671,554	0.949	0.657	4,628,170	0.964	0.772
I/M/M	2,836,477	0.912	0.305	3,632,157	0.939	0.589	4,588,749	0.955	0.720
I/F75/F75	2,907,238	0.935	0.486	3,680,049	0.951	0.672	4,641,805	0.966	0.789
I/F85/F85	2,920,016	0.939	0.518	3,688,549	0.953	0.687	4,651,683	0.968	0.802
I/F95/F95	2,939,965	0.946	0.569	3,710,781	0.959	0.726	4,672,727	0.973	0.830
M/M/M	2,836,678	0.913	0.305	3,643,351	0.942	0.608	4,626,463	0.963	0.769
F75/F75/F75	2,907,425	0.935	0.486	3,695,051	0.955	0.698	4,664,076	0.971	0.818
F85/F85/F85	2,920,087	0.939	0.518	3,695,696	0.955	0.699	4,671,432	0.973	0.828
F95/F95/F95	2,939,476	0.946	0.568	3,714,240	0.960	0.732	4,681,701	0.975	0.841
I/I/I	3,108,583	1	1	3,868,564	1	1	4,803,474	1	1

The following tables report the results of all of the ‘mean price’ scheme model runs.

### Appendix 3: “Variable Price” Model Runs

This appendix contains the results for the “variable price” scheme as figures and tables. We consider the effect of forecast uncertainty by fixing the representation of uncertainty (i.e. I/I\* or a stochastic programming model) and changing the quality of the forecast. It is observed in the chapter that as the forecast improves, the *Eff* also generally improves. To examine how the storage capacity affects this assumption, consider the following figures, in which the turbine size is fixed but the size of the reservoir is varied.

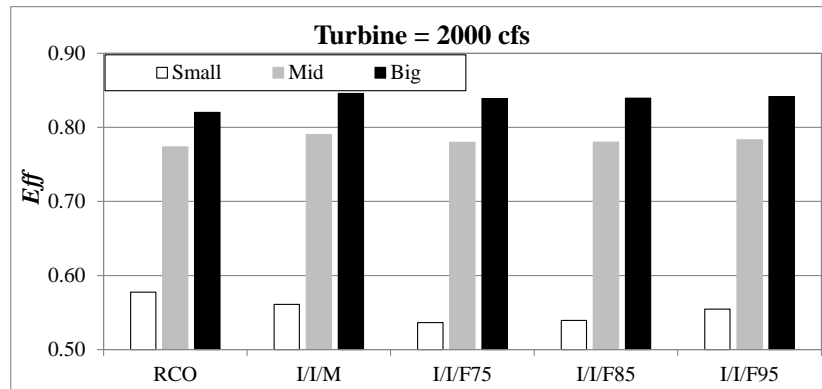


Figure 4-31: The effect of forecast precision and reservoir size on *Eff* for stochastic programming models, with fixed turbine capacity (2000 cfs), ‘variable price’ scheme.

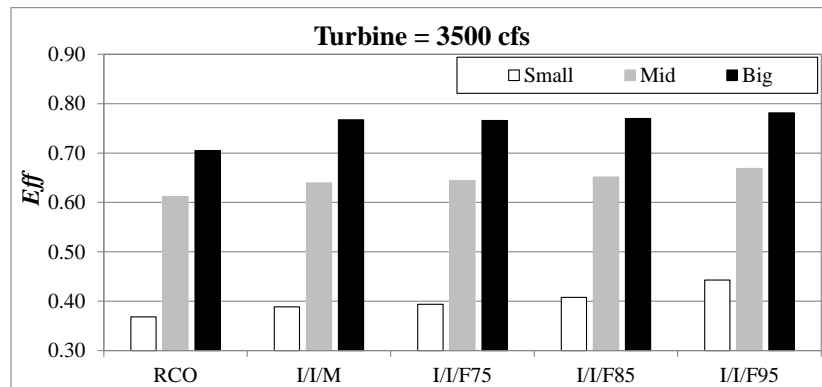


Figure 4-32: The effect of forecast precision and reservoir size on *Eff* for stochastic programming models, with fixed turbine capacity (3500 cfs), ‘variable price’ scheme.

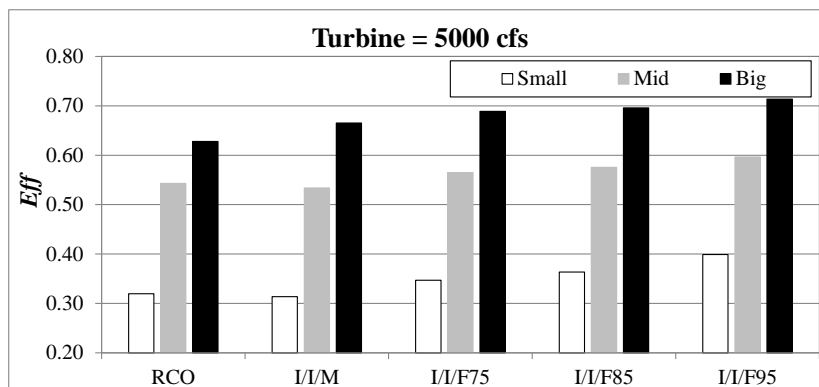


Figure 4-33: The effect of forecast precision and reservoir size on *Eff* for stochastic programming models, with fixed turbine capacity (5000 cfs), ‘variable price’ scheme.

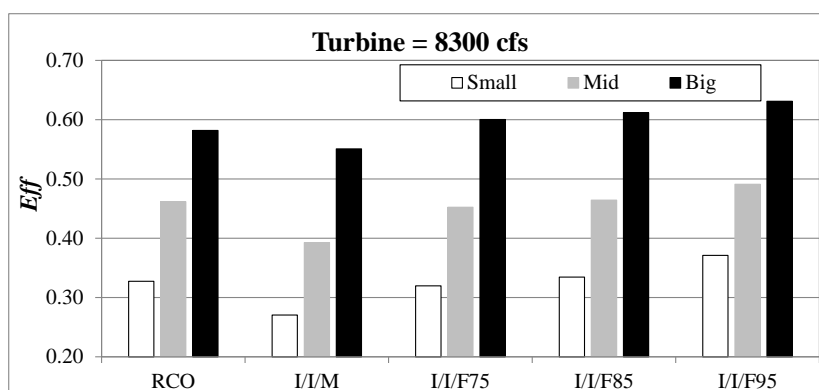


Figure 4-34: The effect of forecast precision and reservoir size on *Eff* for stochastic programming models, with fixed turbine capacity (8300 cfs), ‘variable price’ scheme.

The following figures consider the effect of forecast precision and turbine capacity by plotting efficiency for the same stochastic programming models, but with fixed storage capacity.

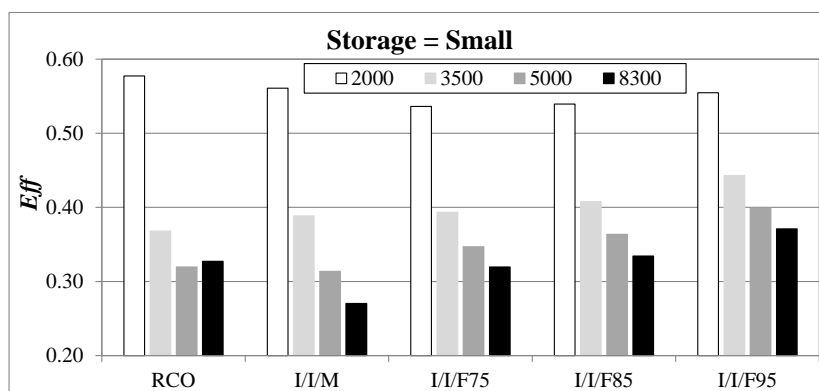


Figure 4-35: The effect of forecast precision and turbine capacity on *Eff* for stochastic programming models, with fixed storage capacity (Small), ‘mean price’ scheme.

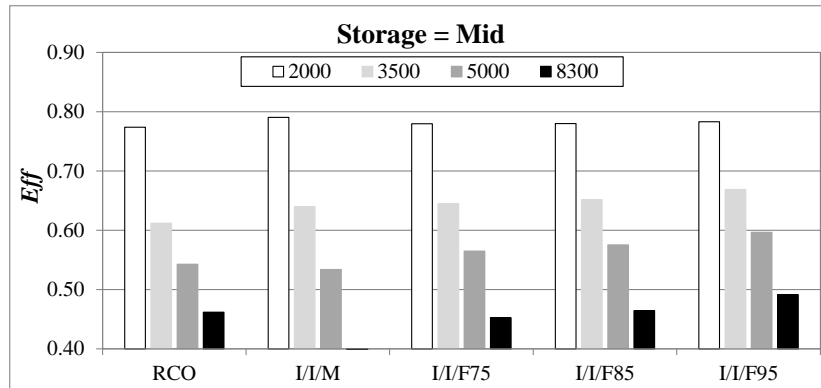


Figure 4-36: The effect of forecast precision and turbine capacity on  $Eff$  for stochastic programming models, with fixed storage capacity (Mid), 'mean price' scheme.

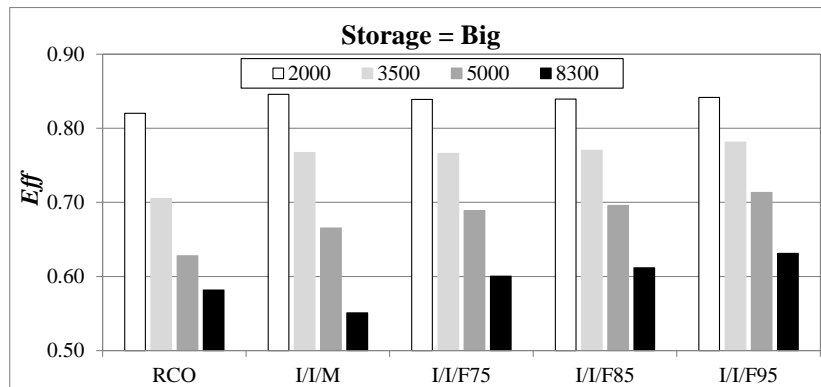


Figure 4-37: The effect of forecast precision and turbine capacity on  $Eff$  for stochastic programming models, with fixed storage capacity (Big), 'mean price' scheme.

Table 4-8: Benefits (*Ben*), Performance Ratio (*PR*), and Efficiency (*Eff*) for systems with turbine capacity 2000 and “variable price” scheme.

Model	(Small, 2000)			(Mid, 2000)			(Big, 2000)		
	<i>Ben</i>	<i>PR</i>	<i>Eff</i>	<i>Ben</i>	<i>PR</i>	<i>Eff</i>	<i>Ben</i>	<i>PR</i>	<i>Eff</i>
ROR	1,834,976	0.819	0	2,301,259	0.793	0	2,827,429	0.858	0
RCO	2,069,437	0.923	0.577	2,765,227	0.953	0.774	3,211,921	0.974	0.820
I/I/M	2,062,756	0.920	0.561	2,775,242	0.957	0.791	3,224,016	0.978	0.846
I/I/F75	2,052,786	0.916	0.536	2,768,837	0.955	0.780	3,220,724	0.977	0.839
I/I/F85	2,054,007	0.917	0.539	2,768,949	0.955	0.780	3,220,995	0.977	0.840
I/I/F95	2,060,221	0.919	0.555	2,770,873	0.955	0.783	3,222,028	0.977	0.842
I/M/M	2,055,829	0.917	0.544	2,770,419	0.955	0.783	3,222,417	0.978	0.843
I/F75/F75	2,044,999	0.913	0.517	2,762,418	0.952	0.769	3,219,027	0.977	0.835
I/F85/F85	2,045,758	0.913	0.519	2,762,276	0.952	0.769	3,219,113	0.977	0.836
I/F95/F95	2,051,329	0.915	0.533	2,764,494	0.953	0.773	3,219,767	0.977	0.837
M/M/M	2,054,196	0.917	0.540	2,764,177	0.953	0.772	3,218,601	0.976	0.834
F75/F75/F75	2,046,473	0.913	0.521	2,753,081	0.949	0.754	3,213,990	0.975	0.825
F85/F85/F85	2,047,201	0.913	0.523	2,752,079	0.949	0.752	3,213,435	0.975	0.823
F95/F95/F95	2,054,530	0.917	0.541	2,752,576	0.949	0.753	3,212,837	0.975	0.822
I/I/I	2,241,064	1	1	2,900,820	1	1	3,296,223	1	1

Table 4-9: Benefits (*Ben*), Performance Ratio (*PR*), and Efficiency (*Eff*) for systems with turbine capacity 3500 and “variable price” scheme.

Model	(Small, 3500)			(Mid, 3500)			(Big, 3500)		
	<i>Ben</i>	<i>PR</i>	<i>Eff</i>	<i>Ben</i>	<i>PR</i>	<i>Eff</i>	<i>Ben</i>	<i>PR</i>	<i>Eff</i>
ROR	2,285,134	0.822	0	2,793,600	0.774	0	3,455,863	0.778	0
RCO	2,467,494	0.887	0.368	3,291,931	0.912	0.612	4,150,761	0.935	0.705
I/I/M	2,477,573	0.891	0.388	3,314,584	0.919	0.640	4,212,004	0.948	0.767
I/I/F75	2,480,080	0.892	0.394	3,318,504	0.920	0.644	4,210,780	0.948	0.766
I/I/F85	2,487,108	0.894	0.408	3,324,252	0.921	0.652	4,214,796	0.949	0.770
I/I/F95	2,504,522	0.901	0.443	3,338,504	0.925	0.669	4,225,823	0.952	0.781
I/M/M	2,470,457	0.888	0.374	3,303,959	0.916	0.627	4,200,624	0.946	0.756
I/F75/F75	2,480,779	0.892	0.395	3,308,118	0.917	0.632	4,201,491	0.946	0.757
I/F85/F85	2,488,295	0.895	0.410	3,312,879	0.918	0.638	4,205,376	0.947	0.761
I/F95/F95	2,502,634	0.900	0.439	3,326,635	0.922	0.654	4,215,727	0.949	0.771
M/M/M	2,470,176	0.888	0.374	3,298,396	0.914	0.620	4,181,965	0.942	0.737
F75/F75/F75	2,481,858	0.893	0.397	3,306,885	0.917	0.630	4,187,675	0.943	0.743
F85/F85/F85	2,489,992	0.896	0.414	3,311,270	0.918	0.636	4,190,944	0.944	0.746
F95/F95/F95	2,505,029	0.901	0.444	3,324,975	0.922	0.652	4,200,206	0.946	0.755
I/I/I	2,780,521	1	1	3,608,056	1	1	4,441,212	1	1

Table 4-10: Benefits (*Ben*), Performance Ratio (*PR*), and Efficiency (*Eff*) for systems with turbine capacity 5000 and “variable price” scheme.

Model	(Small, 5000)			(Mid, 5000)			(Big, 5000)		
	<i>Ben</i>	<i>PR</i>	<i>Eff</i>	<i>Ben</i>	<i>PR</i>	<i>Eff</i>	<i>Ben</i>	<i>PR</i>	<i>Eff</i>
ROR	2,522,492	0.822	0	3,053,077	0.775	0	3,746,508	0.768	0
RCO	2,697,328	0.879	0.319	3,534,421	0.897	0.543	4,455,785	0.914	0.628
I/I/M	2,694,138	0.878	0.314	3,526,360	0.895	0.534	4,498,150	0.922	0.665
I/I/F75	2,712,354	0.884	0.347	3,553,971	0.902	0.565	4,524,798	0.928	0.689
I/I/F85	2,721,513	0.887	0.364	3,563,309	0.904	0.575	4,532,550	0.930	0.696
I/I/F95	2,740,778	0.893	0.399	3,582,120	0.909	0.597	4,552,482	0.934	0.714
I/M/M	2,690,606	0.876	0.307	3,513,032	0.892	0.519	4,480,674	0.919	0.650
I/F75/F75	2,724,337	0.887	0.369	3,550,031	0.901	0.560	4,514,697	0.926	0.680
I/F85/F85	2,731,858	0.890	0.383	3,559,234	0.903	0.571	4,524,256	0.928	0.689
I/F95/F95	2,746,661	0.895	0.410	3,575,741	0.908	0.589	4,540,896	0.931	0.703
M/M/M	2,691,117	0.877	0.308	3,522,303	0.894	0.529	4,473,650	0.917	0.644
F75/F75/F75	2,726,930	0.888	0.374	3,562,303	0.904	0.574	4,512,191	0.925	0.678
F85/F85/F85	2,734,558	0.891	0.388	3,570,764	0.906	0.584	4,519,704	0.927	0.685
F95/F95/F95	2,749,327	0.896	0.415	3,587,331	0.911	0.603	4,534,592	0.930	0.698
I/I/I	3,069,733	1	1	3,939,799	1	1	4,876,079	1	1

Table 4-11: Benefits (*Ben*), Performance Ratio (*PR*), and Efficiency (*Eff*) for systems with turbine capacity 8300 and “variable price” scheme.

Model	(Small, 8300)			(Mid, 8300)			(Big, 8300)		
	<i>Ben</i>	<i>PR</i>	<i>Eff</i>	<i>Ben</i>	<i>PR</i>	<i>Eff</i>	<i>Ben</i>	<i>PR</i>	<i>Eff</i>
ROR	2,753,582	0.821	0	3,321,862	0.782	0	4,024,188	0.762	0
RCO	2,950,104	0.880	0.327	3,748,722	0.883	0.462	4,754,899	0.901	0.582
I/I/M	2,915,930	0.869	0.270	3,684,765	0.868	0.392	4,716,186	0.893	0.551
I/I/F75	2,945,580	0.878	0.320	3,739,996	0.881	0.452	4,778,347	0.905	0.600
I/I/F85	2,954,475	0.881	0.334	3,751,232	0.883	0.464	4,792,471	0.908	0.612
I/I/F95	2,976,501	0.887	0.371	3,776,069	0.889	0.491	4,816,998	0.912	0.631
I/M/M	2,932,224	0.874	0.297	3,693,998	0.870	0.402	4,712,978	0.893	0.548
I/F75/F75	2,970,158	0.885	0.361	3,748,744	0.883	0.462	4,775,289	0.904	0.598
I/F85/F85	2,979,061	0.888	0.375	3,760,538	0.886	0.474	4,788,574	0.907	0.609
I/F95/F95	2,997,949	0.894	0.407	3,780,400	0.890	0.496	4,812,638	0.911	0.628
M/M/M	2,934,253	0.875	0.301	3,711,261	0.874	0.421	4,734,233	0.897	0.565
F75/F75/F75	2,973,227	0.886	0.366	3,769,553	0.888	0.484	4,799,014	0.909	0.617
F85/F85/F85	2,981,525	0.889	0.379	3,781,531	0.891	0.497	4,810,009	0.911	0.626
F95/F95/F95	3,000,174	0.894	0.411	3,800,914	0.895	0.518	4,834,123	0.916	0.645
I/I/I	3,354,230	1	1	4,246,495	1	1	5,280,286	1	1

## CHAPTER 5

### CORRIDOR DYNAMIC PROGRAMMING FOR HIGH DIMENSIONAL PROBLEMS

Solving high-dimensional dynamic programming (DP) problems continues to be a challenging problem in engineering and science. This is because as the dimension of state space increases, the computational burden of solving the associated optimization model with traditional techniques increases exponentially. For deterministic problems, one can successively solve the problem in a small corridor, where the corridor is adjusted as the optimization proceeds [Heidari et al., 1971]. However, when solving the general SDP problem, one needs to approximate the cost-to-go value function over the range of states to which the system might evolve. In water resources systems analysis this has had the practical consequence of limiting water resources studies using traditional DP studies to 4 reservoirs [Yakowitz, 1982; Yeh, 1985; Labadie 2004]. However there are many techniques for reducing the computational burden including aggregation, Benders decomposition, higher-order approximations of the future value function, and sparse or selective sampling of the state space. Drawing on elements of these techniques, a new Corridor SDP procedure is proposed in this chapter. The Corridor SDP idea is to focus the optimization efforts on the regions of the state space where the system is most likely to visit by developing a set of basis points in a “corridor”, and to represent the future value function with radial basis functions (RBFs) which are effective for scattered data approximations. Section 5.1 provides an introductory explanation of the well-known ‘Curse of Dimensionality’ and explains the motivation of the Corridor SDP concept. Section

5.2 introduces DP for reservoir operations optimization, Section 5.3 describes previous efforts at addressing the ‘Curse’, and Section 5.4 introduces the Corridor SDP concept. 0 and Section 5.6 introduce regular and Hermite RBF interpolation and least-squares approximation, and provide a discussion of common basis functional forms and their parameterization. Section 5.7 describes an objective procedure for basis selection when using Corridor DP. Section 5.8 provides a demonstration of the performance of the Corridor DP procedure, with a discussion in Section 5.8.3 and concluding remarks in Section 5.10. Finally an appendix discusses two simple but effective diagnostic procedures for identifying when numerical solution of the Bellman equation has terminated prematurely, which can result in gross errors.

### ***Section 5.1 Introduction and motivation for Corridor Concept***

A well-documented problem in stochastic dynamic programming is that the computational effort required to solve the optimization problem increases exponentially with the dimension of the state space. This is sometimes referred to as Bellman’s “Curse of Dimensionality,” though that “Curse” originally referred to the growth in required memory allocation rather than computational effort [Bellman, 1961]. Because the storage in each reservoir of a system is typically assigned a state variable, practical applications of traditional dynamic programming to reservoir systems has been limited to at most four-reservoir systems [Yeh, 1985; Labadie, 2004].

This work introduces the Corridor SDP approach, which aims to reduce the computational burden of solving high dimensional SDP problems by focusing

optimization efforts on areas of the state-space where the system is most likely to visit in typical operation, the so called Corridor.

In many systems it is easy to empirically demonstrate that much of state space is not visited in regular operation. More formally, Saad et al. [1992] and used principle component analysis to show that 97% of the variability in a four reservoir system was described by two eigenvalues (linear combinations of storage values). The ‘corridor’ concept is exploited in stochastic dual dynamic programming (SDDP) [Pereira and Pinto, 1985], which builds a representation of the DP future value function through iterative simulation and optimization of the system. That work uses Benders decomposition and linear representations of the value function, enabling solution of high-dimensional problems [Tilmant and Kelman, 2007; Goor et al., 2011].

The work presented here draws on the Corridor concept used in SDDP, but applies it to a traditional SDP framework and does not require a piece-wise linear approximation of the cost-to-go function. This is achieved using Radial Basis Function (RBF) interpolating and approximating surfaces, which can represent a wide range of surface shapes and do not require regular, square lattices. To select an efficient and well-spaced set of basis points an algorithm is developed which places points in the Corridor region where they are needed to achieve a good representation of a DP future value function. This is similar to the idea underlying adaptive sparse grids [Bungartz, and Griebel, 2004], but is specifically focused on a specific Corridor region, and does not allow for evolution of the set of basis points over time.

### ***Section 5.1.1 Corridor SDP and the use of corridors in deterministic DP***

Before moving on it is important to distinguish the Corridor DP work presented here from previous work in deterministic DP which used a state-space corridor. Discrete Differential Dynamic Programming (DDDP) is such a method [Heidari et al., 1971; Hall et al., 1969; Trott and Yeh, 1985]. DDDP solves a deterministic DP model by beginning with an initial decision-state trajectory through time which satisfies initial and final storage constraints. Because it is a deterministic problem, a corridor can be defined about the initial decision-state trajectory, and the state space need not be sampled beyond that corridor. A new, improved trajectory through the state space is found using optimization, and the width and location of the corridor evolves to encompass the new trajectory. This iterative procedure continues until the change in the optimal trajectory between iterations satisfies some convergence criteria [Yeh, 1985].

Such a methodology would not work for the stochastic case because it is impossible to predict where the reservoir system will travel because inflows are random. For this reason previous applications of corridors with deterministic DP problems are not appropriate for the stochastic case. While the example presented in this chapter is a deterministic problem, the true advantage of the Corridor DP approach is for stochastic problems.

### ***Section 5.2 Dynamic Programming (DP) for Reservoir Operation***

Chapter 2 of this thesis introduces DP, SDP, and SSDP algorithms and provides a more general discussion of the topic. Furthermore, Chapter 2 discusses the evolution of DP and SDP models in reservoir operations optimization. The intent in

this section is to provide enough background to preface the following Corridor SDP development.

The objective in reservoir operation is to maximize benefits by selecting a sequence of releases over a planning period. . In the case of SDP, this is a sequential decision problem because we will not know exactly what states will be visited in the future. In practice, time is often broken into discrete time steps in which a release decision,  $R_t$ , must be made. In each time step, the state of the system is described by a state variable, which is often storage in the reservoir  $S_t$ . For each state  $S_t$ , each  $R_t$  results in an incremental benefit  $B_t(R_t, S_t)$ . For each time step  $t$ , and each potential initial system state  $S_t$ , a DP optimization selects an optimal release  $R_t^*$  which maximizes the sum of the present incremental benefits  $B_t(R_t, S_t)$  and the future benefits  $f_{t+1}(S_t)$ . This is solved numerically by recursively solving equation (5-1) backwards from planning horizon  $T$  to the present time  $t = 1$ :

$$f_t(S_t) = \max_{R_t} (B_t(R_t, S_t) + f_{t+1}(S_{t+1}))$$

$$\forall S_t \text{ and } t \in \{1, \dots, T\}$$
(5-1)

$$S_{t+1} = S_t + Q_t - R_t - e(S_t, S_{t+1})$$
(5-2)

where  $Q_t$  is the reservoir inflow in time  $t$  and  $e(S_t, S_{t+1})$  is an evaporation/seepage loss term. To solve equation (5-1), the state space is often discretized and solved at  $N$  specified points, generally on a grid. If  $f_t$  is non-linear, then as  $N$  increases the precision of an approximation of  $f_t$  should also increase.

In the case that a  $k$ -reservoir system is considered,  $S_t$ ,  $R_t$ , and  $Q_t$  become  $k$ -dimensional vectors of reservoir storage  $\mathbf{S}_t$ , releases,  $\mathbf{R}_t$ , and inflows  $\mathbf{Q}_t$  at each of the

$k$  reservoirs in time  $t$ . The state space becomes a  $k$ -dimensional cube, and if each dimension is divided into  $d$  discrete points (assume that the same  $d$  is used in each direction though it needn't be), then equation (5-1) must be solved at  $N = d^k$  points, resulting in an exponential growth of computational effort and memory required to resolve equation (5-1) with an increase in  $k$ . An additional problem is that solving equation (5-1) at each point becomes more difficult as  $k$  increases, further adding to the computational burden of traditional DP in high dimension. In a SDP there is typically an extra dimension describing the hydrologic state of the system. Moreover, an expectation is added to (5-1). Both add to the computational burden of solving the problem.

### ***Section 5.3 Addressing the Curse***

There are four common approaches to reducing the burden of high-dimensional DP problems in reservoir optimization studies: aggregation, stochastic dual dynamic programming, approximation of the future value function, and sparse sampling of the state space.

#### ***Aggregation Approaches***

Perhaps the most obvious approach to reduce the computational burden of high-dimensional DP models is aggregation, wherein several reservoirs are represented by a combined state variable such as total storage or total energy [Arvanitidis and Rosing, 1970; Quintana and Chikhani, 1981; Gilbert and Shane, 1982; Duran et al., 1985; Saad and Turgeon, 1988; Turgeon and Charbonneau, 1998]. This approach can be very effective, particularly in systems where the critical operation is well represented by a subset of the original state variables (eigenvectors for the full

state space). Saad et al. [1992] demonstrate such an example using principle component analysis to determine which state variables account for the majority of the variability in system performance. For their 4-reservoir example, upwards of 90% of the variability was described by a single state variable, and upwards of 97% of the variability was described by two state variables. This suggested that modeling the system with two state variables is sufficient to capture the critical aspects of system operation. A potential downside of such a representation is that aggregation can often result in a loss of modeling resolution of constraints and system dynamics which may not be acceptable.

### ***Stochastic Dual Dynamic Programming***

A second approach to addressing the “curse” has been through use of Bender’s Decomposition in Sampling Dual Dynamic Programming (SDDP) [Pereira and Pinto, 1985]. That algorithm uses simulation of the system to obtain points where the future value function is evaluated. The future value function is approximated by piecewise linear Benders cuts. This involves iterative optimization and simulation till the desired precision is achieved and the analysis converges. The linear approximation allows evaluation of the future value function over the entire volume of the state space. Remarkably, the Pereira and Pinto [1985] solve a 39 reservoir problem using this method. The SDDP approach has also been successfully applied more recently [see Tilmant and Kelman, 2007; Goor et al., 2011]. However, if  $f_t$  is particularly non-linear, the SDDP piecewise linear approximation might struggle with precision.

### ***Surrogate Approximation of Future Value Function***

A third approach is to use a surrogate surface to represent  $f_t$  between discrete points in the state space at which equation (5-1) has been solved. Define  $\mathcal{S}_B$  as set of  $N$  discrete points in the state space  $\mathcal{S}$  at which equation (5-1) has been solved. This allows for a coarser grid of discrete points to achieve the desired precision in  $f_t$  (i.e. allows for smaller  $N$  to achieve the same accuracy). A simple method is to use linear, or multi-linear interpolation between discrete  $\mathcal{S}_i \in \mathcal{S}_B$ . This can work well when  $f_t$  is nearly linear, but will require an increasingly fine mesh (i.e. larger  $N$ ) as  $f_t$  becomes more non-linear. Another concern is that a piecewise linear representations will have discontinuous first derivatives at the discrete evaluation points  $\mathcal{S}_i \in \mathcal{S}_B$ , which make solution of equation (5-1) more difficult. This point is explored in more detail in Section 5.8.4.

Johnson et al. [1993] compare cubic splines, Hermite polynomials, and multi-linear interpolation for a multi-reservoir problem. They demonstrate that for a 4-reservoir system, using cubic splines resulted in a 330 times speed-up compared to multi-linear interpolation in order to achieve a 0.5% mean relative error. The speed up is both because a coarser lattice of points is sufficient, and because a faster, derivative based, quasi-Newton optimizer was used to solve equation (5-1) because cubic splines have continuous first and second derivatives.

### ***Sparse Sampling of the State Space***

The previous discussion has assumed that the selected discrete state-space points,  $\mathcal{S}_B$ , are arrayed on a regular grid, or lattice of points. This is called a full-factorial lattice because the same discretization level is used in all dimensions, and a

basis point is placed at every combination of discretization levels across the dimensions [Chen et al., 1999]. Full factorial lattices are preferable for fitting multi-linear and cubic-spline interpolation surfaces. However, other work has explored the use of irregularly placed points and partial grid designs as a means of reducing the required size of  $\mathcal{S}_B$ .

One example of partial grid design is the use of sparse grids [see Bungartz and Griebel, 2004]. Sparse grids are built using a hierarchical discretization scheme. In this approach, rather than having discrete levels in each dimension, the discretization is divided into degrees characterized by the distance between adjacent points in a degree. As the degree of discretization increases the distance between adjacent points in that degree is smaller. Under certain conditions, sparse grids can be shown to achieve the same accuracy as full grids, with a fraction of the points. Adaptive sparse grids change the degree of the discretization adaptively across the state-space in response to the complexity of the function being approximated [Brumm and Scheidegger, 2014].

Another example of partial grid design is provided Chen et al. [1999] who use orthogonal arrays to select discrete points in the state-space. To represent  $f_t$  they use multivariate adaptive regression splines, which do not require a regular lattice of points. A potential downside of MARS is that it has discontinuous first derivatives at the knots, which slow an optimization algorithm. The work presented in this chapter uses irregularly placed points, with radial basis functions (RBFs) to approximate  $f_t$ . Rather than using orthogonal arrays to select the points to sample in the state space,

this work uses *a priori* knowledge of system behavior to select points particularly relevant to likely system operation.

The corridor approach described in the next section borrows from three of the four common methods described in this section. Like SDDP the Corridor DP focuses on a limited region of the state-space. The Corridor DP utilizes RBF surrogate surfaces to approximate the future value function between discrete points where the Bellman equation has been solved. Finally, like sparse grids, the Corridor DP basis selection criteria presented in this chapter concentrates basis points in the corridor region where the surface behavior is more irregular. If the value function is linear, then it could easily be approximated by linear functions.

#### ***Section 5.4 Corridor DP***

The standard discretization lattice (or full factorial lattice) is built by discretizing each of the  $k$  dimensions into  $d$  levels, then placing a basis point at each of the  $d^k$  combinations of discrete reservoir storage in each dimension. Figure 5-1 shows a 3-dimensional projection of a 4-dimensional lattice, with 10 discrete points in each dimension, resulting in  $d^k = 10,000$  points in the state-space.

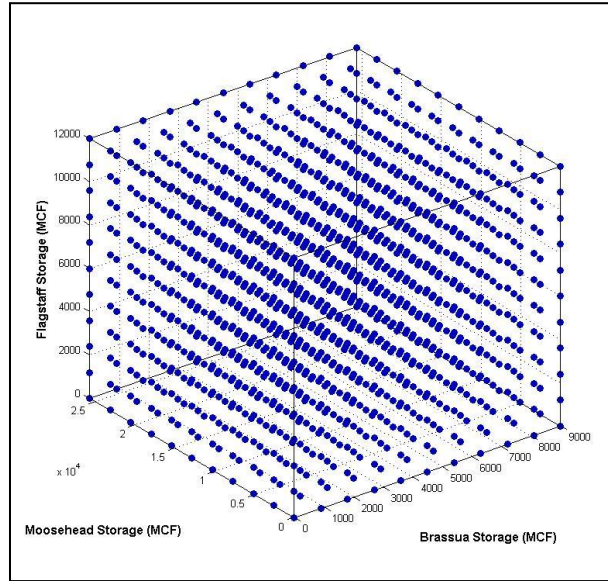
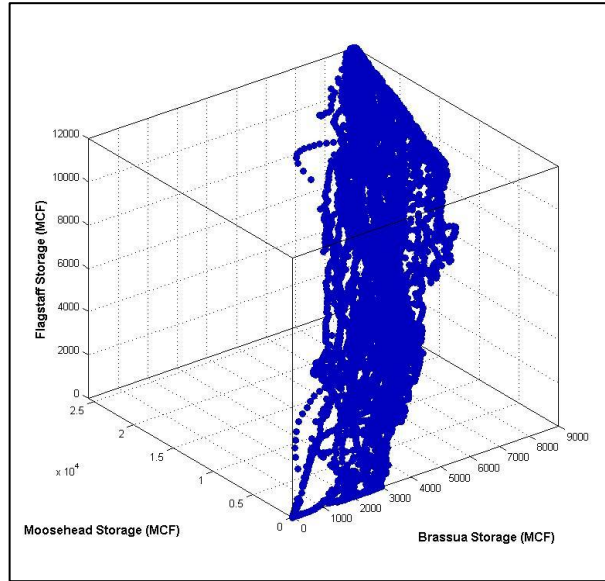


Figure 5-1: 3-dimensional projection of a 4-dimensional lattice with 10 discrete points evaluated in each dimension.

It is easy to demonstrate that much of the volume of the state space represents storage vectors which are not reasonable. When a reservoir system is operated reasonably it is unlikely that one storage reservoir will be full while others are empty. Rather, the system state will tend to travel in a corridor, as demonstrated by Saad and Turgeon [1988] and Saad et al. [1992]. This can be seen by simulating a hypothetical reservoir system (described in Section 5.8.2). Each point in Figure 5.1 is a storage vector visited when the system operation is simulated. It is clear that the system tends to travel in a corridor and never visits much of the state space during 20 years of simulation. Thus, a great deal of work can be avoided by developing the future value function approximation across a set of reasonable storages, called a Corridor.



**Figure 5.1:** Path of a 4-reservoir system in a 4-dimensional storage state space over 20-years of simulated operation.

Pereira and Pinto [1985] developed their corridor for SDDP by simulating the system iteratively as they derived the operating policy. Here it is proposed to gather a compact set of reasonable system storage vectors from at least three sources:

- (1) Storage vectors that occurred during the simulation of the historical streamflow record.
- (2) Storage vectors obtained for the system over time as a result of simulating the system yesterday, or last week (which has the advantage that they should be very close to the values of interest when decisions are optimized today).
- (3) Storage vectors obtained by simulating the anticipated solution to the optimization model for today, perhaps with some perturbation of the initial storage volumes so as to generate a neighborhood of storage stages in the state-space near today's solution.

The first approach is taken in the example in Section 5.8.2. One reason that SDP applications have not taken advantage of the corridor idea is that the approximation techniques often used to numerically solve equation (5-1), such as cubic splines or linear interpolation, work best on uniformly spaced  $k$ -dimensional lattices. New approximation techniques can deal with irregularly placed points in the

state space. One such method is radial basis function (RBF) approximation [Buhman, 2003; Wendland, 2005]. The idea in Corridor DP with RBF approximation is to concentrate basis points within the Corridor to achieve the desired precision in the important region of the state space with as few discrete points as possible.

Section 5.5 describes regular and Hermite RBF interpolation and least-squares approximation methods. Section 5.6 describes basis functional forms and their parameterization, and Section 5.7 details a procedure for selecting a good set of basis points.

### ***Section 5.5 RBF Interpolation and Least-Squares Approximation***

The RBF approximation of function  $f_t(j)$  at point  $j$  in  $k$ -dimensional space is given by:

$$\hat{f}(j) = \sum_{i=1}^M \beta_i \phi(\|\mathbf{S}(i) - \mathbf{S}(j)\|) + p(\mathbf{S}(j)) \quad (5-3)$$

where where  $\|\cdot\|$  is the Euclidean norm,  $\beta_i \in \mathbb{R}$ ,  $M$  is the number of basis points,  $\phi(\cdot)$  is the basis function,  $\mathbf{S}(i)$  is the location vector of basis point  $i$ , and  $p(\mathbf{S})$  is some polynomial function over the state space  $\mathbf{S}$ . Basis functions can take several functional forms, as summarized in Table 5-1.

In interpolation, the RBF approximation must match the function value at every basis point. This model can be obtained by solving the system of equations (Regis and Shoemaker, 2007):

$$\begin{pmatrix} \Phi & \mathbf{P} \\ \mathbf{P}^T & \mathbf{0}_k \end{pmatrix} \begin{pmatrix} \boldsymbol{\beta} \\ \mathbf{c} \end{pmatrix} = \begin{pmatrix} \mathbf{F} \\ \mathbf{0} \end{pmatrix} \quad (5-4)$$

where

$\Phi$  is an  $M \times M$  matrix where  $\Phi_{i,j} = \phi(\|\mathbf{S}(i) - \mathbf{S}(j)\|)$  for all  $i, j = 1, \dots, M$ ,  
 $\mathbf{P}$  is an  $M \times k$  matrix where  $\mathbf{P}(i, l) = p(\mathbf{S}(i, l))$ ,  
 $\mathbf{S}(i, l)$  is the value of the  $l^{th}$  dimension of the  $i^{th}$  basis point,

$\boldsymbol{\beta}$  is a  $M \times 1$  vector of model parameters,  
 $\mathbf{F}$  is an  $M \times 1$  vector where  $\mathbf{F}(i) = f_t(i)$ ,  
and  $\mathbf{0}_k$  and  $\mathbf{0}$  are zero vectors of sizes  $k \times k$  and  $k \times 1$  respectively.

Hermite interpolating RBF surfaces match the function value  $f_t(j)$  and the partial derivatives of  $f_t(j)$  with respect to each dimension of  $\mathbf{S}$ . The Hermite interpolating RBF approximation of function  $f_t(j)$  at point  $j$  in  $k$ -dimensional space is given by (Ong et al., 2008):

$$\hat{f}(j) = \sum_{i=1}^M \beta_i \phi(\|\mathbf{S}(i) - \mathbf{S}(j)\|) + \sum_{i=1}^M \sum_{l=1}^k \tilde{\beta}_{i,l} \frac{\partial \phi}{\partial S(l)}(\|\mathbf{S}(i) - \mathbf{S}(j)\|) \quad (5-5)$$

where  $\tilde{\beta}_{i,l} \in \mathbb{R}$  and  $\frac{\partial \phi}{\partial S(l)}$  is the partial derivative of  $\phi$  with respect to  $S(l)$  (the  $l^{\text{th}}$  dimension of  $\mathbf{S}$ ). In order to satisfy the condition that the partial derivatives of  $\hat{f}$  match those of  $f_t$  at each basis point,  $\phi$  must be twice differentiable. The parameters of the Hermite RBF surface in equation (5-5) can be computed by solving the equation:

$$\mathbf{A}\boldsymbol{\theta} = \mathbf{Z} \quad (5-6)$$

where  $\boldsymbol{\theta}$  is a column vector of model parameters with length  $M(k + 1)$  arranged as

$$\boldsymbol{\theta} = \{\beta_1, \tilde{\beta}_{1,1}, \tilde{\beta}_{1,2}, \dots, \tilde{\beta}_{1,k}, \beta_2, \tilde{\beta}_{2,1}, \tilde{\beta}_{2,2}, \dots, \tilde{\beta}_{2,k}, \dots, \beta_M, \tilde{\beta}_{M,1}, \tilde{\beta}_{M,2}, \dots, \tilde{\beta}_{M,k}\}$$

and  $\mathbf{Z}$  is a vector of function values and partial derivative values with length  $M(k + 1)$

arranged as

$$\mathbf{Z} = \begin{bmatrix} f_t(1), \frac{\partial f_t}{\partial S(1)}(\mathbf{S}(1,1)), \frac{\partial f_t}{\partial S(2)}(\mathbf{S}(1,2)), \dots, \frac{\partial f_t}{\partial S(k)}(\mathbf{S}(1,k)) \\ \vdots \\ f_t(M), \frac{\partial f_t}{\partial S(1)}(\mathbf{S}(M,1)), \frac{\partial f_t}{\partial S(2)}(\mathbf{S}(M,2)), \dots, \frac{\partial f_t}{\partial S(k)}(\mathbf{S}(M,k)) \end{bmatrix}$$

The coefficient matrix  $\mathbf{A}$  has size  $M(k + 1) \times M(k + 1)$  can be written in terms of  $M$  submatrices as

$$A = \begin{bmatrix} \mathbf{a}_{1,1} & \mathbf{a}_{1,2} & \cdots & \mathbf{a}_{1,M} \\ \mathbf{a}_{2,1} & \mathbf{a}_{2,2} & \cdots & \mathbf{a}_{2,M} \\ \vdots & \vdots & \ddots & \vdots \\ \mathbf{a}_{M,1} & \mathbf{a}_{M,2} & \cdots & \mathbf{a}_{M,M} \end{bmatrix}$$

where  $\mathbf{a}_{i,j}$  is a  $(k + 1) \times (k + 1)$  matrix having the form

$\mathbf{a}_{i,j}$

$$= \begin{bmatrix} \phi(\|\mathbf{S}(i) - \mathbf{S}(j)\|) & \frac{\partial \phi}{\partial S(1)}(\|\mathbf{S}(i) - \mathbf{S}(j)\|) & \cdots & \frac{\partial \phi}{\partial S(k)}(\|\mathbf{S}(i) - \mathbf{S}(j)\|) \\ \frac{\partial \phi}{\partial S(1)}(\|\mathbf{S}(i) - \mathbf{S}(j)\|) & \frac{\partial^2 \phi}{\partial S(1)^2}(\|\mathbf{S}(i) - \mathbf{S}(j)\|) & \cdots & \frac{\partial^2 \phi}{\partial S(1)\partial S(k)}(\|\mathbf{S}(i) - \mathbf{S}(j)\|) \\ \vdots & \vdots & \ddots & \vdots \\ \frac{\partial \phi}{\partial S(k)}(\|\mathbf{S}(i) - \mathbf{S}(j)\|) & \frac{\partial^2 \phi}{\partial S(k)\partial S(1)}(\|\mathbf{S}(i) - \mathbf{S}(j)\|) & \cdots & \frac{\partial^2 \phi}{\partial S(k)^2}(\|\mathbf{S}(i) - \mathbf{S}(j)\|) \end{bmatrix}$$

The discussion thus far has focused on interpolating RBF surfaces which match the function value (and the partial derivatives for Hermite RBFs) at each basis point. If the selected basis points are not distributed across the region of interest in a semi-uniform way, the resulting surface may not be smooth. Surfaces that are not smooth are particularly problematic when using derivative based methods to solve equation (5-1) in DP problems. ‘Wiggles’ in the RBF surface can cause the solver to terminate at a suboptimal solution. Because the numerical solution of DP models requires recursive solution of equation (5-1), small errors can compound over time and can become severe. Good selection of basis points can help prevent this problem, as described in Section 5.7. Another solution to the problem is to relax the interpolating conditions using a least-squares fit to the specified value of the function.

In the interpolation approach using equations (5-4) and (5-6) to solve for the parameters of equations (5-3) and (5-5), a basis function is centered at every basis point. In least-squares function approximation, the condition that the surface match

the data (and the derivatives for Hermite RBF) at each of the basis points is relaxed. Instead the model parameters are selected to minimize the sum of squared residual errors. In approximation  $d$  extra points are added for which the function value (and the partial derivatives for Hermite RBF) are known but at which no basis function is centered. This provides degrees of freedom, resulting in a smoother surface. Least-squares approximation is a very reasonable alternative to interpolation in the numerical solution of DP problems because the true values of  $f_t$  are not known with certainty. There is error due to the tolerance of the numerical optimization and errors from using some function as a surrogate for the true future value function surface. In SDP errors are also introduced from the discrete representation of continuous stochastic processes.

The least squares approximate RBF surface is still provided by equation (5-3), but now the condition that  $\hat{f}(i) = f_t(i)$  for all points  $i$  in the basis is relaxed. Thus,  $\hat{f}(i) = f_t(i) + e(i)$ .  $d$  additional points,  $\check{\mathbf{S}}$ , are added, but no basis functions are centered at the new points. The model parameters which minimize the sum of squared errors are given by:

$$\begin{pmatrix} \mathbf{B} \\ \mathbf{c} \end{pmatrix} = (\mathbf{D}^T \mathbf{D})^{-1} \mathbf{D}^T \begin{pmatrix} \mathbf{F} \\ \check{\mathbf{F}} \end{pmatrix} \quad (5-7)$$

where  $\check{\mathbf{F}}$  is a  $d \times 1$  vector where  $\check{\mathbf{F}}(i) = f_t(i)$ , and  $\mathbf{D}$  is a  $(M + d) \times (M + k)$  matrix

$$\mathbf{D} = \begin{pmatrix} \mathbf{\Phi} & \mathbf{P} \\ \check{\mathbf{\Phi}} & \check{\mathbf{P}} \end{pmatrix}$$

where

$\check{\mathbf{\Phi}}$  is a  $d \times M$  matrix where  $\check{\Phi}_{i,j} = \phi(\|\check{\mathbf{S}}(i) - \mathbf{S}(j)\|)$  for all  $i = 1, \dots, d$  and  $j = 1, \dots, M$ ,

$\check{\mathbf{P}}$  is a  $d \times k$  matrix where  $\check{P}_{i,l} = p(\check{\mathbf{S}}(i, l))$  for all  $i = 1, \dots, d$  and  $l = 1, \dots, k$ , and  $\mathbf{\Phi}$  and  $\mathbf{P}$  are as defined before.

Similarly the least-squares approximate Hermite RBF surface is still provided by equation (5-5), but the conditions that  $\hat{f}(i) = f_t(i)$  and  $\frac{\partial \hat{f}}{\partial s(j)}(i) = \frac{\partial f_t}{\partial s(j)}(i)$  at all points  $i$  in the basis and all dimensions  $j$  is relaxed. Thus,  $\hat{f}(i) = f_t(i) + e(i)$  and  $\frac{\partial \hat{f}}{\partial s(j)}(\mathbf{S}(i, j)) = \frac{\partial f_t}{\partial s(j)}(\mathbf{S}(i, j)) + \tilde{e}(i, j)$ .  $d$  additional points,  $\ddot{\mathbf{S}}$ , are added, but no basis functions are centered at the new points. The model parameters which minimize the sum of squared errors are given by:

$$\begin{pmatrix} \boldsymbol{\beta} \\ \tilde{\boldsymbol{\beta}} \end{pmatrix} = (\mathbf{G}^T \mathbf{G})^{-1} \mathbf{G}^T \begin{pmatrix} \mathbf{Z} \\ \ddot{\mathbf{Z}} \end{pmatrix} \quad (5-8)$$

where  $\ddot{\mathbf{Z}}$  is a  $d(k+1) \times 1$  vector:

$$\ddot{\mathbf{Z}} = \begin{bmatrix} f_t(1), \frac{\partial f_t}{\partial S(1)}(\ddot{\mathbf{S}}(1,1)), \frac{\partial f_t}{\partial S(2)}(\ddot{\mathbf{S}}(1,2)), \dots, \frac{\partial f_t}{\partial S(k)}(\ddot{\mathbf{S}}(1,k)) \\ \vdots \\ f_t(M), \frac{\partial f_t}{\partial S(1)}(\ddot{\mathbf{S}}(M,1)), \frac{\partial f_t}{\partial S(2)}(\ddot{\mathbf{S}}(M,2)), \dots, \frac{\partial f_t}{\partial S(k)}(\ddot{\mathbf{S}}(M,k)) \end{bmatrix}$$

and  $\mathbf{G}$  is a  $(M+d)(k+1) \times M(k+1)$  matrix:

$$\mathbf{G} = \begin{bmatrix} \mathbf{A} \\ \ddot{\mathbf{A}} \end{bmatrix}$$

where  $\mathbf{A}$  is as previously defined and  $\ddot{\mathbf{A}}$  is matrix of size  $d(k+1) \times M(k+1)$  that can be written in terms of  $M$  submatrices as:

$$\ddot{\mathbf{A}} = \begin{bmatrix} \ddot{\mathbf{a}}_{1,1} & \ddot{\mathbf{a}}_{1,2} & \cdots & \ddot{\mathbf{a}}_{1,M} \\ \ddot{\mathbf{a}}_{2,1} & \ddot{\mathbf{a}}_{2,2} & \cdots & \ddot{\mathbf{a}}_{2,M} \\ \vdots & \vdots & \ddots & \vdots \\ \ddot{\mathbf{a}}_{d,1} & \ddot{\mathbf{a}}_{d,2} & \cdots & \ddot{\mathbf{a}}_{d,M} \end{bmatrix}$$

where  $\ddot{\mathbf{a}}_{i,j}$  is a  $(k+1) \times (k+1)$  matrix having the form

$\mathbf{a}_{i,j}$

$$= \begin{bmatrix} \phi(\|\check{\mathbf{s}}(i) - \check{\mathbf{s}}(j)\|) & \frac{\partial \phi}{\partial S(1)}(\|\check{\mathbf{s}}(i) - \check{\mathbf{s}}(j)\|) & \cdots & \frac{\partial \phi}{\partial S(k)}(\|\check{\mathbf{s}}(i) - \check{\mathbf{s}}(j)\|) \\ \frac{\partial \phi}{\partial S(1)}(\|\check{\mathbf{s}}(i) - \check{\mathbf{s}}(j)\|) & \frac{\partial^2 \phi}{\partial S(1)^2}(\|\check{\mathbf{s}}(i) - \check{\mathbf{s}}(j)\|) & \cdots & \frac{\partial^2 \phi}{\partial S(1)\partial S(k)}(\|\check{\mathbf{s}}(i) - \check{\mathbf{s}}(j)\|) \\ \vdots & \vdots & \ddots & \vdots \\ \frac{\partial \phi}{\partial S(k)}(\|\check{\mathbf{s}}(i) - \check{\mathbf{s}}(j)\|) & \frac{\partial^2 \phi}{\partial S(k)\partial S(1)}(\|\check{\mathbf{s}}(i) - \check{\mathbf{s}}(j)\|) & \cdots & \frac{\partial^2 \phi}{\partial S(k)^2}(\|\check{\mathbf{s}}(i) - \check{\mathbf{s}}(j)\|) \end{bmatrix}$$

Both interpolation and least-squares approximation methods can be used to fit RBF and Hermite RBF surfaces to the future value function in numerical DP experiments, as described in Section 5.8.2.

### ***Section 5.6 Basis Functional Forms and Parameterization***

The previous section described RBF interpolation and least-squares approximation techniques. This section describes some common basis functional forms, discusses their parameterization, and provides some visualizations of fitted RBF surfaces. Experience suggests that the performance of numerical DP models using RBFs to represent the future value function are highly dependent on the set of basis points and the parameterization of the basis functions. This section focuses on the parameterization of basis functions, while Section 5.7 describes a greedy algorithm for selecting basis points that are where they best help improve the approximation.

Table 5-1 summarizes commonly used basis functional forms, but others are also commonly applied. Each of the functions, except the tri-cube have global support. Tri-cubes have compact support because they take non-zero values only at distances less than  $B$ , where  $B$  is the bandwidth parameter. Gaussian functions are globally supported, but rapidly approach to zero at some distance from the basis point. The Gaussian scale parameter  $\gamma$  is essentially like a bandwidth parameter in that it

controls how quickly  $\phi$  decreases. Similarly, inverse multiquadrics vanish to zero at infinite distance from the basis point, and have a scale parameter  $\gamma$  which controls the shape of the function and how quickly  $\phi$  begins to decrease.

Table 5-1: Basis Functional Forms and Conditions (Regis and Shoemaker, 2007)

Name	Functional Form	Conditions
Surface Splines	$\phi(r) = r^\kappa$	$\kappa \in \mathbb{N}, \kappa$ odd
	$\phi(r) = r^\kappa \log(r)$	$\kappa \in \mathbb{N}, \kappa$ even
Multiquadrics	$\phi(r) = (r^2 + \gamma^2)^\kappa$	$\kappa \notin \mathbb{N}, \kappa > 0$
Inverse Multiquadrics	$\phi(r) = (r^2 + \gamma^2)^\kappa$	$\kappa < 0$
Gaussian	$\phi(r) = e^{-\gamma r^2}$	$\gamma > 0$
Tri-cube	$\phi(r) = \max\left(0, \left(1 - \left(\frac{r}{B}\right)^3\right)^3\right)$	$B > 0$

RBF cubic splines ( $\phi(r) = r^3$ ) and RBF thin-plate splines ( $\phi(r) = r^2 \log(r)$ )

are special cases of the surface splines. RBF cubic splines have continuous second derivatives over the whole surface. RBF thin-plate splines have infinite second derivatives at the basis points, which is troubling in our application. Surface splines take increasingly large values at increased distance from the basis point, and have no scale or bandwidth parameter, which makes their use simpler. In particular, with the cubic polynomial, the basis functions are global polynomials, and not local, so that the problem of having too small a bandwidth does not arise. On the other hand, because the surface splines do not approach zero at large distances, the surface spline approximation anywhere depends on the value of the function  $f$  everywhere.

### ***Section 5.6.1 RBF Function Shape and Parameterization for two-dimensional test cases***

To help visualize how the choice of RBF functional form and parameterization affect the shape of the fitted surface, consider the following 2-dimensional quadratic test function:

$$\begin{aligned}
y = & -1(10 - x_1)^2 - 1(10 - x_2)^2 + (10 - x_1)(10 - x_2) + (10 - x_1) \\
& + (10 - x_2) + 90 \\
& x_1 \in [0,10], x_2 \in [0,10]
\end{aligned}
\tag{5-9}$$

Figure 5-2 plots the resulting surface.

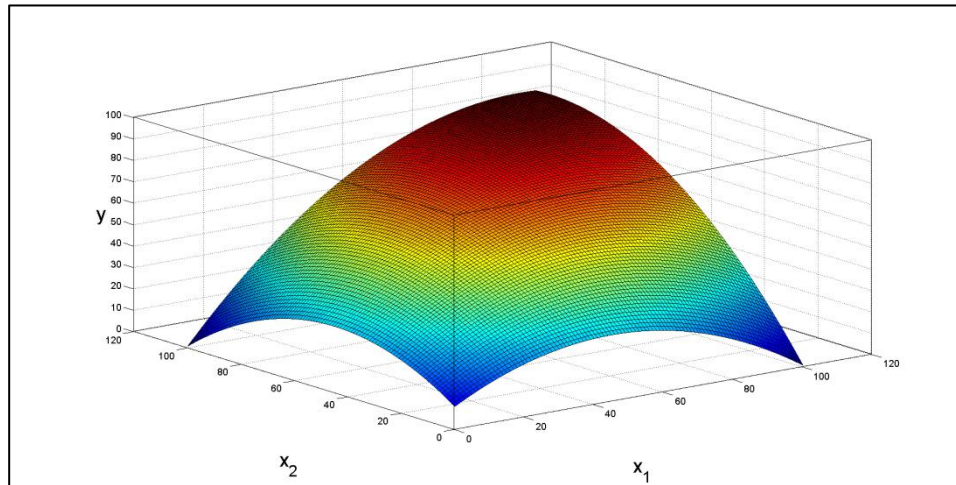


Figure 5-2: Quadratic Test Function

For our example each dimension is discretized at three levels, and a basis point is placed at each combination of the levels (a full factorial grid). Figure 5-3, Figure 5-4, Figure 5-5, and Figure 5-6 plot an interpolating Gaussian surface fit with scale parameters,  $\gamma$ , of 0.1, 0.6, and 2.1, and 4.6 respectively. Figure 5-7 plots the RBF cubic spline fit.

Note that for small  $\gamma$  the Gaussian functions quickly fade to zero, and the interpolating RBF surface essentially becomes a plane, with spikes where basis points are located. As  $\gamma$  becomes larger, the Gaussian functions overlap, creating a smooth surface which closely resembles the real function in Figure 5-2. The cubic function has no scale parameter, and the cubic functions at each basis point overlap, creating a smooth approximation.

However, it should be noted that the lack of a scale parameter means that RBF cubic spline functions are potentially less sensitive to local features of a non-smooth function, and there is no parameter or adjustment to make them more sensitive. As an example consider the Matlab test function ‘Peaks’ plotted in Figure 5-8. Each dimension is divided into five levels and a basis point is placed at each combination of level (a full factorial grid). Figure 5-9 plots the interpolating Gaussian RBF function ( $\gamma = 0.65$ ), and Figure 5-10 plots the interpolating Cubic Spline RBF function. Note that much of the detail is missed by both RBF surfaces due to the coarse discretization: there are only 9 grid points. However, the Gaussian functions are able to resolve more of the irregular surface details because they are better able to represent local features.

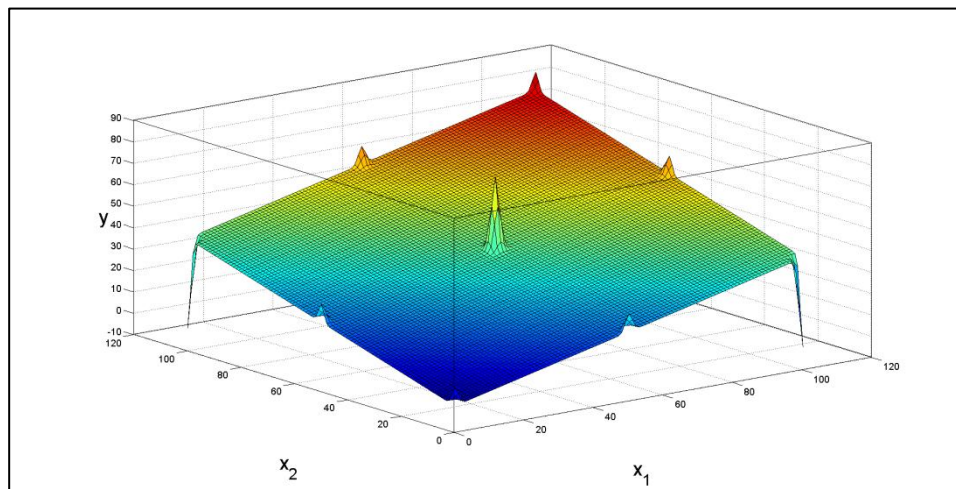


Figure 5-3: Interpolating Gaussian RBF surface ( $\gamma = 0.1$ ) with 9 grid points

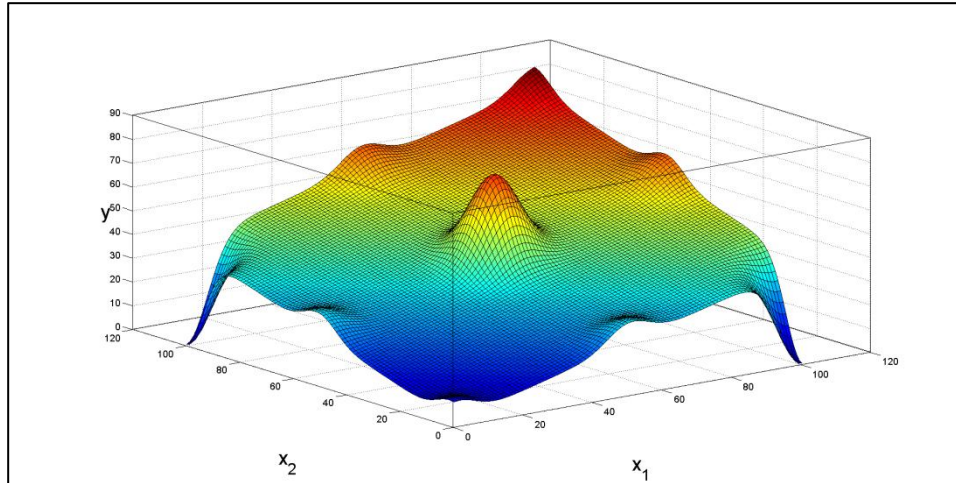


Figure 5-4: Interpolating Gaussian RBF surface ( $\gamma = 0.6$ ) with 9 grid points

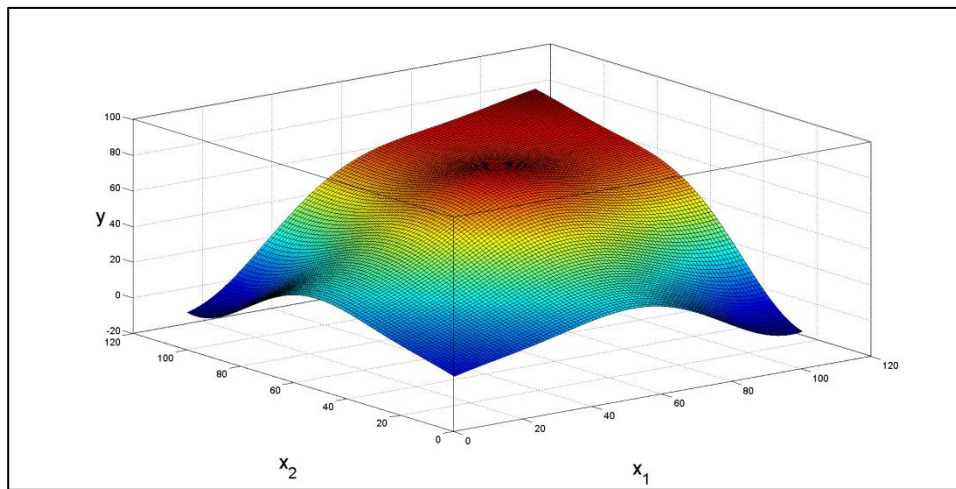


Figure 5-5: Interpolating Gaussian RBF surface ( $\gamma = 2.1$ ) with 9 grid points

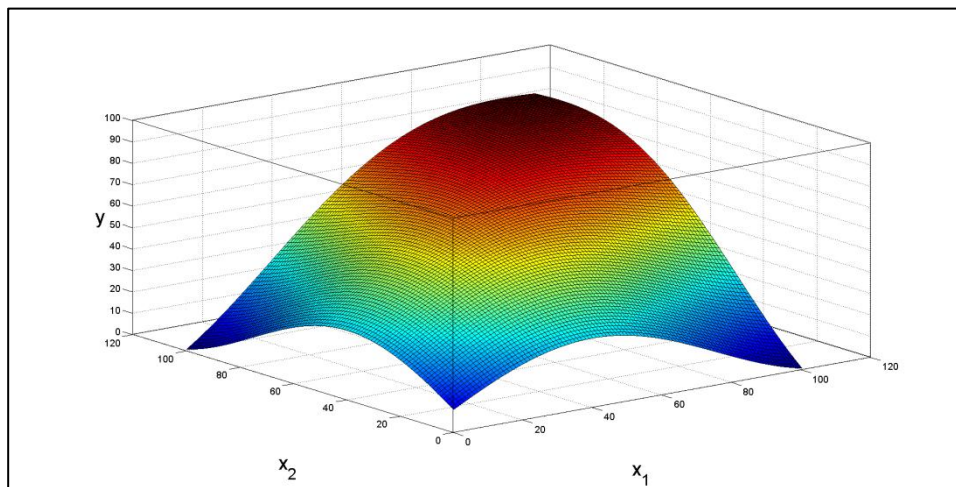


Figure 5-6: Interpolating Gaussian RBF surface ( $\gamma = 4.6$ ) with 9 grid points

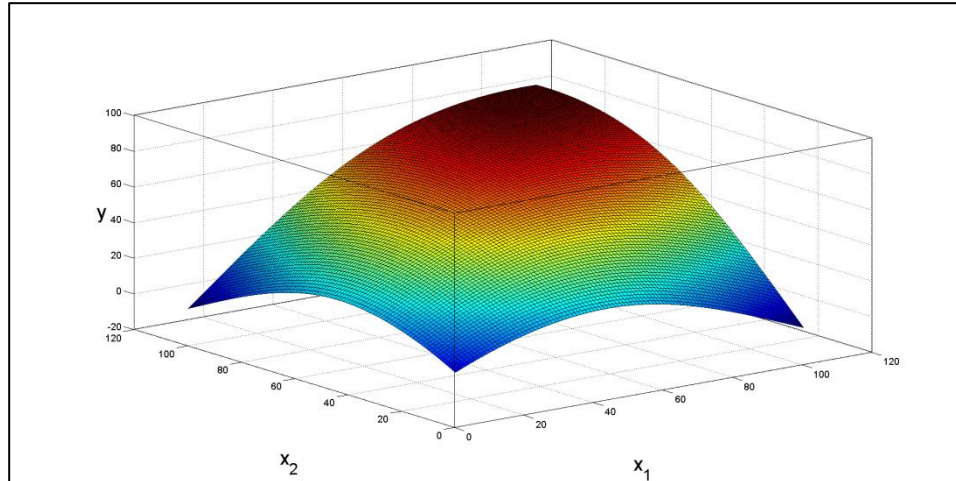


Figure 5-7: Interpolating RBF cubic Spline RBF surface with 9 grid points

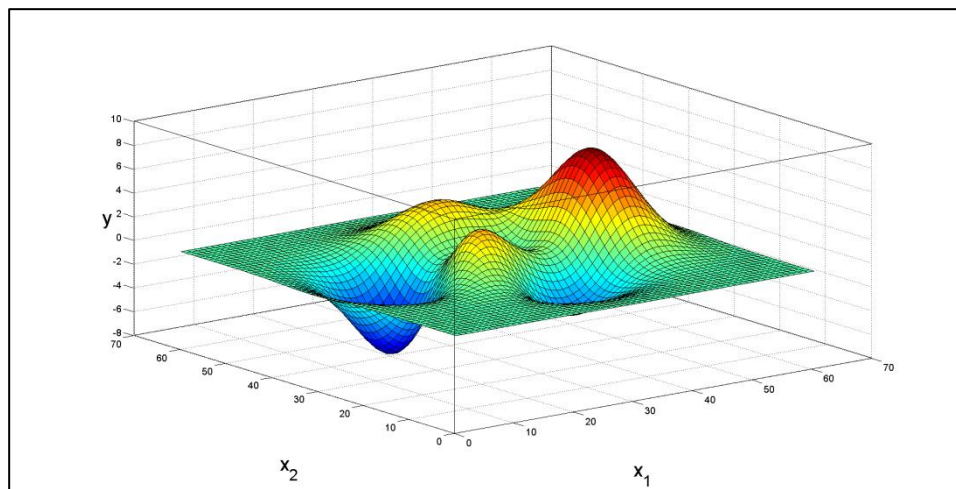


Figure 5-8: Matlab 'Peaks' Function

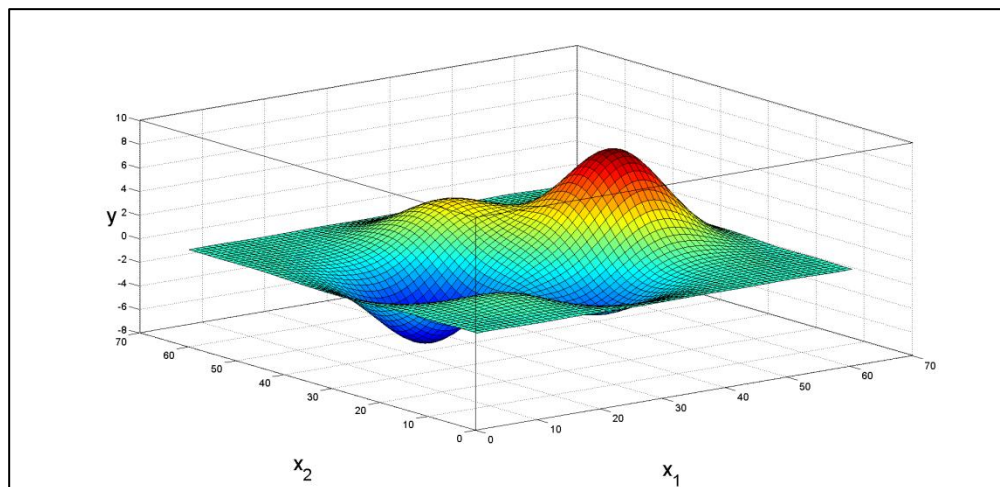


Figure 5-9: Interpolating Gaussian RBF ( $\gamma = 0.65$ ) surface for Matlab 'Peaks' with 9 grid points

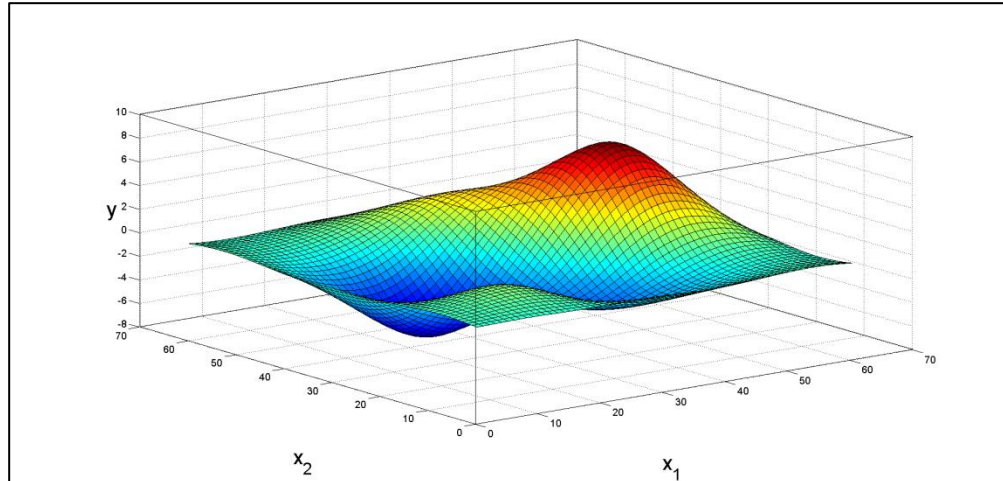


Figure 5-10: Interpolating Cubic Spline RBF surface for Matlab 'Peaks' with 9 grid points

As is clear from the test cases, the choice of basis function and the parameterization of the function can have a large impact on the shape of the fitted RBF surface. The choice of function surface can be informed by *a priori* knowledge of the shape of the true surface or through experimentation with available data. The latter approach was taken in this work, as described in Section 5.8.

There is a significant body of results that describe how basis points should be spaced and how basis functions should be parameterized. For an excellent reading on the topic, see Wendland [2005] or Buhmann [2003]. Many of those results are based on the *separation distance* and *fill distance*. *Separation distance* is  $\frac{1}{2}$  the minimum distance between separate basis points. This can be interpreted as the maximum radius of two spheres centered at different basis points that are disjoint. For an extensive discussion of the effect of separation distance on RBF interpolation see Ball et al. [1992].

*Fill distance* is the maximum radius of a sphere contained in the state space which does not include a basis point: i.e. the largest gap in the data sites. Using these

two metrics, Wendland [2005] details several results on basis function parameterization, and point selection for stable and well-conditioned RBF interpolates. Unfortunately many of the results which rely on *fill distance* and *separation distance* are based on semi-uniform distributed points. By design, the *fill distance* will be very large compared to the *separation distance* in Corridor DP applications. On the other hand, the *separation distance* is an important metric, as closely spaced points can cause the RBF surface to ‘wobble.’ When applying the Corridor selection methodology in Section 5.7 the separation distance provides a useful diagnostic metric.

### ***Section 5.7 Selection of Corridor Points***

As described in Section 5.4, candidate corridor points might be generated from simulation or repeated optimization with different starting conditions. However these points may not represent a good basis for RBF interpolation. Many points might be redundant: they might be very close and represent essentially the same storage state. Furthermore, there might be holes or gaps in the Corridor coverage where the system could easily travel but did not happen to go during the simulation period. Another concern is that the basis points might not be concentrated where they are needed to obtain a good approximation (i.e. where the future value function becomes very non-linear). Finally, the solution of the Bellman equation (equation (5-1)) requires a reasonable approximation of the future value function in the extremes of the state-space even if it does not choose to go that direction, and such points will not be included in a record of typical system operation. This section describes a procedure for selecting a set of points which address the concerns above. This could be justified

with a diffusion or thermal analogy of shaking the initial set of points so that they moved around randomly

### ***Section 5.7.1 Step One: Filling***

Filling is simply the process of eliminating in any holes or gaps which might exist in the Corridor. Define  $\mathbf{B}$  as the current set of basis points in our  $k$ -dimensional optimization problem which have been obtained using one of the procedures described in Section 5.4.  $\mathbf{B}(j)$  is the  $j^{th}$  point in set of points  $\mathbf{B}$ . The simplest approach to filling is to add  $n$  new points for each of the current points, with a multivariate normal random displacement about each current point,  $\epsilon \sim MVN(\mathbf{0}, \mathbf{\Sigma})$ , where  $\mathbf{0}$  is a  $k \times 1$  vector of zeros and  $\mathbf{\Sigma}$  is a  $k \times k$  covariance matrix.

Selecting a reasonable  $\mathbf{\Sigma}$  is not trivial, particularly in high dimensional space. If the elements of  $\mathbf{\Sigma}$  become too large, then new points will be placed beyond the Corridor region, but if the elements of  $\mathbf{\Sigma}$  are too small then the new points will fail to fill gaps in the Corridor coverage. Furthermore, an appropriate scale for each dimension should be selected – should it be percentage of active storage, or cubic meters?

A major consideration when selecting a reasonable  $\sigma^2$  is that the density of points might vary widely across the Corridor region. For this reason, it was found useful to define a point-specific covariance matrix,  $\mathbf{\Sigma}$ . In particular, a covariance matrix was selected so that the 95% of generated points fall within a  $k$ -sphere enclosing the 30 nearest points. The choice of 30 is somewhat arbitrary, but seemed to produce good results.

The selection of  $\Sigma$  is achieved by assuming that the variance in each dimension (i.e. the diagonal elements of  $\Sigma$ ) are equal (say  $\sigma$ ), that there is no correlation (i.e. the off diagonal elements of  $\Sigma = 0$ ) and observing that:

$$\left(\frac{r}{\sigma}\right)^2 \sim \chi_k^2 \quad (5-10)$$

where  $\chi_k^2$  denotes the chi-distribution with  $k$  degrees of freedom and  $r$  is the distance between a newly generated point and the original point. Let  $v$  be the inverse of the CDF of  $\chi_k^2$  and  $r_{30}$  be the distance to the 30<sup>th</sup> nearest point.  $\sigma^2$  is then given by:

$$\sigma^2 = \left(\frac{r}{v}\right)^2 \quad (5-11)$$

This ensures that the range over which the  $n$  new points are distributed reflects the sparsity of the Corridor coverage about point  $i$ . Figure 5-11 plot the Corridor region before, and after filling.

It should be noted that random diffusion as described above can result in basis points which are outside the state space. In reservoir problems this means that the storage vector includes storages which are either negative or greater than the maximum reservoir storage. This is a common problem for points on the boundary of the state space: on average 94% randomly generated new points about a vertex of a 4-dimensional hypercube will not be valid. An easy solution to this problem is to re-draw when an infeasible point is generated. A second solution is to simply set the dimension of the state vector which lies outside the state space to the boundary (either 0 or the maximum allowed in that direction). The second approach can result in many points concentrated along the edges of the state space. This might be desirable if the future value function is very non-linear at the boundaries. On the other hand it can

result in many redundant points, which prevents proper filling of the Corridor region. For this reason the re-sample approach was adopted in this study.

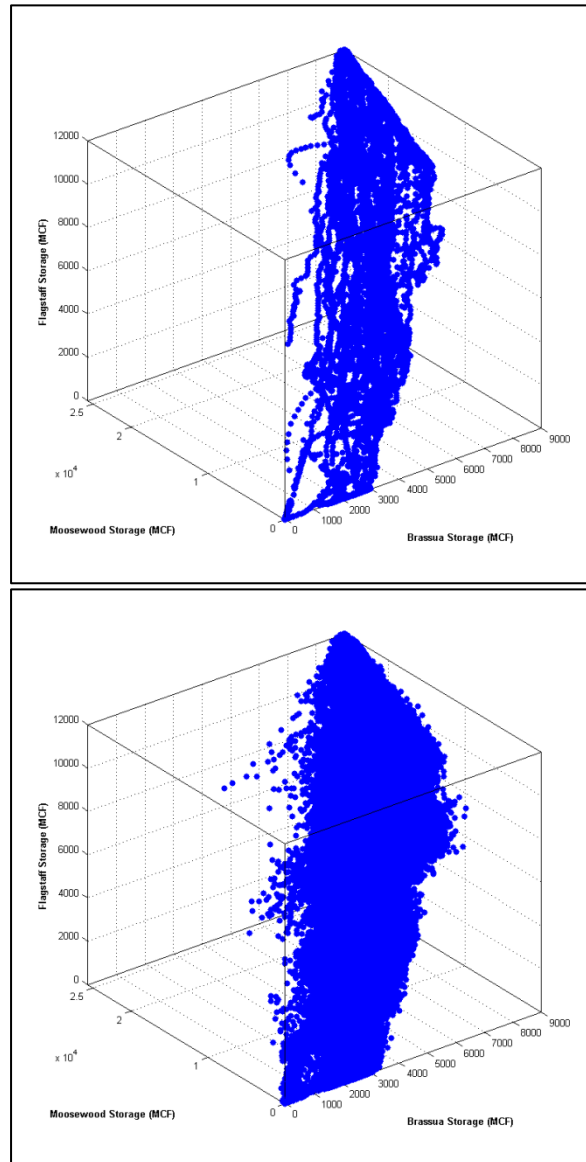


Figure 5-11: Corridor Basis Points before and after Filling.

### ***Section 5.7.2 Step Two: Inserting a Backbone***

As was noted at in the introduction to this section, the solution of equation (5-1) in DP problems will consider transitions into the extreme regions (or vertices) of the state-space. Thus it is desirable that the fitted RBF surface have a reasonably accurate representation of the future value function in the extremes. This is achieved

by inserting ‘backbone’ points outside of the Corridor, allowing the RBF surface to maintain a reasonable representation of the future value function. Figure 5-12 plot the basis points after ‘backbone’ points are added.

Different discretization levels of the backbone were tested it was found that placing points at the vertices of the state space (16 backbone points) performed as well as having four discrete levels in each dimension (256 backbone points), while being substantially less computationally expensive.

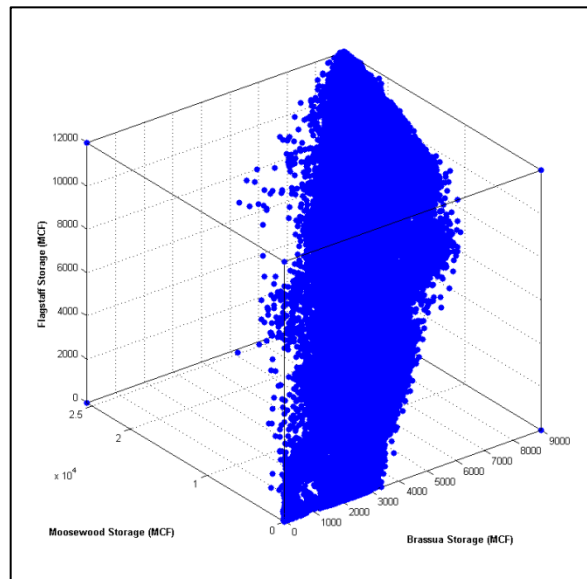


Figure 5-12: Corridor Basis Points with Backbone points

### ***Section 5.7.3 Step Three: Corridor Thinning***

As described in the beginning of this section, two additional concerns when selecting a good basis are that 1) the basis does not contain redundant points, and 2) that the basis contain points where the surface of the future value function is highly non-linear. To address both of these concerns a greedy algorithm is proposed to generate a well-conditioned basis for the RBF approximation. For simplicity, the following discussion will focus on RBF interpolation. While not explicitly described here, the procedure can also be easily be extended to RBF least-squares

approximation, Hermite RBF interpolation, and Hermite RBF least-squares approximation. The algorithm for an RBF interpolating surface has 4 steps, as described in Table 5-2.

If basis functions with compact support are used, the algorithm in Table 5-2 will be much faster than if basis functions with global support are used (Wendland, 2005). This is because only the coefficients of nearby points need be updated when a new basis point is added, rather than the coefficients of every basis point. Brumm and Scheidegger [2014] utilizes the same principle to achieve quick convergence in an adaptive sparse grid framework. In that work, hierarchical basis functions with disjoint support are used so that the coefficient of a new basis point is simply the residual error at that point. In this work, globally supported basis functions are used. But basis point selection is an ‘off-line’ process which is run separate from the Corridor DP algorithm, so the speed of the basis selection process is not a major concern.

**Table 5-2: Greedy Algorithm for basis selection for Interpolating RBF Surface**

**Input:** Set of candidate basis points  $\mathbf{B}$ , and corresponding function values  $\mathbf{F}$ . Set of initial points  $\mathbf{S}_0$ , and corresponding  $\mathbf{F}_0$ . RBF functional form and parameterization. Desired maximum squared error,  $\varepsilon^2 > 0$

**Output:** Set of basis points  $\hat{\mathbf{S}}$  whose fitted interpolating surface  $\hat{\mathbf{F}}$  satisfies accuracy criterion.

**Step 1:** Iteration  $i = 0$ . Fit RBF surface  $\hat{\mathbf{F}}_0$  to basis  $\mathbf{S}_0$ .

**Step 2:** Iteration  $i = i + 1$ . Compute maximum squared residual error and record

$$\text{index } e_i^2 = \max \left( (\hat{\mathbf{F}}_{i-1}(\mathbf{B}) - \mathbf{F})^T (\hat{\mathbf{F}}_{i-1}(\mathbf{B}) - \mathbf{F}) \right)$$

Identify index  $j$  corresponding to  $e_i^2$

**Step 3:** IF  $e_{k_i}^2 < \varepsilon^2$ , DONE

ELSE Add  $\mathbf{B}(j)$  to basis  $\mathbf{S}_i$

**Step 4:** Fit RBF surface  $\hat{\mathbf{F}}_i$  to basis  $\mathbf{S}_i$ , move to Step 2

Because the algorithm is greedy, it will be somewhat sensitive to the choice of the initial basis points,  $\mathcal{S}_0$ . A natural choice for  $\mathcal{S}_0$  are the ‘backbone’ points. In this way, one starts with a very coarse representation of the surface and progressively adds points to the Corridor region where they are needed. Figure 5-13 plots the maximum residual error versus iteration number for a sample run of the Greedy Algorithm described in Table 5-2, where the ‘backbone’ points were used as  $\mathcal{S}_0$ .

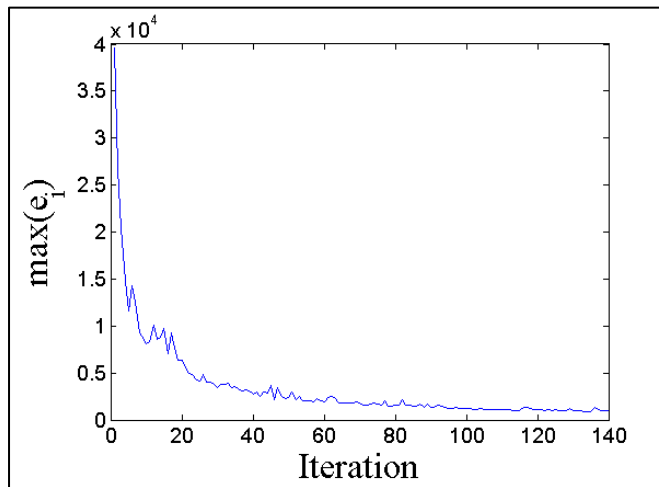


Figure 5-13: Maximum Residual Error ( $\max(e_i)$ ) versus Iteration of the Greedy Basis Selection Algorithm

Note that  $\max(e_i)$  sometimes increases, which is counter-intuitive for a greedy algorithm. However this occurs because when using globally supported basis functions an improvement in one region might result in a distortion and greater errors in another. The algorithm quickly responds to this by placing additional points where the error in the fit is worst. Figure 5-14 plot an example of a thinned Corridor using the Greedy Algorithm in Table 5-2 for the *easy case* in Section 5.8.2. Figure 5-15 plots a thinned Corridor using the Greedy Algorithm in Table 5-2 for the *hard case* in Section 5.8.3.

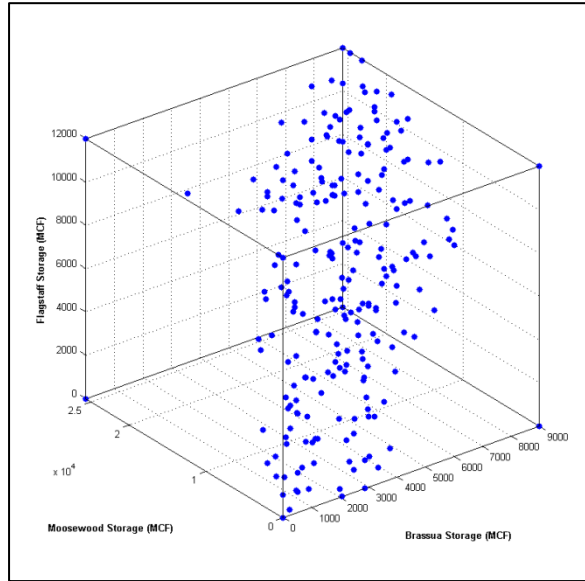


Figure 5-14: Corridor Basis Points with Backbone after thinning using the Greedy Algorithm, for the *easy case*

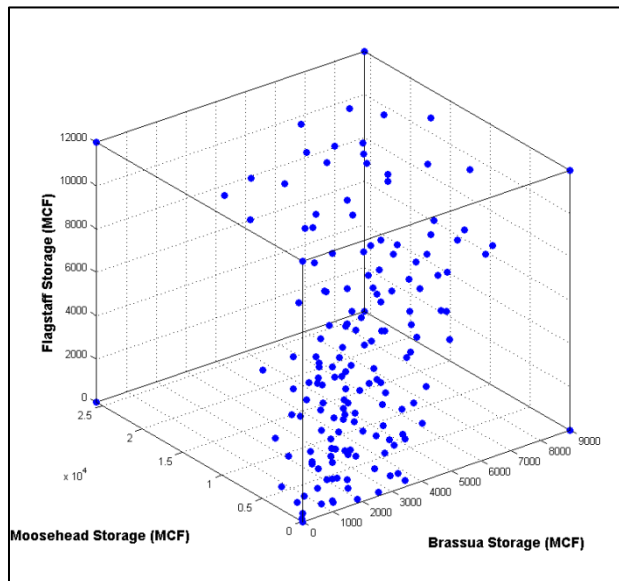


Figure 5-15: Corridor Basis Points with Backbone after thinning using the Greedy Algorithm, for the *hard case*

For the run plotted in Figure 5-14, and for all runs of the Greedy Algorithm reported in this thesis the values of  $\mathbf{F}$  were generated using the highest resolution spline from the test problem in Section 5.8.2. The high resolution spline is paired with standard (full lattice) DP, and that algorithm recursively iterates three steps. The

resulting cubic spline approximation of  $f_{T-3}(\mathbf{B})$  is used as  $\mathbf{F}$  for the greedy algorithm. Of course the extent to which  $\mathbf{F}$  resembles the real surface will affect the performance of the greedy algorithm. Experience suggests that practitioners likely have a reasonable estimate of  $\mathbf{F}$  from repeatedly solving similar optimization problems on their system.

For all of the Corridor SDP results presented in this thesis,  $\mathbf{S}_0$  is the 16 backbone points. Following the algorithm in Table 5-2, the RBF surface of choice is fit to  $\mathbf{S}_0$ . For the example in Figure 5-13 and Figure 5-14 cubic RBFs are used.

### ***Section 5.8 Results***

To demonstrate the Corridor SDP concept, a four reservoir example is provided in this section. Section 5.8.1 provides a brief discussion of the hydropower system used as a test case, with a more extensive discussion of the hydrologic characteristics of that basin included in Chapter 3. Section 5.8.2 provides a comparative analysis of the Corridor DP algorithm and DP algorithms using full-factorial grids with multi-linear and cubic spline interpolants.

#### ***Section 5.8.1 Test Basin***

The Kennebec River basin is located in north-central Maine in the eastern United States. The river originates near the US/Canada border and flows 150 miles to the Atlantic Ocean at Merrymeeting Bay. The river has a drainage area of 5,870 square miles and includes a wide range of topography from mountains in the headwaters to flat coastal plains.

There are ten hydro-electric generation facilities as well as two storage-only reservoirs (Moosehead and Flagstaff Lakes) located along the length of the river. The

elevation change from the first facility to the last is 1073 vertical feet. The total installed hydro-electric generation capacity is 256 MW. The available storage in the Kennebec's three primary reservoirs, Moosehead Lake, Flagstaff Lake, and Brassua Lake is 44.7 billion cubic feet, or about 15% of the average annual runoff. Figure 5-16 shows a schematic of the Kennebec Hydropower system.

Essentially the system contains three storage reservoirs and two generating reservoirs, followed by seven run-of-river plants. Run-of-river plants have virtually no storage so the only water available in stage  $t$  is the inflow.

For the demonstration in this chapter a four reservoir sub-system of the Kennebec hydropower system is modeled, as shown in Figure 5-17. Here the Lower Kennebec is not modeled, and Harris Station and Moosehead Lake are modeled as a composite reservoir. There is relatively little unregulated inflow between Harris Station and Moosehead Lake, and Harris Station has a relatively small storage, but significant head effects. Thus, the optimal operating policy of the whole system would include using Moosehead to keep Harris Station as full as possible, without spilling. Thus modeling Harris Station and Moosehead Lake as a composite reservoir is appropriate.

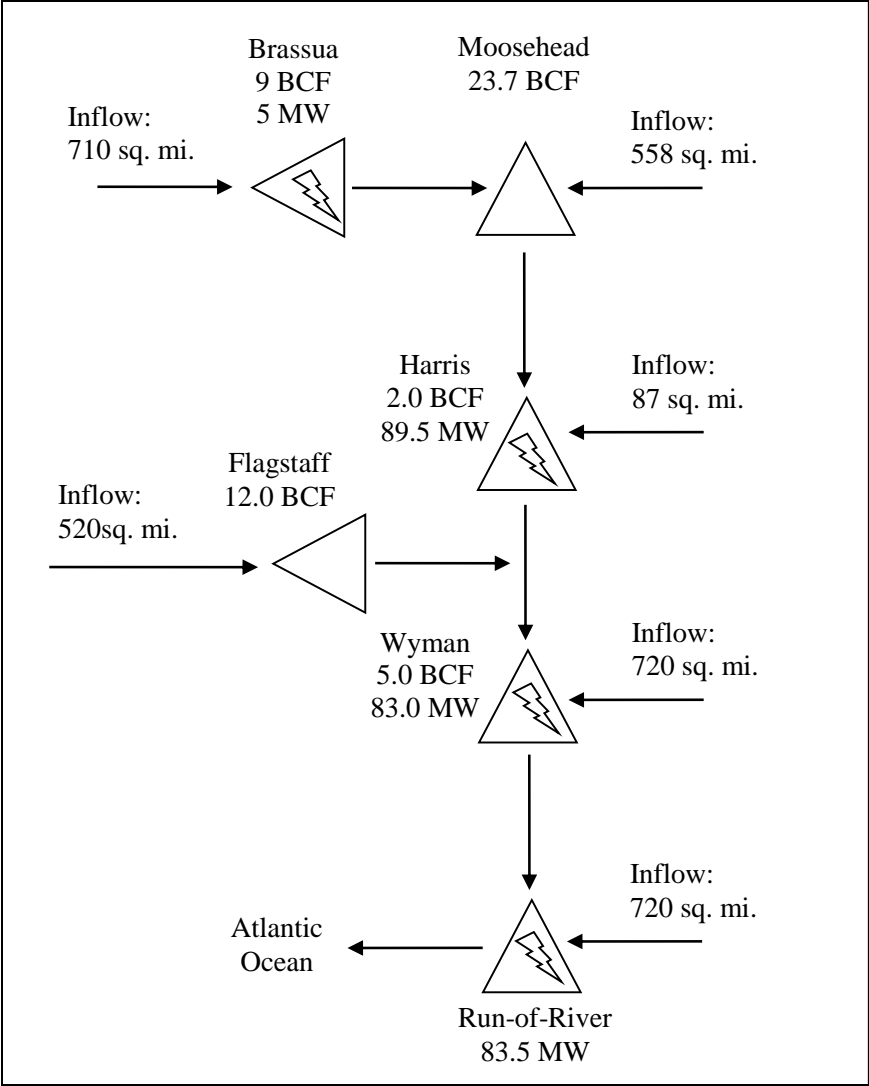


Figure 5-16: Schematic of the Kennebec Hydropower System

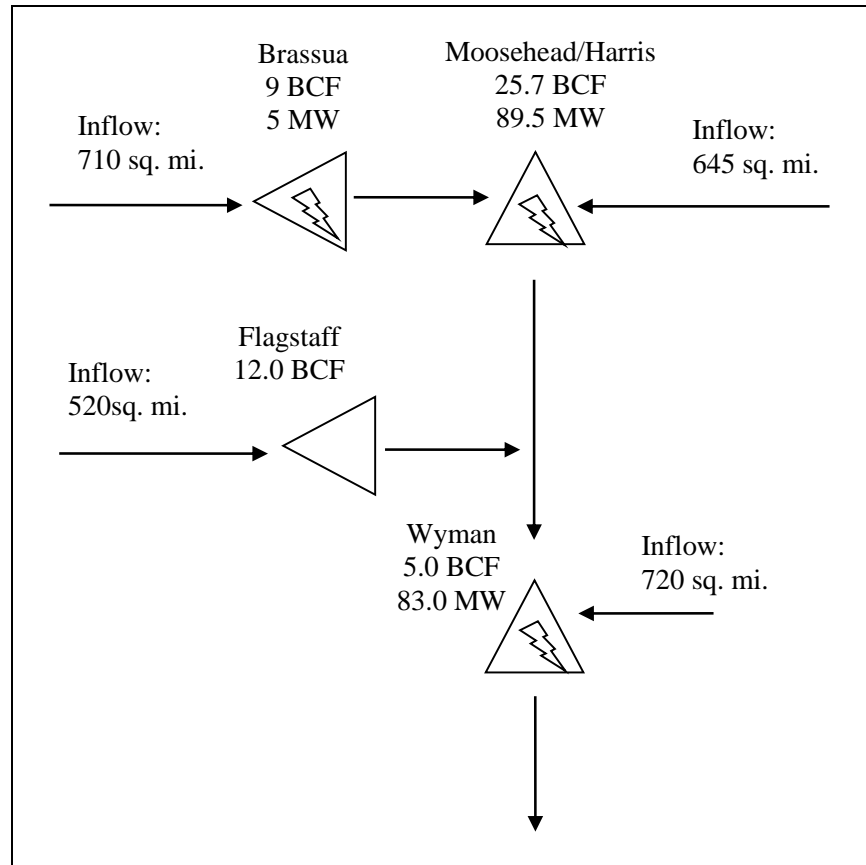


Figure 5-17: Schematic of four-reservoir test system used in Section 5.8.2.

**Section 5.8.2 Comparison of Traditional and Corridor SDP: Easy Case**

A three-stage, four reservoir DP model of the system in Figure 5-17 was constructed. This model was run using various representations of  $f_t$ . Of interest is the error in  $\hat{f}_t$  after several (3) DP stages associated with different representations of the future value function and different basis sizes. It is expected that as the number of points in the basis increases, the accuracy of  $\hat{f}_t$  should also improve. Unfortunately, increasing the size of the basis also increases the burden of solving the DP problem. This section explores the question: given a desired accuracy of solution in the Corridor (accuracy of  $\hat{f}_t$  inside the Corridor region), what basis selection and future value function representation method achieves the desired accuracy with the smallest basis?

Our examples start with what is called the *easy case* because there are no penalties, and the value function  $f$  is very smooth and well behaved. The next sections considers our *hard case* wherein the reservoir management problems includes penalties should low flows fall below several thresholds. .

Table 5-3 summarizes the DP algorithms compared in this section. These utilize two basis selection methods: full-grid and Corridor with backbone as described in Section 5.7. Multi-linear interpolation and cubic spline interpolation are used with full grids. A variety of thinplate RBF and cubic RBF interpolation and least-squares approximation techniques were paired with the Corridor method for basis selection. Other basis functional forms were also tested, but with less success. This last point is explored more in 0.

Table 5-3: Summary of DP Schemes tested, *easy case*

	Name	Abbreviation	Representation of $f_t$	Basis Selection
1	Multi-Linear DP	(ML-Full)	Multi-linear interpolation.	Full grid
2	Cubic-Spline DP	(CS-Full)	Cubic spline interpolation	Full grid
3	Thinplate RBF Interpolating Corridor DP	(TI-Corr)	Gaussian RBF interpolation	Corridor and backbone
4	Cubic RBF Interpolating Corridor DP	(CI-Corr)	Cubic RBF interpolation	Corridor and backbone

The test problem considered here is based on a real system, for which analytical solutions are not available. Thus, it was necessary to construct a ‘perfect’ surface against which to measure relative error. Following the work by Johnson et al. [1993], a high-density cubic spline (CS-Full), with 15 discrete levels in each dimension was used as the benchmark against which all other surfaces are compared. Unlike Johnson et al. [1993], this work is not interested in a good fit throughout the

entire state-space, but rather the fit inside the Corridor region. To this end, 360 test points which span the empirical Corridor region were selected so as to ensure they are semi-uniformly distributed across the corridor region. The measure of algorithm performance is the sum of the squared deviations of a test surface and the ‘perfect’ surface at the 360 test points.

Figure 5-18 plots the SSE in the Corridor region versus the size of the basis for the DP schemes described in Table 5-3. Figure 5-19 plots the % Relative RMSE in the Corridor region versus the size of the basis for the DP schemes described in Table 5-3. % Relative RMSE is defined as:

$$\% \text{ Relative RMSE} = 100 \times \sqrt{MSE} \times (1/\bar{F})$$

where  $MSE$  is the mean squared error in the corridor of a DP scheme, and  $\bar{F}$  is the average of function values at the test points.

Cubic splines on full factorial grids (CS-Full) do significantly better than multi-linear interpolation on a full grid (ML-Full). This confirms the very important finding reported by Johnson et al. [1993] on a realistic system, whereas Johnson et al.’s tests were on a very simple test problem. For this example, CS-Full with 625 basis points has less error than ML-Full with 50,625 basis points. This is remarkable. The improvement of CS-Full over ML-Full grows as the density of the grid increases.

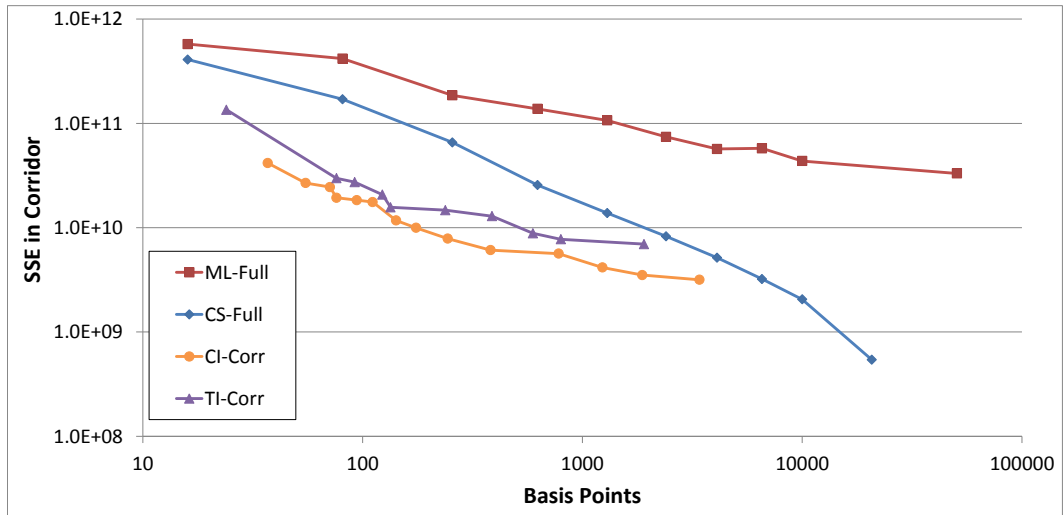


Figure 5-18: SSE in the Corridor Region vs. Number of Basis Points, *easy case*

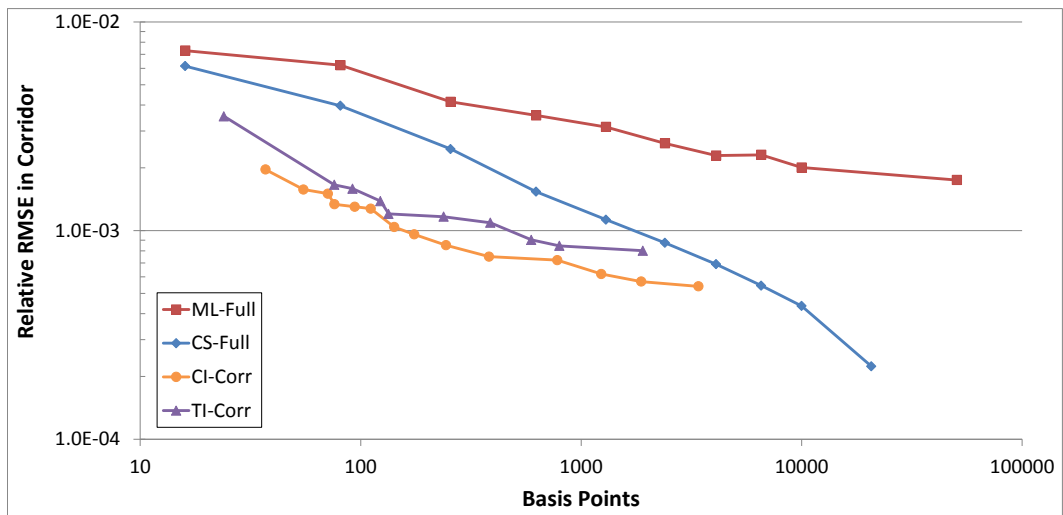


Figure 5-19: Relative RMSE in the Corridor Region vs. Number of Basis Points, *easy case*

Both CI-Corr and TI-Corr beat CS-Full, and CI-Corr (Cubic radial basis functions for the corridor) seems to consistently out-perform TI-Corr (thin-plate with corridor). It is not clear why this should be the case, but it was found over a wide range of basis sizes. CI-Corr generally beats CS-Full by an order of magnitude: meaning that with about 1/10 the CI-Corr can achieve the same SSE in the Corridor region as CS-Full points. Both CI-Corr and TI-Corr significantly outperform ML-

Full. In-fact CI-Corr with as few as 76 basis points returns smaller SSE in the Corridor than ML-Full with 50,625 basis points.

Clearly, CS-Full provides a significant improvement over ML-Full, and CI-Corr provides about an order of magnitude improvement over CS-Full in this easy case. For some cases, careful manual selection of basis points showed even greater improvements were possible with Corridor DP and RBF interpolation. However, this was a purely subjective selection, depending on the skill of the selector, and is not reproducible.

### ***Convergence Analysis***

Interpolations with piecewise linear polynomials and cubic splines is a well-studied topic in one dimension. Kahaner et al. (1977, p. 98) indicate that linear interpolation  $L(x)$  between points in one-dimension should result in an error in approximating a smooth function with a continuous second derivative  $g(x)$  that decreases quadratically with the spacing  $h$  between points:

$$e_L = |L(x) - g(x)| < \left(\frac{1}{8}\right) h^2 \max|g''(x)|$$

for some point  $x$  in the interval. In our case in dimension  $k = 4$ , the number of points  $N$  increases as  $h$  decreases according to  $N = r/h^4$  where  $r$  represents the width of the intervals being divided. Putting these two relationships together yields

$$e_L < \kappa_L \left(\frac{r}{N}\right)^{0.5}$$

or

$$\ln[e_L] = \ln[\kappa_L r^{0.5}] - 0.5 \ln[N]$$

Thus on a log-log plot such as Figure 5-18,  $\ln[e_L]$  should decrease linearly with  $\ln[N]$  with a slope of -0.5. We see in Figure 5-18 that the relative error inside the corridor for the linear DP (ML-Full) has a slope of -0.44, or nearly the same as one might expect from the theory. The deviation from the theoretical convergence is in part explained by the effects of the nested optimization, which also contributes error and can decrease the rate of convergence for the DP approximation of the future value function.

Similarly, Kahaner et al. (1977, p. 111) indicate that the error when using a cubic spline  $C(x)$  with appropriate end conditions to approximate a function  $g(x)$  that has a continuous fourth derivative should have the bound

$$e_c = |C(x) - g(x)| < \kappa_c h^4 \max|g^{(4)}(x)|$$

for some constant  $\kappa_c$ , so that

$$e_c = |C(x) - g(x)| < \kappa_c \left(\frac{r}{N}\right)$$

or,

$$\ln[e_c] = \ln[\kappa_c r] - \ln[N]$$

Thus on a log-log plot such as Figure 5-18,  $\ln[e_c]$  should decrease linearly with  $\ln[N]$  with a slope of -1. Examination of Figure 5-18 reveals the error of the spline DP (CS-full) has a slope of -0.92, or very nearly what is suggested by the theory. As before it is believed that the error convergence rate is slower than suggested by theory due to the errors introduced through the numerical solution of the DP.

Assuming that these error bounds apply in our case when  $g(x)$  may not have the hoped for smoothness, one can understand why the error for the cubic spline

approximations decrease so much more rapidly with an increasing number of points. A slope of  $-1$  versus  $-0.5$  on a log-log plot makes a major difference if one is hoping to obtain a very small error.

In general, if one were working in dimension  $k$ , then the coefficient of  $\ln [N]$  would be  $-2/k$  for linear interpolation, and  $-4/k$  for cubic spline interpolation. Carl de Boor [1997] indicated that in many cases the behavior of the error in the multivariate case is the same as that in the univariate case, when appropriately reducing the mesh size in the different dimensions.

The corridor approximation has smaller errors than splines with relative few points reflecting the intelligence that went into selecting the location of the corridor points. However, because the points are located in advantageous locations, rather than in a regular grid, one cannot expect the higher-order reduction in the error that is possible with cubic splines. The data in Figure 5-18 suggests that the rate of decrease in the corridor error with the number of points more closely matches that of linear interpolation with a log-log slope of  $-0.52$ . Thus it does appear that cubic splines though not initially as accurate as the corridor approach, do over take the corridor approach as  $N$  increases.

### ***Section 5.8.3 Comparison of Traditional and Corridor DP: Hard Case***

The future value function surface resulting from the analysis in Section 5.8.2 was fairly well behaved in that it was relatively smooth and nearly linear over a wide range of the state-space. However in real applications there can be penalties which could potentially add significant and potentially localized curvature to the future value function. These penalties might be incurred due to a failure to provide a minimum

generation, for violation of flow constraints (either low or high) or for violation of environmental quality constraints. The Corridor SDP algorithm, paired with the Greedy Algorithm point selection is particularly well suited to such a problem because it places basis points precisely where such problematic curvature exists.

As an example, consider the hypothetical system introduced in Section 5.8.1 and Section 5.8.2, with the addition of minimum flow constraints from each project:

$$\mathbf{R}_{\min} = \begin{bmatrix} 1000 \text{ cfs} \\ 2000 \text{ cfs} \\ 1000 \text{ cfs} \\ 3000 \text{ cfs} \end{bmatrix}$$

where the elements of  $\mathbf{R}_{\min}$  are the minimum release constraints from Brassua, Moosehead/Harris, Flagstaff, and Wyman respectively. These constraints were selected to ensure that in low storage states it is very difficult or impossible for the system to meet the constraints in some simulation periods. If the constraints are not met, a linear penalty is applied:

$$\begin{aligned} \mathit{pen}(i) &= 10^6 \times \frac{\mathbf{R}_{\min}(i) - \mathbf{R}(i)}{\mathbf{R}_{\min}(i)} && \text{if } \mathbf{R}(i) < \mathbf{R}_{\min}(i) \\ \mathit{pen}(i) &= 0 && \text{otherwise, } i = 1,2,3,4 \end{aligned}$$

The sum of the elements of  $\mathit{pen}$  are subtracted from the benefit function in each time period. As in the previous section a 3-stage DP model is solved for the hypothetical 4-reservoir system, but now with the introduction of the linear penalty for violations of the minimum release. This will be known as the *hard case*.

Three algorithms are compared, as summarized in Table 5-4. Each algorithm is used to solve the 3-stage DP problem with an increasing number of basis points. The relative error in the estimate of the future value function after three DP stages is

compared. As before a spline surface constructed using 50,625 basis points is assumed to be perfect.

Figure 5-20 plots the MSE inside the corridor region versus the number of basis points for the three algorithms tested and Figure 5-21 plots the relative RMSE inside the corridor region. The difference with the *easy case* (Figure 5-18) is striking. The error rate for the Cubic-Spline DP is much closer to the error in Multi-Linear DP than in the *easy case* in the previous section. For example in the *easy case* Cubic-Spline DP with 625 points had smaller relative error than Multi-Linear DP with 50,625 points. In the *hard case* Cubic-Spline DP with 625 points does about as well as Multi-linear with about 4,000 points. And the difference between cubic splines and thin-plate splines has all but disappeared.

Table 5-4: Summary of DP Schemes tested with flow penalty, *hard case*

	Name	Abbreviation	Representation of $f_t$	Basis Selection
1	Multi-Linear DP	(ML-Full)	Multi-linear interpolation.	Full grid
2	Cubic-Spline DP	(CS-Full)	Cubic spline interpolation	Full grid
3	Cubic RBF Interpolating Corridor DP	(CI-Corr)	Cubic RBF interpolation	Corridor and backbone
4	Thinplate RBF Interpolating Corridor DP	(TI-Corr)	Thinplate RBF interpolation	Corridor and backbone

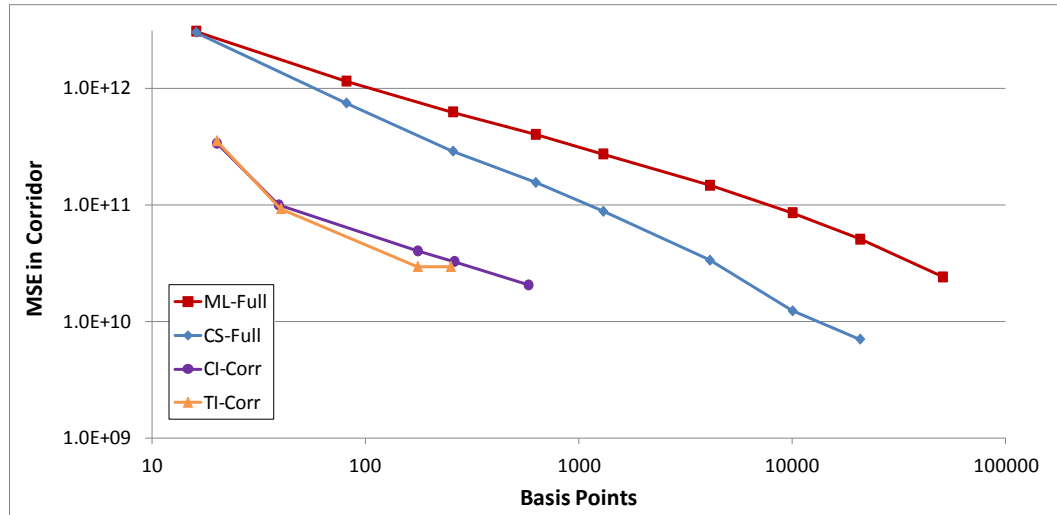


Figure 5-20: MSE in the Corridor Region vs. Number of Basis Points, *hard case*

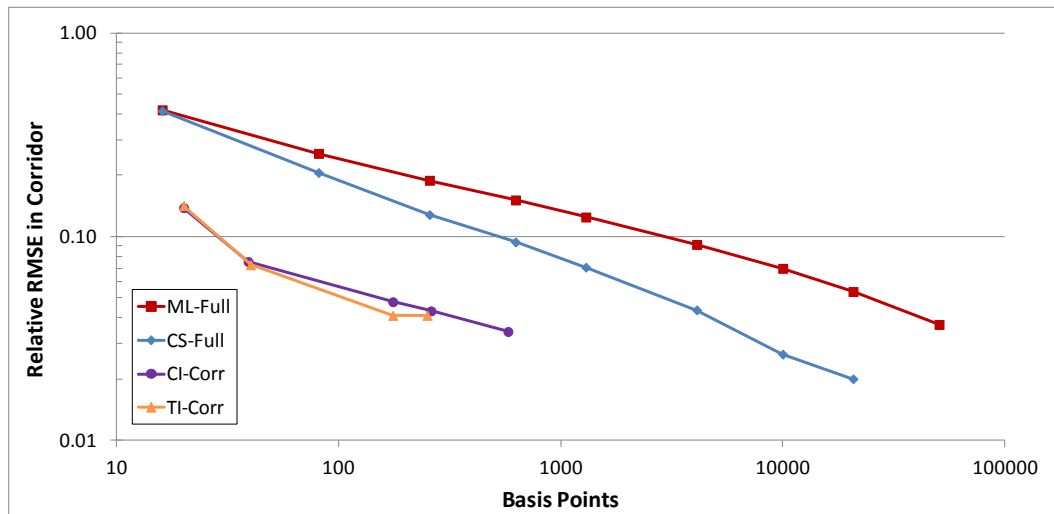


Figure 5-21: Relative RMSE in the Corridor Region vs. Number of Basis Points, *hard case*

The most striking difference of the *hard case* results versus the *easy case* results is that the error convergence rate of splines (CS-Full) is now much closer to that of multi-linear (ML-Full). Whereas in the *easy case* CS-Full with 625 points achieved better accuracy than ML-Full with 50,625 points, in the *hard case* CS-Full with 625 points achieves the same error as ML-Full with about 4,000 points (interpolating). Thus we conclude that CS-Full achieves greater accuracy than ML-Full, but that the improvement is not nearly as dramatic as in the *easy case*.

The improvement of the Corridor DP method over splines is even more dramatic in the *hard case* than in the *easy case* (see Figure 5-18). In the *easy case* the CI-Corr achieved about the same error as CS-Full with about 1/10 the points, but in the *hard case* CI-Corr matches the error of CS-Full with about 1/30 the number of points. This exciting result is largely because the Greedy Algorithm described in Section 5.7.3 places points where the minimum flow constraints introduce curvature to the future value function. As with the linear and spline methods, it seems the error convergence rate for the Corridor DP RBFs is slower than in the *easy case*. As can be seen, the relative efficiency of Splines over Multi-linear increases as the specified error decreases (point density increases). Thus to do as well as CS with 4000 points, ML requires 30,000 points.

#### ***Section 5.8.4 Speed-up from smooth surfaces***

An important assertion in Johnson et al. [1993] was that, for a given discretization level, DP with splines was actually faster than DP with linear interpolation because much faster, gradient based methods were able to be applied. Johnson et al. [1993] estimates this speedup to be about 10 times for their 4-reservoir system, despite the fact that spline interpolation and gradient evaluation takes roughly 20 times more flops than in the linear case. The analysis of errors in Section 5.8.2 and Section 5.8.3 are reported in terms of the number of basis points, which completely misses this aspect of the findings by Johnson et al. [1993].

As a test of the speed-up achieved by using a smooth surface to approximate the future value function a time trial was performed. The three stage DP models from

Section 5.8.2 and Section 5.8.3 were run with a fixed discretization, but with either spline or linear interpolation, and the run times are compared.

Johnson et al. [1993] note that the cost of constructing a cubic spline interpolating surface increases with the discretization level, but also noted that this cost is likely small compared to the overall cost of the many optimization problems required to solve a DP. To test the effect of discretization time trials are conducted at various discretization levels.

In order to make the results more robust, the time trial for each discretization level is repeated many times, using the MATLAB function ‘testit,’ and the median run time is reported [Mathworks, 2014]. The median run time and the relative RMSE in the corridor for different discretization levels are reported in Table 5-5 for the *easy case* (i.e. the model reported in Section 5.8.2).

Table 5-5: Run time and relative RMSE in the Corridor for the 4-reservoir system for various discretization levels for DP with spline and linear interpolation for the *easy case*

$N$	Linear		Spline	
	Median Run Time (sec)	% RMSE in the Corridor	Median Run Time (sec)	% RMSE in the Corridor
16	13	0.729	13	0.615
81	46	0.621	38	0.397
256	144	0.414	131	0.246
625	298	0.357	253	0.154

Like the findings reported by Johnson et al. [1993], we find that Spline DP optimizes faster than Linear DP, though not by an order of magnitude. Instead the speed up is somewhat minor, and there is no strong evidence that the relative speed up of spline over linear decreases or increases with increased discretization. It is clear,

however, that as the discretization level increases, the relative error in the corridor decreases more rapidly with splines than with linear. Thus we can conclude that for the *easy case* using splines to interpolate improves the accuracy of the DP solution, while not incurring an increased computational burden from the increased difficulty of fitting and evaluating the spline surface.

The same test was conducted on the *hard problem* (as described in Section 5.8.3). Table 5-6 reports the median run time, and relative RMSE for linear and spline DP with different discretization levels. As before the median solution time for spline DP is nearly the same, or slightly less than the solution time for linear DP. As before the relative error in the corridor is less for spline DP than linear DP. As described in Section 5.8.3, the rate of improvement of Spline DP over Linear DP is lower than in the *hard case*. It is, however, still the case that for the same, or slightly less computation time, spline DP still returns a more accurate solution than linear DP.

Table 5-6: Run time and relative RMSE in the Corridor for various discretization levels for DP with spline and linear interpolation for the *hard case*

$N$	Linear		Spline	
	Median Run Time (sec)	% RMSE in the Corridor	Median Run Time (sec)	% RMSE in the Corridor
16	13	42.0	14	41.5
81	50	25.6	37	20.6
256	151	18.9	142	12.8
625	295	15.1	262	9.4

The results in this section agree with the findings of Johnson et al. [1993]: using splines instead of linear interpolation speeds up the nested optimization which compensates (or more than compensates) for the increased computational burden of evaluating the spline surface.

However, we find the speed-up to be much less than reported by Johnson et al. [1993]. This is for at least two reasons. First, the test case used by Johnson et al. had much more curvature than the test cases considered here, having a quadratic objective function. It should be noted that even the *hard case* reported in Table 5-6 is relatively linear over a wide range of the state-space. The second reason for the disagreement with Johnson et al.'s findings is that a derivative based procedure was used in this section for the DP on both surfaces (linear and spline). In contrast, Johnson et al. use a derivative based method for the spline DP and a non-derivative method for the linear DP. Thus, it is not at all surprising that a significant speed up was achieved with splines: that solver was given more information about the surface (the gradient) than was the solver for linear DP.

In conclusion, solution of DP problems with fixed discretization levels was found to go slower (and often faster) when splines are used to approximate the future value function rather than linear interpolation. This finding is important, and validates the decision in the previous sections to report relative error for approximation surfaces versus the number of basis points rather than versus computation time.

#### ***Section 5.8.5 On the Selection of Basis Functional Form***

It was stated earlier that cubic basis functions were generally found to perform the best of all the functional forms examined in this Chapter, with thinplate spline basis functions also performing well. This conclusion was reached through testing with both objective and subjective basis point selection over a wide range of point densities applied to the *easy case* in Section 5.8.2. This point is examined in more detail here.

To test the accuracy achieved using different basis functional forms, the 3-stage Corridor DP model used in Section 5.8.2 (i.e. the *easy case*) is run using a fixed number of basis points, but with different functional forms. To make the analysis more robust, this test is done with two different basis sizes: 40 and 175 basis points.

The Greedy algorithm described in this chapter is used for point selection. Experience suggests the Greedy algorithm for point selection is relatively stable in that when run multiple times, the resulting point bases return similar relative errors from the Corridor SDP optimization. Thus, in the following analyses, the filling procedure described in Section 5.7.1 is run only once, and the resulting ‘filled’ basis is used for all subsequent runs of the Greedy algorithm. Furthermore each RBF functional form is tested once rather than repeatedly.

This approach is justified by examination of Figure 5-18. Clearly some of the scatter and dis-uniformity in the error rate of the RBF surfaces is due to the randomness of the Greedy algorithm point selection. However the fact that the cubic and thinplate RBF error monotonically decreases with increased basis size, and are always ranked consistently across the range of basis sizes suggests the Greedy Algorithm returns relatively stable results.

Figure 5-22 reports the SSE in the Corridor Region for various functional forms and for two basis sizes for the *easy case*. Note that cubic RBFs outperform the other functional forms at both basis sizes, but thinplate splines return similar accuracy. These results are typical of the findings across a wide range of basis sizes. Here the notation of (-) indicates the value of the  $\gamma$  parameter. For multiquadrics two separate  $\gamma$

values are used for  $N = 40$  and  $N = 175$  and the notation  $(-, -)$  indicates the  $\gamma$  for those basis sizes respectively.

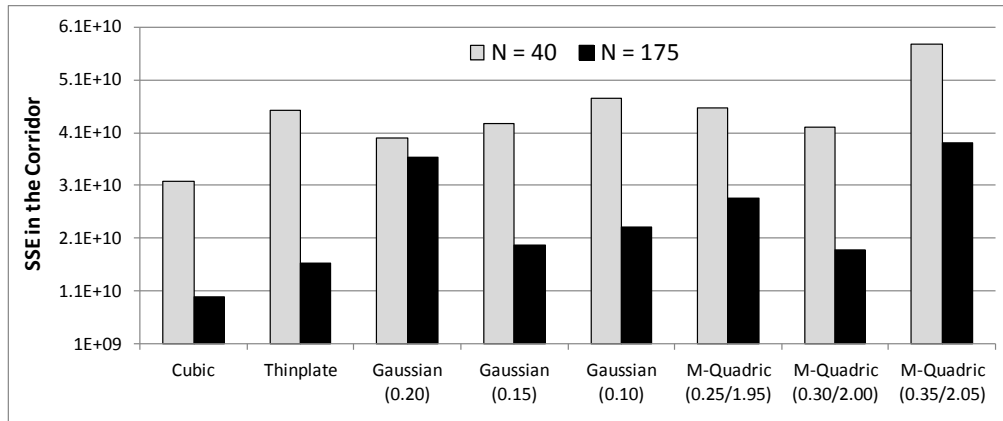


Figure 5-22: SSE in Corridor for various RBF functional forms, for two discretization levels, *easy case*

One great advantage (or a possible disadvantage) of cubic and thinplate spline RBFs is that they require no additional parameter, the way Gaussian and multiquadrics do (see Section 5.6). This is an advantage because they can be easily applied to a new problem, without the needed tuning. On the other hand, it is impossible to tune the surface parameters to a specific problem.

The best  $\gamma$  for Gaussian and Quadric basis functions depends on the size of the basis (i.e. the density of the basis points). If one considers Gaussian functions, for instance, one expects that as the basis point density decreases and points are farther apart, the best  $\gamma$  should become larger. This is because a ‘fatter’ Gaussian function is needed to cover more of the state space if points are sparse. This is precisely what we see in Figure 5-22: for larger  $N$  the best  $\gamma$  is smaller.

Figure 5-25 reports the SSE in the corridor for various RBF functional forms for two basis sizes for the *hard case*. We see now that each of the functional forms achieve about the same accuracy for  $N = 40$ , and interestingly multiquadrics (when

properly parameterized) provide the best fit. However, as the basis size increases the cubic and thinplate spline functional forms achieve the best accuracy. These functional forms require no parameterization and can be used without trial and error on the functional surface.

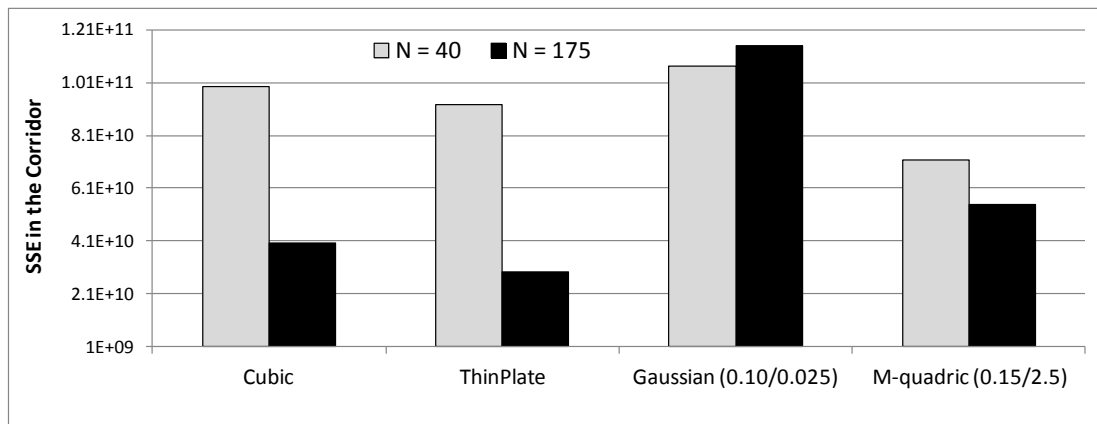


Figure 5-23: SSE in Corridor for various RBF functional forms, for two discretization levels with gamma ( $N = 40/N = 175$ ), *hard case*

One reason that Gaussian basis functions perform so poorly is that they employ a uniform  $\gamma$  parameter across the entire state space. In the *easy case* points were distributed somewhat uniformly in the corridor region, so a uniform  $\gamma$  is appropriate. However, in the *hard case* the basis points are concentrated in a corner of the state space, so a single  $\gamma$  parameter is very problematic: the Gaussian functions are bound to be too ‘fat’ in dense regions and too ‘thin’ in sparse regions. This might explain why the accuracy achieved with Gaussian functions actually became slightly worse with more basis points.

Despite their good performance, the use of thinplate splines is not recommended for numerical solution of DP problems because the second derivative of the RBF surface is infinite at each basis point. This is particularly a problem if one is using a quasi-Newton solution method to solve equation (5-1). Cubic basis functions

avoid this problem, and seem to perform as well or better than thinplate splines in the test cases presented.

Multiquadrics and Gaussian RBFs should be used with great care, as their parameterization can greatly affect the quality of the function approximation. One is often forced to use ‘trial and error’ to pick parameter values that work well for a problem in hand, and this might prove prohibitively expensive. It is observed in this section that the optimal parameterization of multiquadric and Gaussian RBF depends greatly on the size of the basis (density of points). This presents a great challenge for the Greedy Algorithm, which adaptively selects points based on where the approximation fits the function the worst. Without extensive *a priori* knowledge of the evolution optimal parameterization of the RBF surface with change in basis size this it is difficult to effectively apply the Greedy Algorithm for point selection with Gaussian or multiquadric RBFs.

Gaussian RBFs have the helpful feature that they can provide a local and limited feature to the surface which can capture localized curvature (explored in Section 5.6.1). One concern when pairing the Gaussian RBFs with a quasi-Newton solver is that the significant curvature introduced by the Gaussian functions could result in an irregular second derivative. A potential solution to this problem is to employ Gaussian functions which, beyond some bandwidth, become linear. This would reduce the curvature of the surface and might improve the performance of quasi-Newton search over the surface.

In conclusion, it seems the cubic and thinplate spline basis functions perform the best on the surfaces tested. Because of concern for the behavior of the second

derivative of RBF thinplate splines, RBF cubic splines are generally deemed better for this application.

### ***Section 5.9 Discussion***

The results in Section 5.8.2 and Section 5.8.3 show that the Corridor DP algorithm has the potential to reduce the computational burden of solving DP problems by as much as 10 times over CS-Full for the *easy case* and by as much as 30 times over CS-Full for the *hard case*. The great difficulty in Corridor DP is the selection of a good basis. In fact a poorly selected basis can cause Corridor DP algorithms to perform much worse than ML-Full. The Greedy algorithm presented in Section 5.7.3 provides a reliable and objective method for selecting an appropriate basis: in every basis generated using that algorithm, the corresponding Corridor DP configuration beat CS-Full.

It was found that manual basis selection can at times outperform the Greedy Algorithm selection criteria. This is an interesting result, as operational application of the Corridor DP algorithm would likely involve re-solving the same or similar problems many times, so that a practitioner will likely have a good set of basis points in hand.

The choice of basis functional form seems critical to the performance of the Corridor DP algorithm. It is difficult *a priori* to know what functional form is best suited to a problem in hand. For the relatively smooth problem in this application cubic and thin-plate RBFs performed best as described in 0. However, in problems with local, irregular features, Gaussian or tri-cube functions might perform better. 0

describes further considerations when searching over the RBF surface using derivative based methods.

### ***Section 5.10 Conclusions***

The solution of high dimensional DP models continues to be a challenging problem, more than 50 years after Bellman coined the ‘Curse of Dimensionality.’ However increased computing power and improved numerical techniques continue to push the boundaries of what is possible. New work on Q-Q iteration DP [Castelletti, 2010] and adaptive sparse grids [Brumm and Scheidegger, 2014] as well as past work using cubic splines [Johnson et al., 1993] and SDDP [Pereira and Pinto, 1985] allow significant improvement over traditional DP solution techniques. In this vein, Corridor DP seeks to reduce the computational burden of high-dimensional DP by focusing the optimization effort in the region of the state space where the system is likely to reside. Results presented here show that with careful basis selection, Corridor DP paired with RBF interpolation can outperform Cubic Spline interpolation in that it achieves the same accuracy more than an order of magnitude less effort.

It is anticipated that this exciting work can be improved upon further through use of least-squares approximation and Hermite RBF interpolation.

## REFERENCES

- Arvanitidis, N.V. & Rosing, J. 1970, "Optimal operation of multireservoir systems using composite representation", *IEEE Trans Power Appl Syst*, vol. 89, no. 2, pp. 327.
- Bellman, R. 1961, *Adaptive Control Processes: A Guided Tour*, 1st edn, Princeton University Press, Princeton, NJ.
- Buhmann, M.D. 2003, *Radial Basis Functions*, Cambridge University Press, New York, N.Y.
- Bungartz, H. & Griebel, M. 2004, "Sparse Grids", *Acta Numerica*, , pp. 1-123.
- Castelletti, A., Galelli, S., Restelli, M. & Soncini-Sessa, R. 2010, "Tree-based reinforcement learning for optimal water reservoir operation", *Water Resources Research*, vol. 46, no. W09507.
- Castelletti, A., Pianosi, F. & Restelli, M. 2013, "A multiobjective reinforcement learning approach to water resources systems operation: Pareto frontier approximation in a single run", *Water Resources Research*, vol. 49.
- Castelletti, A., Pianosi, F. & Soncini-Sessa, R. 2008, "Water reservoir control under economic, social and environmental constraints", *Automatica*, vol. 44, no. 6, pp. 1595-1607.
- Chen, V.C.P., Ruppert, D. & Shoemaker, C.A. 1999, "Applying experimental design and regression splines to high-dimensional continuous-state stochastic dynamic programming", *Operations Research*, vol. 47, no. 1, pp. 38-53.
- Cote, P., Haguma, D., Leconte, R. & Krauc, S. 2011, "Stochastic Optimization of Hydro-Quebec hydropower installations: a statistical comparison between SDP and SSDP methods", *Canadian Journal of Civil Engineering*, vol. 38, no. 12, pp. 1427-1434.
- deBoor, C. 1997, "The error in polynomial tensor-product , and in Chung-Yao interpolation" in *Surface Fitting and Multiresolution Methods*, eds. A. LeMehaute, C. Rabut & L.L. Schumaker, Vanderbilt University Press, Nashville, TN, pp. 35.

- Draper, N.R. & Smith, H. 1966, *Applied Regression Analysis*, 1st edn, John Wiley & Sons, Inc., New York.
- Duran, H., Puech, C., Diaz, J. & Sanchez, G. 1985, "Optimal operation of multireservoir systems using an aggregation-decomposition approach", *IEEE Trans Power Appl Syst*, vol. 104, no. 8, pp. 2086.
- Goor, Q., Kelman, R. & Tilmant, A. 2011, "Optimal Multipurpose-Multireservoir Operation Model with Variable Productivity of Hydropower Plants", *Journal of Water Resources Planning and Management*, vol. 137, no. 3, pp. 258-267.
- Hall, W.A., Harboe, R.C., Yeh, W.W. & Askew, A.J. 1969, *Optimum firm power output from a two reservoir system by incremental dynamic programming*, Water Resources Center, University of California at Los Angeles.
- Heidari, M., Chow, V.T., Kokotovic, P.V. & Meredith, D.D. 1971, "Discrete differential dynamic programming approach to water resources systems optimization", *Water Resources Research*, vol. 7, no. 2, pp. 273.
- Johnson, S.A., Stedinger, J.R., Shoemaker, C.A., Li, Y. & Tejada-Guibert, J.A. 1993, "Numerical Solution of Continuous-State Dynamic Programs Using Linear and Spline Interpolation", *Operations Research*, vol. 41, no. 3.
- Kahaner, D., Moler, C. & Nash, S. 1989, *Numerical Methods and Software*, Prentice-Hall Inc, Englewood Cliffs, New Jersey.
- Labadie, J.W. 2004, "Optimal Operation of Multireservoir Systems: State-of-the-Art Review", *Journal of Water Resources Planning and Management*, vol. 130, no. 2, pp. 93-111.
- Ong, Y.S., Lum, K.Y. & Nair, P.B. 2008, "Hybrid evolutionary algorithm with Hermite radial basis function interpolants for computationally expensive adjoint solvers", *Comput Optim Appl*, vol. 39, pp. 97-119.
- Pereira, M.V.F. & Pinto, L.M.V.G. 1985, "Stochastic optimization of a multireservoir hydroelectric system-a decomposition approach", *Water Resources Research*, vol. 21, no. 6.

- Pianosi, F., Castelletti, A. & Restelli, M. 2013, "Tree-based fitted Q-iteration for multi-objective Markov decision processes in water resource management", *Journal of Hydroinformatics*, vol. 15, no. 2, pp. 258-270.
- Quintana, V.H. & Chikhani, A.Y. 1981, "A Stochastic Model for Mid-Term Operation Planning of Hydro-Thermal Systems with Random Reservoir Inflows", *IEEE Trans Power Appl Syst*, vol. 100, no. 3, pp. 1119.
- Regis, R.G. & Shoemaker, C.A. 2007, "A Stochastic Radial Basis Function Method for the Global Optimization of Expensive Functions", *INFORMS Journal of Computing*, vol. 37, no. 2, pp. 113-135.
- Saad, M. & Turgeon, A. 1988, "Application of principal component analysis to long-term reservoir management", *Water Resources Research*, vol. 24, pp. 907-912.
- Saad, M., Turgeon, A. & Stedinger, J.R. 1992, "Censored-data Correlation and Principle Component Dynamic Programming", *Water Resources Research*, vol. 28, no. 8, pp. 2135-2140.
- Tilmant, A. & Kelman, R. 2007, "A stochastic approach to analyze trade-offs and risks associated with large-scale water resources systems", *Water Resources Research*, vol. 43, no. W06425, pp. 1-11.
- Turgeon, A. & Charbonneau, R. 1998, "An aggregation-disaggregation approach to long-term reservoir management", *Water Resources Research*, vol. 34, no. 12, pp. 3585-3594.
- Wendland, H. 2005, *Scattered Data Approximation*, Cambridge University Press, United Kingdom.
- Yakowitz, S. 1982, "Dynamic programming applications in water resources", *Water Resources Research*, vol. 18, no. 4, pp. 673-679.
- Yeh, W.W. 1985, "Reservoir Management and Operations Models: A State-of-the-Art Review", *Water Resources Research*, vol. 21, no. 12, pp. 1797-1818.

### ***Appendix: SDP Diagnostics***

The numerical solution of DP models requires one to solve equation (5-1) many times in each time step. For instance, the most extreme case considered in 0 solved equation (5-1) more than 50,000 times in each time step. For such problems to be tractable, fast solution methods must be used. Such methods, whether they are derivative based or not, are prone to pre-mature termination, which returns sub-optimal solutions. This is particularly troubling in DP because the solution process is recursive: the solutions for one iteration inform the solutions for the next iteration, so errors can compound over time. To address this concern two simple diagnostic procedures are presented.

The first procedure depends on the fact that the future value function in many applications should be non-decreasing with increase in the state variables. For reservoir operations optimization, without spill and storage penalties, more water in storage should always translate to the same or more benefits. This fact can easily be leveraged into a diagnostic check. After equation (5-1) has been solved for each point in the basis  $\mathbf{X}$ , the following check is performed for each basis point  $i$ :

$$\begin{aligned} f_t(i) &\geq f_t(j) \\ \forall j \in \tilde{\mathbf{F}}(i) \end{aligned} \tag{5-12}$$

where  $\tilde{\mathbf{F}}(i)$  is a set of basis point indices satisfying the condition that

$$\begin{aligned} \mathbf{X}(i, l) &\geq \mathbf{X}(j, l) \\ l &= 1, 2, \dots, k \end{aligned}$$

The condition in equation (5-12) ensures that the future value function at point  $i$ ,  $f_t(i)$  is greater than or equal to the future value function at every other point with

equal or less storage. If this condition is violated it indicates that the maximization of equation (5-1) likely terminated prematurely at point  $i$ .

The second diagnostic procedure is based on regression. It follows from the observation that the  $k$ -dimensional future value function (in our case  $k = 4$ ) is well approximated by a simple non-linear function when transformed to a suitable 1-dimensional space. It was found that the simple linear transformation in equation (5-13) worked well:

$$\mathbf{T} = \mathbf{aX} \quad (5-13)$$

where  $\mathbf{a}$  is a row vector of weights and  $\mathbf{T}$  is a vector of transformed storages. The elements of  $\mathbf{a}$  correspond to the fraction of system powerhouse generation which is downstream of each reservoir, including the power house associated with that reservoir:

$$\mathbf{a} = [0.3625 \quad 0.3279 \quad 0.1550 \quad 0.1545]$$

The following non-linear model of the future value function is fit using the transformed storage total  $\mathbf{T}$ :

$$f_t(i) = \lambda_1 + \lambda_2 T(i) + \lambda_3 \sqrt{T(i)} + e(i) \quad (5-14)$$

where the parameters  $\lambda_1$ ,  $\lambda_2$ , and  $\lambda_3$  are selected to minimize the total sum of squared errors:

$$SSE = \mathbf{e}^T \mathbf{e}$$

where  $\mathbf{e}$  is a vector of residual errors whose  $i^{th}$  element is  $e(i)$ . The significance of each residual is tested using the statistic:

$$t_{stat}(i) = \frac{e(i)}{s} \quad (5-15)$$

where

$$s^2 = \frac{SSE}{N - 3}$$

Assuming the residual errors are normal distributed yields the result that  $t_{stat}$  is distributed Student T [Draper and Smith, 1966]. Any desired significance level can be used when testing the residuals. A significant residual suggests that the optimizer terminated pre-maturely at a sub-optimal solution when solving equation (5-1).

As an example of these methodologies the Corridor DP algorithm with interpolating RBFs which is described in 0 was run for one time step.  $f_t$  is plotted in the transformed space Figure 5-24. Note that the  $f_t$  for a single basis point deviates significantly from trend in the rest of the  $f_t$ .

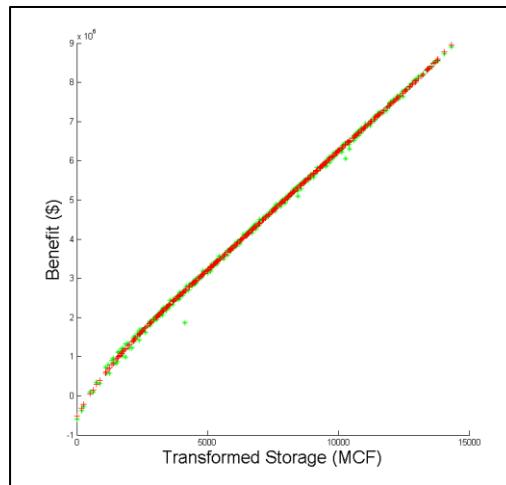


Figure 5-24: Future Value Function of Corridor DP after one time step (green) and fitted polynomial (red).

At first this deviation is ignored, and the recursive DP problem continues backwards another two time steps. Figure 5-25 plots the final future value function in transformed space.

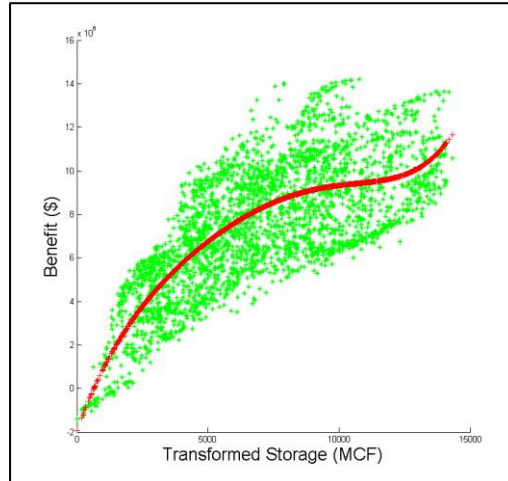


Figure 5-25: Future Value Function of Corridor DP after three time step (green) and fitted polynomial (red) if the sub-optimal termination in Figure 5-24 is ignored.

The future value function now fluctuates wildly, and the condition in equation (5-12) is now widely violated. Clearly the single sub-optimal termination seen in Figure 5-24 has caused the entire DP solution to fail. Figure 5-26 plots the future value function in transformed space if the initial problematic basis point is identified, and equation (5-1) is solved with a more robust, and slower, optimization routine. Note that the wild behavior has disappeared and the condition in equation (5-12) is now satisfied at every basis point.

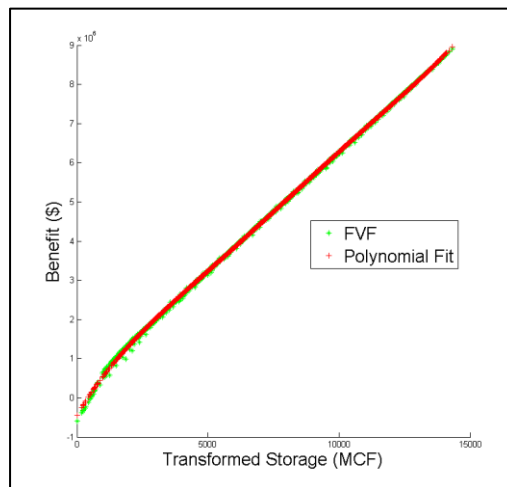


Figure 5-26: Future Value Function of Corridor DP after three time step (green) and fitted polynomial (red) if the sub-optimal termination in Figure 5-24 is addressed.

The two diagnostic approaches recommended in this appendix are simple, quick, and have proven useful in experience.

## CHAPTER 6

When modeling any system, it is important to understand the underlying system dynamics and the time scales (or inversely the frequencies) at which those dynamics are acting. This chapter proposes three diagnostic metrics and analyses for identifying the important operational time scales for hydropower systems. First, a number of simple diagnostic statistics are proposed which help the analyst diagnose the operational time scales for a hydropower system to any advanced analysis or policy simulation. The second approach is based on regression analysis on optimized system operations. The third is based on spectral analysis of optimized system operation. As an example, the operation of a hypothetical single-reservoir system on the Kennebec River in Maine is considered with all three sets of metrics.

### ***Section 6.1 Introduction***

When designing a system model it is critical that the dynamics which drive the system operation are adequately represented. An important consideration is the time scale of system processes and how this influences system operation. For instance, an important consideration for the model in Chapter 4 was hourly energy price fluctuations, so a model that assumes constant generation over the week would miss that critical process. On the other hand, a system that moves large quantities of water and energy between different seasons can perhaps be represented by a model with a weekly or monthly time scale, with appropriate parameterized within-week or within-month operation.

A related consideration is the streamflow forecast horizon which is most useful for system operation. In some applications this is obvious: for instance in a fill period in snowmelt hydrology (like in Faber [2000], Kelman et al. [1990], and Tejada-Guibert et al., 1995, and others), the obvious forecast is the seasonal snowmelt runoff. In the operational context one might be constrained by the actual forecasts which are available. But in other cases, like the short-term planning model in Chapter 4, or in cases where multiple forecast products are available, the choice is less obvious.

The aim of this chapter is to explore several sets of diagnostic statistics to help answer these questions in reservoir system modeling problems. It should be noted that system operators can often identify a good modeling approach for the various system processes. The diagnostics presented here do are not intended to replace valuable operator insight. Rather it provides basic diagnostic metrics to confirm such insight, or for the case that such input is not available. They may be particularly valuable in regional or climate change studies that are considering a host of systems and reservoir configurations that could be developed.

## ***Section 6.2 Literature Search***

Section 6.3 describes the use of non-dimensional metrics as diagnostic tools when building models of hydropower operations. In this thesis these metrics are used in two ways: 1) to provide metrics by which an analyst might understand and compare the scale and mode of operation of different hydropower projects of different sizes across a wide geographical range, and 2) to provide a dimensionless presentation of results (or at least use of a common dimension, such as ‘days’) in order to draw more generalized conclusions.

An early example of the use of non-dimensional statistics is provided by Klemes [1977]. That work examines the value of hydrologic information to optimal reservoir management, and reports its findings in non-dimensional form in order to be more generalizable, in the same way the results in Chapter 4 of this thesis are presented. Klemes reports the value of hydrologic information in terms of the ratio of reservoir storage and mean annual inflow and the ratio of annual draft (demand) to annual inflow. Karamouz and Houck [1987] compare the performance of SDP and deterministic DP models on hypothetical reservoirs with different sizes in several basins in different hydrology across the United States, and use dimensionless storage (ratio of mean storage capacity and mean annual inflow) to compare across basins and hypothetical reservoirs.

An early example of this kind of approach comes from reliability analysis for storage reservoirs, which is concerned with determining the likelihood that a reservoir will fail to deliver its annual yield [Vogel, 1985; Vogel and Stedinger, 1987; Vogel, 1987; Vogel and Bolognese, 1995]. As part of this effort Vogel [1985] and Vogel and Stedinger [1987] derive the distribution of over-year storage given different assumptions.

Taking dimensionless metrics of reservoir reliability, Vogel et al. [1995] develop regional relationships for storage reliability and resilience for the Northeast United States. That analysis is extended by Vogel et al. [1999] to include the entire United States, and by McMahon et al. [2007] to include basins across the whole world. Montesari and Adeloeye [1999] also provide a more limited example comparing reservoirs in Iran and England. In this way the relationships first derived to generalize

the findings of a specific analysis (in Vogel [1985]) are extended to develop regional storage-reliability/storage-resilience relationships for an entire region (Vogel et al. [1995, 1999]; McMahon et al. [2007]).

More recent examples of the application of dimensionless statistics include Hejazi et al. [2008], who conducts a regional study (for the Great Plains and California) of what hydrologic variables are most related to reservoir operations using a data-mining approach. By using dimensionless statistics, that work is able to compare reservoirs of vastly different scales by a common metric. Another recent work is Vogel et al. [2007] who uses the dimensionless statistics derived by Vogel [1985] and Vogel [1987] to derive relationships between storage-yield and new measures of downstream ecological health. Zhao et al. [2012] use the dimensionless metrics of reservoir storage capacity developed by Vogel and Stedinger [1987] to examine the effects of forecast and forecast horizon on optimal reservoir operation.

The analysis by Zhao et al. [2012] is also notable because it seeks to identify the critical forecast length for real-time reservoir operations, similar to the objective of the analyses in Section 6.3.1 and Section 6.3.2. Unlike the analysis presented in this chapter, that work considers the diminishing accuracy of longer forecasts.

### ***Section 6.3 Diagnostic Metrics***

The test case here is a single reservoir system on the Kennebec River in Maine. As in Chapter 4, summer operation with various system configurations (combinations of storage and turbine capacity) are considered. By changing the system characteristics it is possible to show how the diagnostic metrics illustrate the

differences among different systems, or the same system but with different hydrologic inputs.

The summer period of operation runs from May 1 to October 31. In each year, it is assumed that the system starts May 1 as full. This is a reasonable assumption because the total storage on the Kennebec River hydropower system is about 1/3 the mean annual inflow, so that even in dry years the reservoir is able to refill. On October 31 the system must be drawn down to meet flood storage. The beginning of the modeled operation period marks the end of the freshet, and the reservoir inflows generally become smaller as the summer proceeds, with the exception of occasional high flows due to large storms.

The summer-long planning period is divided into 6-hour time steps, and the optimal release in each time step is selected using an optimization model which assumes perfect foresight of hydrologic and economic conditions for the entire planning horizon. That is, for each 6-hour time step a release,  $R_t$ , is selected as if the operator knew the exact hydrologic and economic condition in each 6-hour time step from the present time till the end of the planning horizon. System performance is over 20 independent years summer operation is simulated. Three approaches for identifying the time scale of interests are presented: simple diagnostic metrics, a regression approach, and a spectral analysis approach.

### ***Section 6.3.1 Simple Diagnostic Metrics***

This section explores several simple diagnostic metrics which describe system characteristics. These metrics have the advantage of being simple to compute, requiring no model simulations, and are applicable to systems of varying orders of

magnitudes in capacity and flow. For simplicity, the discussion here will focus on a hydropower system with a single reservoir.

The most common bifurcation in hydropower project classification is ‘run-of-river’ projects which have no variable storage, and ‘reservoir’ projects which have variable storage. In reality many projects are somewhere in-between (see Creager and Justin [1950] for a discussion). In particular Creager and Justin define two classes of run-of-river projects: those with ponding ability, roughly meaning they can shape inflows on a daily basis, and those which have no such ability. At the opposite end of the spectrum a ‘storage-only’ project is one which has no powerhouse and only stores water in support of some downstream use.

In some cases the time scale of interest will dictate whether the system is considered a run-of-river or storage project. The storage capacity factor,  $C_S(\tau)$ , considers the size of the active reservoir storage relative to the average inflow, given inflow variability:

$$C_S(\tau) = \frac{V_a - \mu_\tau}{\sigma_\tau} \quad (6-1)$$

where  $V_a$  is the volume of active reservoir storage,  $\mu_\tau$  and  $\sigma_\tau$  are the mean and standard deviation of inflow volume over discrete time steps of length  $\tau$  respectively. Similar statistics were proposed by Vogel [1985] for reservoir reliability studies (see earlier discussion). Figure 6-1 plots  $C_S(\tau)$  versus  $CV = \sigma_\tau/\mu_\tau$  for various  $V_a$ . If one is concerned that serial correlation in the inflows will affect  $\sigma_\tau$ , a correction could be applied (see Wilks, 2011pg. 148).

As  $C_S(\tau)$  becomes smaller the project is more like the ‘run-of-river’ classification and as  $C_S(\tau)$  becomes larger the project is more like the ‘reservoir’

classification. A purely run-of-river project will have no active storage ( $V_a = 0$ ) so  $C_S(\tau)$  will take negative values. As  $V_a$  increases, so too will  $C_S(\tau)$ . Importantly  $C_S(\tau)$  decreases with increasing  $CV$ : as inflow variability increases a larger reservoir is needed to regulate inflows and shape releases. As  $\tau$  becomes larger  $C_S(\tau)$  will generally become smaller, reflecting the fact that a medium sized project might be able to regulate inflows on an hourly basis, but would be unable to store water over multiple weeks. Thus the chosen time step of a given model affects how a project should be modeled.

Because  $C_S(\tau)$  is dimensionless it can be difficult to intuitively understand its meaning. Clearly the value  $C_S(\tau)$  will change greatly depending on the chosen  $\tau$ . For example the distribution of flows for duration  $\tau = 1 \text{ year}$  will be very different than those for  $\tau = 1 \text{ day}$ . An alternative is the storage-days ( $ST_{\text{days}}$ ) statistic:

$$ST_{\text{days}} = \frac{V_a}{\mu_{\text{day}}} \quad (6-2)$$

where  $\mu_{\text{day}}$  is the mean daily inflow.  $ST_{\text{days}}$  has daily units and can be understood as the number of days of average inflow which can be stored in the active storage. It should be noted that both  $V_a$  and  $\mu_{\text{day}}$  can vary greatly across seasons, so in some applications it might be advantageous to define a season specific  $ST_{\text{days}}$ . A similar term, except with yearly average inflows is used by Hejazi et al. [2008] for a study of reservoir characteristics across the western United States. Unlike  $C_S(\tau)$ ,  $ST_{\text{days}}$  does not take inflow variability into account.

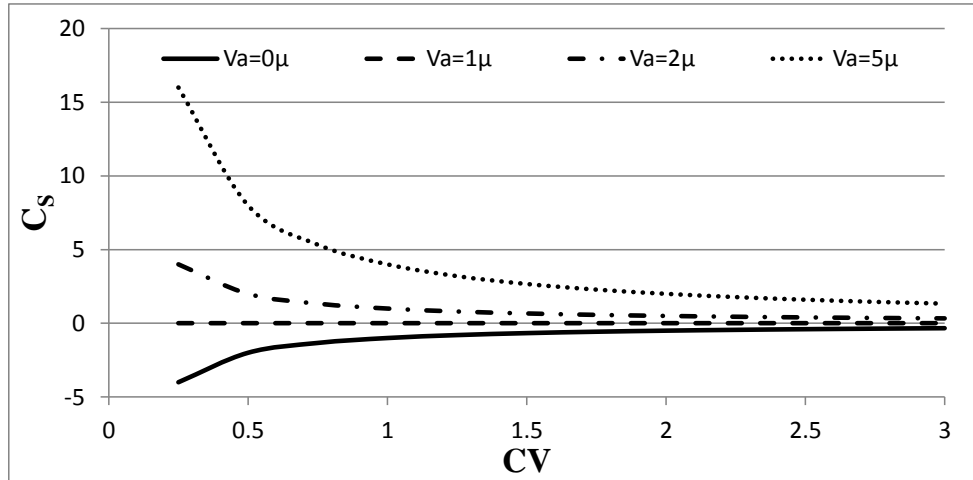


Figure 6-1: Storage Capacity Factor,  $C_s$ , versus coefficient of variation for various active storage volumes,  $V_a$ .

Another consideration when modeling hydropower reservoirs is the size of the powerhouse hydraulic capacity relative to the active storage. The storage-powerhouse ratio,  $Y$ , is the number of days it would take to empty the reservoir active storage, absent of any inflow, at the peak powerhouse hydraulic capacity:

$$PH_{days} = \frac{V_a}{V_{PH}} \quad (6-3)$$

where  $V_{PH}$  is the maximum volume which a project's powerhouse(s) can release during a day. Note that a purely 'run-of-river' project will have no active storage, so  $PH_{days} = 0$ . As  $PH_{days}$  increases, the project will become more of a 'reservoir' project. In the extreme, a storage only reservoir will have no powerhouse, so  $V_{PH} = 0$  and  $PH_{days} = \infty$ . Table 6-1 reports  $PH_{days}$  for some notable projects on the Upper Kennebec, Merrimack, and Columbia Rivers.

Brassua Lake is primarily used as a storage reservoir, though it has recently been retrofitted with a small powerhouse with a single turbine. Thus, as one might expect  $PH_{days}$  for Brassua is very large. Remarkably, Bonneville on the Columbia

has nearly the same storage, but has a very small  $PH_{days}$ . This is because Bonneville has very large powerhouse capacity: and is essentially operated as a run-of-river project at the time scale of daily and over-day operations. This highlights the danger of simply comparing storage volumes in the absence of power house capacity when attempting to understand the operation of a facility.

Table 6-1:  $V_a$ ,  $V_{PH}$ , and  $PH_{days}$  for projects on the Kennebec, Merrimack and Columbia Rivers.

Project	$V_a$ ( $10^6$ ft <sup>3</sup> )	$V_{PH}$ ( $10^6$ ft <sup>3</sup> )	$PH_{days}$ (days)
Brassua Lake (Kennebec)	9,000	149	60.56
Harris Station (Kennebec)	1,970	717	2.75
Wyman Station (Kennebec)	4,950	726	6.82
Amoskeag Dam (Merrimack)	188	487	0.39
Grand Coulee (Columbia)	225,876	23,328	9.68
Chief Joseph (Columbia)	4,147	19,613	0.21
John Day (Columbia)	28,737	33,610	0.86
Bonneville (Columbia)	9,711	28,685	0.34

One limitation of  $PH_{days}$  is that it makes no consideration for complex operational constraints. For example,  $PH_{days} = 9.68$  for Grand Coulee suggests that Grand Coulee could draft more than 80 ft in less than 10 days without spilling. While this is hydraulically possible it is operationally infeasible because Grand Coulee has a maximum drawdown rate of 1.5 feet per day. On the other hand as a simple metric of a project's flexibility, the storage-powerhouse factor is effective in placing projects on the 'run-of-river' to 'storage' spectrum. It correctly identifies that Brassua Lake has very limited capacity to quickly draft without spilling, while projects like Chief Joseph and Bonneville have large turbine capacity but limited storage and are incapable of long (several day), major storage drafts. In the intermediate, Wyman, Harris, and

Grand Coulee have appreciable storage with sufficient power-house capacity to significantly draft on the order of a few days.

Considering the magnitude of the powerhouse hydraulic capacity alone leaves an incomplete picture: one must consider powerhouse capacity relative to average inflows and inflow variability. The powerhouse flexibility capacity factor,  $C_{PH}$ , is given by:

$$C_{PH} = \frac{PH_{max} - \mu}{\sigma} \tag{6-4}$$

where  $\mu$  and  $\sigma$  are the mean and standard deviation of the project inflow rate respectively, and  $PH_{max}$  is the maximum flow rate through the powerhouse. Figure 6-2 displays  $C_{PH}$  for various  $PH_{max}$  and  $CV = \sigma/\mu$ . Again, one might wish to adjust  $\sigma$  to account for serial correlation.

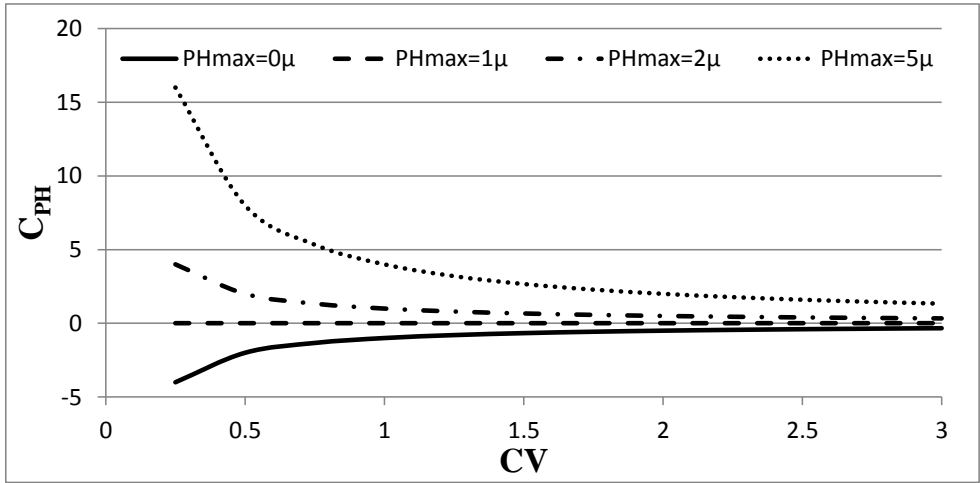


Figure 6-2: Powerhouse Flexibility Factor,  $C_{PH}$ , versus coefficient of variation for various powerhouse hydraulic capacities,  $PH_{max}$ .

It should also be noted that  $\mu$  and  $\sigma$  likely vary greatly over the year, so a single system likely has different  $C_{PH}$  for different seasons. During the refill season

for a ‘reservoir’ project,  $C_{PH}$  might very well be negative, while during the summer operational period it is likely to be positive.

The four diagnostic metrics introduced in this section are applied to a variety of hydropower systems in the Section 6.4.

### ***Section 6.3.2 The Regression Approach***

The metrics in the previous section give the analyst some indication of a project’s operational flexibility, but they do not indicate what time scales are important to system operation, or the forecast length of interest. This section proposes a regression approach to determine both.

A natural approach to determining the inflow time scale of importance is to consider the correlation between the optimal decision,  $R_t$ , and the cumulative inflow volume over a lead time  $\tau$ ,  $V_t(\tau)$ . Here  $V_t(\tau)$  is the cumulative inflow into the reservoir from time  $t + 1$  to time  $t + 1 + \tau$  (note the use of  $t + 1$  rather than  $t$  derives from the assumption in Chapter 4 that the current inflow is known). One can then identify the most important inflow time scale as the  $\tau$  which has the maximum correlation with  $R_t$ . This is essentially analogous to regressing  $R_t$  on  $V_t(\tau)$ . Viewing the analysis in terms of regression allows for easy expansion of the analysis to other explanatory variables, and to the use of non-linear models. In the case of understanding the relationship between release and inflow, an important explanatory variable is storage in the present time  $S_t$ . The diagnostic metric of interest would then be the coefficient of determination ( $R^2$ ) for models with varying  $\tau$ . The  $\tau$  which results in the highest  $R^2$  corresponds to the critical time scale of reservoir inflows.

The operation of the single reservoir on the Kennebec River in Chapter 4 was driven by energy price as much as by hydrologic conditions, one might also regress the optimal decision on the mean energy price over a lead  $\tau$  to determine the economic time scale of operation which is most important.

The results section of this chapter contains examples of the regression approach considering hydrologic explanatory variables for a variety of hydropower systems.

Before moving on, it is important to draw a distinction between this methodology and previous similar work which uses regression paired with optimization to derive an optimal policy. An early example of this work is Houck and Karamouz [1982] who derive annual and monthly operating rules using this approach. First they use deterministic DP to derive an optimal policy, then use regression on the optimal policy to identify relationships between variables of interest and the optimal release.

The method proposed here takes a similar but different tack. This work uses first applies a deterministic DP optimization for the given system over 20 years of operation. Rather than using regression to derive operating rules from this result, we use regression analysis to inform us of the best hydrologic state variable and forecast duration for subsequent stochastic optimization.

### ***Section 6.3.3 The Spectral Density Function Approach***

Spectral density estimation is commonly used in signal processing and fluid mechanics to determine the frequency content of sampled data. This can reveal the frequency bands (or inversely periodicities) which contain the most variation in the

sampled data. In this application the sampled data are the optimal policy derived by a deterministic optimization over a summer season operation with perfect foresight. This is viewed as a continuous optimal decision rule which has been sampled with frequency corresponding to the time step of the model. Spectral density estimation is then used to identify the important frequencies of system operation.

The Fourier transformation transforms sampled data from the temporal domain to the frequency domain. The discrete Fourier transformation is defined as

$$G_k = \sum_{t=0}^{T-1} R_t e^{-2i\pi(\frac{t}{T})k} \quad (6-5)$$

$$k = 0, 1, 2, \dots, T - 1$$

where  $k$  is the index of the sample record in the frequency domain and  $n$  is the index of the sample record in the temporal domain. Let  $\mathbf{G}$  be a vector of  $G_k$  for an optimal release sequence. The power spectral density function (PSDF) is defined as

$$\mathbf{S}_{RR} = \frac{\Delta t}{T} \mathbf{G} \mathbf{G}^* = \frac{\Delta t}{T} |\mathbf{G}^2| \quad (6-6)$$

where  $\Delta t$  is the time step length of the model and  $\mathbf{G}^*$  is the complex conjugate of  $\mathbf{G}$ .

The cross power spectral density function (CPSDF) of  $R$  and another data series  $h$  is defined as

$$\mathbf{S}_{gh} = \frac{\Delta t}{T} \mathbf{G} \mathbf{H}^* \quad (6-7)$$

where  $\mathbf{H}$  is a vector of the Fourier transformed data series  $h$ , and  $\mathbf{H}^*$  is the complex conjugate of  $\mathbf{H}$ .

The PSDF describes the portion of the data variance which is contained in each frequency band. Similarly, the CPSDF describes the portion of the covariance of two variables which is contained in each frequency band. By identifying the frequency

bands which contain significant variation in reservoir operation, we can infer the critical frequencies of the system's operation. The resolution of the frequency band is dictated by the length of the data record:

$$\Delta f = \frac{1}{T} \quad (6-8)$$

where  $\Delta f$  is the frequency band.

The PSDF can be noisy, so it is customary to repeat experiments several times, and to report the ensemble average PSDF,  $\langle \mathbf{S}_{RR} \rangle$ . In this application optimal decision sequences are derived for many independent summer seasons of operation, the PSDF and CPSDF are computed for each, and the ensemble average is reported in the Results section.

## ***Section 6.4 Results***

This section provides examples of the diagnostic tools developed in Section 6.3 applied to various study systems based on the single reservoir system on the Kennebec River described in Chapters 3 and 4.

### ***Section 6.4.1 Study Systems***

The diagnostic metrics described in the previous section are applied to the hypothetical single reservoir systems on the Kennebec described in Chapters 3 and 4. Twelve different systems are created by varying the turbine capacity and the reservoir storage, as described in Table 6-2. The same 20 summer inflow sequences are used for each of the 12 system configurations. The systems are assumed to start each summer operating period (May 1) with full storage. At the end of the summer operating period (October 31), the system must draw down to flood storage level.

The system operational objective is to maximize revenue from power sales:

$$\max_{R_t} \left\{ \sum_{t=1}^T B_t \right\} \quad (6-9)$$

where the incremental benefit in each time,  $B_t$  is a function of  $R_t$ , the current and next time period's reservoir storage,  $S_t$  and  $S_{t+1}$  respectively, and the energy price profile in the present time. A time step of 6-hours is considered here. The power generated by release  $R_t$  during period  $t$  with a given storage is:

$$P_t = \frac{\alpha R_t [0.5(\Delta H(S_t, R_t) + \Delta H(S_{t+1}, R_t))]}{\zeta}, \quad R_t \geq 140 \frac{ft^3}{s} \quad (6-10)$$

$$P_t = 0, \quad \text{otherwise}$$

where  $\alpha$  is an efficiency factor,  $\zeta$  is a unit conversion factor,  $\Delta H$  is the net head which is a function of storage and release, The incremental benefits resulting from  $P_t$ ,  $B_t$ , are computed as:

$$B_t = \int_0^{P_t} Price_t(p) dp \quad (6-11)$$

where  $Price_t$  is the price profile for timestep  $t$ . Over a 6-hour period, the  $Price_t$  is a continuous function of the power generated during that 6-hour period, given by:

$$Price_t(p) = c + a \times \cos(b \times p) \quad (6-12)$$

where  $a$  and  $c$  are profile parameters, and  $b$  is

$$b = \frac{\pi}{P_t(\max)} \quad (6-13)$$

where  $P_t(\max)$  is the maximum possible generation level given the system's current state. For more discussion of the price profile formulation see Chapter 4.

The real Kennebec hydropower system is part of the ISO New England market. In that market prices vary throughout the day and across days. Two price schemes are considered in the following runs. To isolate the effect of hydrologic processes on the

system a ‘mean price’ scheme is used. In this case each day is divided into three ‘on-peak’ periods and one ‘off-peak’ period. Every ‘on-peak’ period has the same price parameters  $a$  and  $c$ , and each ‘off-peak’ period has the same price parameters  $a$  and  $c$ . Thus prices vary within each day but have the same values from day-to-day.

Price variability is important to the operation of the real system, so a ‘real price’ scheme is also used. In this case each time period has a unique  $a$  and  $c$  based on real day-ahead price data from New England ISO.

Table 6-2: Turbine Capacity and Storage Capacity for each of the 12 system configurations.

System Name	Turbine Capacity (ft <sup>3</sup> /s)	Storage Capacity (million ft <sup>3</sup> )
(Small, 1000)	1000	1970
(Mid, 1000)	1000	9850
(Big, 1000)	1000	19700
(Small, 2000)	2000	1970
(Mid, 2000)	2000	9850
(Big, 2000)	2000	19700
(Small, 3500)	3500	1970
(Mid, 3500)	3500	9850
(Big, 3500)	3500	19700
(Small, 5000)	5000	1970
(Mid, 5000)	5000	9850
(Big, 5000)	5000	19700
(Small, 8300)	8300	1970
(Mid, 8300)	8300	9850
(Big, 8300)	8300	19700

A deterministic model assuming perfect foresight was applied to each of the fifteen hypothetical systems for 20 years of summer operation, and using both the ‘mean price’ and ‘real price’ economic schemes. The ‘real price’ scheme will allow evaluation of energy market variations on optimal system operations during the summer period that is modeled. The following section describes the application of the diagnostic metrics described in Section 6.3.

### Section 6.4.2 Application of Diagnostic Metrics

Table 6-3 reports the storage capacity factor, storage days, powerhouse days, and powerhouse flexibility factor for the fifteen systems described in Table 6-2. Note that when  $PH_{max} = 1000$ ,  $C_S(PH) < 0$  indicating that the powerhouse capacity is smaller than the average inflow, so that the system must either fill (excess water is stored) or spill (there is no room to store excess water) over much of the planning period. In fact, for system (Big,1000),  $PH_{days}$  is greater than the planning period length. This means that if the system were to start full, it would take longer than the planning period to reach flood storage draw-down, even if the powerhouse ran at capacity for the entire planning period; in this case no optimization model is needed.

Table 6-3: Storage Capacity Factor  $C_S(\tau = 1 \text{ Day})$ , Storage-days  $ST_{days}$ , Powerhouse-days  $PH_{days}$ , and the Powerhouse Flexibility Factor  $C_{PH}$  for twelve system configurations

System Name	$C_S$	$ST_{days}$	$PH_{days}$	$C_{PH}$
(Small, 1000)	12.34	16.19	22.80	-0.19
(Mid, 1000)	64.95	82.19	114.00	-0.19
(Big, 1000)	130.70	162.14	228.01	-0.19
(Small, 2000)	12.34	16.19	11.40	0.39
(Mid, 2000)	64.95	82.19	57.00	0.39
(Big, 2000)	130.70	162.14	114.00	0.39
(Small, 3500)	12.34	16.19	6.51	1.27
(Mid, 3500)	64.95	82.19	32.57	1.27
(Big, 3500)	130.70	162.14	65.15	1.27
(Small, 5000)	12.34	16.19	4.56	2.47
(Mid, 5000)	64.95	82.19	22.80	2.47
(Big, 5000)	130.7	162.14	45.60	2.47
(Small, 8300)	12.34	16.19	2.75	4.08
(Mid, 8300)	64.95	82.19	13.74	4.08
(Big, 8300)	130.70	162.14	27.47	4.08

At the opposite end of the spectrum, when  $PH_{max} = 8300$ ,  $C_{PH} = 4.08$ , meaning that  $PH_{max}$  is bigger than most inflows so spilling is not a concern. Instead

systems with  $PH_{max} = 8300$  can largely shape outflows to take advantage of on-peak pricing. The ability of those systems to store water to take advantage of higher prices on some days than others is dictated by the available storage.  $PH_{days}$  varies by an order of magnitude between systems (Small, 8300) and (Big, 8300): 2.75 and 27.47 respectively. Thus one expects shorter-term planning to be more critical for system (Small, 8300) than for system (Big, 8300).

### ***‘Mean Price’ Scheme Results***

The regression approach described in Section 6.3.2 was applied to the optimization results for each of the twelve systems in Table 6-2 for the ‘mean price’ economic scheme. In the ‘mean price’ scheme energy price functions vary during each day but not across days. To eliminate the effect of within day peaking, daily cumulative releases ( $\ddot{R}_d$ ) are used in the regression analysis. A non-linear model of  $R_t$  as a function of available reservoir storage and inflow over a duration  $\tau$  is fit using non-linear ordinary least squares. The non-linear model has the form:

$$\ddot{R}_d = \max \left[ PH_{max} \times v, \beta_1 + \beta_2 \sum_{u=t}^{\tau} I_u + \beta_3 \sum_{u=t}^{\tau} (V_a - S_u) \right] + e_t \quad (6-14)$$

Durations  $\tau$  ranging from 1 day to 10 days were considered. The  $R^2$  statistic was computed for twelve of the systems and for each of the ten values of  $\tau$ . Figure 6-3, Figure 6-4, Figure 6-5, and Figure 6-6 plot  $R^2$  versus duration for various  $PH_{max}$  and  $V_a$  combinations.

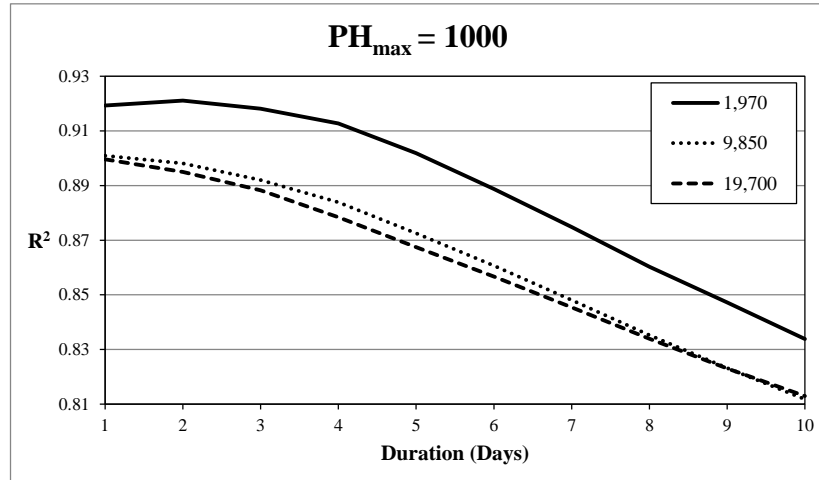


Figure 6-3:  $R^2$  vs. Duration ( $\tau$ ) for various reservoir storages (in  $10^6 ft^3$ ) for  $PH_{max} = 1000$  (in  $ft^3/s$ ).

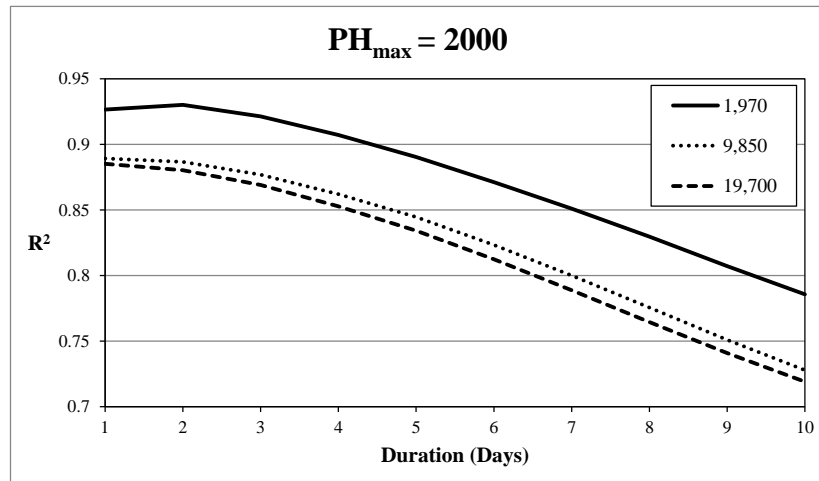


Figure 6-4:  $R^2$  vs. Duration ( $\tau$ ) for various reservoir storages (in  $10^6 ft^3$ ) for  $PH_{max} = 2000$  (in  $ft^3/s$ ).

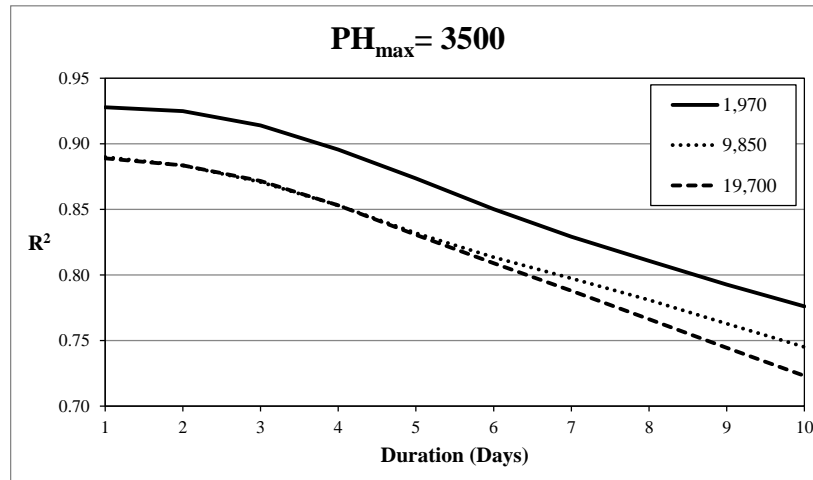


Figure 6-5:  $R^2$  vs. Duration ( $\tau$ ) for various reservoir storages (in  $10^6 ft^3$ ) for  $PH_{max} = 3500$  (in  $ft^3/s$ ).

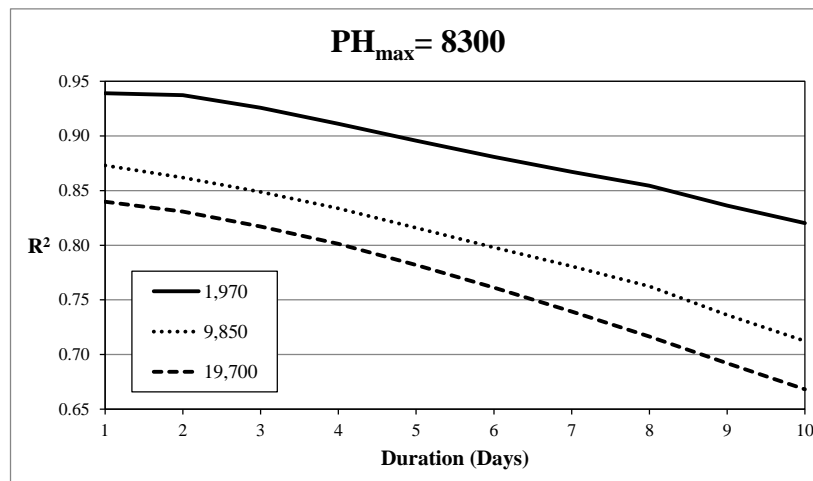


Figure 6-6:  $R^2$  vs. Duration ( $\tau$ ) for various reservoir storages (in  $10^6 ft^3$ ) for  $PH_{max} = 8300$  (in  $ft^3/s$ ).

For nearly every  $PH_{max}$  considered  $R^2$  decreases with increased reservoir storage, indicating that near-term hydrologic conditions (inflows and storages up to 10-days) have a weaker relationship with the current day release as the storage increases. This is expected: larger storage allows the system to hold inflows longer and to plan on longer time scales, and thus releases are determined less by the immediate inflow.

$R^2$  generally decreases with duration, though the maximum  $R^2$  occurs at two days duration for  $PH_{max} = 1000$  and  $2000$ . We draw the conclusion from these results that the most important flow information to provide to a decision model for the twelve systems considered here is an estimate of the expected flow in the next day. This is somewhat surprising, as the twelve systems considered represent a wide range of  $PH_{days}$ . On the other hand, the serial correlation of daily flows is very high (see Figure 6-7) so the flow for the next day includes a lot of information about the next 2-6 days of inflow.

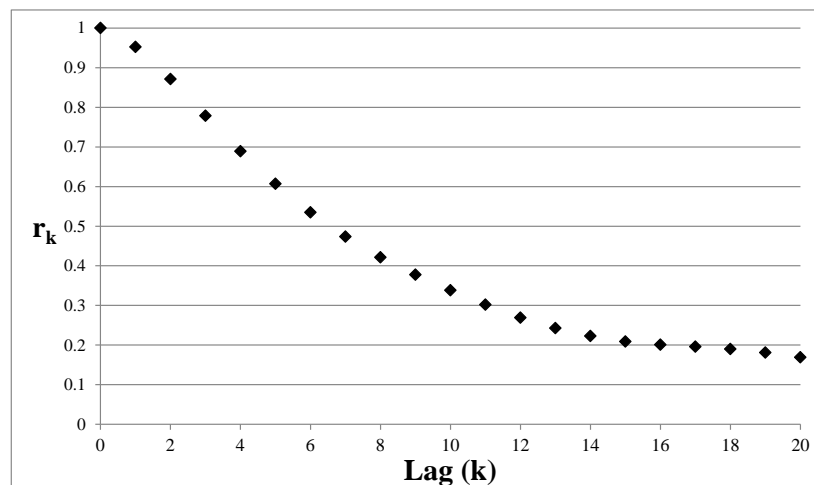


Figure 6-7: Autocorrelation vs. Lag for daily inflow volume into hypothetical Kennebec reservoir.

A more detailed discussion of the special steps taken in this regression procedure is expected in a forthcoming journal publication of this work.

The spectral analysis approach described in Section 6.3.3 is applied to twelve of the systems described in Table 6-2. Each of the 20 years of simulated operation is treated as an independent experiment, and a unique PSDF is fit to the optimal releases. The 20 PSDFs are then averaged to produce an ensemble averaged PSDF of  $\langle S_{RR} \rangle$ .

Figure 6-8 plots  $\langle S_{RR} \rangle$  versus frequency for (Big, 2000), which has  $V_a = 19,700$  and  $PH_{max} = 8300$ .

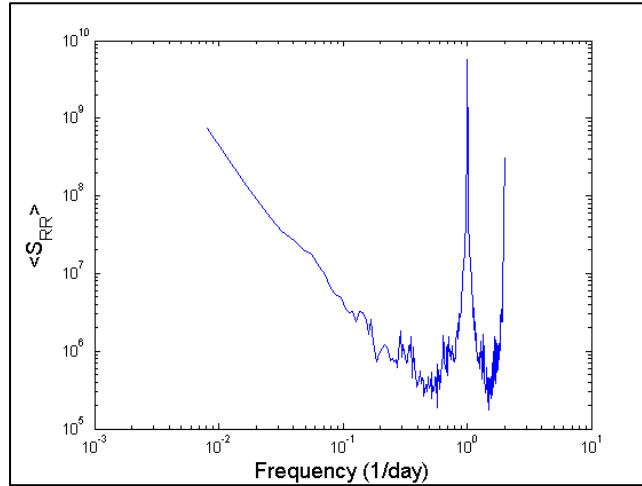


Figure 6-8: Ensemble PSDF of optimal release  $R$  for System (Big, 2000),  $ST_{days} = 162.1$ ,  $PH_{days} = 114$ , with the ‘mean-price’ economic scheme.

Peaks in the ensemble PSDF indicate frequencies which contain a significant portion of the variability in the system operation. The maximum peak is at frequency 1/day. This is caused by the diurnal price fluctuations. The significant low frequency variability is the seasonal drawdown of the reservoir to meet flood storage, which occurs on longer time scales (thus smaller frequencies in Figure 6-8). It is clear, however, that the two major time scales that drive system (Big, 2000) operation are daily and monthly (multiple weeks).

Figure 6-9 plots the ensemble CPSDF for the optimal release and the inflow for the system (Big, 2000) with the mean economic scheme ( $\langle S_{IR} \rangle$ ). Peaks in the CPSDF indicate frequencies at which significant portions of the covariance of two signals is contained. Note that unlike  $\langle S_{RR} \rangle$  in Figure 6-8, the maximum peak of  $\langle S_{IR} \rangle$  does not correspond to a frequency of 1/day, but instead corresponds to low frequencies corresponding to monthly or seasonal periods. This is caused by the

seasonal fluctuation in inflows which seem to dominate the covariance between  $R$  and  $I$  rather than the diurnal cycle of prices.

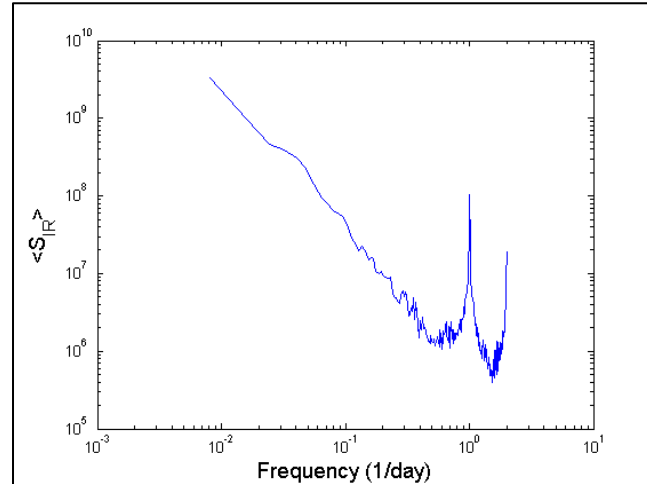


Figure 6-9: Ensemble CPSDF of optimal release  $R$  and inflow  $I$  for System (Big, 2000),  $ST_{days} = 162.1$ ,  $PH_{days} = 114$ , with the ‘mean-price’ economic scheme

Figure 6-10 plots the Ensemble PSDF of optimal release for system (Small, 2000), which has  $V_a = 1,970$ ,  $PH_{max} = 2000$ ,  $ST_{days} = 16.9$ , and  $PH_{days} = 11.4$ . As in Figure 6-8 there is a peak of the ensemble PSDF occurs at the frequency 1/day because of the diurnal peaking cycle. Unlike the ensemble PSDF in Figure 6-8, the highest peak of the PSDF is at low frequencies corresponding to seasonal fluctuations in reservoir operation. This is in part attributable to the smaller storage: the system must act more like a ‘run of river’ plant and is more sensitive to seasonal fluctuations in inflow.

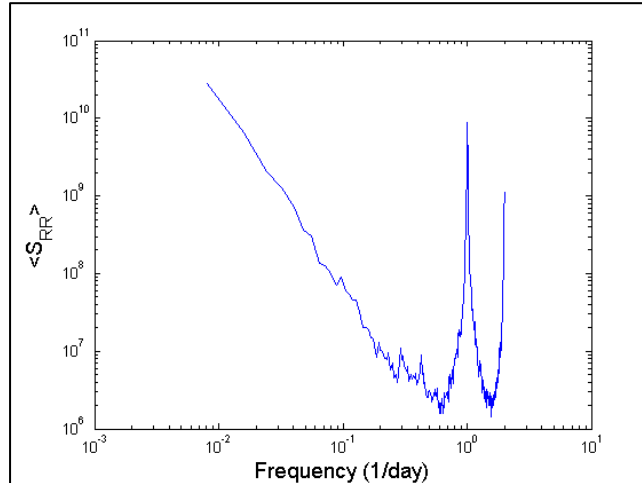


Figure 6-10: Ensemble PSDF of optimal release  $R$  for System (Small, 2000),  $ST_{days} = 16.9$ ,  $PH_{days} = 11.4$ , with the ‘mean-price’ economic scheme.

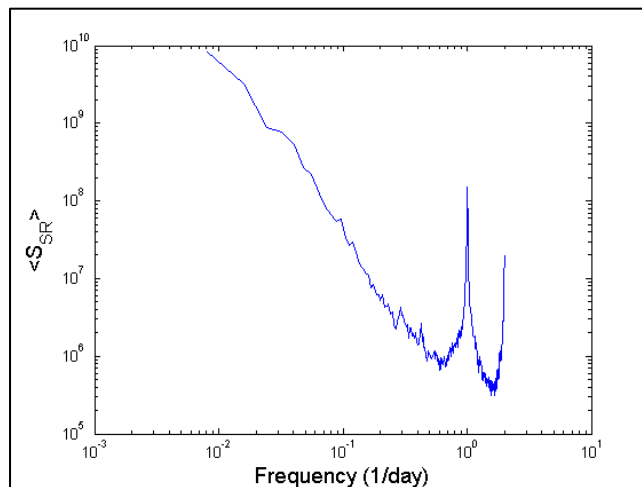


Figure 6-11: Ensemble CPSDF of optimal release  $R$  and reservoir storage  $S$  for System (Small, 2000),  $ST_{days} = 16.9$ ,  $PH_{days} = 11.4$ , with the ‘mean-price’ economic scheme.

Figure 6-11 plots the ensemble CPSDF of optimal release and reservoir storage for system (Big, 2000). As in the plot of  $\langle S_{RR} \rangle$  in Figure 6-10 there is a notable peak at a frequency of 1/day, which is caused by the diurnal cycling of energy prices, but as before, the most notable peak in the CPSDF are located at low frequencies corresponding to seasonal changes in hydrology and end-of-year drawdown targets.

Ensemble PSDF and CPSDF plots for twelve systems for the ‘mean price’ scheme are available in the appendix of this chapter. It was noted that in for some of those runs a small peak of the PSDF  $\langle S_{RR} \rangle$  periodicities corresponding to weekly cycling. While it is not clear if those peaks are statistically significant, it is precisely what one expects in real systems, as examined in the next section.

### ***‘Real Price’ Scheme Results***

In the ‘real price’ scheme the parameters of the price model (equation (6-12)) are based on real energy prices from the New England ISO. Thus, rather than having a single pair of ‘on peak’ and ‘off peak’ prices for every day in the simulation period, the price function parameters vary from day to day, and week to week. Because the prices add an extra element of uncertainty to system operation, it is more difficult to draw conclusions about the hydrologic time scales of interest than in the ‘mean price’ scheme. On the other hand, comparing the ensemble PSDF to those for the ‘mean price’ is interesting. And if hydrologic variability is not that important, then the lesson is that perhaps our modeling efforts should be directed elsewhere, specifically the impact of energy market price variability.

Figure 6-12 plots the ensemble PSDF for system (Big, 2000) for the ‘real price’ economic scheme. As before, the peak of the PSDF is found at the 1/day frequency, indicating that the diurnal fluctuation in energy price is very important to system operation. In fact the peak at 1/day is even more pronounced than in the ‘mean price’ case, indicating that diurnal peaking is even more important now, likely because the variability in ‘on-peak’ and ‘off-peak’ prices is much greater now. Interestingly there is a striking peak of the PSDF at the 0.1429/day frequency, corresponding to a

weekly cycle. This is likely due to a weekly cycle in energy prices in which prices are generally lower on the weekends and higher during the week. This weekly cycle is not present in the ‘mean price’ scheme.

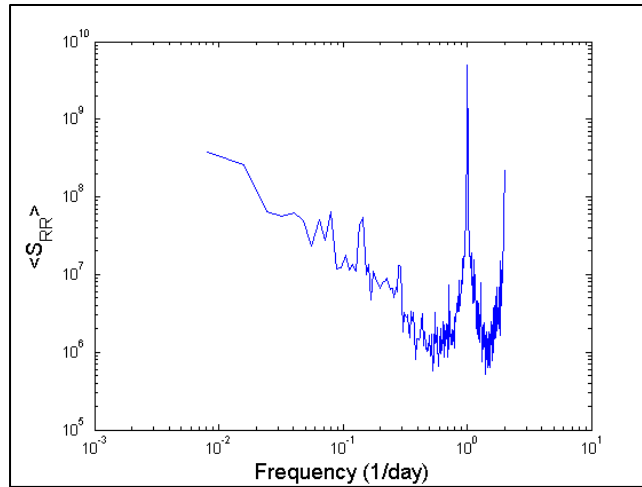


Figure 6-12: Ensemble PSDF of optimal release  $R$  for System (Big, 2000),  $ST_{days} = 162.14$ ,  $PH_{days} = 114$ , with the ‘real-price’ economic scheme.

Figure 6-13 plots the CPSDF of the optimal release,  $R$ , and inflow,  $I$ ,  $\langle S_{IR} \rangle$  for the variable price scheme. As in the case of mean price schemes, the maximum peak of  $\langle S_{IR} \rangle$  occurs at low frequencies corresponding to seasonal changes in the inflows. There are small peaks at frequencies corresponding to 1/day and 1/week, but these are much less pronounced than in  $\langle S_{RR} \rangle$  in Figure 6-12.

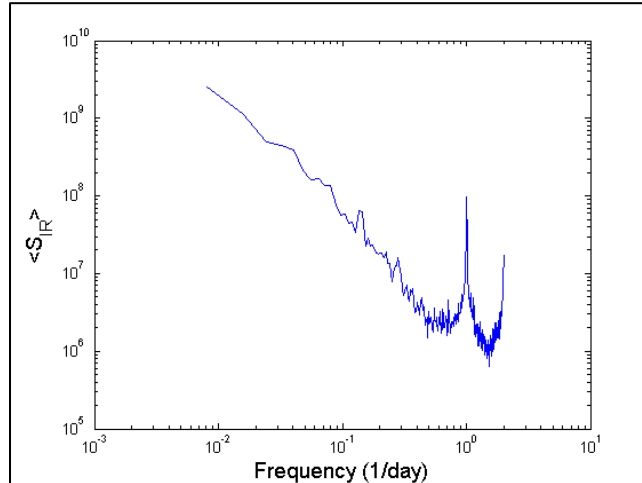


Figure 6-13: Ensemble CPSDF of optimal release  $R$  and inflow  $I$  for System (Big, 2000),  $ST_{days} = 162.14$ ,  $PH_{days} = 114$ , with the ‘real-price’ economic scheme.

Figure 6-14 plots the ensemble PSDF for system (Big, 8300), which has  $V_a = 19,700$ ,  $PH_{max} = 8300$ ,  $ST_{days} = 162.14$ , and  $PH_{days} = 27.47$  for the ‘real price’ scheme. Like the PSDF in Figure 6-12 there is a significant peak at frequency 0.14/day ( or 1/week), but the striking feature is that this peak is now much more pronounced. This is because with bigger turbines, the system is able to take greater advantage of the weekly weekend/weekday pricing cycle. There is more variation explained at frequencies corresponding to multi-day periodicities because the price now changes from day to day, and the system is willing to withhold ‘on peak’ generation in some days in order to generate more on higher price days. This is not seen as much in Figure 6-12 because for that system the turbines are smaller so there is much less potential for peaking.

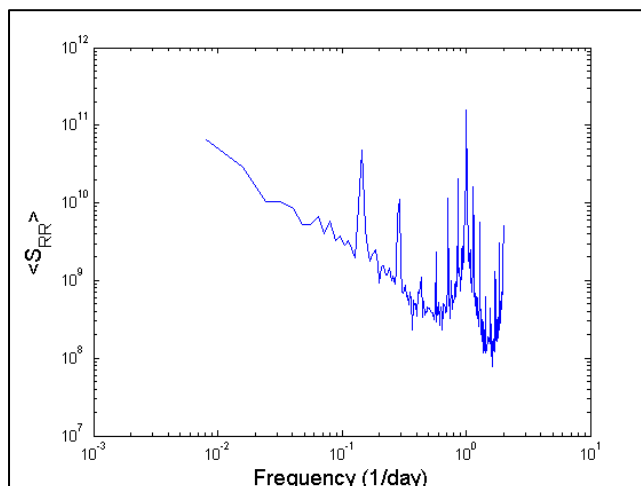


Figure 6-14: Ensemble PSDF of optimal release  $R$  for System (Big, 8300),  $ST_{days} = 162.14$ , and  $PH_{days} = 27.47$ , with the ‘real-price’ economic scheme.

Figure 6-15 plots the CPSDF of the optimal release,  $R$ , and inflow,  $I$ ,  $\langle S_{IR} \rangle$  for the variable price scheme. As in the case of mean price schemes, the maximum peak of  $\langle S_{IR} \rangle$  occurs at low frequencies corresponding to seasonal changes in the inflows. There are small peaks at frequencies corresponding to 1/day and 1/week, but these are much less pronounced than in  $\langle S_{RR} \rangle$  in Figure 6-14. With a large storage capacity and large turbines, releases are not tied to short-term variations in inflow.

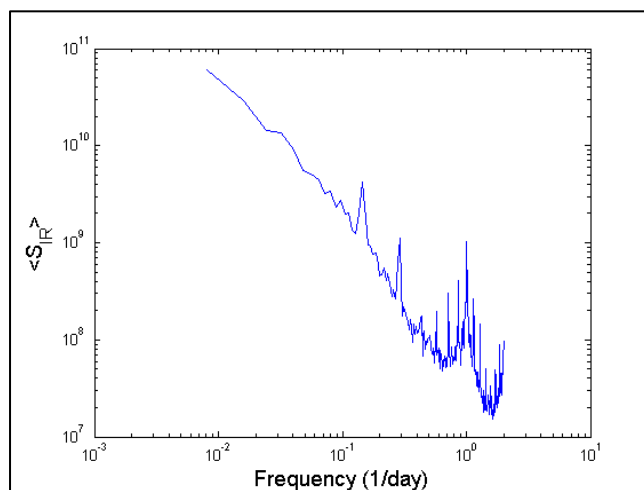


Figure 6-15: Ensemble CPSDF of optimal release  $R$  for System (Big, 8300),  $ST_{days} = 162.14$ , and  $PH_{days} = 27.47$ , with the ‘real-price’ economic scheme.

Figure 6-16 plots the ensemble PSDF for  $R$  for (Small, 8300). The shape is very similar to the PSDF for (Big, 8300) in Figure 6-14, but a key difference is that the magnitude of the variability explained in at 0.14/day frequency (1-week periodicity) is much less. This is because with much smaller storage, system (Small, 8300) is fairly limited in its ability to hold inflows long enough take advantage of the weekly price cycle.

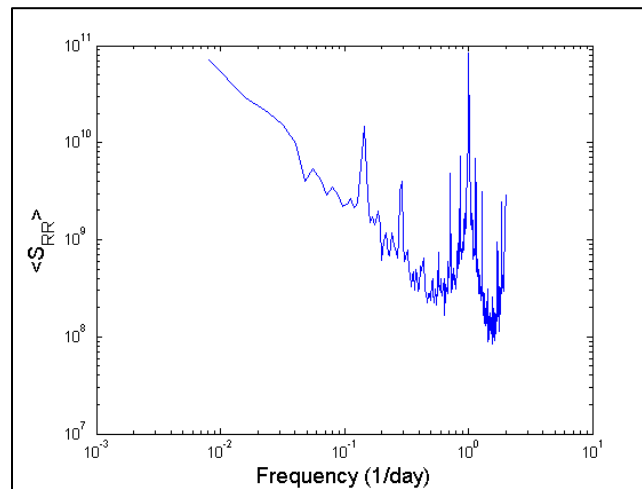


Figure 6-16: Ensemble PSDF of optimal release  $R$  for System (Small, 8300),  $ST_{days} = 16.19$ , and  $PH_{days} = 2.75$ , with the ‘real-price’ economic scheme.

Ensemble PSDF and CPSDF plots for twelve systems for the ‘real price’ scheme are available in the appendix of this chapter.

### ***Section 6.5 The value of the Spectral Density Analysis***

A concern expressed in multi-tiered SSDP model framework Chapter 4 of this thesis is that the short-term SSDP model might engage in myopic behavior in the last few time steps of each week if the terminal value function provided by the long-term SSDP model has some small error. Steps that might be taken to remedy this situation would add to the run time of the overall SSDP model so there was hesitancy to alter

take precautionary measures. Examination of the optimal operating rule didn't seem to indicate any myopic behavior, so it was assumed that all was well. However, when the PSDF of the optimal release for the 'mean price' scheme was examined a clear weekly cycle was present (see Figure 6-17). This was odd, because there was no weekly signal in the inflows or the price.

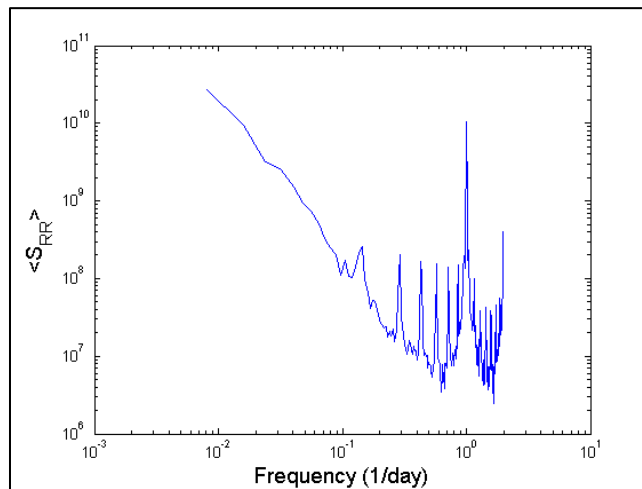


Figure 6-17: Ensemble PSDF of optimal release  $R$  for System (Small, 8300), 'mean price' scheme, 1-week short-term SSDP horizon.

This odd occurrence indicated that the model framework was adversely affecting the optimal decisions and introducing a weekly cycle that was otherwise undetectable. When the short-term SSDP planning horizon was extended to two weeks the erroneous weekly signal vanished (see Figure 6-18). Without the spectral density analysis performed in this chapter it is doubtful that this error in the model framework would have been apparent.

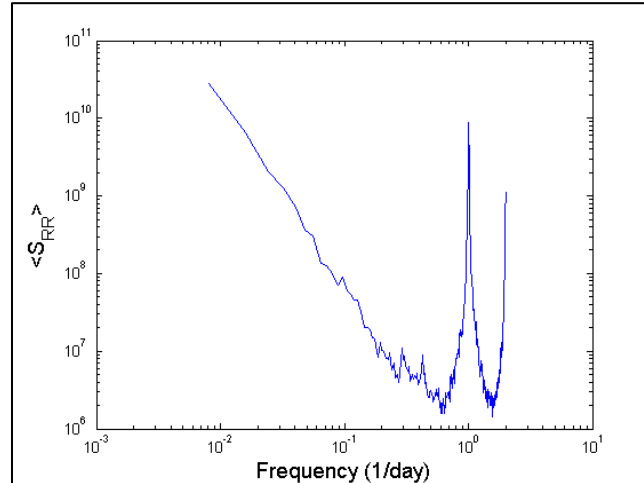


Figure 6-18: Ensemble PSDF of optimal release  $R$  for System (Small, 8300), 'mean price' scheme, 2-week short-term SSDP horizon.

### **Section 6.6 Conclusion**

This chapter focuses on diagnostic tools which can be used to identify the type of operation one is likely to see, the important time scales of operation to a system, and the amount of variability in the optimal control policy which is explained in different frequency bands. The simple diagnostic measurements are very easy to apply and can be very revealing. Chief Joseph Dam is in the top 5 power producing dams in the United States, and yet it is essentially a run of river plant. This is counterintuitive: Chief Joseph dam has an enormous storage and is nearly 200 ft high. However the operational constraints on the active storage, and the enormous flows in the Columbia River result in this massive project operating as a run of river project. The simple diagnostic tools allow this characteristic of the system to be immediately identified, and explained.

The regression analysis approach to identifying potential state variables and important duration periods is inspired by past work that derives optimal operating policies by regressing on the results of deterministic optimization (see Karamouz and

Houck [1982] for an early example). However, in the analysis proposed here, the optimal policy is not derived from the regression analysis; but rather the regression analysis informs the structure of the stochastic optimization model. In the examples provided in Chapter 6 it is shown that inflow in the next 7-24 hours is most related to the optimal perfect policy over a wide range of hypothetical systems. From this observation it was concluded that the inflow forecast for the next 24-hours was the most informative for the optimization models applied in Chapter 4.

The spectral analysis approach to diagnosing hydropower reservoir operating frequencies is new. Additional exploration of the results of this analysis would be advantageous. In our case it clearly shows that the diurnal peaking cycle in the energy market explains a huge amount of the variability in the system operation, though the largest fluctuations are due to the multi-week seasonal drawdown to meet end-of-period flood storage targets.

## REFERENCES

- Creager, W.P. & Justin, J.D. 1950, *Hydro-Electric Handbook*, 2nd edn, John Wiley & Sons, New York.
- Faber, B.A. 2001, *Real-Time Reservoir Optimization Using Ensemble Streamflow Forecasts*, PhD edn, Cornell University, Ithaca, NY.
- Hejazi, M.I., Cai, X.M. & Ruddell, B.J. 2008, "The role of hydrologic information in reservoir operation – Learning from historical releases", *Advances in Water Resources*, vol. 31, pp. 1636-1650.
- Karamouz, M. & Houck, M.H. 1987, "Comparison of Stochastic and Deterministic Dynamic Programming for Reservoir Operating Rule Generation", *Water Resources Bulletin*, vol. 23, no. 1, pp. 1.
- Karamouz, M. & Houck, M.H. 1982, "Annual and Monthly Reservoir Operating Rules Generated by Deterministic Optimization", *Water Resources Research*, vol. 18, no. 5, pp. 1337.
- Kelman, J., Stedinger, J.R., Cooper, L.A., Hsu, E. & Yuan, S. 1990, "Sampling stochastic dynamic programming applied to reservoir operation", *Water Resources Research*, vol. 26, no. 3, pp. 447-454.
- Klemes, V. 1977, "Value of Information in Reservoir Optimization", *Water Resources Research*, vol. 13, no. 5, pp. 837.
- Loucks, D.P., Stedinger, J.R. & Haith, D.A. 1981, *Water Resources Systems Planning and Analysis*, 1st edn, Prentice-Hall, Englewood Cliffs, N.J.
- McMahon, T.A., Vogel, R.M., Pegram, G.G.S., Peel, M.C. & Etkin, D. 2007, "Global streamflows - Part 2: Reservoir storage-yield performance", *Journal of Hydrology*, vol. 347, pp. 260.
- Montaseri, M. & Adedoye, A.J. 1999, "Critical period of reservoir systems for planning purposes", *Journal of Hydrology*, vol. 224, no. 115.

- Tejada-Guibert, J.A., Johnson, S.A. & Stedinger, J.R. 1995, "The value of hydrologic information in stochastic dynamic programming models of a multireservoir system", *Water Resources Research*, vol. 31, no. 10, pp. 2571-2579.
- Vogel, R.M. 1987, "Reliability Indices for Water Supply Systems", *Journal of Water Resources Planning and Management*, vol. 113, no. 4, pp. 563.
- Vogel, R.M. 1985, *The Variability of Reservoir Storage Estimates*, Cornell University.
- Vogel, R.M. & Bolognese, R.A. 1995, "Storage-reliability-resilience-yield relations for over-year water supply systems", *Water Resources Research*, vol. 31, no. 3, pp. 645-654.
- Vogel, R.M., Fennessey, N.M. & Bolognese, R.A. 1995, "Storage-Reliability-Resilience-Yield Relations for Northeastern United States", *Journal of Water Resources Planning and Management*, vol. 121, no. 5.
- Vogel, R.M., Lane, M., Ravindiran, R.S. & Kirshen, P. 1999, "Storage Reservoir Behavior in the United States", *Journal of Water Resources Planning and Management*, vol. 125, no. 5, pp. 245.
- Vogel, R.M., Sieber, J., Archfield, S.A., Smith, M.P., Apse, C.D. & Huber-Lee, A. 2007, "Relations among storage, yield, and instream flow", *Water Resources Research*, vol. 43, no. W05403.
- Vogel, R.M. & Stedinger, J.R. 1987, "Generalized storage reliability yield relationships", *Journal of Hydrology*, vol. 89, pp. 303-327.
- Wilks, D.S. 2011, *Statistical Methods in the Atmospheric Sciences*, 3rd edn, Academic Press, New York.
- Zhao, T., Yang, D., Cai, X., Zhao, J. & Wang, H. 2012, "Identifying effective forecast horizon for real-time reservoir operation under a limited inflow forecast", *Water Resources Research*, vol. 48, no. W01540.

*Appendix: 'Mean Price' Economic Scheme PSDF  $\langle S_{RR} \rangle$*

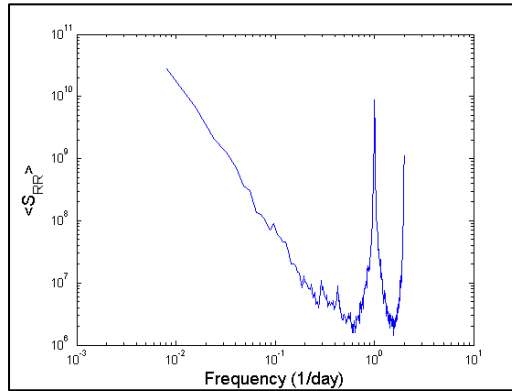


Figure 6-19: Ensemble PSDF of optimal release  $R$  for System (Small, 2000),  $ST_{days} = 16.19$ ,  $PH_{days} = 11.4$ , with the 'mean-price' economic scheme.

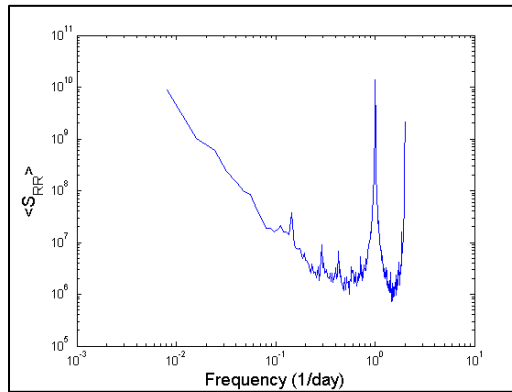


Figure 6-20: Ensemble PSDF of optimal release  $R$  for System (Mid, 2000),  $ST_{days} = 82.19$ ,  $PH_{days} = 57.00$ , with the 'mean-price' economic scheme.

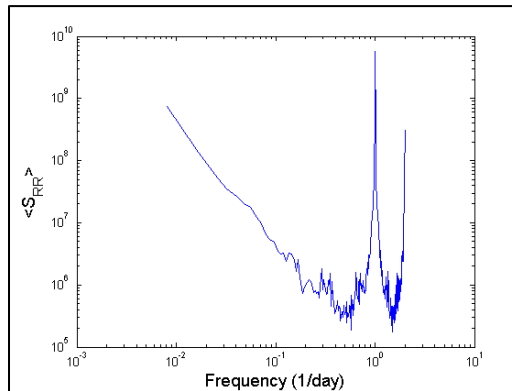


Figure 6-21: Ensemble PSDF of optimal release  $R$  for System (Big, 2000),  $ST_{days} = 162.14$ ,  $PH_{days} = 114$ , with the 'mean-price' economic scheme.

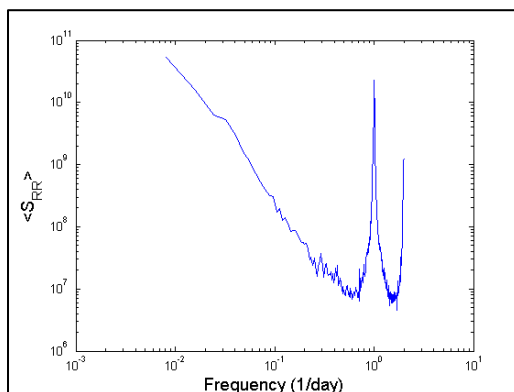


Figure 6-22: Ensemble PSDF of optimal release  $R$  for System (Small, 3500),  $ST_{days} = 16.18$ ,  $PH_{days} = 6.51$ , with the ‘mean-price’ economic scheme.

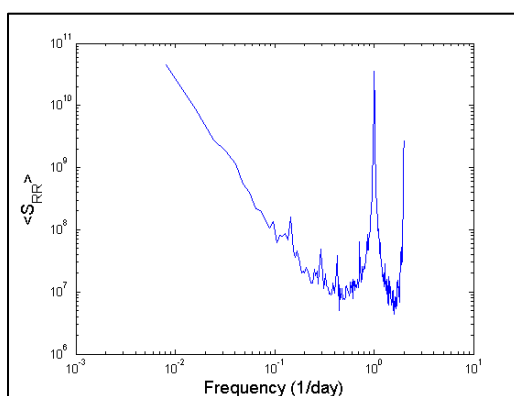


Figure 6-23: Ensemble PSDF of optimal release  $R$  for System (Mid, 3500),  $ST_{days} = 82.19$ ,  $PH_{days} = 32.57$ , with the ‘mean-price’ economic scheme.

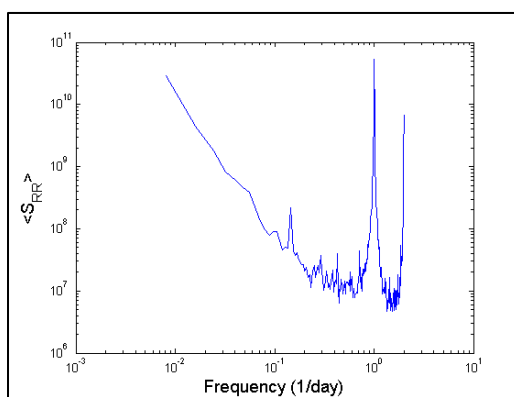


Figure 6-24: Ensemble PSDF of optimal release  $R$  for System (Big, 3500),  $ST_{days} = 162.14$ ,  $PH_{days} = 65.15$ , with the ‘mean-price’ economic scheme.

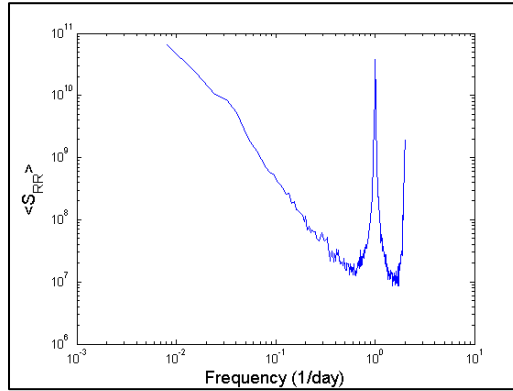


Figure 6-25: Ensemble PSDF of optimal release  $R$  for System (Small, 5000),  $ST_{days} = 16.19$ ,  $PH_{days} = 4.56$ , with the ‘mean-price’ economic scheme.

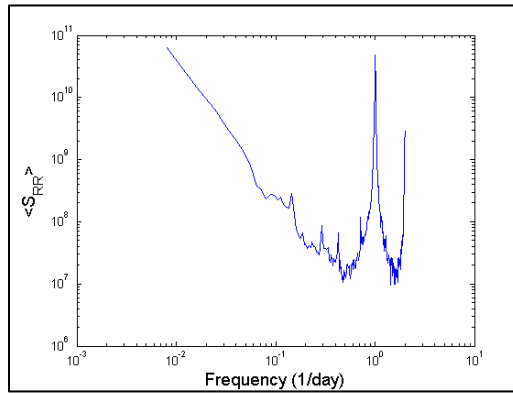


Figure 6-26: Ensemble PSDF of optimal release  $R$  for System (Mid, 5000),  $ST_{days} = 82.19$ ,  $PH_{days} = 22.8$ , with the ‘mean-price’ economic scheme.

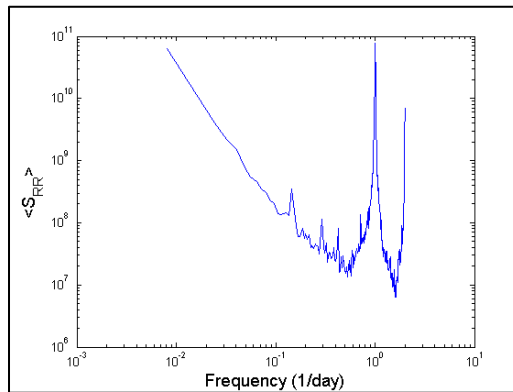


Figure 6-27: Ensemble PSDF of optimal release  $R$  for System (Big, 5000),  $ST_{days} = 162.14$ ,  $PH_{days} = 45.60$ , with the ‘mean-price’ economic scheme.

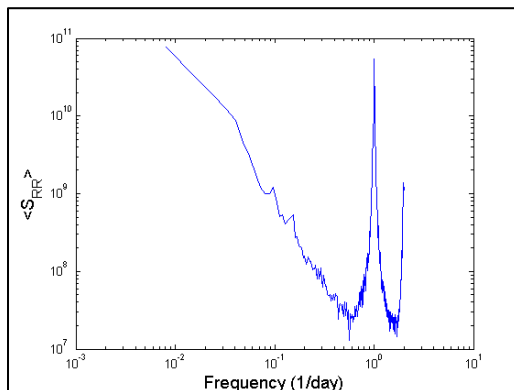


Figure 6-28: Ensemble PSDF of optimal release  $R$  for System (Small, 8300),  $ST_{days} = 16.19$ ,  $PH_{days} = 2.75$ , with the ‘mean-price’ economic scheme.

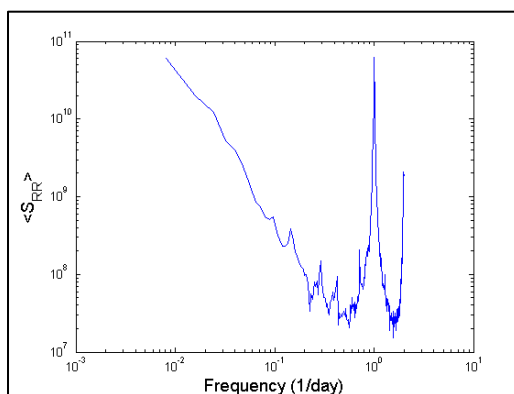


Figure 6-29: Ensemble PSDF of optimal release  $R$  for System (Mid, 8300),  $ST_{days} = 82.19$ ,  $PH_{days} = 13.74$ , with the ‘mean-price’ economic scheme.

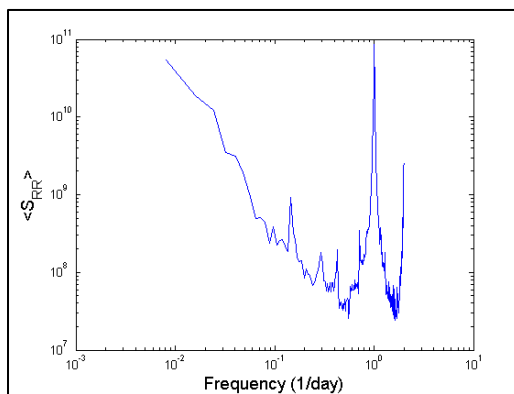


Figure 6-30: Ensemble PSDF of optimal release  $R$  for System (Big, 8300),  $ST_{days} = 162.14$ ,  $PH_{days} = 27.47$ , with the ‘mean-price’ economic scheme.

*Appendix: 'Mean Price' Economic Scheme CPSDF  $\langle S_{IR} \rangle$*

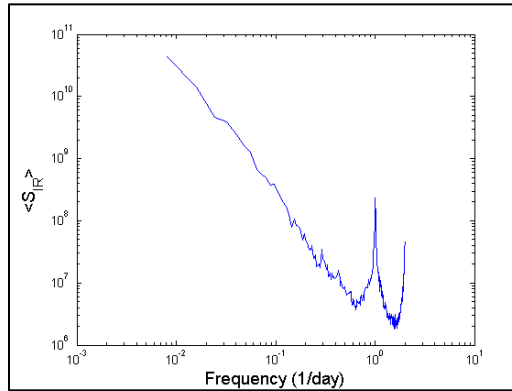


Figure 6-31: Ensemble CPSDF of optimal release  $R$  and inflow  $I$  for System (Small, 2000),  $ST_{days} = 16.19$ ,  $PH_{days} = 11.40$ , with the 'mean-price' economic scheme.

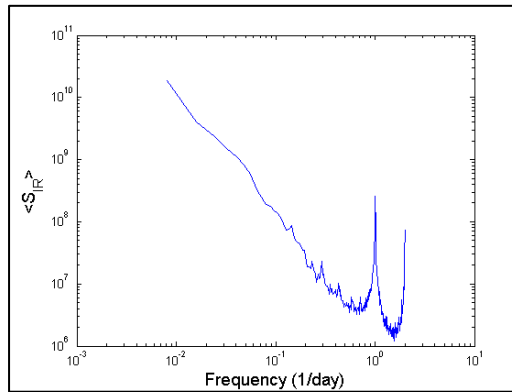


Figure 6-32: Ensemble CPSDF of optimal release  $R$  and inflow  $I$  for System (Mid, 2000),  $ST_{days} = 82.19$ ,  $PH_{days} = 57.00$ , with the 'mean-price' economic scheme.

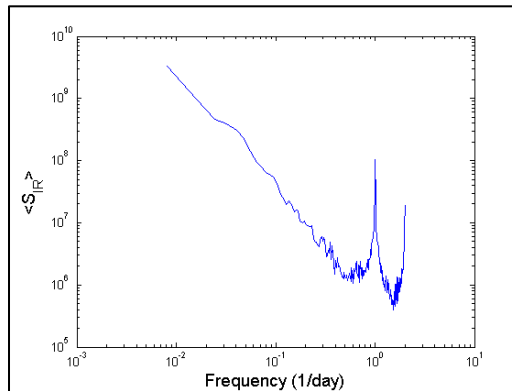


Figure 6-33: Ensemble CPSDF of optimal release  $R$  and inflow  $I$  for System (Big, 2000),  $ST_{days} = 162.14$ ,  $PH_{days} = 114.00$ , with the 'mean-price' economic scheme.

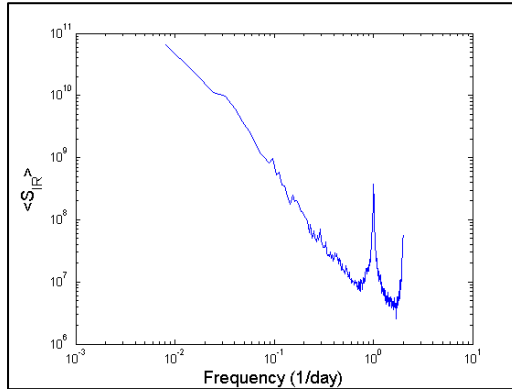


Figure 6-34: Ensemble CPSDF of optimal release  $R$  and inflow  $I$  for System (Small, 3500),  $ST_{days} = 16.19$ ,  $PH_{days} = 6.51$ , with the ‘mean-price’ economic scheme.

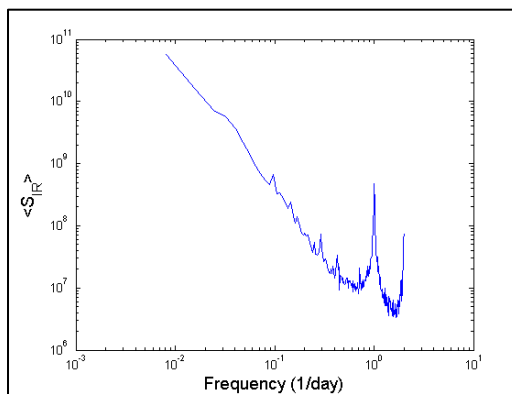


Figure 6-35: Ensemble CPSDF of optimal release  $R$  and inflow  $I$  for System (Mid, 3500),  $ST_{days} = 82.19$ ,  $PH_{days} = 32.57$ , with the ‘mean-price’ economic scheme.

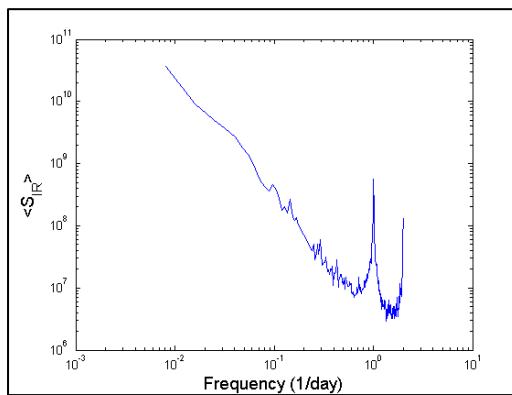


Figure 6-36: Ensemble CPSDF of optimal release  $R$  and inflow  $I$  for System (Big, 3500),  $ST_{days} = 162.14$ ,  $PH_{days} = 65.15$ , with the ‘mean-price’ economic scheme.

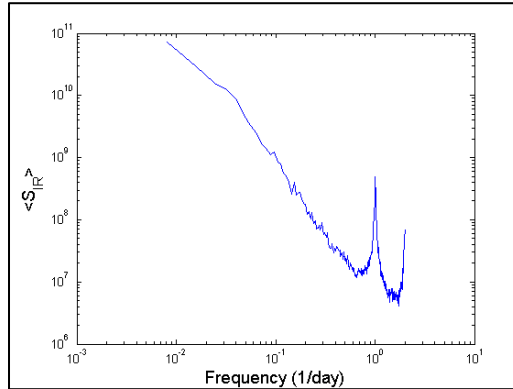


Figure 6-37: Ensemble CPSDF of optimal release  $R$  and inflow  $I$  for System (Small, 5000),  $ST_{days} = 16.19$ ,  $PH_{days} = 4.56$ , with the ‘mean-price’ economic scheme.

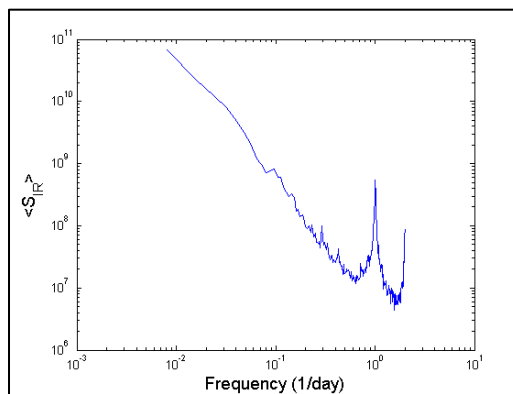


Figure 6-38: Ensemble CPSDF of optimal release  $R$  and inflow  $I$  for System (Mid, 5000),  $ST_{days} = 82.19$ ,  $PH_{days} = 22.8$ , with the ‘mean-price’ economic scheme.

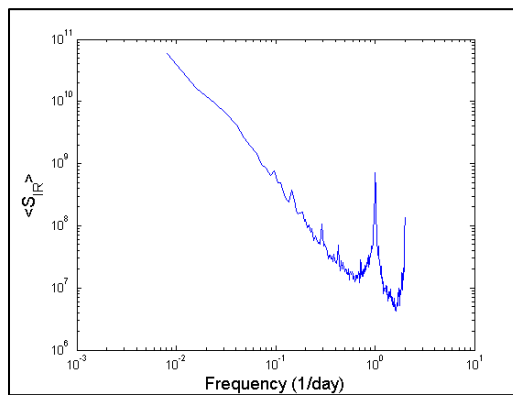


Figure 6-39: Ensemble CPSDF of optimal release  $R$  and inflow  $I$  for System (Big, 5000),  $ST_{days} = 162.14$ ,  $PH_{days} = 45.6$ , with the ‘mean-price’ economic scheme.

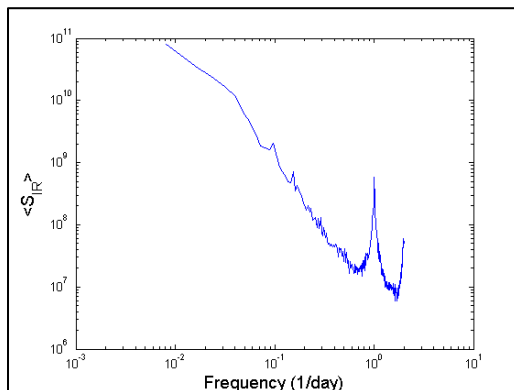


Figure 6-40: Ensemble CPSDF of optimal release  $R$  and inflow  $I$  for System (Small, 8300),  $ST_{days} = 16.19$ ,  $PH_{days} = 2.75$ , with the ‘mean-price’ economic scheme.

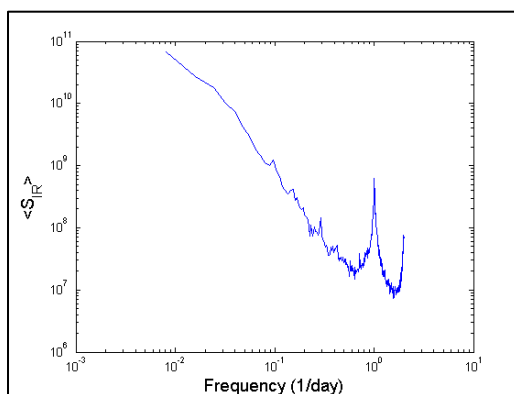


Figure 6-41: Ensemble CPSDF of optimal release  $R$  and inflow  $I$  for System (Mid, 8300),  $ST_{days} = 82.19$ ,  $PH_{days} = 13.74$ , with the ‘mean-price’ economic scheme.

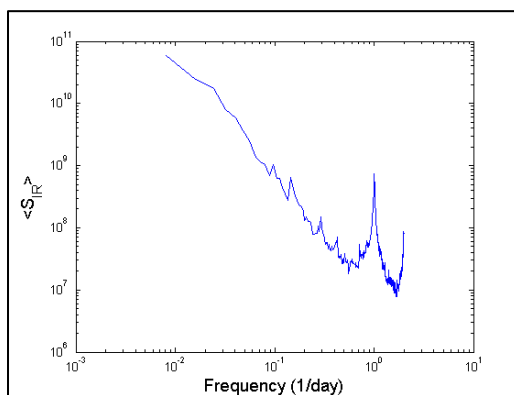


Figure 6-42: Ensemble CPSDF of optimal release  $R$  and inflow  $I$  for System (Big, 8300),  $ST_{days} = 162.14$ ,  $PH_{days} = 27.47$ , with the ‘mean-price’ economic scheme.

**Appendix: ‘Mean Price’ Economic Scheme CPSDF  $\langle S_{SR} \rangle$**

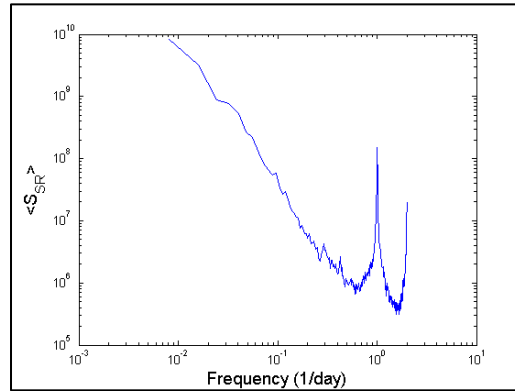


Figure 6-43: Ensemble CPSDF of optimal release  $R$  and reservoir storage  $S$  for System (Small, 2000),  $ST_{days} = 16.19$ ,  $PH_{days} = 11,40$ , with the ‘mean-price’ economic scheme.

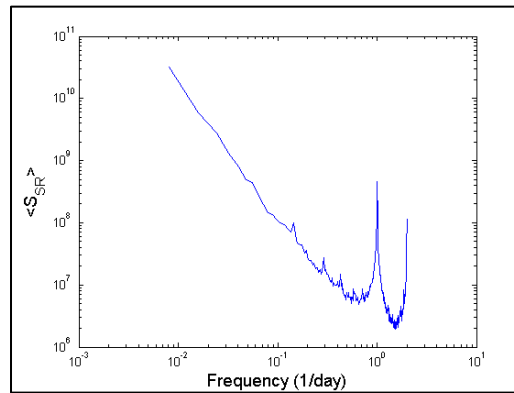


Figure 6-44: Ensemble CPSDF of optimal release  $R$  and reservoir storage  $S$  for System (Mid, 2000),  $ST_{days} = 82.19$ ,  $PH_{days} = 32.57$ , with the ‘mean-price’ economic scheme.

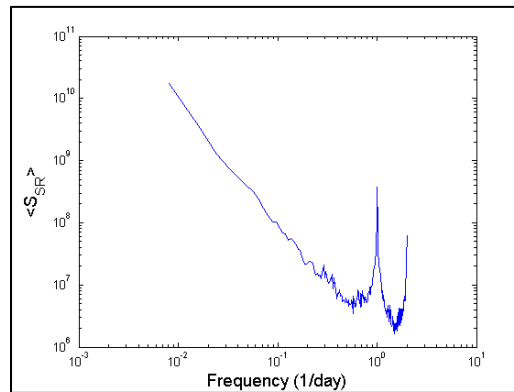


Figure 6-45: Ensemble CPSDF of optimal release  $R$  and reservoir storage  $S$  for System (Big, 2000),  $ST_{days} = 162.14$ ,  $PH_{days} = 114.00$ , with the ‘mean-price’ economic scheme.

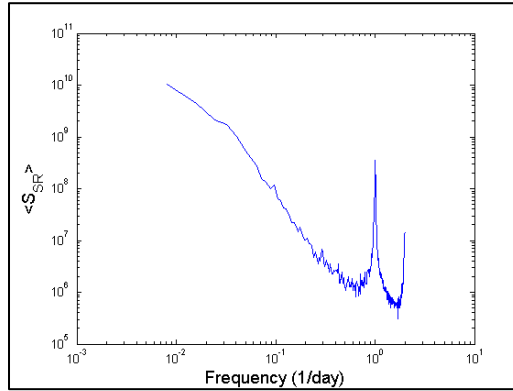


Figure 6-46: Ensemble CPSDF of optimal release  $R$  and reservoir storage  $S$  for System (Small, 3500),  $ST_{days} = 16.19$ ,  $PH_{days} = 6.51$ , with the ‘mean-price’ economic scheme.

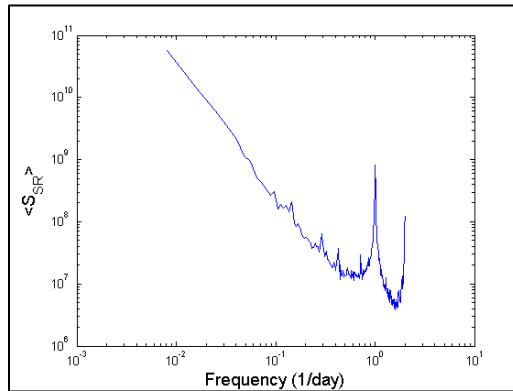


Figure 6-47: Ensemble CPSDF of optimal release  $R$  and reservoir storage  $S$  for System (Mid, 3500),  $ST_{days} = 82.19$ ,  $PH_{days} = 32.57$ , with the ‘mean-price’ economic scheme.

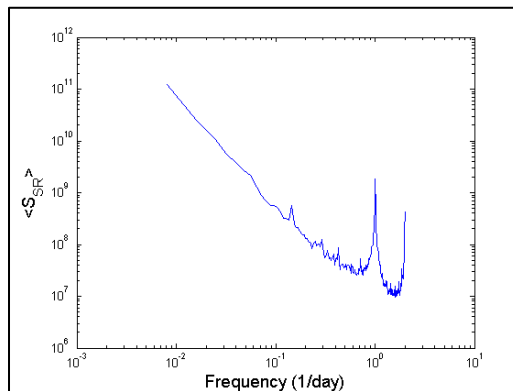


Figure 6-48: Ensemble CPSDF of optimal release  $R$  and reservoir storage  $S$  for System (Big, 3500),  $ST_{days} = 162.14$ ,  $PH_{days} = 65.15$ , with the ‘mean-price’ economic scheme.

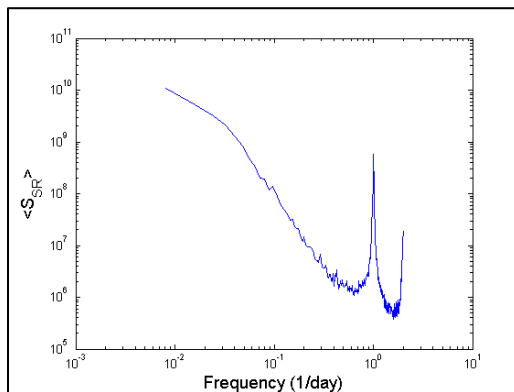


Figure 6-49: Ensemble CPSDF of optimal release  $R$  and reservoir storage  $S$  for System (Small, 5000),  $ST_{days} = 16.19$ ,  $PH_{days} = 4.56$ , with the ‘mean-price’ economic scheme.

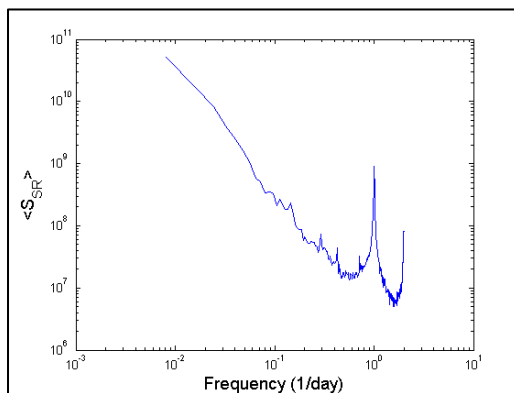


Figure 6-50: Ensemble CPSDF of optimal release  $R$  and reservoir storage  $S$  for System (Mid, 5000),  $ST_{days} = 82.19$ ,  $PH_{days} = 22.80$ , with the ‘mean-price’ economic scheme.

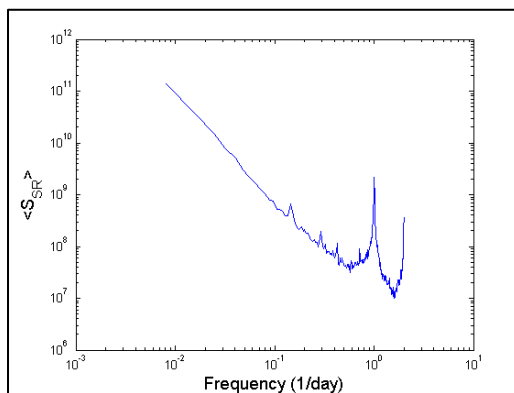


Figure 6-51: Ensemble CPSDF of optimal release  $R$  and reservoir storage  $S$  for System (Big, 5000),  $ST_{days} = 162.14$ ,  $PH_{days} = 45.60$ , with the ‘mean-price’ economic scheme.

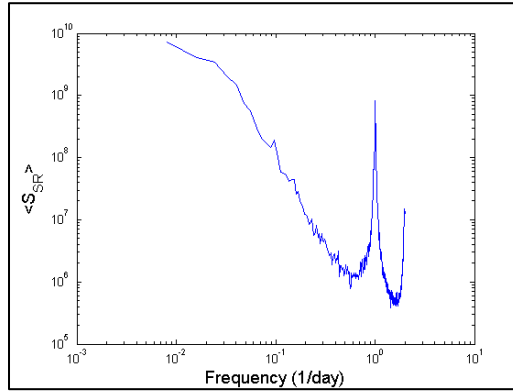


Figure 6-52: Ensemble CPSDF of optimal release  $R$  and reservoir storage  $S$  for System (Small, 8300),  $ST_{days} = 16.19$ ,  $PH_{days} = 2.75$ , with the ‘mean-price’ economic scheme.

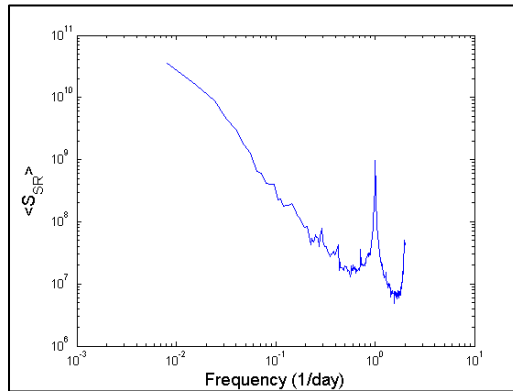


Figure 6-53: Ensemble CPSDF of optimal release  $R$  and reservoir storage  $S$  for System (Mid, 8300),  $ST_{days} = 82.19$ ,  $PH_{days} = 13.74$ , with the ‘mean-price’ economic scheme.

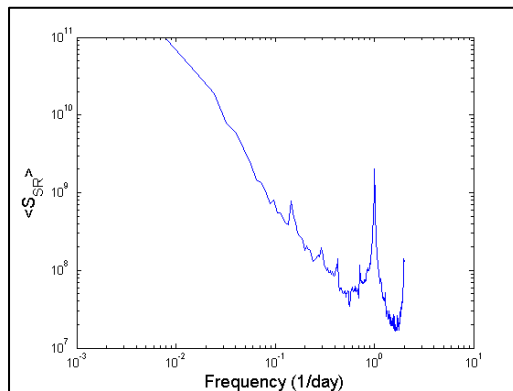


Figure 6-54: Ensemble CPSDF of optimal release  $R$  and reservoir storage  $S$  for System (Big, 8300),  $ST_{days} = 162.14$ ,  $PH_{days} = 27.47$ , with the ‘mean-price’ economic scheme.

*Appendix: 'Real Price' Economic Scheme PSDF  $\langle S_{RR} \rangle$*

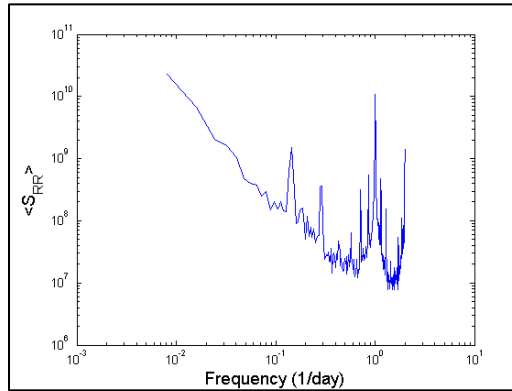


Figure 6-55: Ensemble PSDF of optimal release  $R$  for System (Small, 2000),  $ST_{days} = 16.19.14$ ,  $PH_{days} = 11.40$ , with the 'real-price' economic scheme.

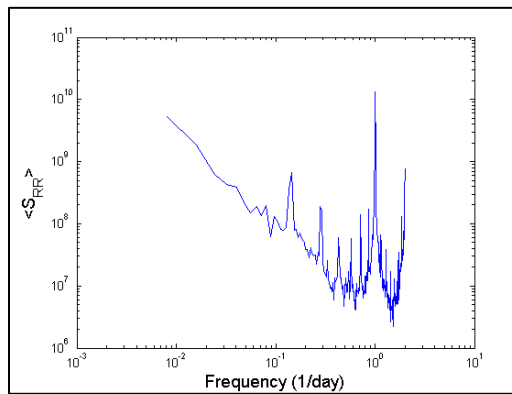


Figure 6-56: Ensemble PSDF of optimal release  $R$  for System (Mid, 2000),  $ST_{days} = 82.19$ ,  $PH_{days} = 57.00$ , with the 'real-price' economic scheme.

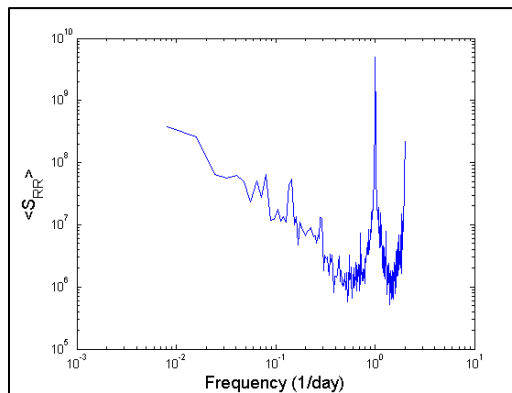


Figure 6-57: Ensemble PSDF of optimal release  $R$  for System (Big, 2000),  $ST_{days} = 162.14$ ,  $PH_{days} = 114.00$ , with the 'real-price' economic scheme.

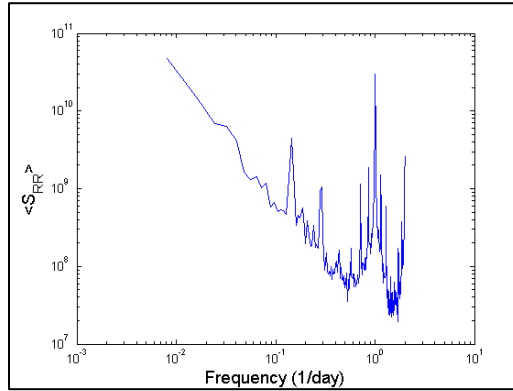


Figure 6-58: Ensemble PSDF of optimal release  $R$  for System (Small, 3500),  $ST_{days} = 16.19$ ,  $PH_{days} = 6.51$ , with the 'real-price' economic scheme.

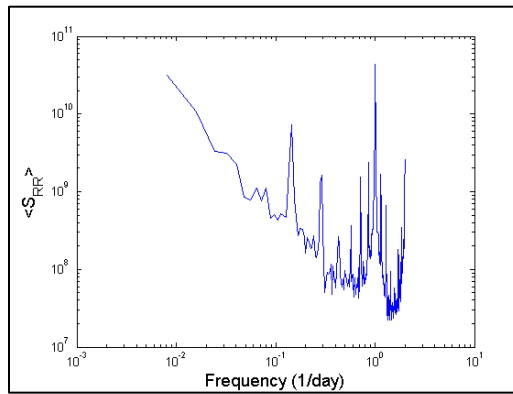


Figure 6-59: Ensemble PSDF of optimal release  $R$  for System (Mid, 3500),  $ST_{days} = 82.19$ ,  $PH_{days} = 32.57$ , with the 'real-price' economic scheme.

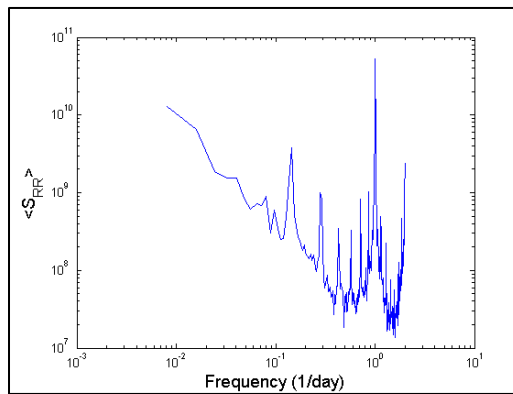


Figure 6-60: Ensemble PSDF of optimal release  $R$  for System (Big, 3500),  $ST_{days} = 162.14$ ,  $PH_{days} = 65.15$ , with the 'real-price' economic scheme.

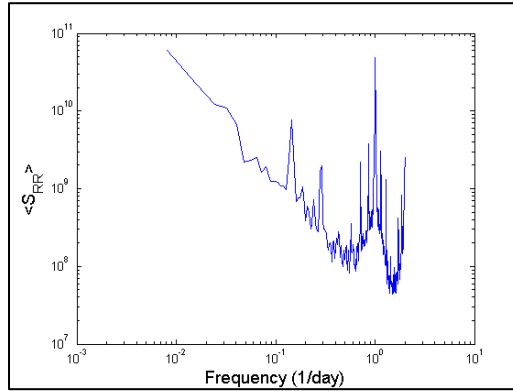


Figure 6-61: Ensemble PSDF of optimal release  $R$  for System (Small, 5000),  $ST_{days} = 16.19$ ,  $PH_{days} = 4.56$ , with the 'real-price' economic scheme.

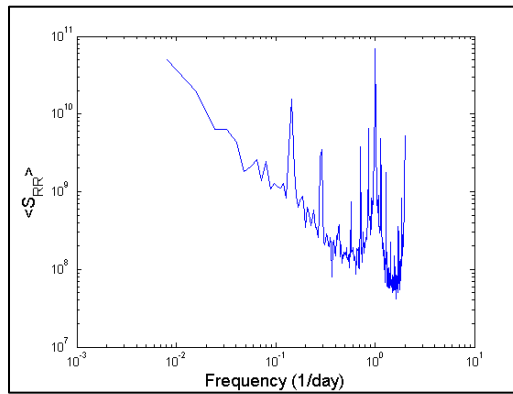


Figure 6-62: Ensemble PSDF of optimal release  $R$  for System (Mid, 5000),  $ST_{days} = 82.19$ ,  $PH_{days} = 22.8$ , with the 'real-price' economic scheme.

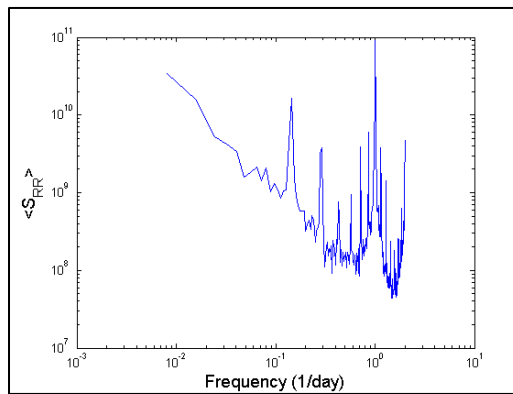


Figure 6-63: Ensemble PSDF of optimal release  $R$  for System (Big, 5000),  $ST_{days} = 162.14$ ,  $PH_{days} = 45.60$ , with the 'real-price' economic scheme.

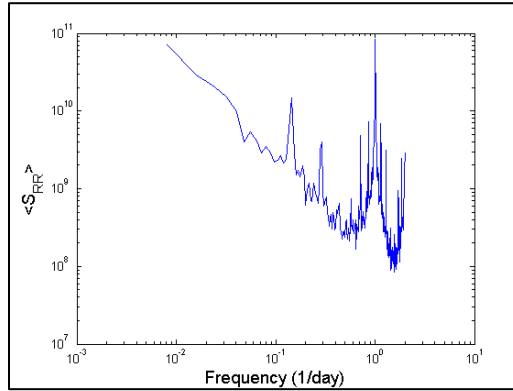


Figure 6-64: Ensemble PSDF of optimal release  $R$  for System (Small, 8300),  $ST_{days} = 16.19$ ,  $PH_{days} = 2.75$ , with the 'real-price' economic scheme.

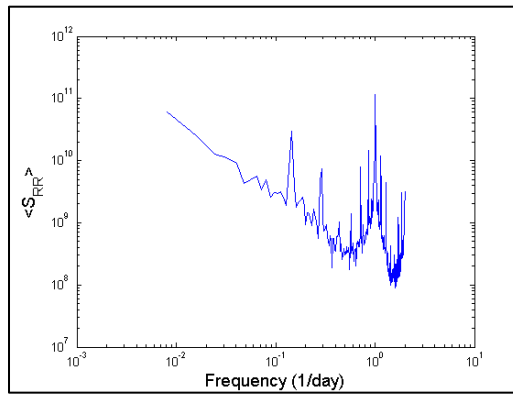


Figure 6-65: Ensemble PSDF of optimal release  $R$  for System (Mid, 8300),  $ST_{days} = 82.19$ ,  $PH_{days} = 13.74$ , with the 'real-price' economic scheme.

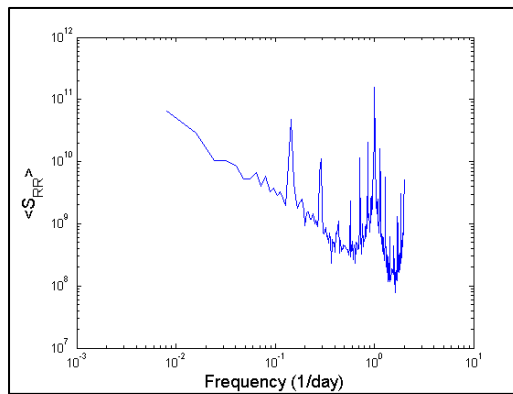


Figure 6-66: Ensemble PSDF of optimal release  $R$  for System (Big, 8300),  $ST_{days} = 162.14$ ,  $PH_{days} = 27.47$ , with the 'real-price' economic scheme.

*Appendix: 'Real Price' Economic Scheme CPSDF  $\langle S_{IR} \rangle$*

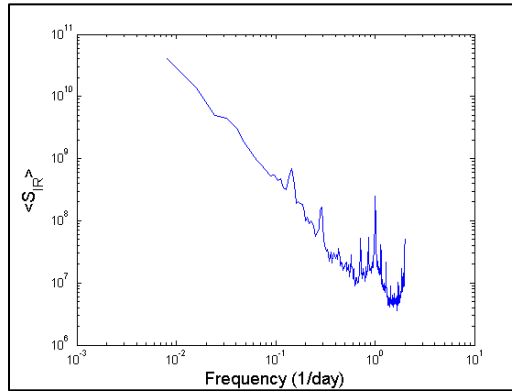


Figure 6-67: Ensemble CPSDF of optimal release  $R$  and inflow  $I$  for System (Small, 2000),  $ST_{days} = 16.19$ ,  $PH_{days} = 11.40$ , with the 'real-price' economic scheme.

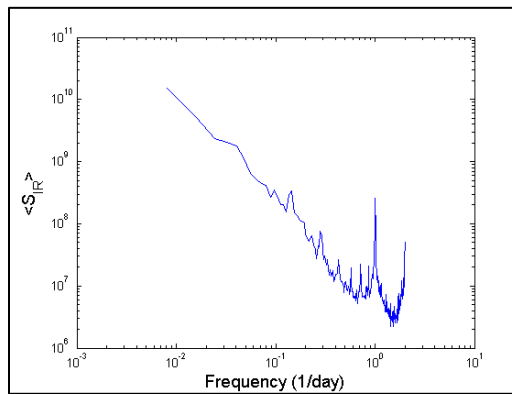


Figure 6-68: Ensemble CPSDF of optimal release  $R$  and inflow  $I$  for System (Mid, 2000),  $ST_{days} = 82.19$ ,  $PH_{days} = 57.00$ , with the 'real-price' economic scheme.

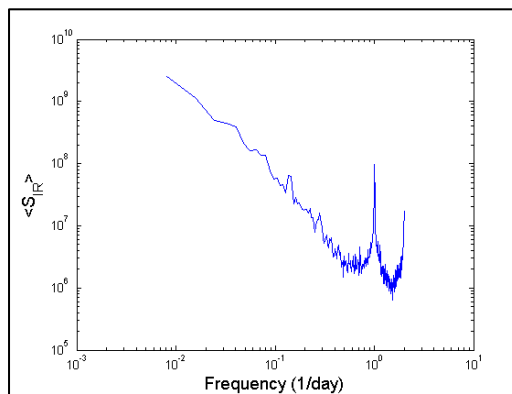


Figure 6-69: Ensemble CPSDF of optimal release  $R$  and inflow  $I$  for System (Big, 2000),  $ST_{days} = 162.14$ ,  $PH_{days} = 114$ , with the 'real-price' economic scheme.

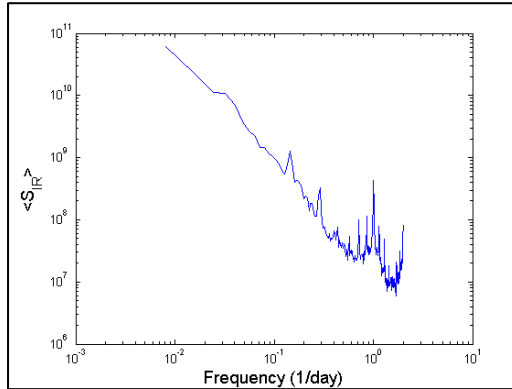


Figure 6-70: Ensemble CPSDF of optimal release  $R$  and inflow  $I$  for System (Small, 3500),  $ST_{days} = 16.19$ ,  $PH_{days} = 6.51$ , with the ‘real-price’ economic scheme.

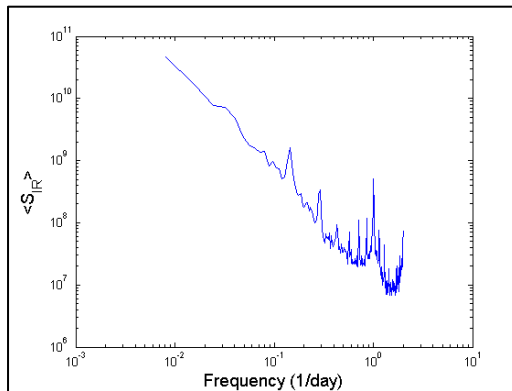


Figure 6-71: Ensemble CPSDF of optimal release  $R$  and inflow  $I$  for System (Mid, 3500),  $ST_{days} = 82.19$ ,  $PH_{days} = 32.57$ , with the ‘real-price’ economic scheme.

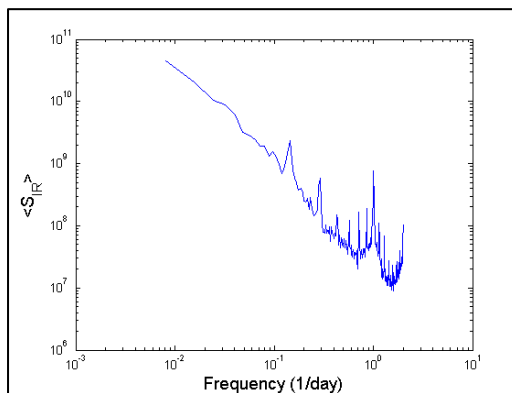


Figure 6-72: Ensemble CPSDF of optimal release  $R$  and inflow  $I$  for System (Big, 3500),  $ST_{days} = 162.14$ ,  $PH_{days} = 65.15$ , with the ‘real-price’ economic scheme.

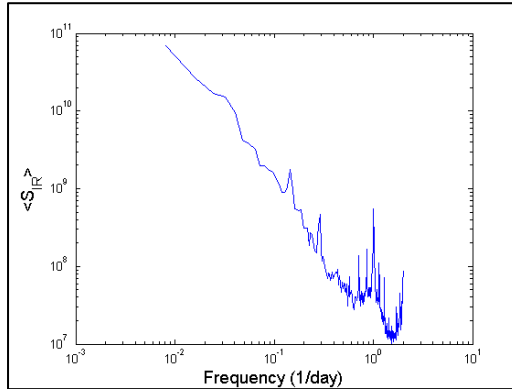


Figure 6-73: Ensemble CPSDF of optimal release  $R$  and inflow  $I$  for System (Small, 5000),  $ST_{days} = 16.19$ ,  $PH_{days} = 4.56$ , with the 'real-price' economic scheme.

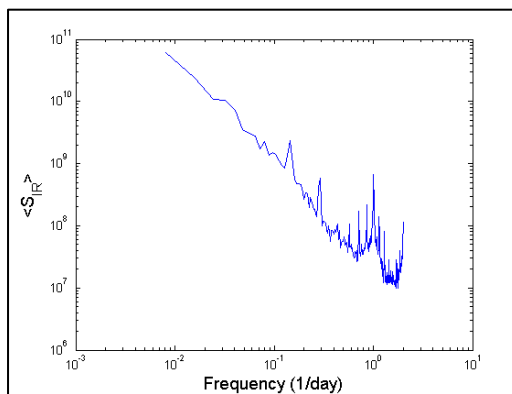


Figure 6-74: Ensemble CPSDF of optimal release  $R$  and inflow  $I$  for System (Mid, 5000),  $ST_{days} = 82.19$ ,  $PH_{days} = 22.8$ , with the 'real-price' economic scheme.

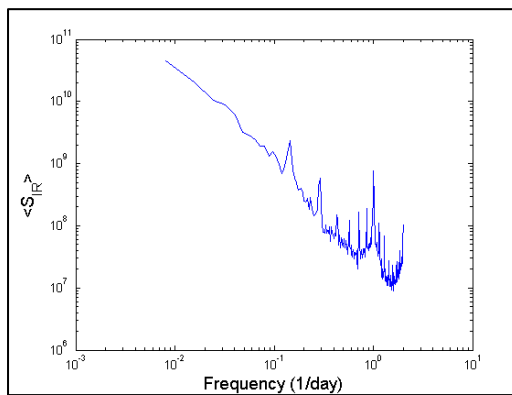


Figure 6-75: Ensemble CPSDF of optimal release  $R$  and inflow  $I$  for System (Big, 5000),  $ST_{days} = 162.14$ ,  $PH_{days} = 45.6$ , with the 'real-price' economic scheme.

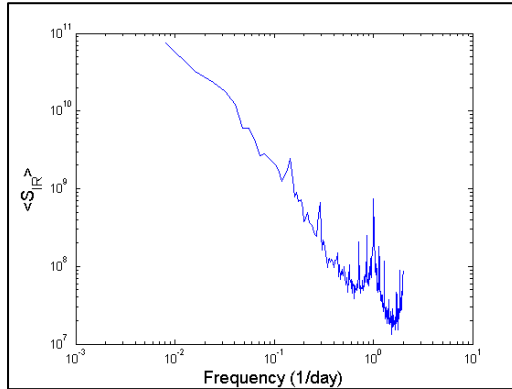


Figure 6-76: Ensemble CPSDF of optimal release  $R$  and inflow  $I$  for System (Small, 8300),  $ST_{days} = 16.19$ ,  $PH_{days} = 2.75$ , with the ‘real-price’ economic scheme.

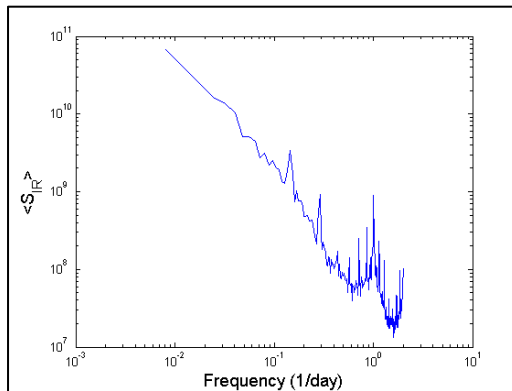


Figure 6-77: Ensemble CPSDF of optimal release  $R$  and inflow  $I$  for System (Mid, 8300),  $ST_{days} = 82.19$ ,  $PH_{days} = 13.74$ , with the ‘real-price’ economic scheme.

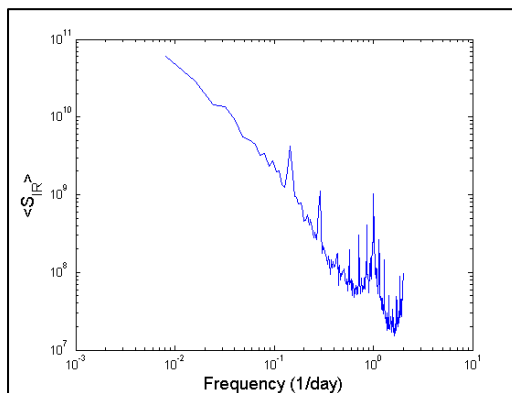


Figure 6-78: Ensemble CPSDF of optimal release  $R$  and inflow  $I$  for System (Big, 8300),  $ST_{days} = 162.14$ ,  $PH_{days} = 27.47$ , with the ‘real-price’ economic scheme.

*Appendix: 'Real Price' Economic Scheme CPSDF  $\langle S_{SR} \rangle$*

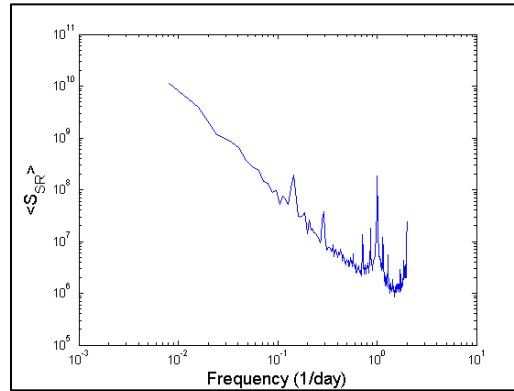


Figure 6-79: Ensemble CPSDF of optimal release  $R$  and reservoir storage  $S$  for System (Small, 2000),  $ST_{days} = 16.19$ ,  $PH_{days} = 11.4$ , with the 'real-price' economic scheme.

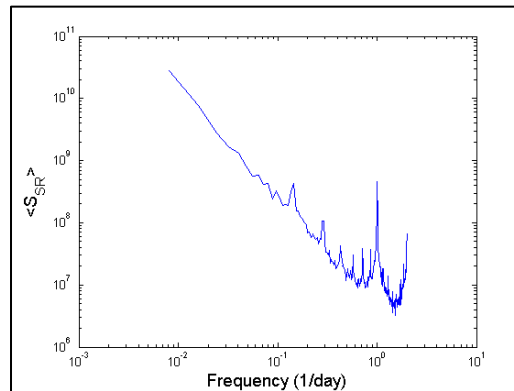


Figure 6-80: Ensemble CPSDF of optimal release  $R$  and reservoir storage  $S$  for System (Mid, 2000),  $ST_{days} = 82.19$ ,  $PH_{days} = 57.00$ , with the 'real-price' economic scheme.

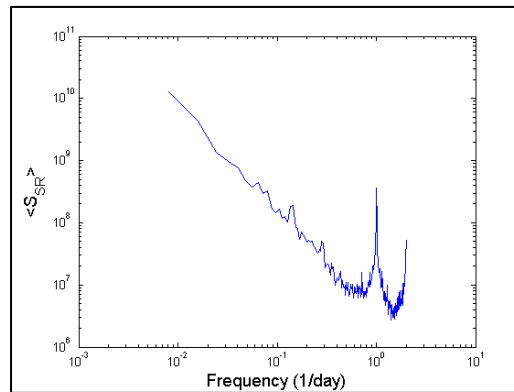


Figure 6-81: Ensemble CPSDF of optimal release  $R$  and reservoir storage  $S$  for System (Big, 2000),  $ST_{days} = 162.14$ ,  $PH_{days} = 114.00$ , with the 'real-price' economic scheme.

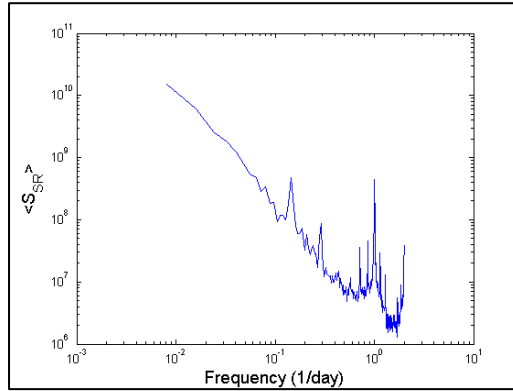


Figure 6-82: Ensemble CPSDF of optimal release  $R$  and reservoir storage  $S$  for System (Small, 3500),  $ST_{days} = 16.19$ ,  $PH_{days} = 6.51$ , with the ‘real-price’ economic scheme.

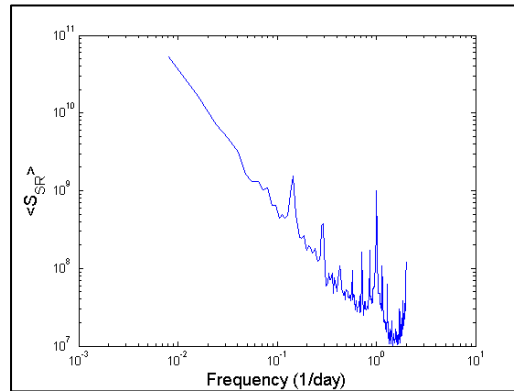


Figure 6-83: Ensemble CPSDF of optimal release  $R$  and reservoir storage  $S$  for System (Mid, 3500),  $ST_{days} = 82.19$ ,  $PH_{days} = 32.57$ , with the ‘real-price’ economic scheme.

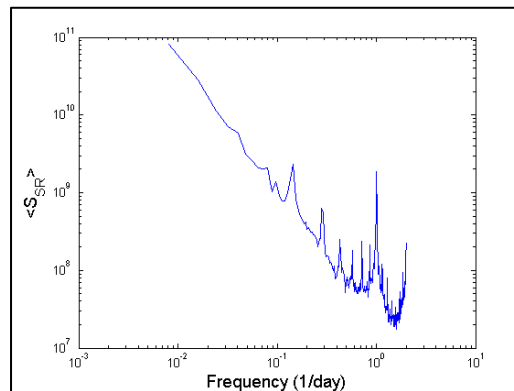


Figure 6-84: Ensemble CPSDF of optimal release  $R$  and reservoir storage  $S$  for System (Big, 3500),  $ST_{days} = 162.14$ ,  $PH_{days} = 65.15$ , with the ‘real-price’ economic scheme.

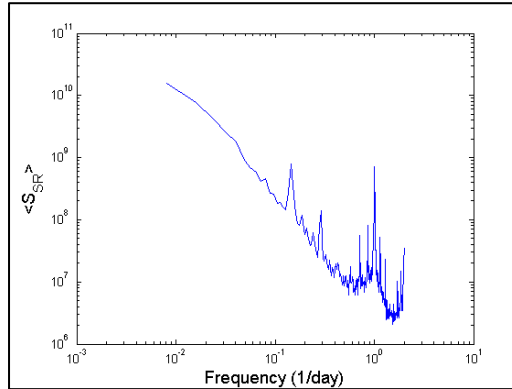


Figure 6-85: Ensemble CPSDF of optimal release  $R$  and reservoir storage  $S$  for System (Small, 5000),  $ST_{days} = 16.19$ ,  $PH_{days} = 4.56$ , with the 'real-price' economic scheme.

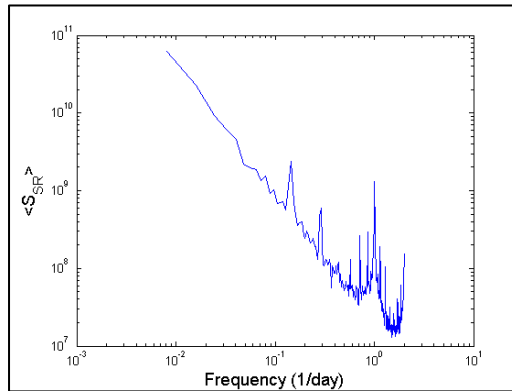


Figure 6-86: Ensemble CPSDF of optimal release  $R$  and reservoir storage  $S$  for System (Mid, 5000),  $ST_{days} = 82.19$ ,  $PH_{days} = 22.80$ , with the 'real-price' economic scheme.

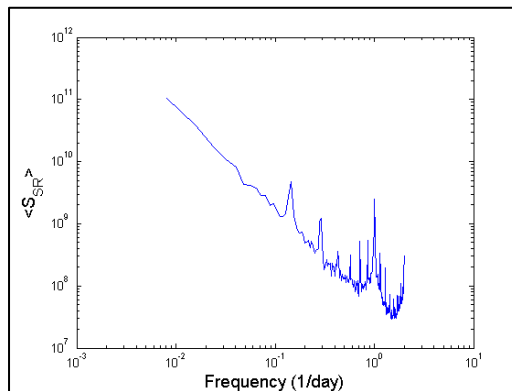


Figure 6-87: Ensemble CPSDF of optimal release  $R$  and reservoir storage  $S$  for System (Big, 5000),  $ST_{days} = 162.14$ ,  $PH_{days} = 45.60$ , with the 'real-price' economic scheme.

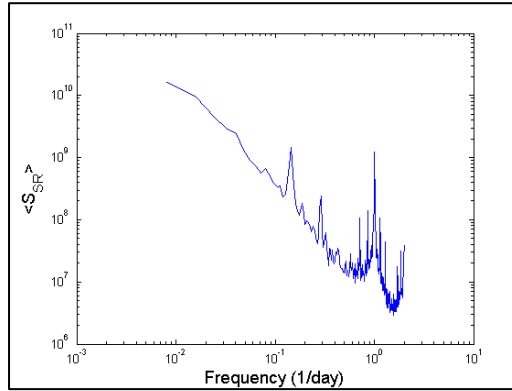


Figure 6-88: Ensemble CPSDF of optimal release  $R$  and reservoir storage  $S$  for System (Small, 8300),  $ST_{days} = 16.19$ ,  $PH_{days} = 2.75$ , with the ‘real-price’ economic scheme.

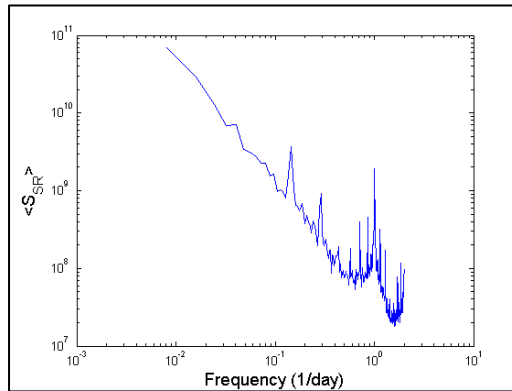


Figure 6-89: Ensemble CPSDF of optimal release  $R$  and reservoir storage  $S$  for System (Mid, 8300),  $ST_{days} = 82.19$ ,  $PH_{days} = 13.74$ , with the ‘real-price’ economic scheme.

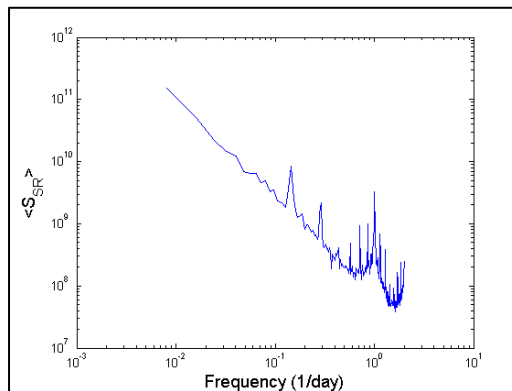


Figure 6-90: Ensemble CPSDF of optimal release  $R$  and reservoir storage  $S$  for System (Big, 8300),  $ST_{days} = 162.14$ ,  $PH_{days} = 27.47$ , with the ‘real-price’ economic scheme.



## CHAPTER 7

### SUMMARY AND CONCLUSIONS

This thesis has focused on the optimization of hydropower reservoirs using dynamic programming (DP) algorithms, with a particular emphasis on stochastic DP (SDP) and sampling SDP (SSDP). The thesis has six major chapters, but three research foci. The first three chapters of the thesis provide introduction and motivation for this work (Chapter 1), a review of past work on DP and SDP models for reservoir operations (Chapter 2), and a description of the Kennebec River system which serves as the case study for this work.

The first research focus, discussed in Chapter 4, is how inflow and forecast uncertainty should best be represented in stochastic hydropower optimization models? The Second research focus, discussed in Chapter 5, is the development of a new and efficient solution technique for multi-reservoir SDP models. The third and final focus, discussed in Chapter 6, is the development of diagnostic analyses which can be used to study a reservoir system and aid in the evaluation of simulation or optimization model performance, or actual operations. The following sections describe the conclusions from each of the three research foci.

#### ***Chapter 4 Conclusions***

In Chapter 4 the single-reservoir SSDP algorithm is leveraged to answer three research questions. First, what is the utility of various representations of uncertainty? Second, what is the value of forecast precision to hydropower operations? And third,

how do the answers to the first two questions depend on the characteristics of the system under study?

To explore each of these questions the operation of a number of hypothetical reservoir systems is simulated over 60 summer operating periods. Two economic models were used: one with a constant energy price profile for each day and one with a variable energy price profile.

It was found that in many cases more complex models, with many uncertainty transition points outperformed simpler two-stage representations of uncertainty and deterministic models which do not consider uncertainty. However, it was found that for large reservoirs with small turbine capacities, simple two-stage uncertainty models perform as well as more complex multi-stage uncertainty models. And with small reservoirs with little storage, operation is essentially run-of-river, and forecasts are of little value.

Furthermore, improved forecast precision generally improved algorithm performance, though it was found that as turbine size becomes smaller the efficiency of the optimization algorithm is less sensitive to the precision of the forecast. This is particularly true for reservoirs with large storage, and in the 'variable price' case where energy prices change from day-to-day.

Finally in Chapter 4 it was shown that algorithm efficiency is generally very low for the 'variable price' case compared to the 'mean price' case. This is partially because there is now an added layer of uncertainty and partially because the algorithm efficiency is distorted by an improvement in the 'perfect' decision rule performance.

### ***Chapter 5 Conclusions***

Chapter 5 addresses the solution of multi-dimensional SDP models, which continues to be a challenging problem more than 50 years after Bellman coined the ‘Curse of Dimensionality.’ However increased computing power and improved numerical techniques continue to push the boundaries of what is possible. New work on Q-Q iteration DP [Castelletti, 2010] and adaptive sparse grids [Brumm and Scheidegger, 2014] as well as past work using cubic splines [Johnson et al., 1993] and SDDP [Pereira and Pinto, 1985] allow significant improvement over traditional SDP solution techniques. In this vein, Corridor DP seeks to reduce the computational burden of high-dimensional DP by focusing the optimization effort in the region of the state space where the system is likely to reside. Results presented in Chapter 5 show that with careful basis selection, Corridor SDP paired with RBF interpolation can outperform DP with Cubic Spline interpolation in that it achieves the same accuracy with about a 1/10 the effort for a smooth (nearly linear) test surface and about 1/30 the effort for a curved surface (with penalties to enforce minimum targets). Corridor SDP paired with RBF interpolation can achieve the same accuracy as linear-DP with 1/1100 and 1/215 the number of points for the smooth and curved objectives respectively.

### ***Chapter 6 Conclusions***

This short chapter focuses on diagnostic tools which can be used to evaluate the character of system one is dealing with, the important time scales of operation to a system, and the amount of variability in the optimal control policy which is explained in different frequency bands. The dimensionless diagnostic measurements are simple

to apply and can be very revealing. Chief Joseph Dam is in the top 5 power producing dams in the United States, and yet it is essentially a run of river plant. This is counterintuitive: Chief Joseph dam has an enormous storage and is nearly 200 ft high. However the operational constraints on the active storage, and the enormous flows in the Columbia River, reduce this massive project to essentially run of river and daily regulation operations.

The regression analysis approach to identifying potential state variables and important duration periods is inspired by past work that derives optimal operating policies by regressing on the results of deterministic optimization (see Karamouz and Houck [1982] for an early example). However, in the analysis proposed here, the optimal policy is not derived from the regression analysis; but rather the regression analysis informs the structure of the stochastic optimization model. In the examples provided in Chapter 6 it is shown that inflow in the next 7-24 hours is most related to the optimal perfect policy over a wide range of hypothetical systems. From this observation it was concluded that the inflow forecast for the next 24-hours was the most informative for the optimization models applied in Chapter 4.

The spectral analysis approach to diagnosing hydropower reservoir operating frequencies is new, and needs more explanation, but it clearly shows that the diurnal peaking cycle in the energy market explains a huge amount of the variability in the system operation, though the largest fluctuations are due to seasonal drawdown to meet flood storage targets.

### ***Future Work***

I see great opportunities for SSDP models for two reasons. First the affordability of high-end computation is becoming such that running short-term SSDP models is becoming operationally feasible for even unsophisticated system operators (like the small utilities in New England). Second, ensemble forecasts of many types are becoming very popular in the fields of hydrology and meteorology, and water resource planners and managers are becoming increasingly interested in incorporating such forecasts into their models. SSDP provides a natural DP framework to incorporate such forecasts. There appears to be two reasons why there has been a resurgence of interest in SSDP [Kim et al., 2007; Vicuna et al., 2010; Cote et al., 2011; Eum et al., 2011]. Given this trend there is great value and will be great appeal for the type of research in Chapter 4, which is exploratory in nature and might easily be applied to draw general conclusions about the value of model classes for reservoir types given a basin's hydrology.

A significant achievement in Chapter 5 was the demonstration that cubic splines worked so well on a realistic system, as Johnson et al. [1993]'s results were based on a simple example. The fact that Corridor DP can beat splines by an order of magnitude (or more) in some cases is a significant result. There are two areas of future research here. The first is to extend the Corridor study to higher dimensions. The cost of cubic spline interpolation on a full grid will increase exponentially, but it seems very doubtful that the cost of Corridor DP will increase that fast. Thus I believe that Corridor DP will become more attractive in higher dimensions, and we hope to pursue that idea.

Secondly, it seems that Hermite RBFs and least-squares RBFs have the potential to significantly improve the performance of the Corridor DP algorithm. The Hermite RBF surface provides much more information about the shape of the function surface than regular RBFs, thus one expects that fewer points should be required to achieve a desired accuracy. Hermite RBFs are described in Chapter 5, and it is my hope to pursue this research immediately upon graduation. Least-squares RBFs become attractive as the size of the basis becomes larger. This is because as the basis becomes larger, separation distance becomes smaller, and an interpolating surface can develop irregular ‘wiggles,’ which can be disastrous when using quasi-Newton search over the RBF surface. By freeing the surface from the interpolation constraint, a smoother surface results, and this should result in better results at high densities (i.e. large basis).

Finally the exploratory analysis in Chapter 6 represents an initial investigation of novel approaches to reservoir system diagnostics, especially the use of spectral analysis. I am excited to continue the study started in Chapter 6 as I see real potential for that work. Future work using the regression analysis procedure from Chapter 6 will explore the nuances and special considerations required for to develop good regression relationships so as to better identify key variables.

## REFERENCES

- Brumm, J. & Scheidegger, S. 2014, "using Adaptive Sparse Grids to Solve High-Dimensional Dynamic Models", *Social Science Research Network*, .
- Castelletti, A., Galelli, S., Restelli, M. & Soncini-Sessa, R. 2010, "Tree-based reinforcement learning for optimal water reservoir operation", *Water Resources Research*, vol. 46, no. W09507.
- Cote, P., Haguma, D., Leconte, R. & Krauc, S. 2011, "Stochastic Optimization of Hydro-Quebec hydropower installations: a statistical comparison between SDP and SSDP methods", *Canadian Journal of Civil Engineering*, vol. 38, no. 12, pp. 1427-1434.
- Eum, H., Kim, Y. & Palmer, R.N. 2011, "Optimal Drought Management Using Sampling Stochastic Dynamic Programming with a Hedging Rule", *Journal of Water Resources Planning and Management*, vol. 137, no. 1.
- Johnson, S.A., Stedinger, J.R., Shoemaker, C.A., Li, Y. & Tejada-Guibert, J.A. 1993, "Numerical Solution of Continuous-State Dynamic Programs Using Linear and Spline Interpolation", *Operations Research*, vol. 41, no. 3.
- Karamouz, M. & Houck, M.H. 1982, "Annual and Monthly Reservoir Operating Rules Generated by Deterministic Optimization", *Water Resources Research*, vol. 18, no. 5, pp. 1337.
- Kim, Y., Eum, H., Lee, E. & Ko, I. 2007, "Optimizing Operational Policies for a Korean Multireservoir System using Sampling Stochastic Dynamic Programming with Ensemble Streamflow Prediction", *Journal of Water Resources Planning and Management*, vol. 133, no. 1, pp. 4-14.
- Labadie, J.W. 2005, "Closure to "Optimal Operation of Multi-Reservoir Systems: State-of-the-Art Review"", *Journal of Water Resources Planning and Management*, vol. 131, no. 5, pp. 407.
- Labadie, J.W. 2004, "Optimal Operation of Multireservoir Systems: State-of-the-Art Review", *Journal of Water Resources Planning and Management*, vol. 130, no. 2, pp. 93-111.

- Little, J.D.C. 1955, "Use of Storage Water in a hydroelectric System", *Journal of Operations Research*, vol. 3, pp. 187-197.
- Pereira, M.V.F. & Pinto, L.M.V.G. 1985, "Stochastic optimization of a multireservoir hydroelectric system-a decomposition approach", *Water Resources Research*, vol. 21, no. 6.
- Powell, W.B. 2007, *Approximate Dynamic Programming*, 2nd edn, Wiley, New York.
- Vicuna, S., Dracup, J.A., Lund, J.R., Dale, L.L. & Maurer, E.P. 2010, "Basin-scale water system operations with uncertain future climate conditions: Methodology and case studies", *Water Resources Research*, vol. 46, no. W04505, pp. 1-19.